Geopolymers and Geocements: Low Environmentally Impact Ceramic Materials

Edited by

Pietro VINCENZINI
and Cristina LEONELLI

TRANS TECH PUBLICATIONS

12th INTERNATIONAL CERAMICS CONGRESS

PART H

12th INTERNATIONAL CERAMICS CONGRESS

Proceedings of the 12 th International Ceramics Congress, part of CIMTEC 2010-12 th International Ceramics Congress and 5th Forum on New Materials
Montecatini Terme, Italy, June 6-11, 2010

PART H *including:*

Symposium CK – Geopolymers and Geocements: Low Environmental Impact Ceramic Materials

Edited by

Pietro VINCENZINI
World Academy of Ceramics and
National Research Council, Italy

Co-edited by

Cristina LEONELLI
University of Modena and Reggio Emilia, Italy

TRANS TECH PUBLICATIONS LTD
Switzerland • UK • USA

on behalf of TECHNA GROUP
Faenza • Italy

Published by Trans Tech Publications Ltd., on behalf of Techna Group Srl, Italy

Trans Tech Publications Ltd
Laubisrutistr. 24
CH-8712 Stafa-Zuerich
Switzerland
http://www.ttp.net

Volume 69 of
Advances in Science and Technology
ISSN 1661-819X

Full text available online at http://www.scientific.net

The listing of the other Volumes (1-61) of the Series "Advances in Science and Technology" are available at TECHNA GROUP website: http://www.technagroup.it

Distributed worldwide by

Trans Tech Publications Ltd
Laubisrutistr. 24
CH-8712 Stafa-Zuerich
Switzerland

Fax: +41 (44) 922 10 33
e-mail: sales@ttp.net

and in the Americas by

Trans Tech Publications Inc.
PO Box 699, May Street
Enfield, NH 03748
USA

Phone: +1 (603) 632-7377
Fax: +1 (603) 632-5611
e-mail: sales-usa@ttp.net

PREFACE

CIMTEC 2010 was held in Montecatini Terme, Italy on June 6-18, 2010. This high qualitative and comprehensive congressional event, similarly to the previous editions, has been designed to encompass and derive synergism from a broad interdisciplinarity network capable of offering opportunities for identifying and exploring new directions for research and production. The above based on the view that ongoing and future innovations require at an ever increasing extent a complex array of interconnections among scientific research, innovating technology and industrial infrastructure.

CIMTEC 2010 consisted of two major events: the 12th INTERNATIONAL CERAMICS CONGRESS (June 6-11, 2010) and the 5th FORUM ON NEW MATERIALS (June 13-18, 2010). The World Academy of Ceramics and the International Ceramic Federation (ICF) acted as principal endorsers for the first one, and the International Union of Materials Research Societies (IUMRS) for the FORUM.

The 12th INTERNATIONAL CERAMICS CONGRESS included 12 International Symposia, two Focused Sessions and two Serial International Conferences ("Disclosing Materials at Nanoscale" and "Advanced Inorganic Fibre Composites for Structural and Thermal Management Applications") which covered recent progress in almost all relevant fields of ceramics science and technology. The 5th FORUM ON NEW MATERIALS consisted of 11 International Symposia primarily concerned with energy technologies, one Focused Session and two Serial International Conferences ("Science and Engineering of Novel Superconductors" and "Medical Applications of Novel Biomaterials and Nano-biotechnology").

A balanced, high quality programme of invited and contributed papers resulted from the over one thousand and seven hundred scientific and technical contributions effectively presented during the working days to a large international audience coming from fifty-seven countries throughout the world.

The 15 volumes which constitute the Official Proceedings of CIMTEC 2010 (10 for the Ceramics Congress, 5 for the Forum) include a selection of the papers presented. Having most of them been written by authors whose mother tongue is not English, considerable revision of the original texts was often required. The partial reworking of several papers and sometimes even complete rewriting was needed to make clear work valid as regards the technical content but difficult to understand because of lack of proficiency in the English language. Even so, in order to allow the scientific and technical community to have access to the proceedings volumes within a reasonable length of time, compromise was necessary in regard to the quality of writing, and papers containing language imperfections were considered acceptable provided that their technical content was adequate and easily understandable.

The Editor, who also acted as the Chairman of CIMTEC 2010, would like to express his sincere appreciation to all the Institutions and Professional Organizations involved in the congress, to the members of the International Advisory Committees, the National Coordinating Committees, the Co-Chairs Prof. Akio Makishima (Japan) for the INTERNATIONAL CERAMICS CONGRESS and Prof. Robert P.H. Chang (USA) for the FORUM ON NEW MATERIALS, the Programme Chairs, the Lecturers, the technical staff of Techna Group, and to the many others who directly or indirectly contributed to the organization. Indeed it was mainly through the involvement of the above bodies and individuals, and the active participation of most internationally qualified experts from major academic and government research institutes and industrial R&D centers that a very valuable scientific programme could be arranged.

It is therefore expected for the Proceedings of CIMTEC 2010-12th INTERNATIONAL CERAMICS CONGRESS & 5th FORUM ON NEW MATERIALS to constitute a further valuable contribution to the literature in the field.

P. VINCENZINI
World Academy of Ceramics
Emeritus Research Manager
National Research Council of Italy

12th INTERNATIONAL CERAMICS CONGRESS

Chairman
Pietro VINCENZINI, *Italy*

Co-Chair
Akio MAKISHIMA, *Japan*

Symposium CK – Geopolymers and Geocements: Low Environmental Impact Ceramic Materials

Programme Chair
Cristina LEONELLI, *Italy*

Members
Erez Allouche, *USA* Mirko Braga, *Italy* Christopher Cheeseman, *UK* Gui Demortier, *Belgium* Katja Dombrowski, *Germany* Constantino Fernandez Pereira, *Spain* Dechang Jia, *P.R. China* Waltraud M. Kriven, *USA* Zongjin Li, *P.R. China* Kenneth J.D. Mackenzie, *New Zealand* Alejandro Manzano Ramirez, *Mexico* Henk Nugteren, *Netherlands* Hassane Oudadesse, *France* Christos G. Papakonstantinou, *USA* Dan S. Perera, *Australia* Vijaya B. Rangan, *Australia* Kwesi Sagoe-Crentsil, *Australia* Frantisek Skvara, *Czekia* Pavel Straka, *Czekia* Bob Talling, *Finland* Amandio Teixeira Pinto, *Portugal* Benjamin Varela, *USA* Marcel Weil, *Germany* Frank Winnefeld, *Switzerland* Yunsheng Zhang, *P.R. China*

Table of Contents

doi:10.4028/www.scientific.net/AST.69.1

STATUS AND PROSPECTS OF RESEARCH AND APPLICATION OF ALKALI-ACTIVATED MATERIALS

PAVEL KRIVENKO
V.D.Glukhovsky Scientific Research Institute for Binders and Materials,
Kiev National University of Civil Engineering and Architecture
31 Vozdukhoflotsky prospect Kiev 03037 Ukraine

e-mail: pavlo.kryvenko@gmail.com

Introduction

Beginning from 1957, a scientific school in Kiev (USSR) headed by Victor Glukhovsky has been developing a new direction in binding/cementitious/ materials. Taken as background was discovery of binding properties of the alkali metal compounds when they act not only as activators of hardening but are responsible for the formation of main structural elements of the alkali- activated cements – zeolite-like compounds of different types.

Just these hydration products, analogues to natural zeolites of the $Na_2O(K_2O)•Al_2O_3$ •(2-4)SiO_2•2H_2O type, were identified in the ancient concretes (Ancient Greece, Ancient Rome, Egypt, Syria). Durability of the ancient concretes and similarity of their structure with that of the alkali-activated cement concretes allowed to predict their high durability. High performance properties of the alkali- activated cement concretes are supported by over 50-year experience of service of the structures made from them.

Theoretical background

Less than a century ago just an idea of the presence of free alkali in a cement composition was considered by cement people as absurd one and this was a basic postulate of fundamentals of exhibiting hydraulic properties by mineral systems. The alkali metal compounds were excluded from traditional hydraulic cements because of their high solubility.

At the same time, the studies held to reveal the reasons explaining excellent durability of the ancient concretes in combination with the data collected on stability and composition of natural mineral formations testified that this postulate was not correct.

In 1957 a scientist from Kiev (USSR) Victor Glukhovsky has discovered that compounds of alkali metals (Li, Na, K, Rb, Cs) - the elements of the first group of the Periodic Table, exhibit hydraulic binding properties similar to compounds of alkali earth metals (Mg, Ca, Sr, Ba)- the elements of the second group.

As a result, an idea of creation of cementitious materials was transformed as the following:

“OLD SCHEME” (ordinary Portland cement (OPC), high-alumina cement)

$$\left.\begin{matrix} CaO-SiO_2 \\ CaO-Al_2O_3 \end{matrix}\right\} + H_2O \rightarrow \begin{matrix} CaO-SiO_2-H_2O \\ CaO-Al_3O_3-H_2O \end{matrix}$$

“NEW SCHEME” (alkali- activated cement)(AAC)

$$\left.\begin{matrix} Al_2O_3-SiO_2 \\ RO-Al_2O_3-SiO_2 \end{matrix}\right\} + R_2O + H_2O \rightarrow \begin{matrix} R_2O-Al_3O_3-SiO_2-H_2O \\ RO-R_2O-Al_2O_3-SiO_2-H_2O \end{matrix}$$

where R- Na, K, Li, Rb, Cs.

The idea itself of using these systems as cementitious ones was based, first of all, on geological data that sodium- potassium- calcium aluminosilicate compounds, which are known to have the higher stability and resistance to atmospheric reagents, are present in the Earth’s Crust. Secondly, this idea was based on the results of experimental studies, which proved that alkali hydroxides and

salts of alkali metals came into interaction with clay minerals, aluminosilicate glasses and crystalline substances of natural and artificial origin with the formation of water resistant alkaline and alkaline- alkali- earth aluminosilicate hydration products analogous to natural minerals of the zeolite and mica types.

3 Terminology

The established possibility of modelling the processes taking place in the Earth's crust based on an interaction between decay products of rock-forming minerals: clays and alkalis, followed by synthesis of these minerals, suggested using natural soils as starting materials for a binder. This explains why the binders/cementitious materials/ developed as long ago as in 1957 have been called "soil cements" and the concretes "soil silicates concretes" [1].

The alkaline and alkali-earth hydroaluminosilicates analogous to natural minerals (hydronepheline, analcime, natrolite, thompsonite, hydrosodalite, etc.) are formed in the soil cement stone during the process of hardening along with calcium hydrosilicates and carbonates.

The soil cements contain alkalis in large amounts (1-20 mass % calculated as R_2O). Just the alkaline oxides are components determining their binding properties. The alkali earth oxides are either absent in them (fly ashes, cakes, clays, field spar minerals) or may be introduced from the outside as the components of the traditional binding materials (lime, Roman-, Portland-, slag Portland or high alumina cements).

In 1973, Professor J. Davidovits was granted his first patents for geopolymers [2]. The technology for manufacturing these cements included the following steps: mixing kaolinite, lime stone, dolomite; burning of the mix and introduction of the alkaline compound solutions. During these processes, the kaolinite transforms into metakaolinite ($Al_2O_3.2SiO_2$), gaining pozzolanic properties, while calcium and magnesium carbonates form calcium and magnesium oxides. Being added to the cement mix, silica or soda or its mixture with potash incorporated with a mixing water produce sodium and potassium hydroxides. The latter initiates a chemical reaction with polysilicate and aluminosilicate oxides with the formation in a composition of the hydration products, represented by analcime and hydrosodalite. Some of these products are known as commercial products (trade names: Pyrament, Geopolycem, Geopolymite, etc.). The cements of this type are known in the art under a general name "geopolymers".

The alkali- activated cements are known among cement people also under other names: alkali-activated cements [3] SKJ- binder [4], F- cement [5], gypsum- free Portland cement [6], geocements [7].

4 Classification

Classification proposed in [8] is based on characteristic features of the products of hydration and hardening of the alkali- activated cements, the "edge" variants of which may be represented by the compounds of two types: alkaline hydrosluminosilicates of the system R_2O-Al_2O_3-SiO_2-H_2O and earth hydrosilicates.

A variety of blended alkaline- alkali- earth hydroaluminosilicates may fall within these "edge" variants. Phase composition of the hydration products of a cement stone is determined by a kind of the initial raw material (Table 1).

Table 1. Mineralogical composition of the cement hydration products vs type of initial aluminosilicate component.

Cement type	Initial soild phase	Alkali content, R_2O, %	Hydration product
OPC	OPC clinker	< 0.6	0% 100% 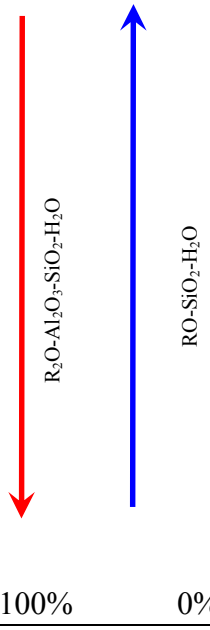 100% 0%
Alkaline OPC	OPC clinker+ R_2O	1-5	
Blended alkaline OPC	OPC clinker+ additive (slag, ash, basalt)+ +Me_2O	2-5	
Slag alkali-activated cement	Metallurgical slag+ R_2O	4-8	
Ash alkali- activated cement	Ash - product of coal combustion	5-10	
Geocement	Clay+ R_2O	10-20	

5 Principles of compositional build-up of the alkali-activated cements

The following postulates have been laid down in their creation:

- alkalis act not only as activators but as structure- forming elements included into the formed phases as well;
- the formed hydration products phases are characteristic of the presence of new formations of the R_2O- Al_2O_3- SiO_2- H_2O and R_2O- CaO- Al_2O_3- SiO_2- H_2O types;
- quantities of alkalis to be introduced are caused by a necessity to meet a stoichiometric composition /stoichiometry requirement/ of the alkaline and alkaline-alkali-earth hydroaluminosilicates analogous to natural zeolites.

In compliance with these principles the alkali content of the cement will be determined by an Al_2O_3 content of the aluminosilicate component (Fig.1).

The introduction into a cement composition of the alkali metal compounds in much larger quantities than was permitted in compliance with the principles of compositional build-up of the traditional cements based on calcium and magnesium compounds suggested to consider that the alkali metal compounds not only act as activators of hardening but as self- functioning components of the binding system Me_2O–MeO–Me_2O_3–SiO_2–H_2O, the main structure-forming products of which are low-basic calcium hydrosilicates and zeolite-like products. A low basicity of the hydration products is caused by specific features of the structure-forming processes taking place in the slag alkali- activated cements, namely: a hydrolytic destruction of the solid phase of the low-basic phases is caused, first of all, by the break of the covalent bonds Si-O-Si, Me^{3+}-O-Me^{3+}, Si-O-Me^{3+} according to a scheme ≡Si-O-Si≡ ↔ [≡Si-O-Si≡]- ↔ ≡Si-OH + ≡Si-O- with protonization of the ion Me^{2+}-O bonds taking place in parallel, as it is known to happen in the high-basic systems [9].

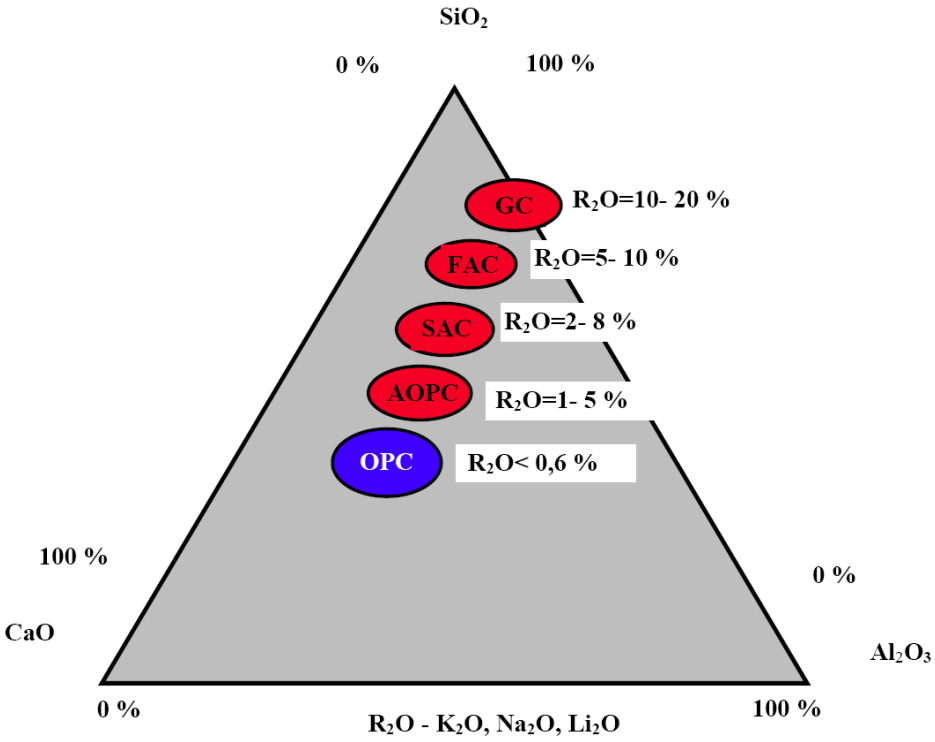

Fig. 1. Comparative chemical analysis of different types of OPC and AAC.

Abbreviations: **OPC**- ordinary Portland cement; **AOPC**- alkali- activated ordinary Portland cement; **SAC** -slag alkali- activated cement; **FAC**- ash alkali- activated cement; **GC**- geocement

An alkaline cation promoting flow of hydrolytic destruction of the low-active low-basic phases acts at early stages of structure formation as a catalyst of destruction. Then, as soon as the condensation processes evolve, it takes an active part as a co-partner of the Ca^{2+} and Mg^{2+} in the structure formation processes. This facilitates its modification due to the formation of the alkaline and alkaline-alkali-earth hydroaluminosilicates that are morphologically homogeneous to low-basic calcium- magnesium hydrosilicate phases.

At early stages of hydration and hardening (for example, of the slag alkali- activated cements), the structure formation is caused, chiefly, by the formation and crystallization of the low- basic hydrosilicates and hydrogarnets. The alkaline and alkali- earth hydro-aluminosilicates, as a result of their slower crystallization, occur at the later stages. Being formed, chiefly, in the pore space, they fill it and promote strong crystallization contacts with primary phases to occur, as well as initiate the formation of more homogeneous and dense structure.

Besides, high pH-values of the medium at which the hydration process takes place block a transfer of the Ca-ions into the solution, thus explaining the absence of $Ca(OH)_2$ and the fact that the resulted calcium hydrosilicate has, as a rule, a basicity exceeding 1.

6 Durability

Specific features of the mechanism of hydration and hardening of the alkali-activated cement determine formation of the more effective microstructure of the cement stone at different levels as compared with the Portland cement stone (Fig.2). This is also clearly seen from comparison of the data on solubility of new hydration products of the alkali-activated and Portland cement stone (Table 2). Specific features of the alkali-activated cement stone structure explain its higher durability (Table 3) compared to other cements.

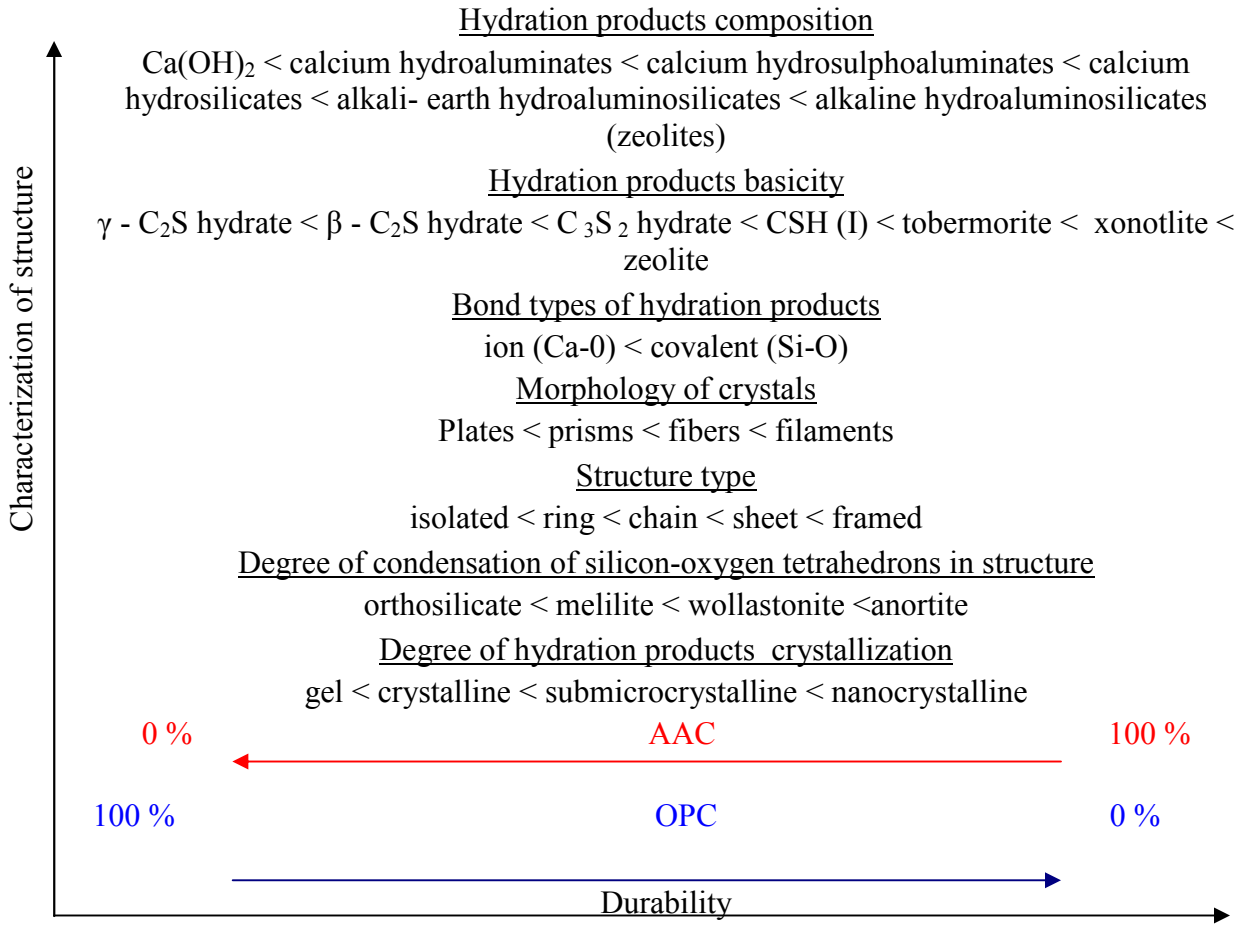

Fig. 2. Dependence between phase compositions of the hydration products, their structure and durability of the cement stone.

Table 2. Solubility of hydration products of the slag alkali- activated and portland cement stones.

Cement	Mineral	Stoichiometric formula	Solubility [kg/m^3]
Slag alkaline cement	CSH(B)	5CaO SiO_2 nH_2O	0.05
	Xonotlite	6CaO 6SiO_2 H_2O	0.035
	Riversideite	5CaO 6SiO_2 3H_2O	0.050
	Plombierite	5CaO 6SiO_2 10.5H_2O	0.05
	Gyrolite	2CaO 3SiO_2 2.5H_2O	0.051
	Calcite	$CaCO_3$	0.014
	Hydrogarnet	3CaO Al_2O_3 1.5SiO_3 3H_2O	0.02
	Na-Ca hydrosilicate	(Na,Ca) SiO_4 nH_2O	0.05
	Thomsonite	(Na,Ca) Si_2O_3 Al_2O_3 6H_2O	0.05
	Hydronepheline	Na_2O Al_2O_3 2SiO_2 2H_2O	0.02
	Natrolite	Na_2O Al_2O_3 3SiO_2 2H_2O	0.02
	Analcime	Na_2O Al_2O_3 4SiO_2 2H_2O	0.02
Portland cement	Calcium hydroxide	$Ca(OH)_2$	1.3
	C_2SH_2	2CaO SiO_2 nH_2O	1.4
	CSH(B)	5CaO 6SiO_2 nH_2O	0.05
	Tetracalcium hydroaluminate	4CaO Al_2O_3 13H_2O	1.08
	Tricalcium hydroaluminate	3CaO Al_2O_3 6H_2O	0.56
	Hydrosulphoaluminate	3CaO Al_2O_3 3$CaSO_4$ 31H_2O	high

Table 3. Properties of different cements.

Cement type	Early strength	Durability	Chemical resistance
Portland cement	++	++	+
Blended cement	+	+++	++
High alumina cement	+++	+	+++
High sulphate cement	+	++	+++
Alkali-activated cement	+++	+++	+++
Sulphoaluminate cement	+++	++	+++

7 Industrial uses

The experience from the small- and large scale industrial uses of the alkali- activated cements gained starting the 1960s in construction (hydropower engineering, road, agricultural, industrial, civil engineering, mining, etc.) gave proofs to high performance properties of the concretes on them. The use of the alkali- activated cement- based materials was found to be especially effective one for specially intended use in many fields besides construction [11].

Below are given some fields of the manufacture and use of the alkali- activated aluminosilicates (Table 4).

Table 4. Some examples of practical uses of the alkali- activated aluminosilicates.

2007		Heavy-duty road pavements Access roads and storage sites of chemical plants					
2000	Inorganic adhesives and glues, protective coatings against action of corrosive environments and high temperatures						
1990				Articles and structures from acid resistant concretes	High-rice building from precast- and cast-in-situ concrete		Compounds for radioactive waste immobili-zation Bodies of precise machine tools
1985				Floors, landings from cast-in-situ concrete	Blocks for buildings, garages, storage houses, etc.		Dies, moulds
1980				Articles and structures from hest resistant concretes	Floor slabs, foundation wall blocks, foundation blocks, piles	Oil well mortars and grouts	Linings of MD-pumps for aluminum melts.

1975		Road bases from strengthened soils					
1970	Tubings of anti-slide systems	Pavements from cast-in-situ concrete and precast reinforced concretes slabs	Pasture sites , storage sites for fertilizes, silo pits from cast-in-situ and precast concrete	Foundation blocks, floor slabs, columns, beams, foundation wall blocs, elements of cleaning-up systems		Reinforced pit props, sleepers	
1960	Sea breakwaters, elements of irrigation systems from cast-in-situ and precast prestressed concrete	Pedestrian way slabs, edges of pavement, landing field slabs					
	Hydraulic	**Road**	**Agricultural**	**Industrial**	**Residential**	**Mining**	
	Constructional engineering						**Non-constructi-onal engineering**

Over 50 years passed since the alkali- activated cements appeared in the field and their efficiency and potential have been proved by extensive researches held not only in the Soviet Union but in many countries over the world: Poland, Finland, The Netherlands, Germany, Czech Republic, Romania, Slovak Republic, Bulgaria, Japan, China, USA, Canada, India, Brazil, Spain, the UK. The experience collected for this period of commercial- scale manufacture and use of structures and articles made from slag alkali- activated cement concrete in various fields of construction testifies to their higher service properties as compared with those of Portland cement. These materials were found to be the most highly effective ones when used in extremely severe conditions as well as in non- civil engineering fields (Fig.3). Moreover, compared from traditional cements, the alkali-activated cements possess polyfunctional properties and can be successfully used as high strength, quick hardening, corrosion resistant, frost resistant, heat- and fire resistant and low exothermal cements [10].

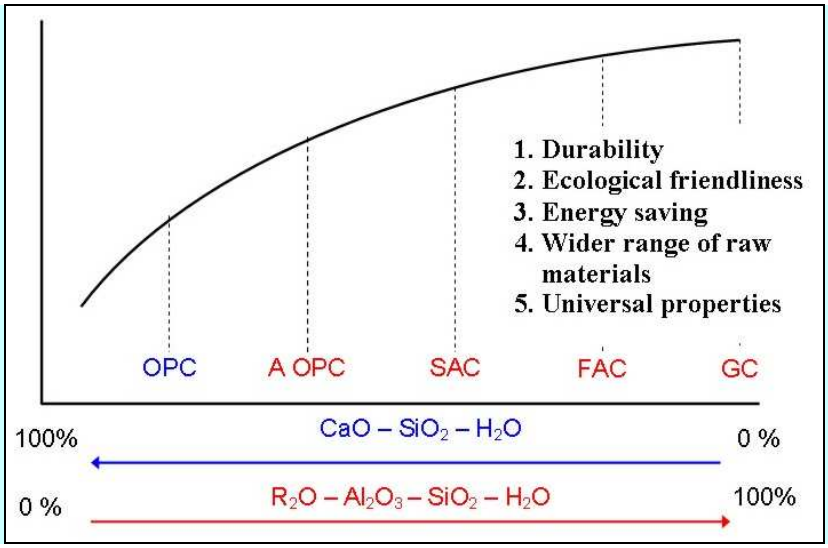

Fig. 3. Benefits of the AACs as compared to OPC-based cements.

More than 50 years practical experience of the Kiev school is connected with a manufacturing technology under which the alkaline activator was introduced into a concrete in a form of aqueous solution- so-called CONCRETE technology. Now there are two technologies, they are:

"CONCRETE" technology– under which all raw materials: aluminosilicate component, alkaline activator and modifying additives/admixtures are introduced in a dry form or in a form of solution during mixing concrete ingredients similar to conventional concrete technology.

"CEMENT" (ALL-IN-ONE) technology– under which all raw materials: aluminosilicate component, alkaline activator and modifying additives/admixtures are ground together and packed in bags for further use similar to other know-in-the-art cements for the use in concrete under traditional OPC- based concrete technology (Fig. 4). This scheme in general is given below. As to required equipment- *the best available techniques* (BET) can be successfully explored in it.

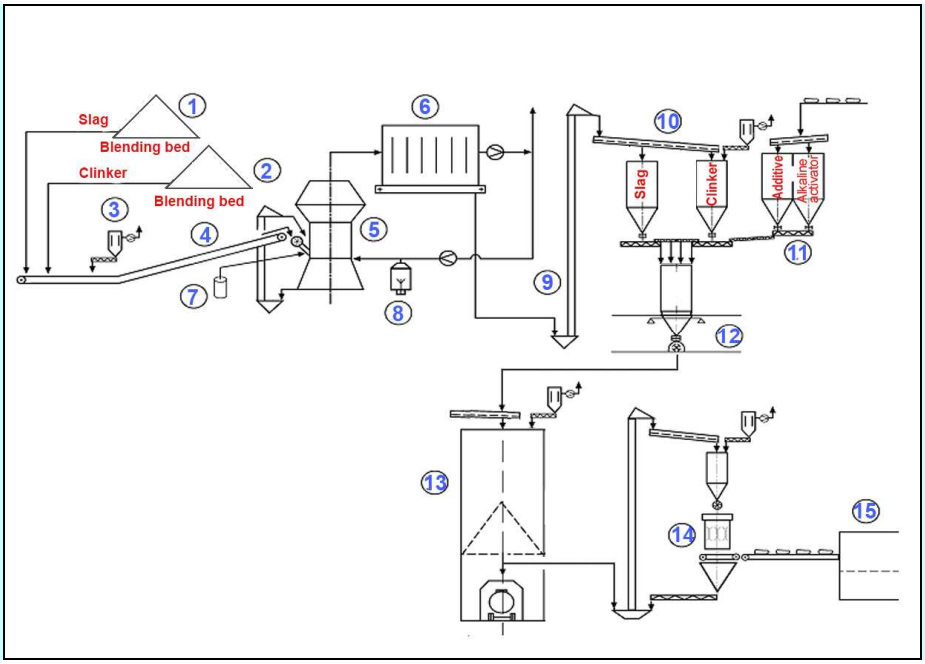

Fig. 4. "CEMENT" (ALL-IN-ONE) technology for the ACC manufacture. 1 – blending bed for slag, 2 – blending bed for clinker, 3 – dust collector, 4 – belt conveyer, 5 – vertical roller mill, 6 – fabric filter, 7 – metering equipment for water repellent, 8 – heat generator for drying, 9 – elevator, 10 – silos for cement constituents, 11 – bunker for additives/admixtures and alkaline activator, 12 – mixer for dry cement constituents, 13 – ready product storage silo, 14 – packer for bags, 15 – palletizer.

8 Standardisation and test procedures

In order to bring a newly delevoped product into a commercial-scale production it should pass all standardisation procedure according to national rules. In the former USSR, the commercialization of the ACCs was possible through its full- scale standardisation: a variety of national and industry standards have been issued. As a result, the AACs were officially approved by the governmental bodies of the USSR for the use in construction for all structures along with OPC (Fig.5).

Fig.5. The first residential house made from alkali- activated cement concrete (Lipetsk, Russian Federation).

The latest achievement in standardisation of the ACCs is a newly issued national standard of Ukraine covering some ACC types [11]. Similar to the EN-196, the standard specifies only strength classes and compressive strength after 2, 7 and 28 days. In substantial composition and strength at an age of 28 days the ACCs are classified as the following: slag alkaline cement, alkaline Portland cement, alkaline pozzolana cement, alkaline slag Portland cement, alkaline composite cement, which differ in combination of such aluminosilicate component as granulated blast furnace slag, OPC clinker, ashes from coal combustion, and basalt taken in combination with the alkaline activator (Table 5). Compressive strength classes under the standard are: 300, 400, 400R, 500, 500R, 600, 600R, 700, 800, 900, 1000. The standard is applicable to making concretes for common application.

Determination of mechanical and physical properties of the alkali- activated cements is carried out in compliance with DSTU B V 2.7-24-95 and ASTM C 109/C 109M. According to these standards a water to cement ratio (W/C) is chosen in order to provide a flow value (measured on cone) =106-115 mm. In case of using these test methods according to EN standards (EN 196-1, 196-3, and 196-6, under which the W/C is restricted to a value of 0.5), the following amendments should be introduced: in determination of flowability of the cement/sand mortar the alkaline solution/solid constituents or water/solid constituents ratio should be chosen experimentally in such a way that to provide the flow values between 160 – 180 mm.

Table 5. Cement types [11]

Cement type		Designation	Content, % by mass				
			Aluminosilicate constituent				Alkali metal compounds (sodium or potassium)
			Granulated blast-furnace slag	OPC clinker	Fly ash	Basalt	
ACEM I	Slag alkaline cement	ACEM I	90-100	0-10	-	-	1.5-12
	Slag alkaline cement with additive of fly ash	ACEM I -3	55-90	0-10	10-35	-	1.5-12
ACEM II	Alkaline portland cement	ACEM II	-	100	-	-	1.5-12
ACEM III	Alkaline pozzolana cement	ACEM III-3	←---------→		36-80	-	1.5-12
		ACEM III-B			-	36-80	
ACEM IV	Alkaline slag portland cement	ACEM IV	36-89	11-64	-	-	1.5-12
ACEM V	Alkaline composite cement	ACEM V	30-50	5-10	40-65	-	1.5-12

9 Conclusions

Now Ukraine has all normative documentation required for a large-scale application of the alkali-activated cementitious materials into practice of construction.

In order to bring this technology into a large-scale world-wide application, the RILEM Technical Committee "Alkali activated materials" was organized in 2007 [12]. Its tasks are:

- to collect and summarize the experience on raw materials; cements; concretes; structures; production; test procedures; durability; intended use.
- to develop basic recommendations "Preparation of performance-based specification for cast-in-place alkali-activated cements and concretes".

The results of this work will allow to develop and approve the national standards for the alkali-activated materials.

References

[1] V.D. Glukhovsky: Soil Silicates (Gruntosilikaty). Budivelnik Publish, Kiev, Ukraine (1967)
[2] J. Davidovich: U.S. Patent 3,950,470 (1976).
[3] Silicate Industry 9, 175 (1983)
[4] Lu Changgo: A new type of durable building material- FKJ, Concr. and Cem. Prod. 6 (1991)
[5] B. Forss: Proceeding of 6th Int. Conference on Alk. Concrete, Denmark (1983), p. 101
[6] R. Odler, J. Skalny, S. Brunauer: Proceeding of 6th Int. Congress on the Chemistry of Cements, Stroiizdat, Moscow (1983), p. 142
[7] P.V. Krivenko, Zh.V. Skurchinskaya: Int. Conference on the Utilization of Fly-Ash and Other Coal Combustion By-Products, Shanghai, China (1991), p. 142
[8] P.V. Krivenko: 10th Int. Congress on the Chemistry of Cements, 4iv046. Sweden, 2-6 June (1997)
[9] P.V. Krivenko: DSc (Eng)Dissertation. Kiev Polytechnic University, Ukraine (1986)
[10] C. Shi, P.V. Krivenko, D. Roy: Alkali-Activated Cement and Concretes. Taylor & Francis, London, New York (2006)
[11] National Standard of Ukraine DSTU B V.2.7-181: 2009 "Alkaline Cements"
[12] www.rilem.net

doi:10.4028/www.scientific.net/AST.69.11

Preparation and Stability of Alkali Activated Materials from Slag and Fly Ashes

BILEK Vlastimil

ZPSV a.s., Krizikova 68, 660 90 Brno, Czech Republic

e-mail: bilek@zpsv.cz

Keywords: Alkali-Activated Materials, slag, fly-ash,

Abstract. Alkali-activated concretes are relatively well-known composites. They show good mechanical properties, good resistance to the attack of a variety of chemical media and some other suitable properties. For their practical application various problems must be solved. In this paper some effects of the composition of the alkali activator and the composition of the binder on setting time, workability, efflorescence, leaching, strengths, shrinkage development, freezing and thawing resistance are studied with respect to a low price of the materials.

Introduction

Alkaline-Activated Materials (AAMs) are considered as materials with mechanical properties, good resistance to the attack of a variety of chemical media and with some other suitable properties [1]. The results are affected especially by the properties of slag and alkali-activator nature. To order to render AAM an interesting material for industry we state these basic conditions:

- concrete must be easily mixed – with a minimum amount of components. There are only usual compounds for the concrete production (slag, fly ash, aggregates, water) and only two new compounds (water glass and NaOH or KOH solution).
- concrete must be easily treated - it is designed as self compacting concrete (exceptionally also as very dry for vibro-pressed elements).
- concrete must bring some quality benefit – for example excellent durability
- concrete must be economically interesting – cheaper than normal concrete for the same purposes - the smallest possible amount of slag and activator is required.

All of these above mentioned requirements limit the development of alkali-activated concrete. At the same time the paper also discusses some problematic properties, such as the low early strength or low freezing and thawing resistance.

Materials

For the preparation of the AAM ground granulated blast furnace slag (GBFS), limestone and fly ashes were used whose composition is shown in Table 1.

Table 1: Chemical composition of used binders [%]

	SiO_2	CaO	Al_2O_3	Fe_2O_3	MgO	SO_3	Na_2O	K_2O	TiO_2
GBFS Stramberk	37.7	41.5	6.5	0.4	10.1	0.8	0.4	0.6	-
GBFS Ukraine	32.3	42.9	6.1	0.04	4.4	1.5	0.42	0.45	0.2
Limestone	0.9	54.1	0.5	0.2	0.3	0.07	-	-	-
Fly ash	49.7	3.6	24.9	14.7	1.15	1.26	0.6	1.9	1.4
Fine fly ash	52	5	26	6	-	-	-	-	-

Specific surface of slag Stramberk was 420 m^2/kg and for slag Ukaine 480 m^2/kg.
Sodium water-glass (M_s = 1.8) and 50% solutions of NaOH and KOH were used as activator.
For the preparation of mortars sand 0/4 mm was used and for concrete, besides sand, also crushed aggregates 4/8 and 8/16 mm were used.

Experimental details

Pastes and mortars were mixed in a laboratory mixer in volume maximum 1l. The workability of mortars was measured using the mini-cone flow (bottom base 100 mm, upper base 70 mm, height 60 mm). Specimens 40x40x160mm were used to determine strengths.
The efflorescence was investigated similarly as it says in the Czech norm for light concrete. In our modification the polystyrene cup was filled with mortar (bottom base 40 mm, upper base 70 mm, height 85 mm). At the age 1 - 3 days (after hardening) the cups were broken and the specimens – cone from the alkali-activated mortar - were placed into small PVC basins. Water was put into the basins reaching the height of 3 cm of the cones. The basin with the cones was left in laboratory conditions and watched for 28 days. The water was kept at the same level during 28 days. The efflorescence on the surface of the cones was observed and evaluated.

Concretes were prepared in a laboratory mixer, one batch represented maximum 35 l. After demoulding at the age of 1 day the specimens were stored in a wet room (r.h. > 95%) or they were wrapped in PE sheet to avoid of water exchange with environment. The workability of the concrete mixtures was evaluated similarly as in the case of usual self-compacting concrete – cone flow for overturned Abrams´ cone. Compressive strengths were measured using cubes 100mm. Beams 80x80x480 mm were also prepared for the measurement of fracture and other mechanical properties. Just before the tests, the beams were notched to 1/3 of their height in the distance of 220 mm from one of their ends. After the fracture test (performed with span S = 400 mm) two fragments of beams were obtained. The longer one ($l \approx 260$ mm) was used for bending strengths measurement (span S = 220 mm). Apart from the test of bending strengths (f_b) also the modulus of elasticity (E) and the modulus of rupture (f_r) was calculated, which is bending strength measured on notched beams (beams 80x80x480 mm). This characteristic reflects the properties of the central region of the beam. It is very sensitive to the occurrence of microcracks and it also reflects the sensitivity of material to the rise of crack growth. The main result of fracture tests is effective fracture toughness K_{IC} in accordance to Karihaloo and Nallathambi method, see [2].

Freezing and thawing resistance was measured in accordance to Czech norm CSN 731322. Testing beams (generally100x100x400mm) are frozen in a freezer where temperatures of -20^{o}C have to be maintained for 4 hours. After this time the beams are put into water +20^{o}C for 2 hours. This represents one cycle. For the most of field applications it is sufficient if the concrete sustains 100 cycles. During preliminary tests, 125 cycles are often required. To evaluate the concrete as frost resistant the freezing and thawing index *I* (ratio of *strength of frosted beams/strength of reference beams*) has to be higher than 0.75.

Results and discussion

Tests of pastes

Time of setting is one of most important technological properties of AAM. A course of setting depends on alkali activator nature and – naturally also on binder – slag – and mineral admixtures – limestone, fly ash,... The course of setting of GBFS is shown in Fig. 1.

There are two types of activator – activator based on sodium water glass and sodium hydroxide and activator based on sodium water glass and potassium hydroxide. It is evident that different compositions of alkali activator allow to reach different times of setting. A very quick setting was recorded for silicate modulus of activator M_s = 0.25 (80%$_{mass}$ of (Na_2O + K_2O) and 20%$_{mass}$ SiO_2) and also optimum setting for $M_s \approx 0.67$. In accordance to literature [3, 4] the setting can be explained by the rate of dissolution of slag (and admixture) and reaction product precipitation. Usually Ca^{2+} ions go into solution more quickly than Si ions. For this reason the setting of mixtures without water glass shows the slowest setting. In contrast, mixtures with high pH and a sufficient source of Si ions show quick setting.

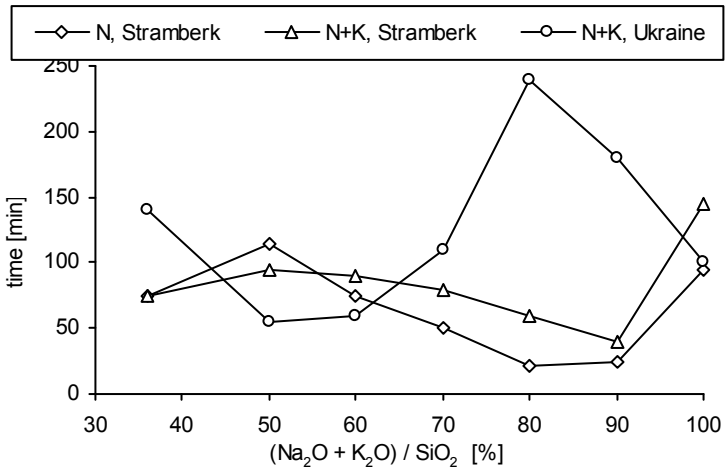

Figure 1: Course of setting of slag-alkaline pastes from different slags Stramberk and Ukraine and different composition of activator (N – only sodium ions (and silicon ions) are present in alkali activator, N+K sodium and potassium ions (and silicon ions) are present in activator

The courses of setting of mixtures with (slag + fly ash) or (slag + limestone) are shown in Fig 2.

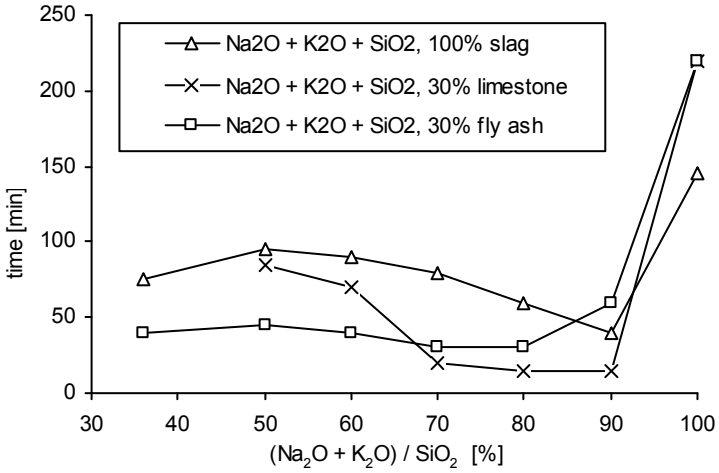

Figure 2: Course of setting of slag-alkaline pastes with different mineral admixture

Despite a different composition of the binder, the optimum composition of alkali activator is in a similar range (Ms ≈ 0.67), which agrees with other authors [3, 4]
The total content of activator also influences setting – the time of setting decreases together with the increase of alkali activator content.

Leaching of the pastes. Basic parameters of pastes used for the analysis of leach are recorded in Table 2. There is paste with sodium ions only, pastes with a combination of sodium and potassium ions in the activator and with various replacements of slag with fly ash and also paste with a lower content of the activator. Four months old pastes were grounded and the powder under 0.3 mm was leached in water. Contents of Na, K and Si are shown in Fig. 3.

Firstly, the comparison of pastes 10-450Na and 10-450 shows that the paste with a combination of sodium and potassium ions shows a significantly lower amount of alkalies (and silicon) in the solution. The content of alkalies in the solution increases as well as the amount of fly ash increases up to some content of fly ash (300g). In the last paste with a lower content of alkali activator, the content of elements in the solution is the lowest, but it is still higher than theoretically computed content in pastes with a higher content of activator in accordance to direct proportion (0.7 x content for 10% mixture). It means that in the poorest paste the leaching proceeds more intensively.

Table 2: Basic parameters of pastes composition

	10-450Na	10-450	10-350	10-300	10-250	7-300
Slag [g]	450	450	350	300	250	300
Fly ash [g]	0	0	100	150	200	150
$Na_2O+K_2O+SiO_2$	10%					7%
$(Na_2O+K_2O) / SiO_2$	60/40					

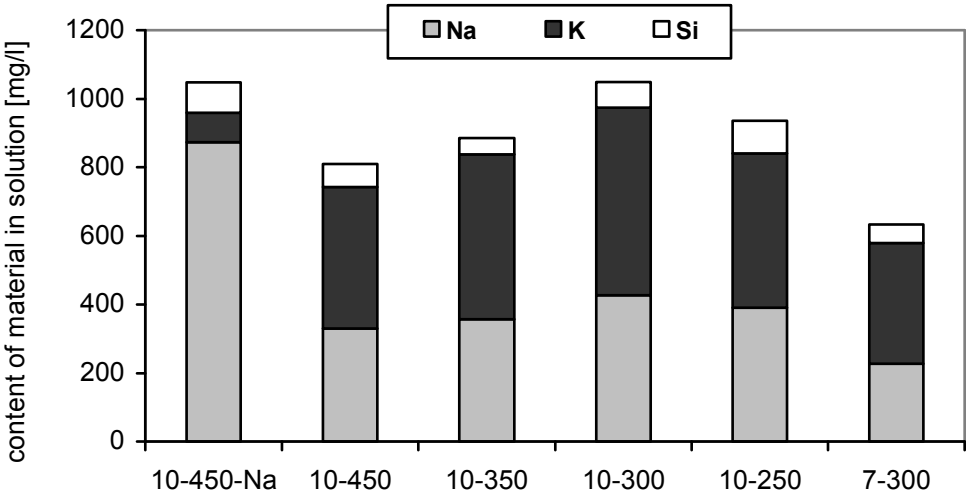

Figure 3: Content of some elements (Na, K and Si) leached from pastes

Tests of mortars

Workability of the mixtures. Alkali-activate mixtures show different workability than mixtures based on portland cement. They show higher plasticity of the mortars and concrete. Contrary to portland cement, it is not necessary to use superplasticizers in alkali-activated self-compacting mixtures. The superplasticizers act poorly - they reduce the strengths and increase the cost of mixtures. The enhancement of workability can be reached by an optimum composition of the mortar. There are two ways - replacement of part of sodium ions by potassium ions and replacement of the slag by appropriate mineral admixture. Both of these ways bring benefit in strengths and also in the reduction of shrinkage.

Efflorescence reduction. Alkali ions are necessary for high pH value of alkali activator and for the decomposition of slag (and admixtures). But later they are bound as a part of CSH gel (CSNH or CSKH gel), where they are only poorly bond or they pass over into pore solution. It means that these ions are tending to create efflorescence. This is one of the big problems of alkali activated materials.

Fig. 4 shows mortars with a different composition of activator. It is evident that presence of potassium ions reduces efflorescence [7, 8]. The reason is not quite clear. Probably, in accordance to [6], potassium ions are able to create a network better than sodium ions. There are probably also other reasons – for example a better bonding between hydrated potassium ions and the base, which is a consequence of (hydrated) ion- radius [9].

Na_2O [%]	100	83	76	17	0
K_2O [%]	0	17	24	83	100

Figure 4: Efflorescence reduction, (Na_2O+K_2O+SiO_2) = 8%, (Na_2O +K_2O)/SiO2=80/20

Strength of mortars is affected by the composition of alkali activator, the dosage of alkali ativator and water to cement ratio. Because the dosage of expensive alkali activator is pressed down and also the water/binder ratio is lowered, the composition of alkali activator can be the most important charasteristic which is possible to change.
Fig. 5 shows compressive strengths of mortars with a different composition of alkali activator and different dosage of the alkali activator. The water to slag ratio was kept at value 0.60, the dosage of slag was 450 g and the dosage of sand was 1450 to 1460.

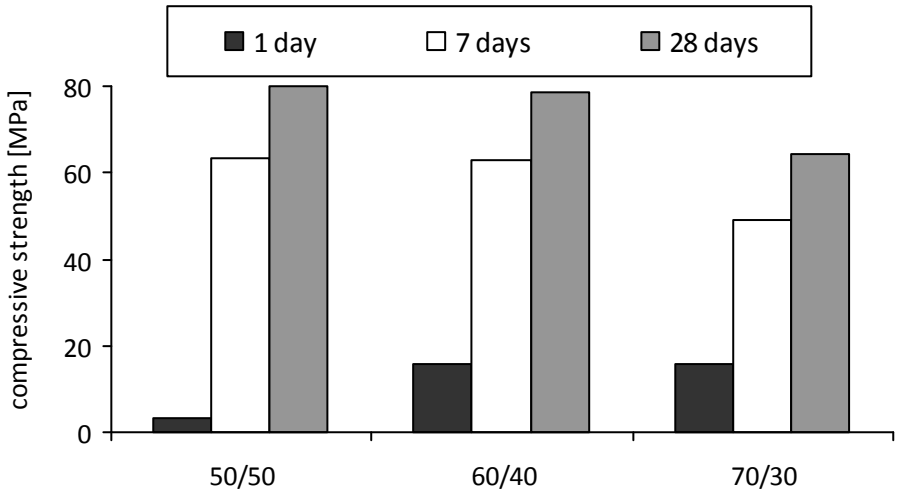

Figure 5: Strengths of alkali activated mortars with different composition of activator. The ratios express mass ratio in dry mass of activator

The strength development of slag-activated mortars with an increasing content of alkali activator is shown in figure 6. It is evident that the strengths increase just as activator content increases. Especially early strength is strongly affected by activator content. From this point of view the content of 12% of activator seems to be convenient.

A similar tendency can be observed also in case of mortars where 30 or 50% of slag was replaced with fly ash (see Fig. 7 and 8). In these cases the early strengths are significantly lower than in the case of mortars without the replacement of slag. Later, the strengths of mortars with 30% fly ash are very high - they are similar as in case of slag only.

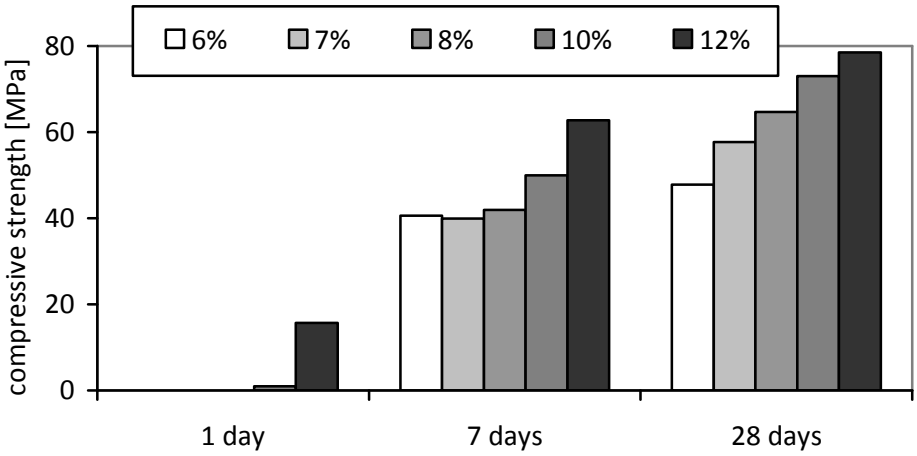

Figure 6: Strength development of alkali activated mortars with different dosage of activator

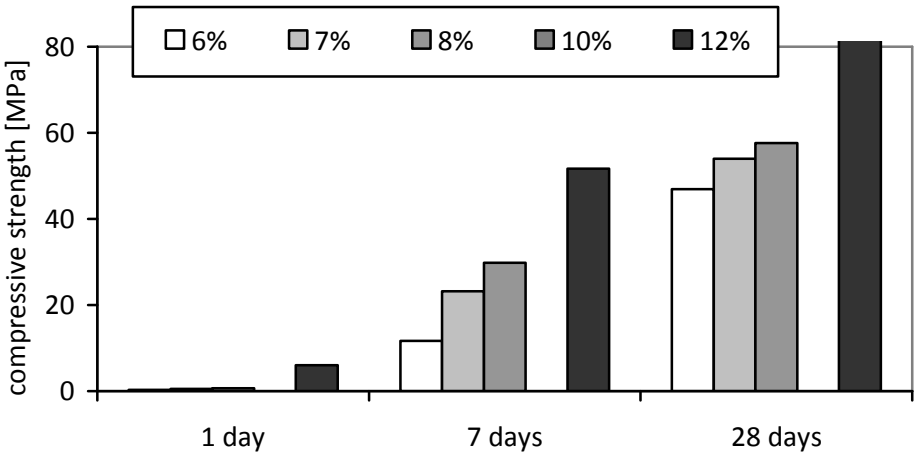

Figure 7: Strength of mortars with slag (67%) and fly ash (33%) with various dosage of activator

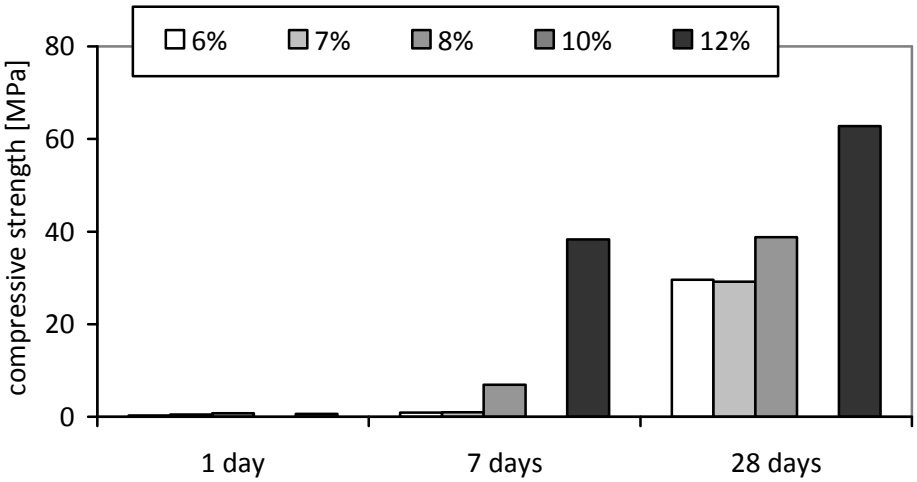

Figure 8: Strength of mortars with slag (50%) and fly ash (50%) with different dosage of activator

Tests of concrete

Concretes were designed as self compacting alkali-activated concretes. This required water/(slag + admixture) ratio ≈ 0.50. For the usual self-compacting concrete some superplasticizer is necessary for a better consistency. Alkali activated concretes show good workability for water/(slag +

admixture) ratio ≈ 0.52, especially if potassium ions are present in the activator and if some mineral admixtures (fly ash, limestone,...) are used. For aerated concrete air entraining admixture was used; the dosage of this admixture was 2 or 3 times higher than in the case of usual concrete and the air content was still very low. Composition of some chosen concretes is shown in the table 3.

Table 3: Composition of some chosen alkali activated concretes

		A	B	C	D	E	F	G
Slag (s)	[kg]	300	450	300	300	450	405	405
Fly ash (f.a.)	[kg]	150	-	150	150	-	-	-
MK	[kg]	-	-	-	-	-	45	-
f.f.a.	[kg]	-	-	-	-	-	-	45
w / (s + f.a.)		0.52	0.52	0.52	0.52	0.52	0.52	0.52
K_2O/(s + f.a.)	[%]	4.2	4.2	0	3.26	3.72	3.72	3.72
$Na_2O+K_2O+SiO_2$/(s + f.a.)	[%]	8	8	11	11	10	10	10
(Na_2O + K_2O)/SiO_2	[%]	70/30	70/30	50/50	50/50	60/40	60/40	60/40
Air content	[%]	-	-	-	-	2.5	-	-
Cone flow	[mm]	660	545	590	670	660	545	590
Cost	[EUR]	65	75	59	65	77	87	87

The **strength development** of concrete is shown in Fig. 9.

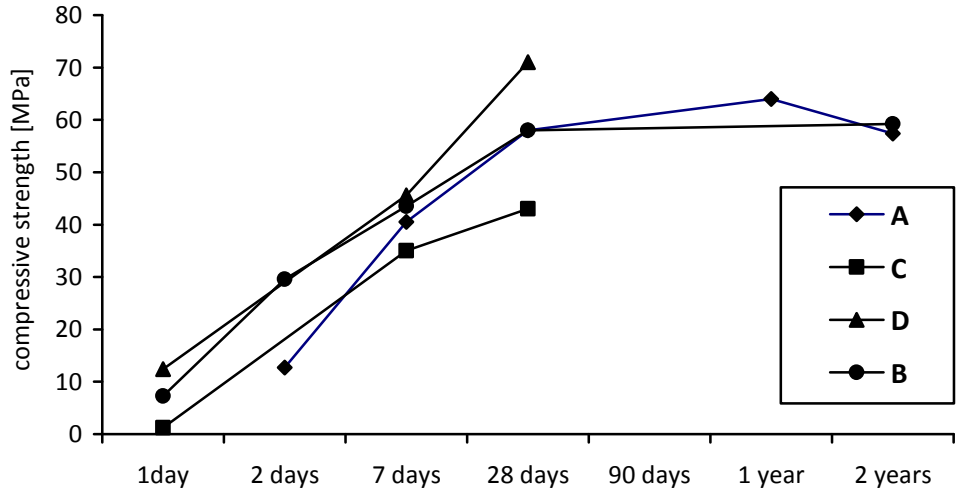

Figure 9: Long term development of compressive strengths, cubes were wrapped in foil

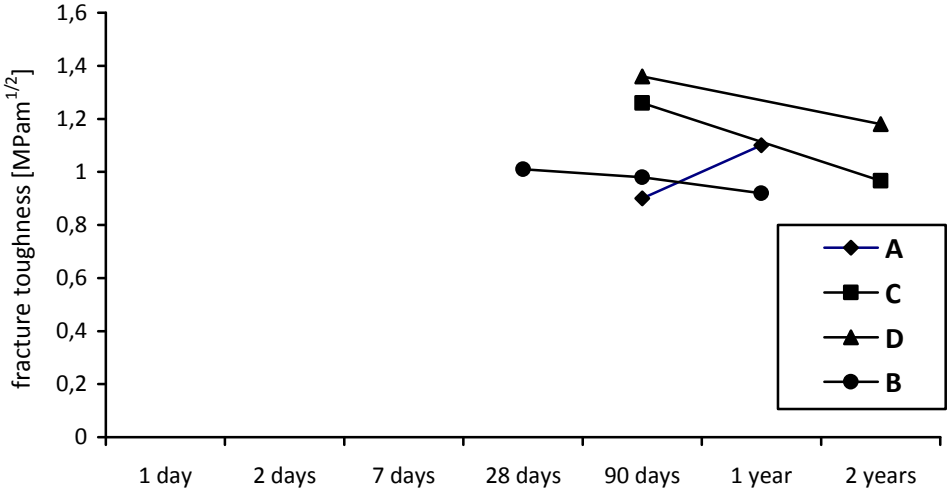

Figure 10: Long term development of fracture toughness, beams were wrapped in foil

The strengths of concretes increase with the increase of alkali activator content. The presence of potassium ions in the activator enhances the strengths of concretes (see concretes C and D). The influence of fly ash or other admixtures is not very important for the development of strengths except for early strengths (see concretes A and B and E-G)

A **long-term development** of mechanical properties brings some interesting results. A reduction of compressive strengths between 1 and 2 year was detected (concrete A). Also, a reduction of fracture toughness was recorded – see Fig. 10. Probably, the development of microcracks which arise as a consequence of shrinkage can be a reason for the fracture toughness reduction. It is also sometimes observed in OPC based concretes, especially with a bigger maximum size of aggregates [10]. Because the shrinkage of alkali activated concretes is bigger than that of OPC based concrete, the formation of microcracks can be detected earlier.

Autogenous shrinkage of alkali activated concretes is shown in figure 11. One day was chosen as the start of measurement. Shrinkage before this was also measured, but it was very small. It is obvious that convenient fly ash is able to reduce the autogenous shrinkage (see concretes A and B). This is a very important result.

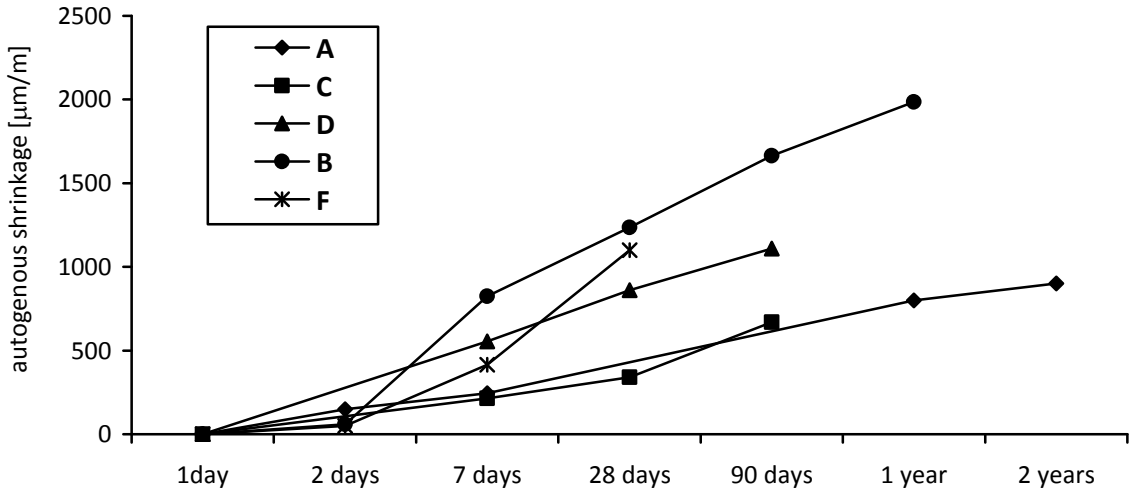

Figure 11: Autogenous shrinkage of alkali activated concretes

Freezing and thawing resistance of alkali-activated concrete. Alkali-activated concretes are generally considered as frost resistant. This phenomenon is explained by a number of aspects [1].

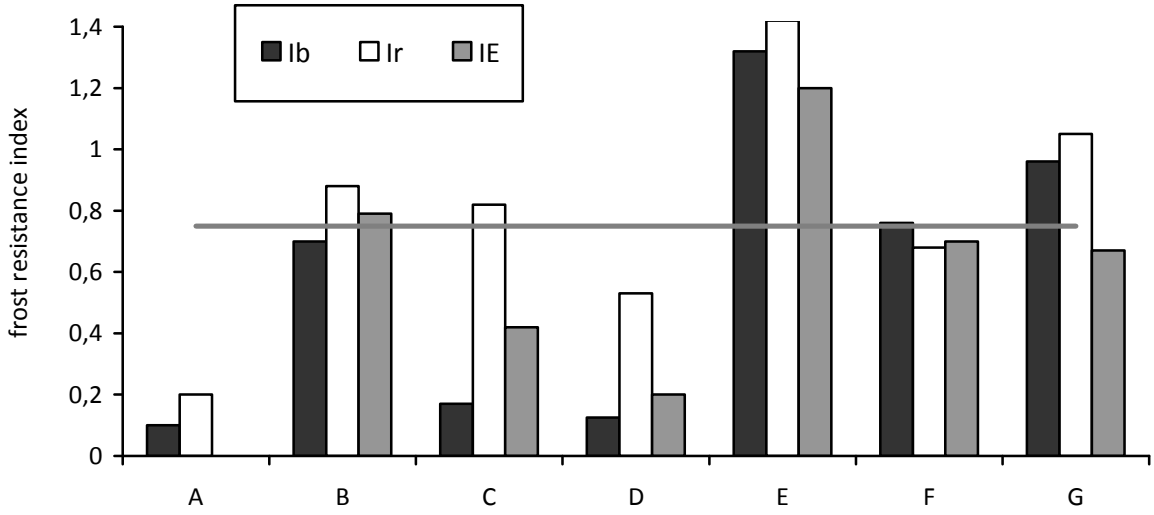

Figure 12: Indexes of frost resistance in terms of bending strength f_b, modulus of rupture f_r and modulus of elasticity E. The line represents frost resistance limit – 0.75

But our results [11] show that the freezing and thawing resistance is not as excellent. Two ways of enhancing of frost resistance were found: 1) the use of a big amount of alkali activator or 2) air-entraining of concrete. The second way is more convenient. The results presented in Fig. 12 show that a small amount of entrained air enhances the freezing and thawing resistance. The application of some mineral admixtures which is very effective in enhancing the frost resistance of usual concrete (metakaoline [12]) doesn´t work in the case of alkali activated concrete.

Comparing the values of indexes of freezing of thawing resistance for bending strength f_b, modulus of rupture f_r and modulus of elasticity E, one can see that the index for modulus of rupture reaches to highest values. This can be interpreted as a consequence of better properties of concrete in the central region of the beams. The failure of the beams starts from the surface of the specimens.

Conclusions

On the basis of the tests of pastes and mortars and on the basis of concrete testing some rules for designing of alkali activated self compacting concrete were specified:

It is convenient to use a combination of sodium water glass and potassium hydroxide in an optimum ratio (optimum time of setting, better workability, efflorescence and leaching reduction). It is also convenient to replace a part of the slag with a convenient fly ash (cost reduction, better workability, reduction of shrinkage). For the production of frost resistant concrete the air entraining of concrete is also necessary. Unfortunately, low early strengths problem persists – only one solution was found – an increase of alkali activator dosage.

Acknowledgement

This work was supported by Ministry of Education, Youth and Sport of Czech Republic, Project No: 2B08024

References

[1] Shi, C., Krivenko, P.V., Roy, D.: Alkali-Activated Cements and Concretes, Taylor & Francis 2006, ISBN I 0: 0-415-70004-3

[2] Karihaloo, B.L.: Fracture mechanics of concrete, Longman Scientific & Technical, New York, 1995

[3] Krizan, D., Zivanovic, B.: Effects of dosage and modulus of water glass on early hydration of alkali-slag cements,Cem.Concr.Res.,Vol.32 (2002), pp.1181 – 1188

[4] Granizo, M.L., Alonso, S., Blanco-Varela, M.T., Palomo, A.: Alkaline activation of Metakaolin: Effect of Calcium Hydroxide in the Product of Reaction, J.Am. Ceram. Soc., 85 (2002) [1], pp. 225-231

[5] Xu, H., Van Deventer, J.S.J.: The geopolymerisation of alumo-silicate minerals, Int. J. Miner. Process. 59 (2000) 247-266

[6] Yip, C.K., Lukey, G.C., Provis, J.L., van Deventer, J.S.J.: Effect of calcium silicate source on Geopolymerisation, Cem Concr. Res. 38 (2008) 554-564

[7] Bilek, V., Urbanova, M., Brus, J., Kolousek, D. 2007. Alkali-Activated Slag Concrete development and their practical use, 12th International Congress on the Chemistry of Cement, J.J.Beaudoin, J.M.Makar and L.Raki Eds., Montreal, Canada, T3-06.6

[8] Szklorzova H., Bilek V.: „Influence of alkali ions in the activator on the performance of alkali activated mortars“, Proc. of 3th Non-Traditional Cement and Concrete Symposium, Bilek and Kersner Eds., Brno, Czech Republic, 2008 ISBN 978-80-214-3642-8, pp. 777 – 784

[9] Kolousek, D., Hajek, P.: personal communication

[10] Bilek., V.: Investigation of Long-Term Mechanical Properties of High Strength Concrete, 6th CANMET/ACI Int. Conf. On Durability of Concrete, Thessaloniky, Greece, Suplementary volume, pp.195-210

[11] Bilek, V., Szklorzova, H.: Freezing and thawing resistance of alkali-activated concretes for the production of building elements, in V.M.Malhotra (Eds) Proceedings of 10th CANMET/ACI Conference on Recent Advances in Concrete Technology, Sevilla, 2009, Supplementary papers, pp. 661-670

[12] Bilek, V., Szklorzova, H.: Influence of metakaoline on enhancing freezing and thawing resistance of concrete, workshop Metakaolin 2009, Brno Technical University, Brno, 2009

doi:10.4028/www.scientific.net/AST.69.21

Recent Development of Magnesium-based Cements - Magnesium Phosphate Cement and Magnesium Oxychloride Cement

Zongjin Li[1, a], Fei Qiao[1, b], and Chung Kong Chau[1, c]

[1]Department of Civil and Environmental Engineering, The Hong Kong University of Science and Technology, Hong Kong, China

[a]zongjin@ust.hk, [b]qiaofei@ust.hk, [c]garrison@ust.hk

Keywords: magnesium oxychloride cement, magnesium phosphate cement, formulation, strength, microstructure, drying shrinkage

Abstract. The recent development of two types of environmental friendly cementitious materials, magnesium oxychloride cement and magnesium phosphate cement, at HKUST are presented. Both of them can develop high strength without heat treatment under elevated temperature, i.e. the bonding of these cementitious materials can be achieved at low temperature through chemical reaction, as opposed to fusion or sintering at high temperature. The preparation process of the two cements can not only save a lot of energy but also emit no carbon dioxide. For magnesium oxychloride cement, our research includes parametric study of the formulation, strength development, water resistance, and also identification of phase composition in the cement paste. Magnesium phosphate cement is mainly applied as rapid repair material in civil engineering. In this paper, the formulation, mechanical properties and performance in patch repair of mortar specimen including strength, bond ability to old concrete substrate, volume stability are studied.

Introduction

The production of Portland cement in the world, especially in many developing countries, is being continuously increased during recent years. For example, the annual output of Portland cement in China reached 1.38 billion tons in 2008, which is 5.2% higher than the product in 2007. The production of one ton of Portland cement generates approximately one ton of carbon dioxide and requires up to 7000 MJ of electrical power and fuel energy. It is evident that the continue rising of cement production would result in serious impacts on energy, resource and environment pollution. Therefore, the use of by-products and wastes to produce cementitious materials with less energy consumption and less waste generation has aroused worldwide concerns and interests [1]. In this paper, two kinds of environmental friendly materials, magnesium oxychloride cement (MOC) and magnesium phosphate cement (MPC), will be introduced and discussed. The bonding of these cementitious materials can be achieved at room temperature through chemical reaction, as opposed to fusion or sintering at high temperature. Therefore, the preparation process of the two cements can not only save a lot of energy but also emit no carbon dioxide.

MOC cement, also known as Sorel cement, is formed by mixing powdered light burnt magnesia (usually calcined at 700-900˚C) with concentrated solution of magnesium chloride ($MgCl_2$). As one of the main representatives of chemically bonded cement, MOC has properties superior to the ordinary Portland cement. It does not need wet curing; has high fire resistance, low thermal conductivity, and good resistance to abrasion as well as chemicals. The rapid setting and hardening properties as well as the excellent bonding ability to large amounts of different fillers such as gravel, sand, marble flour, asbestos, wood, and expanded clays, make MOC an attractive inorganic cement. The four main crystalline phase in the MOC system are $2Mg(OH)_2 \cdot MgCl_2 \cdot 4H_2O$ (Phase 2), $3Mg(OH)_2 \cdot MgCl_2 \cdot 8H_2O$ (Phase 3), $5Mg(OH)_2 \cdot MgCl_2 \cdot 8H_2O$ (Phase 5), and $9Mg(OH)_2 \cdot MgCl_2 \cdot 8H_2O$ (Phase 9) [2]. The well crystallized needle-shaped Phase 5 of MOC cement has been described as scroll-tubular whiskers [3]. The mechanical interlocking and dense microstructure resulting from the intergrowth of these whiskers is a major source for strength

development of MOC cement [4]. One major problem of MOC is the poor water resistance. The strength of hardened MOC paste would be sharply decreased after immersing in water for some time, which evidently limits the engineering application of this material. Until now, the most efficient method to improve the water resistance of MOC is addition of soluble phosphorous compound, such as phosphoric acid, the phosphates of alkali metals, alkali earth metals, iron, aluminum, and phosphates of ammonia. Even a small amount of these compounds can improve the water resistance of MOC significantly.

Magnesium phosphate cement (MPC) is based on the chemical reaction of an aqueous acidic phosphate solution with dead burned magnesia powder [5-7]. On mixing, acid-base reactions lead to the formation of insoluble magnesium phosphate hydrates, which constitute the binding phase in the hardened cement. It usually sets very fast at room temperature and produces a high early strength, low permeability patch with good durability [8-10]. Therefore, such materials have found applications as casting investment in dentistry, in the rapid repair of concrete pavements, and stabilization of toxic and radioactive waste. Since the reaction process of MPC formation is accompanied with strong heat release, MPC based construction products are therefore promoted for application in cold weather. When ammonium dihydrogen phosphate (ADP) is used as acid component, it has been shown by X-ray powder diffraction that the principle reaction products formed is magnesium ammonium phosphate hexahydrate ($MgNH_4PO_4 \cdot 6H_2O$), also known as mineral struvite. Two other reaction products, $(NH_4)_2Mg(HPO_4)_2 \cdot 4H_2O$ (schertelite) and $MgNH_4PO_4 \cdot H_2O$ (dittmarite), may also be present in the system either when the water content used is insufficient to ensure complete reaction of the available ADP or when the heat evolved on setting caused the evaporation of a substantial proportion of the water present.

In the recent years, it is found that mono-potassium phosphate is a good candidate for replacing ammonium phosphate to eliminate the ammonia emitted during processing and storage. In addition, potassium dihydrogen phosphate (KDP) has a lower dissociation constant and lower molar solubility thus reduce the reaction rate [11]. It is interesting that when potassium phosphate is used, the reaction product is invariably magnesium potassium phosphate hexahydrate, $MgKPO_4 \cdot 6H_2O$ (MKP) which binds the aggregates into a uniform mass. The main reaction equation is shown below:

$$MgO + KH_2PO_4 + 5H_2O \rightarrow MgKPO_4 \cdot 6H_2O \quad (1)$$

Previous works [12-16] on MPC paste prepared with KDP indicate that the properties of MPC paste are mainly affected by the reactivity of magnesia, molar ratio of magnesium to phosphate (M/P), as well as borax and water content. Those findings reveal that MPC prepared with KDP also exhibits fast setting and healthy strength development. Besides the mechanical properties, the bond to substrate concrete and shrinkage behavior of the repair material are essential for application in structure rehabilitation. However, little work has been reported on these issues.

Summary of MOC

Formulation of MOC cement. The basic requirements for obtaining high performance MOC cement are to ensure the production of phase 5, minimize of unreacted $MgCl_2$ content, and obtain a reasonable workability with an appropriate setting time. Theoretically speaking, phase 5 can be obtained from a molar ratio of $MgO/MgCl_2$ of 5 along with stoichiometric water. Nevertheless, the correct or theoretical proportions of the starting materials alone are not sufficient to ensure the formation of phase 5 cystals, since the chemical reactions in the MgO - $MgCl_2$ - H_2O system is not complete and many unreacted MgO are expected to left in the final reaction products. Therefore, the formulation of MOC should be optimized to obtain the highest strength.

The strength developments of MOC paste after air curing for 7 days with a wide range of molar ratios of $MgO/MgCl_2$ and $H_2O/MgCl_2$ are presented in Fig. 1. “Hxx” means the molar ratio of $H_2O/MgCl_2$. It shows that with a fixed molar ratio of $MgO/MgCl_2$, the strength is increased with the decrease of the molar ratio of $H_2O/MgCl_2$. Besides, with a fixed molar ratio of $H_2O/MgCl_2$, the

higher the $MgO/MgCl_2$ ratio, the higher the strength. The highest strength is 150 MPa for the mixture M13/H12 ($MgO/MgCl_2$ ratio of 13 and $H_2O/MgCl_2$ of 12). The X-ray diffractograms shown in Fig. 2 give the assemblages of the reaction products for several mixtures. It can be seen that the mixture M13/H12 has the sharpest peaks of phase 5 and the lowest amorphous base as compared to others. As expected, the MgO content of this mixture is in excess and residual MgO is found. More phase 3 is found for the mixtures with a molar ratio of $MgO/MgCl_2$ lower than 11 and $Mg(OH)_2$ phase can be dominant if the $MgO/MgCl_2$ ratio is higher than 17. Therefore, it is recommended the optimal application ranges of the molar ratios for the ternary system of MOC cement are $MgO/MgCl_2$ from 11 to 17, and $H_2O/MgCl_2$ from 12 to 18. The choose of $H_2O/MgCl_2$ is, however, largely dependent on the ratio of $MgO/MgCl_2$ as excess water is required for desired workability.

Microstructure of MOC cement. The well crystallized phases 5 of MOC has been described as scroll-tubular whiskers [3]. However, sporadic evidences of the acicular crystals of MOC phases [4, 17, 18] without enough and consistent details have befuddled researchers in the microstructural studies of MOC cement. In our study, with modern technology and powerful computational capability, more detailed and clarified microstructure of MOC crystalline phases including morphology, crystal habit, grain size, and elemental composition can be revealed.

The typical morphologies and microstructures of fractured surfaces of the selected sample #1 (dominated with phase 3 through XRD examination) and sample #2 (largely with phase 5) are shown in Fig. 3 (a) and (b), respectively. It can be seen that the crystals of mixture #1 are generally in prismatic, spindle and bundled shape but poorly formed and distorted. With a rough surface of granular grains, the crystal aggregation exhibit a variety of shapes and sizes: thin or stout, short or long, straight or arcuate, and prismatic or tabular. As compared to mixture #1, the microstructure of the mixture #2 is more homogenous, and with interlaced needle shaped crystals. The crystals of the phase 5 are largely intergrowth with bundled shape that even spiral bundle can be observed. The interlaced needle shaped crystals and the resulting mechanical interlocking is believed to be responsible for the strength development of MOC cement [3-4].

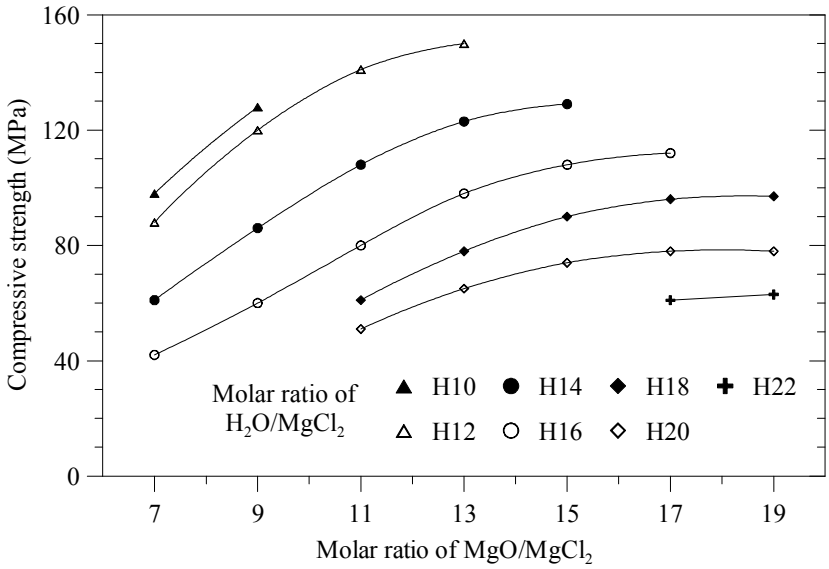

Fig. 1 – Compressive strengths of different mixtures after air curing of 7 days

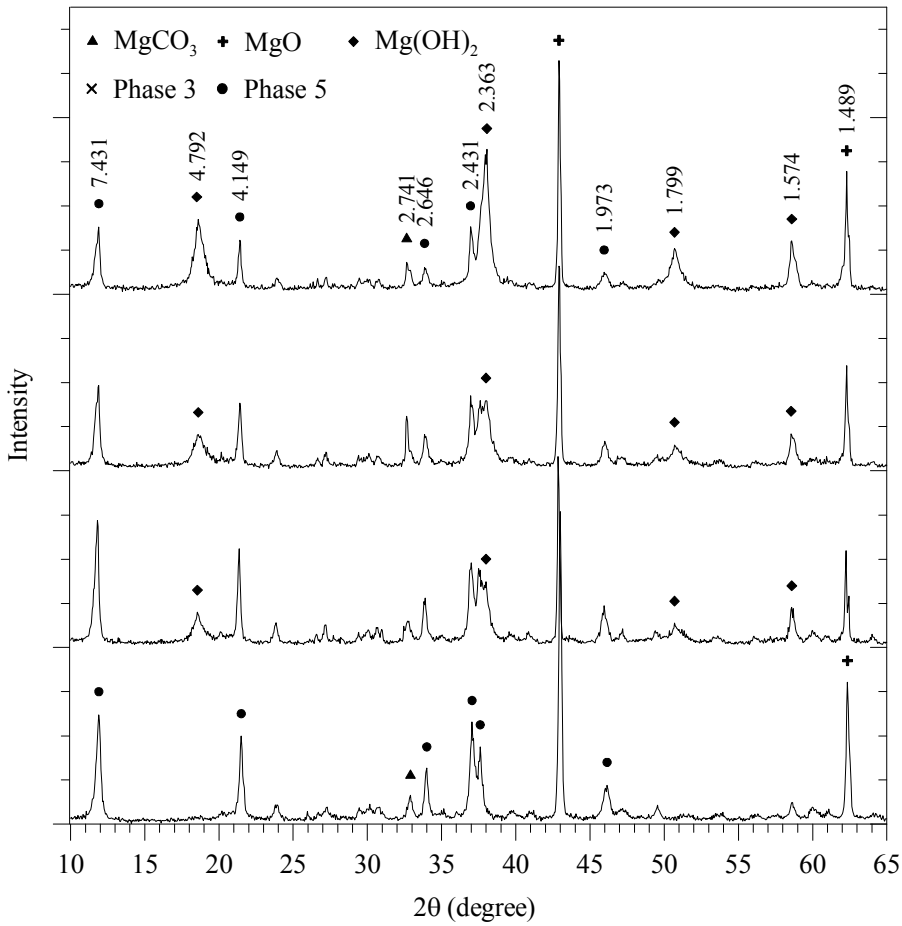

Fig. 2 – XRD patterns of the mixtures (from bottom to top): M13/H12, M13/H16, M17/H16, and M19/H22

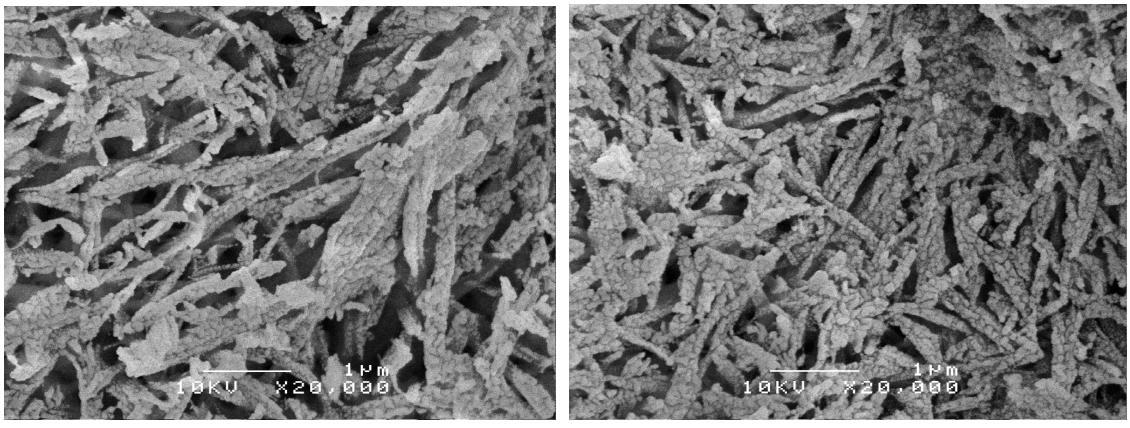

(a) (b)

Fig. 3 – Microstructure of mixture #1 (a) and #2 (b).

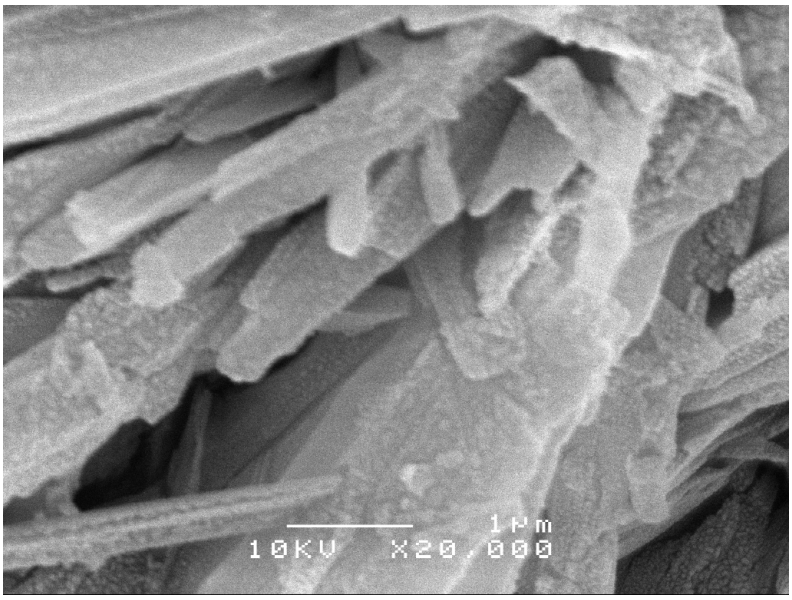

Fig. 4 – Bulky crystalline platelets found from the mixture M7.8/H20

As mentioned in the formulation study, $Mg(OH)_2$ phase can be dominant if the $MgO/MgCl_2$ ratio is higher than 17. The microstructure of the corresponding sample rich with brucite is shown in Fig. 4. It can be seen that the crystals are immense, slender, flattened and blade-like in layered structure, which is very different from those bundled needle shaped crystals shown in the previous figures.

Besides of the phase identification by XRD and observation under SEM, the crystalline phases in MOC paste were further identified by EDS spectra. The measured atomic percentage of the elements from the area scans of the aforementioned 3 mixtures are compared to the theoretically calculated ones of the phase 3, phase 5 and brucite as listed in Table 1. It can be seen that the measured values of the three mixtures show reasonable agreement with the theoretical ones. The insignificant amount of chloride ion detected from the area scan on the brucite crystals may come from the surrounding and background MOC matrix. In general, the amount of measured Mg is higher than the theoretical ones as a significant amount of MgO residual is expected to be existent as the rate of consumption of the MgO powder would not be complete during the chemical reactions.

Table 1. Atomic percentage of the different crystalline phases

MOC phase		Atomic percentage† (%)		
		Mg	O	Cl
Phase 3 – $Mg_2(OH)_3Cl{\cdot}4H_2O$	t	20.0	70.0	10.0
M3.6/H10 (Figure 3a)	m	25.4	66.1	08.5
Phase 5 – $Mg_3(OH)_5Cl{\cdot}4H_2O$	t	23.1	69.2	07.7
M4.7/H14 (Figure 3b)	m	29.3	63.9	06.8
Brucite – $Mg(OH)_2$	t	33.3	66.7	00.0
M7.8/H20 (Figure 4)	m	37.4	60.3	02.3

† - the hydrogen element is not included in the calculation
t - values from theoretical calculation
m - values from the measurements

Influence of fly ash on the water resistance and drying shrinkage of MOC cement. The results of the water resistance as plotted in Fig. 5 exhibit that the water resistance of the MOC mortars would be dramatically boosted when appropriate amount of fly ash is utilized. For the MOC mortar incorporated with fly ash of 30% by weight of MgO, the strength retention coefficient is raised from merely 40% up to about 80% when compared to the reference strength at 14-day air curing (A14). The improvement of the water resistance of the MOC mortars with fly ash incorporation may be due to the amorphous alumino-silicate gel formed by the pozzolanic reaction of the reactive SiO_2 and Al_2O_3 contents of fly ash under the alkaline condition of MOC system. The drying shrinkage test demonstrates that the MOC mortars are in general expansive and most of the expansion taking place in the first week after casting. Besides, it is believed that the expansion of the mortars may only come from the MOC matrix. The fly ash incorporation reduces amount of expansion and the more amount incorporated, the more the deduction as shown in Fig. 6. A slightly expansive nature of the MOC mortars is favorable for being a repair mortar to avoid crack and premature failure due to drying shrinkage.

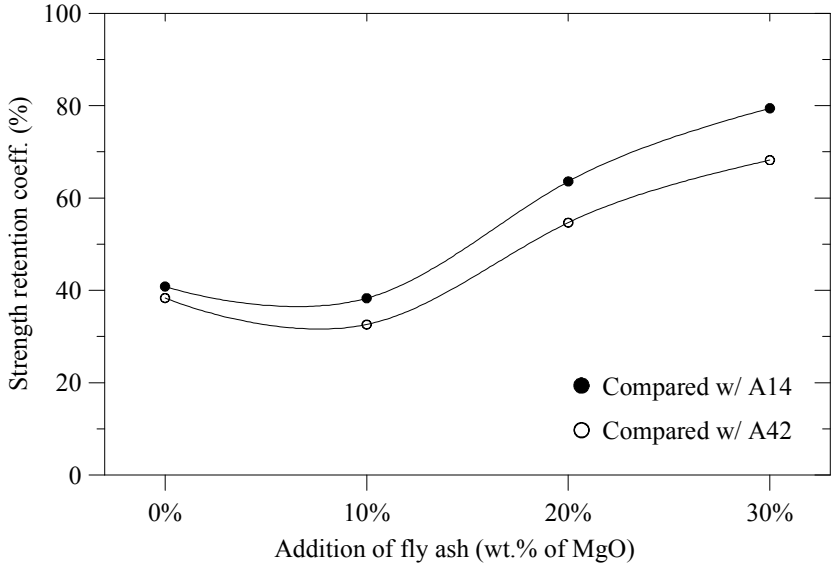

Fig. 5 – Influence of fly ash on the water resistance of MOC mortar

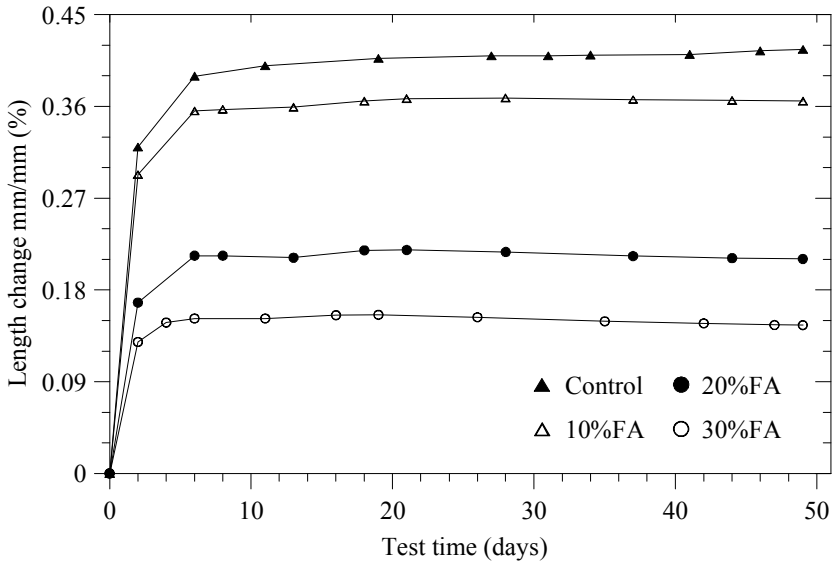

Fig. 6 – Influence of fly ash on drying shrinkage of MOC cement

Summary of MPC

Bond strength with Portland cement concrete substrate. In this study, two kinds of tests were employed to evaluate the bond strength between the MPC repair mortar and the substrate OPC mortar or concrete. One was defined as flexural bond strength, which was a kind of indirect bond test and conducted by four-point bending. The specimen for flexural bond test was a beam made by half of OPC and half of MPC mortar. The other bond test defined as tensile bond strength was carried out by pull-off method according to BS 1881-207:1992. Disk specimens with diameter of 75mm and height of 15mm were cast on the roughed surface of OPC concrete and the bond strength was calculated by dividing the maximum force by the bond area.

The results of the flexural bond strength test are shown in Fig. 7. The results indicate that the bond strength of MPC with OPC mortar is not sensitive to M/P ratio at early stage but at late stage the lower M/P ratio leads to a higher bond strength. Compared with the OPC repaired specimen, MPC shows prominent bond strength which is 77-120% higher than that of OPC mortar at 28d. After the failure of specimen, it is found that the MPC repaired samples always break in MPC mortar before 7d and fail in OPC mortar at 28d while the OPC repaired specimens fail at the interface all the time. The results combined with the flexural strength of OPC at 28d and MPC demonstrate that at early stage, since the MPC repair mortar has not been matured completely, the flexural strength decreases in the order: OPC mortar > bond > MPC. While at 28d, the flexural strength of MPC is maturely developed and over than that of OPC, the flexural strength decreases in the order: MPC mortar > bond > OPC. The bond failure of OPC repaired specimen indicates the OPC mortar has poor bonding with itself.

It can be seen from Fig. 8 that pull-off test provides more conservative value than flexural test but the results are in agreement well with each other. Similar with the results in flexural test, all of MPC repaired samples have obviously higher bond strength than OPC repaired specimen. Since the bond strengths at M/P of 6 and 8 are very close and notably higher than that at M/P of 10 and 12, it is believed that the pull-off strength may not be improved. But if the M/P ratio is further decreased the cost of the repair material would be increased much due to higher cost of KDP.

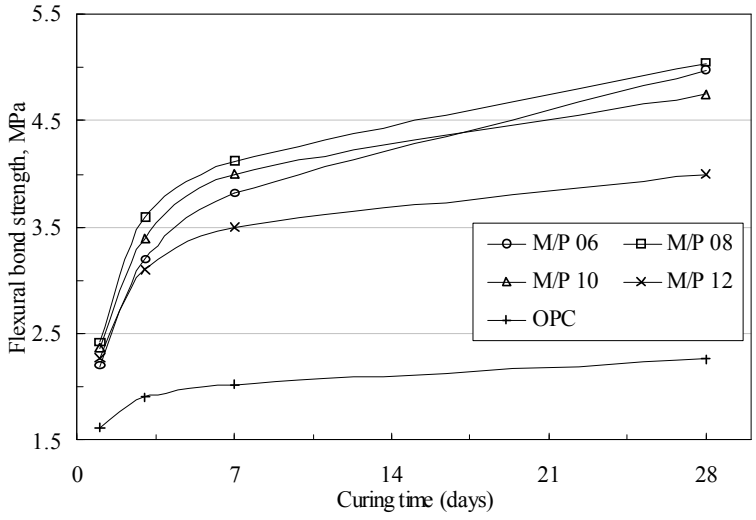

Fig. 7 – Flexural bond strength of MPC mortar with different M/P ratios

It is well accepted that the adhesion of the repair material to the old OPC interface is dependent on material compaction, moisture content of repair surface and roughness of interface. It is believed there should exist some chemical interlock between MPC and OPC substrate that improve the bond performance of MPC. For a small M/P ratio, the more hydrates is available to lubricate the mortar. At the same roughness of interface, the specimen with the better fluidity and sufficient paste to wet the interface would achieve the better adhesion to substrate. This is why the specimen with lower M/P has higher bond strength in both the flexural and pull-off tests.

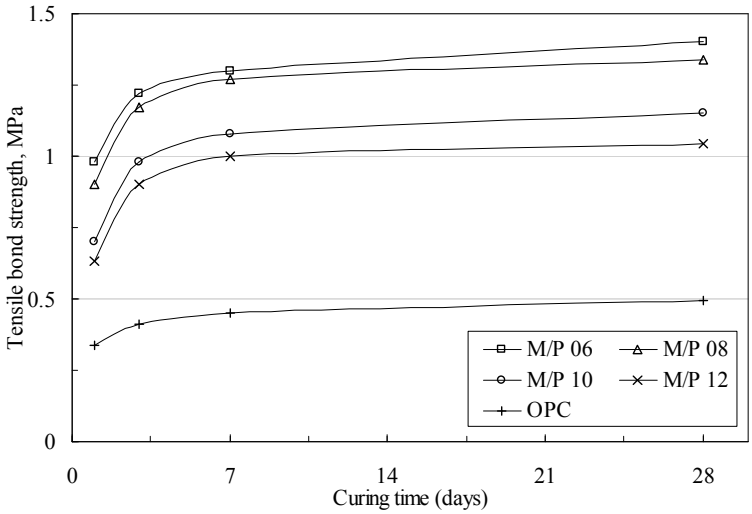

Fig. 8 – Tensile bond strength of MPC mortar with different M/P ratio

Volume stability of MPC mortar. Drying shrinkage of repair material is another major concern of concrete repair because the success of any patch repair depends largely on overcoming the tendency of the patching material to shrink after placement. The shrinkage test results of MPC mortar and reference OPC mortar are shown in Fig. 9. It can be seen that all of the MPC mortars have less shrinkage than OPC mortar at all ages. The shrinkage of OPC increases significantly in the 1st week reaching 700 microstrain at the age of 7-day, while the shrinkage of MPC mortars is only around 40% of OPC mortar at the same age. At early stage the influence of M/P ratio on the shrinkage of MPC mortar is obvious. With the increase of the M/P ratio, the shrinkage is decreased. With the time development, shrinkages tend to be stable and very close for all mixtures except that with M/P ratio of 6 has a little higher value at around 650 microstrain. It is estimated that the early shrinkage is mainly due to the chemical reaction and at the late stage due to the evaporation or migration of free water. From the theoretical volumes of individual ingredient as well as the volume of the reaction product in MPC system given in Table 2, the volume change after reaction can be calculated with Eq. (2):

$$\text{Estimated volume change} = \frac{155.46 - 10.61 - 58.17 - 90}{10.61 + 58.17 + 90} \times 100\% = -2.09\% \quad (2)$$

It can be seen from the calculation that the formation of MKP is accompanied by slight volume shrinkage. Because all of the mixtures have M/P ratio higher than the theoretical value of 1, with the fixed total weight, lowering of the M/P ratio leads to produce more reaction products and cause larger volume shrinkage. From Fig. 9, we can also find the great effect of S/B ratio on the shrinkage of MPC. Regardless the M/P ratio, the lower the S/B ratio, the larger the shrinkage. Involving sand into the paste can restrict the shrinkage of the specimen.

Table 2. Properties of the individual component of the MPC system

	MgO	+	KH_2PO_4	+	$5H_2O$	→	$KMgPO_4 \cdot 6H_2O$
Molar mass (g/mol)	40		136		18		266
Density (g/cm^3)	3.77		2.338		1		1.711
Volume occupied (cm^3/mol)	10.61		58.17		90		155.46

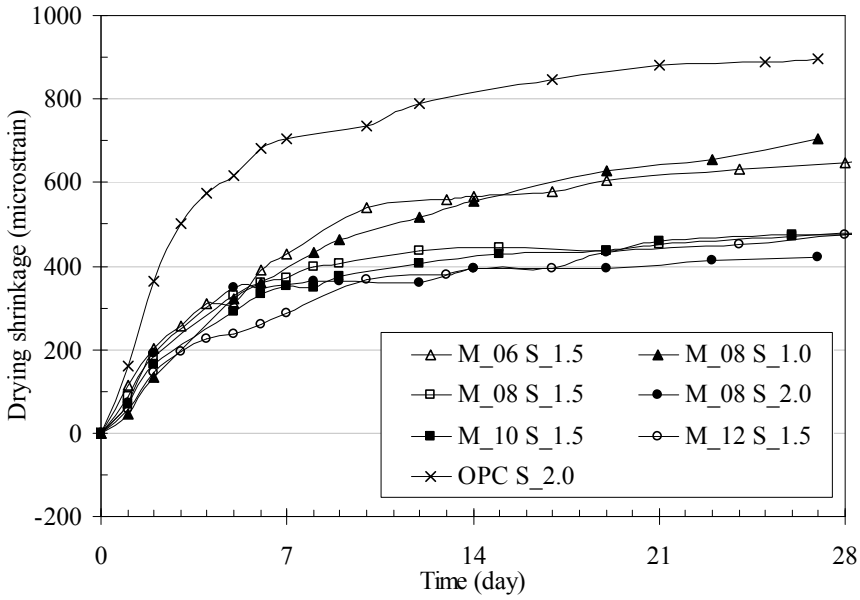

Fig. 9 – Drying shrinkage of MPC mortars and OPC mortar

Conclusions

For MOC cement, the systematic parametric study results demonstrate that the optimal application ranges of the molar ratios for the ternary system of MOC are $MgO/MgCl_2$ from 11 to 17, and $H_2O/MgCl_2$ from 12 to 18. By incorporating fly ash up to 30% by weight of magnesia in the MOC mortars, the workability is enhanced, and more importantly the water resistance is improved, although the final compressive strength decreased. The microstructure of phase 3 crystals is basically in prismatic or spindle shape but poorly formed and distorted, while that of phase 5 crystal is more homogeneous with largely bundled needle shaped crystals. The intergrowth and interlaced network of the bundled needle shaped crystals is believed to be the major mechanism of the strength development of MOC cement.

MPC mortars not only possess high early strength, short setting time, but also have superior bond strength to ordinary Portland cement (OPC) mortar/concrete substrate and the drying shrinkage of MPC based repair mortars is much less than that of OPC mortar. Both the molar ratio of magnesium to phosphate (M/P) and sand ratio can greatly affect the workability, bond strength and drying shrinkage. In this study, the suitable range for preparing MPC mortar are M/P ratio of 8-10 and sand ratio of 1.5.

Acknowledgements

The financial support from Hong Kong Research Grant Council under the grant of 616008 is gratefully acknowledged.

References

[1] P.K. Mehta, in: International symposium on sustainable development of cement and concrete industry, Ottawa, Canada. (1998)

[2] T. Demediuk, W.F. Cole and H.V. Heuber: Australian Journal of Chemistry Vol. 8(1955), p.2133-2152

[3] B. Tooper and L. Cartz: Nature Vol. 211(1966), p.64-66

[4] B. Matkovic and J.F. Young: Nature Physical Science Vol. 246(1973), p.79-80

[5] T. Sugama and L.E. Kukacka: Cement and Concrete Research Vol. 13(1983), p.407-416.

[6] B.E.I. Abdelrazig, J.H. Sharp and B. EI-Jazairi: Cement and Concrete Research Vol. 19(1989), p.247-258

[7] S.S. Seehra, S. Gupta and S. Kumar: Cement and Concrete Research Vol. 23(1993), p.254-266

[8] B.E.I. Abdelrazig, J.H. Sharp and B. EI-Jazairi: Cement and Concrete Research Vol. 18(1998), p.415-425

[9] Q. Yang, S. Zhang and X. Wu: Cement and Concrete Research Vol. 32(2002), p.165-168

[10] H.Y. Jiang and L.M. Zhang: Journal Wuhan University of Technology, Materials Science Edition Vol. 16(2001), p.46-48

[11] A.S. Wagh, Chemically Bonded Phosphate Ceramics. Oxford: Elsevier (2004)

[12] Q. Yang, B. Zhu, S. Zhang and X. Wu: Cement and Concrete Research Vol. 30(2000), p.1807-1813

[13] D.A. Hall, R. Stevens and B. EI-Jazairi: Cement and Concrete Composites Vol. 31(2001), p.455-465

[14] D.A. Hall and R. Stevens: Journal of the American Ceramic Society Vol. 81(1998), p.1550-1556

[15] Z. Ding and Z. Li: Cement and Concrete Composites Vol. 27(2005), p.11-18

[16] F. Qiao, W. Lin, C.K. Chau and Z. Li: Key Engineering Materials Vol. 400-402(2009), p.115-120

[17] W.O. Robinson and W.H. Waggaman: Journal of Physical Chemistry Vol. 13(1909), p.673-678

[18] D.R. Glasson, P. O'Neill and M.A. Sheppard: Journal of Applied Chemistry Vol. 18(1968), p.198-203

doi:10.4028/www.scientific.net/AST.69.31

Geopolymer Binders in Composite Cements and Ceramic-like Materials

Ch. Kaps[1,a] and M. Hohmann[1,b]

[1]Bauhaus-University Weimar, Germany

Chair of Building Chemistry

Coudraystrasse 13C, D-99423 Weimar

[a]christian.kaps@uni-weimar.de , [b]marc.hohmann@uni-weimar.de

Keywords: acidic activation, amorphous networks, burning regime, geopolymer binder, iron-oxyhydroxide, mechanical strength, metaclay, sodium hydroxide, phosphoric acid

Abstract. Two types of geopolymeric networks have been prepared and characterized: aluminosilicatic binders(1) generated of metaclays for composite cements and iron-phosphate binders(2) formed of iron oxyhydroxites for applications in strong acidic environments. The focus of the investigations was on the influence of the thermal(1) or the acidic(2) activation on the structure and properties of the materials. In both cases, the amount of present water plays an essential role.

Introduction

Geopolymers are well-known as alkali activated aluminosilicates forming an inorganic polymer network with advantageous binder properties in the application field of building chemistry. In comparison with Portland-based cements the aluminosilicate networks show a remarkably extended thermal stability (up 1000°C and more) and an improved acid resistivity (wastewater constructions). Moreover, the geopolymer technology is characterized by a CO_2-reduced binder generation. In general two important activation steps are necessary to transform the raw materials in an efficient geopolymer binder. Fig. 1 demonstrates a simplified scheme of the thermal activation as the first step for the generation of an amorphous, energy-rich intermediate product and of the alkaline activation as the second step for a dissolution/polycondensation process forming a geopolymer network.

Whereas the Metakaolin-based geopolymers(a in Fig. 1) are often regarded as 'model systems' [1], the enlarged use of three-layer clay minerals(b in Fig. 1) represents currently an attractive way for the formulation composite cements (*CO_2-poor cements* [2]). The generation of metaclays is possible at temperatures lower than 1000°C (low energy-demand) and a lime-burning with inevitable CO_2-output can be excluded [3].

Fig. 2 shows a view over the compositions of different cement types corresponding to DIN EN 197 in the system Portland clinker(OPC) – slags – pozzolana (left) in comparison with that of geopolymers and alkali-activated slags(AAS [4]) (right). Especially in Portland composite cements (CEM II), Puzzolan cements (CEM IV) and Composite cements (CEM V) a partial substitution of Portland clinker phases by metaclays seems meaningful and the formation of aluminosilicate networks as binder component should be possible compared to C-S-H phases. To find out optimum conditions for the thermal activation of given clay represents a scientific endeavour. This aim is subject of the investigation in the first section.

For extreme acidic conditions with pH $\lesssim$ 3, stable inorganic polymer binders are necessary for special applications in constructions of the chemical industry and in treatment units for highly polluted wastewater of other companies. Under these conditions the aluminosilicate materials break down in every case because of the solubility of the aluminate component.

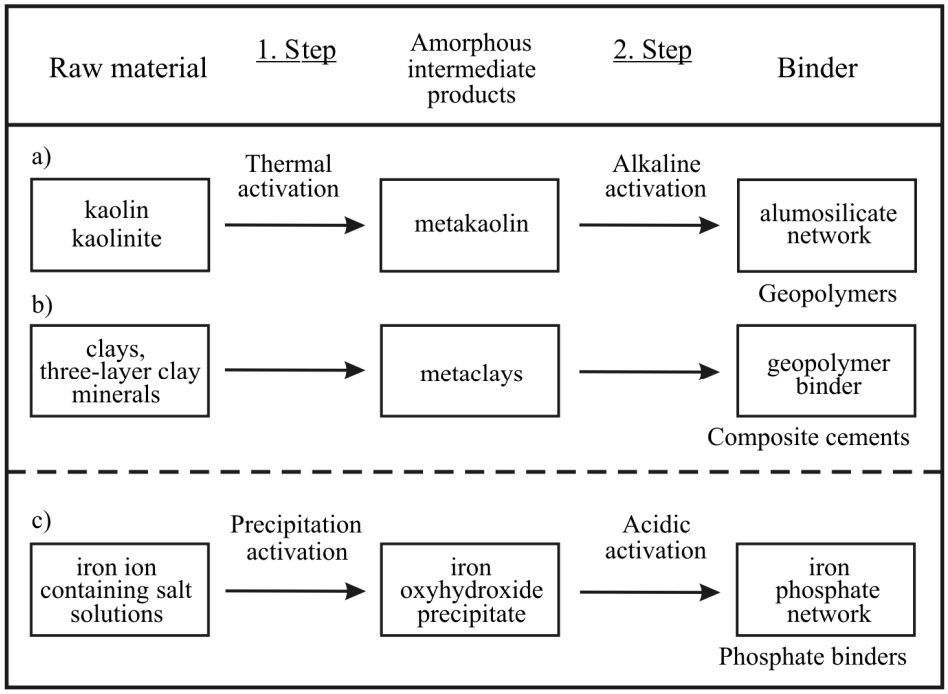

Fig. 1: Two-step procedure for generation of inorganic networks

That is why, other network constituents are required. In accordance with the two-step procedure (Fig. 1) for the generation of geopolymeric networks, the investigation of the second section is focused on the acidic activation of amorphous iron oxyhydroxides, precipitated from an aqueous solution containing iron ions by phosphorous acid (Fig. 1 c, Phosphate binder).

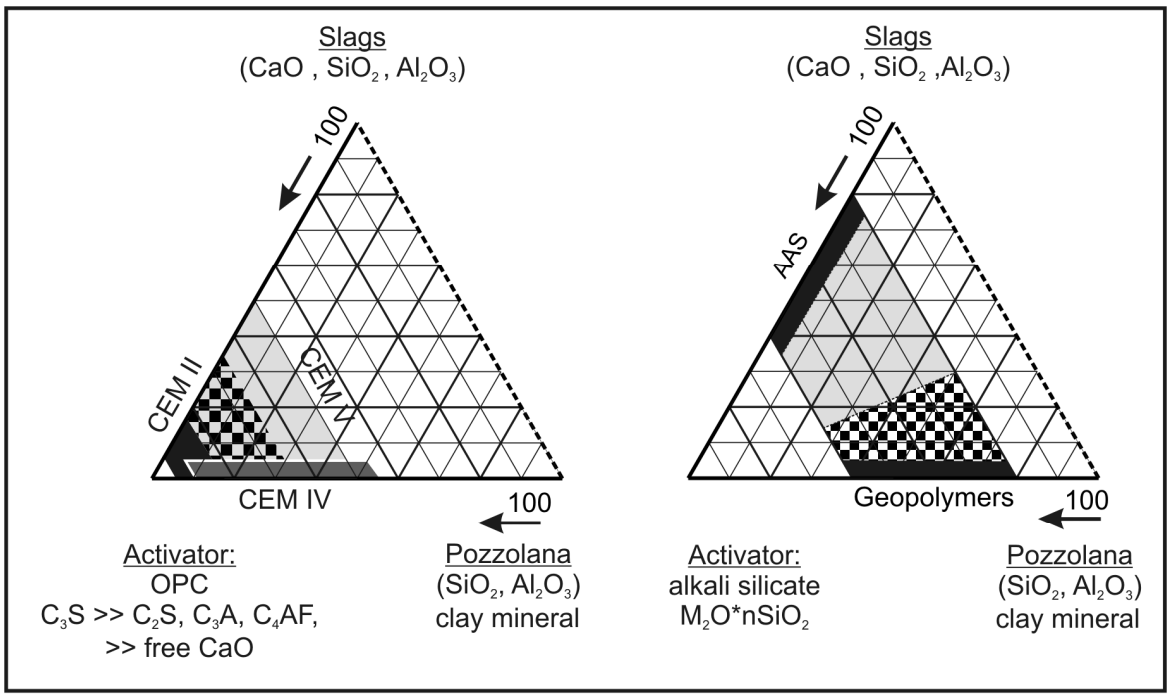

Fig. 2: Compositions of cements (DIN EN 197), alkali-activated slags (AAS) and geopolymers in relation to the activators OPC and alkali silicate

The available iron oxyhydroxide arises in the process of drinking water purification. This study of an acidic activation with phosphorous acid is directed to a comparison with the alkaline activation of aluminosilicates and the main questions consist in: Can iron phosphates form amorphous networks? Is it possible to generate materials with exploitable binder properties? The overall results

of this contribution will demonstrate the general requirement of very detailed investigations for an optimum thermal and acidic activation getting a developed binder.

Geopolymer binders for composite cements by thermal activation of clays

Raw material and thermal activation. For the investigation the smectitic/illitic clay Ndh (Nordhausen, Germany) was used. The chemical analysis is given in Table 1. The content of lime (CaO, MgO) seems to be sufficient low for avoidance of appreciable amounts of C-S-H phases as a result of the subsequent alkaline activation. It was possible to estimate the content of three-layer clay minerals by X-ray diffraction (XRD) into a value of about 58 wt.%.

Table 1: Characterisation of the clay Ndh

Component	SiO_2	Al_2O_3	Fe_2O_3	CaO	MgO	K_2O	Na_2O	SO_3	
Content	64.8	13.7	4.9	1.0	2.6	4.0	0.2	not detectable	wt.%
Three-layer minerals: about 58 wt.% Estimated molar Si/Al ratio: 3.5(total, including quartz), 1.7(only three-layer clay minerals with assumed Si/Al substitution) and 1.1(all clay minerals)									

After a wet processing the clay was extruded in kind of prisms (120x30x15 mm^3) dried and burned at different temperatures between 650 and 950°C in a laboratory furnace. Because of the known influence of the gas atmosphere during the thermal activation process on the reactivity of the burned metaclays we carried out two different activation procedures:
A direct burning in air and a indirect burning in the degassing atmospheres of the clay (water vapour). The detailed conditions of the thermal activation are represented in Table 2.

Table 2: Conditions of the thermal activation

Temperature procedure	Heating rate: 200 K/h Firing temperatures (1 h): 650, 750, 850 and 950°C Cooling: in the furnace, without electronic control
Gas atmosphere over the clay	Direct burning: in air, open (dry, oxidizing) Indirect burning: in degassing atmosphere, encapsulated(wet, reducing)

After the thermal activation the metaclays were grinded up (to 5.7 m^2/g) and analyzed in respect to the phase contents by XRD. Fig. 3 shows the results in dependence on the firing temperature and realized gas atmosphere. Both burning regimes lead to an increasing content of the amorphous components; however the start of the amorphization is already observable at 750°C in the case of indirect burning and at 850°C after direct burning. In exactly the same way, the remarkable high content of unchanged three-layer clay minerals (Illite), indicated by the metaclay (650°C, indirect), is still present in the metaclay (750°C, direct) at 100 K higher firing temperature under dry conditions.

Also, the formation of spinel takes place under the wet condition of indirect burning at temperatures 100 K lower than in the case of direct burning. Obviously the breakdown of the three-layer clay minerals with six-fold coordinated aluminium and the transition to amorphous aluminosilicates with fourfold-coordinated aluminium is favoured at lower activation temperatures in the process of indirect burning in the presence of water vapour.

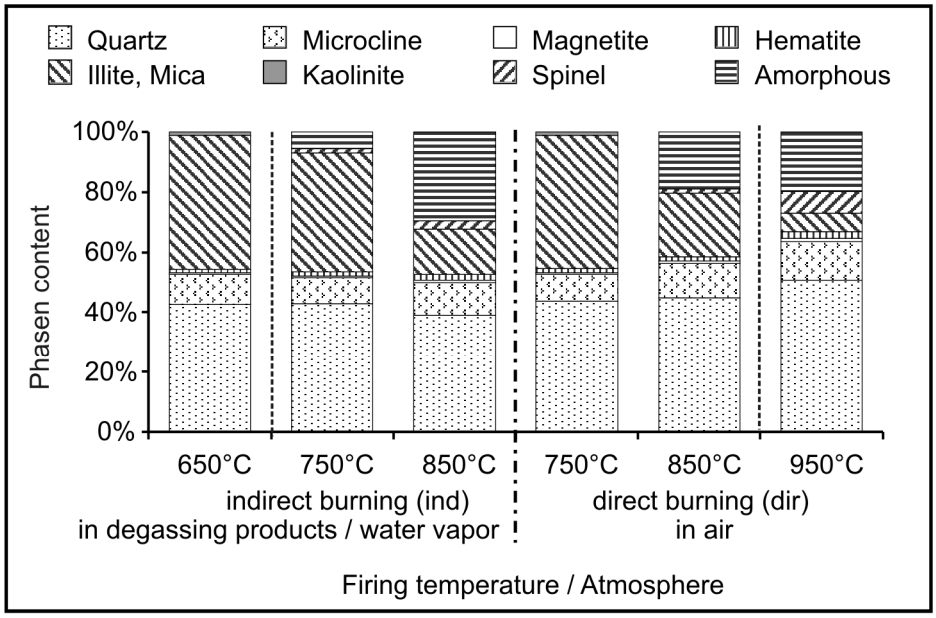

Fig. 3: Phase compositions of the metaclays after direct and indirect burning of the clay Ndh

Alkaline activation: Comparison of the Chapelle test and silicate/aluminate solubility of the metaclays. The Chapelle test represents a characterization method for the pozzolanicity of a raw material in respect to the formation of C-S-H phases in the cement science [5]. The materials are promoted with a $Ca(OH)_2$ solution and the $Ca(OH)_2$ amount, consumed for the reactive setting of solid C-S-H phases, is estimated. To this end, 1 g metaclay was mixed with 2 g CaO and dissolved in 250 ml deionised water. After 16 h at 90°C the surplus of non-reacted $Ca(OH)_2$ was determined by a quantitative titration and the reactive quantity consumed was applied to the amount of pozzolanic material (metaclay).

For the assessment of the reactivity or activity of the metaclays in respect to the formation of geopolymers, the solubility of silicate and aluminate in an alkaline solution is estimated. In detail the metaclay was putted in a 10% NaOH solution (mass ratio: solid/solution = 1/1000) and warm up to 60°C. The dissolved silicate and aluminate contents were determined after 1 day, 3 days and 5 days by ICP-Optical Emission Spectroscopy.

A comparison of the results of the two characterization methods for the metaclays made from the clay Ndh is given in Fig. 4. The Chapelle test and also the sum of the dissolved silicate and aluminate (Si+Al) demonstrate maximum values at the same firing temperature of 750°C for the indirect burning (ind) and as well a maximum at a firing temperature of 850°C for the direct burning (dir). On the hand this result shows a good correspondence of these two characterizations methods for metaclays in respect to their reactivity under the conditions of alkaline activation and on the other hand it gives an evidence of the meaning of the formation of amorphous phases in the thermal activation process. In Fig. 3, the both metaclays (750°C, ind) and (850°C, dir) stand out for a distinct amount of amorphous components, formed from the three-layer minerals at these (lowest) firing temperatures.

Understandably the molar ratio Si/Al of the solved species proves to be decisively important for the formation of aluminosilicatic geopolymers. Since the beginning of the research on geopolymers this ratio is discussed in the range $1 \lesssim Si/Al \lesssim 3$ [6]. For a correct evaluation of the metaclays in respect to the polycondensation of aluminosilicates with an Si/Al ratio, which is only determinated by consumption of the thermally transformed clay, the alkaline activation (solubility test) was carried only with NaOH solution (without water glass) in this investigation. The evolution of the measured molar ratio Si/Al of the dissolved (free) silicate and aluminate of the alkaline solution is presented in Fig. 5.

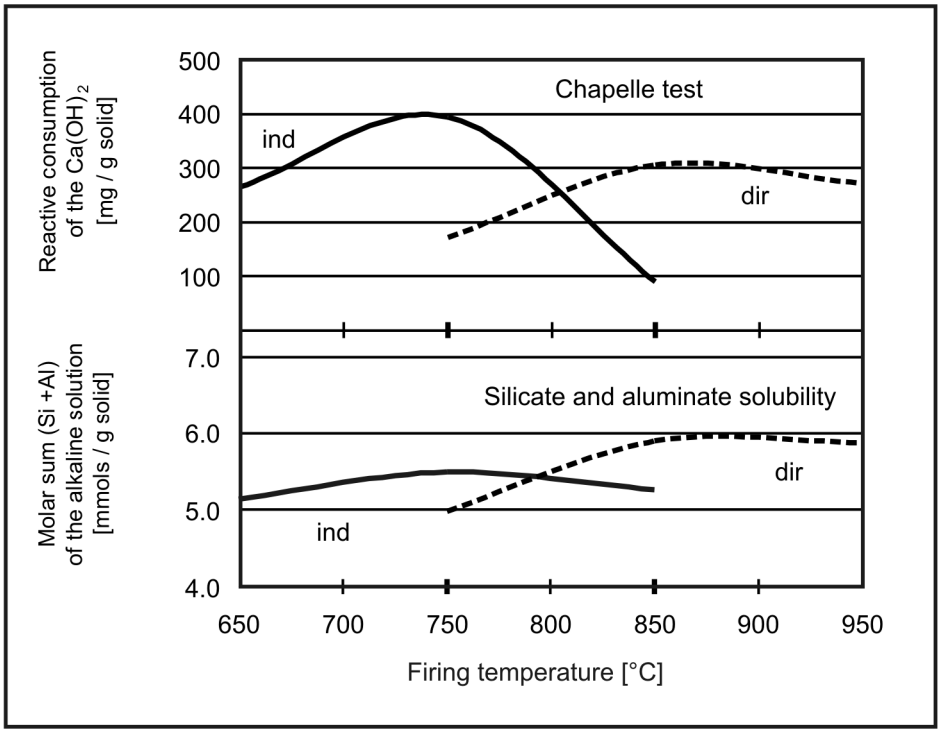

Fig. 4: Correspondence of the results from the Chapelle test to the sum of the silicate and aluminate solubility

At any time the values are the result of the alkaline dissolution and polycondensation forming solid geopolymers.

The metaclay of the indirect burning at 750°C yields an actual Si/Al ratio from 2.2 to 3.0 in the alkaline solution during a time from 1 to 7 days. Under this burning regime, the metaclay from 800°C demonstrates already a ratio Si/Al>3 (silicate excess) 3 days after the beginning of the dissolution process. A comparison with the solubility behaviour of the directly burnt metaclay (850°C, dir) shows similar ratios (2.3<Si/Al<3.2 from 1 to 7 days).

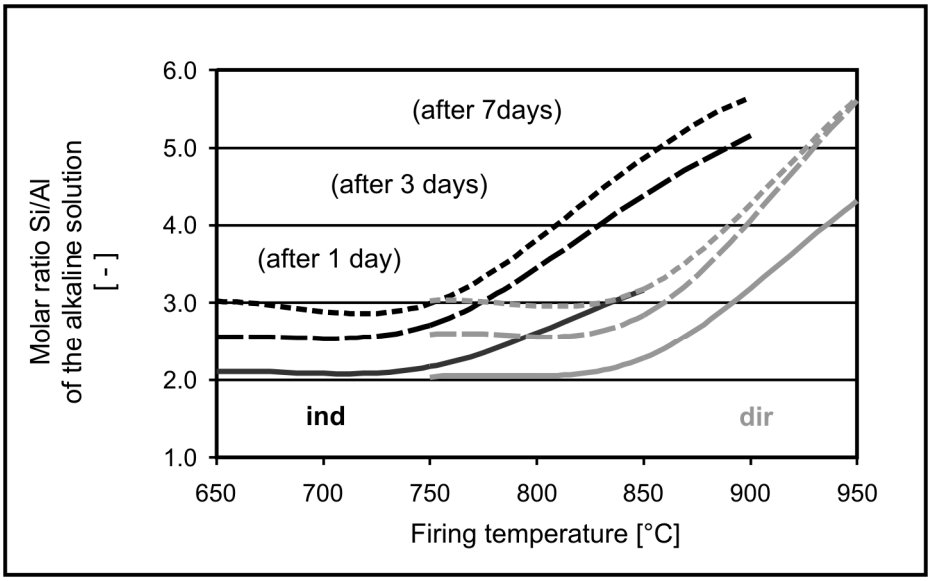

Fig. 5: Evolution of the molar ratio Si/Al of the alkaline solution, comparison of indirect and direct burning of the clay Ndh

However, the firing temperature of 850°C is 100 K higher than that of the indirectly burnt metaclay, and consistently the thermal activation requires a higher amount of energy. Nevertheless the metaclay, burnt at 900°C, generates already a remarkable silicate excess (Si/Al≳4) 3 days after the beginning of the alkaline dissolution. We assume that this silicate excess, generally observed at higher firing temperatures, comes from the alkaline attack on the quartz of the clay Ndh.

Influence of the burning conditions on the strength of the geopolymer binders. Using the metaclays made from the clay Ndh by burning on different ways, geopolymer binders were prepared by an alkaline activation with NaOH solution (8 mole/l) in a mass ratio solid/activator of 0.35 and putted in a mould (10x25x60 mm^3). For setting and harding a storage regime was chosen under 75% r.h. at 20°C with a duration of 90 days. The measurement of the flexural strength represents a very sensitive method for the characterization of the binding strength of a material and proves to be an useful information source on the reaction potential of the metaclays and on the performance of the polycondensation respectively. In Fig. 6 the measured values of the flexural strength are compiled.

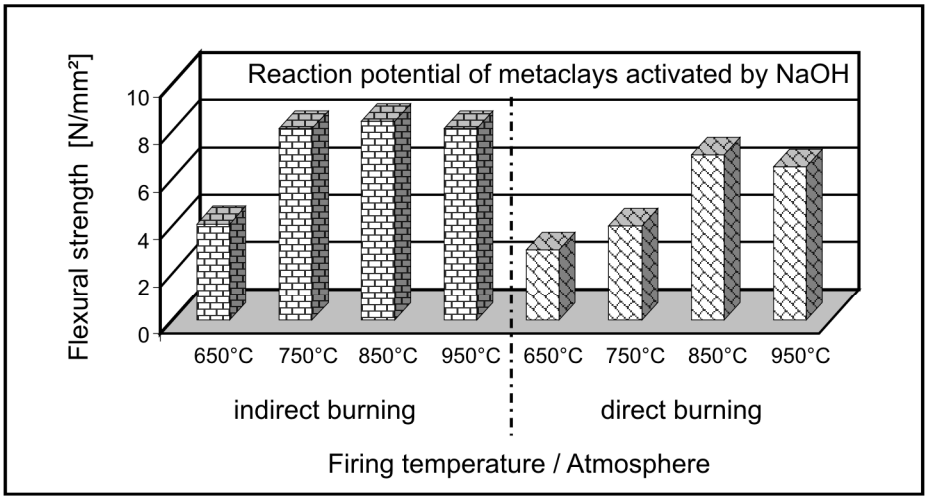

Fig. 6: Flexural strength of the geopolymer binders in dependence on the burning conditions of the metaclays

The strength of the geopolymer binders with metaclays from the indirect burning (650-950°C) is higher than that of the corresponding binders with metaclays from the direct burning (650-950°C). Obviously, the increasing content of amorphous components (see Fig. 3) causes also an enlargement of the geopolymer strength, indicated in both cases of the burning regimes. The indirect burning yields a sharp increase of the strength at the firing temperature of 750°C. In comparison the direct burning demonstrates a gradual rise of the strength. This behaviour depending on the burning regime seems to be characteristic of the geopolymer formation and is not found in the case of ceramic binding of metaclay prisms by sintering of the clay Ndh under identical thermal conditions (dir and ind). Finally the strength of the geopolymer binding drops at higher firing temperatures (950°C, dir and 950°C, ind), corresponding to the noticeable formation of new crystalline phases indicated by the spinel (see, Fig. 3). The late release of silicates from the metaclays during the alkaline dissolution process seeing in Fig. 5 at T≳900°C, provides no remarkable contribution for an increased strength of the geopolymers (Fig. 6, 950°C ind and dir).

Ceramic-like materials based on H_3PO_4- activated iron oxyhydroxides

Preparation and setting behaviour of iron-phosphate networks. The investigation of the formation possibilities for iron-phosphate networks was carried out in relation to aluminosilicate geopolymers under the assumption of a polycondensation reaction [7, 8], presented in a simplified form in Eq. 1.

$$(HO)_2Fe\text{-}OH + HO\text{-}PO(OH)_2 \rightarrow (HO)_2Fe\text{-}O\text{-}PO(OH)_2 + H_2O \quad (1)$$

An iron oxyhydroxide, formed in a precipitation process (Fig. 1), was mixed with phosphoric acid of different degrees of dilution. The raw materials and their characteristic parameters are described in Tab. 3.

Tab. 3: Raw materials and characterization of the iron oxyhydroxide

Iron oxyhydroxide, IO Phosphoric acid; PA Water, W		technical residual product, amorphous (XRD) H_3PO_4, cons. (85%), p.a. H_2O, deionised water								
Analized components of IO	Fe_2O_3	CaO	SiO_2	MnO	P_2O_5	MgO	Al_2O_3	Na_2O	K_2O	TiO_2
[wt.%]	71.3	10.0	14.5	1.5	1.4	0.7	0.3	0.2	0.03	0.01
Mineral phases of IO:	amorphous Ferrihydrite ("FeO(OH)", ≳ 55 wt.%) Calcite (cryst. $CaCO_3$, ≈ 10 wt.%)									

For the study, different compositions of solid iron oxyhydroxide and more or less diluted phosphoric acid were tested. An overview of the realized compositions is illustrated in Fig. 7 by the lines with different degrees of acid dilution (mass ration PA/W: 0.89 (g1), 1.8 (g2), 4.4 (g3) and ∞ (g4) and with iron oxyhydroxide contents of 15, 20, 25 and 30 wt.% IO.

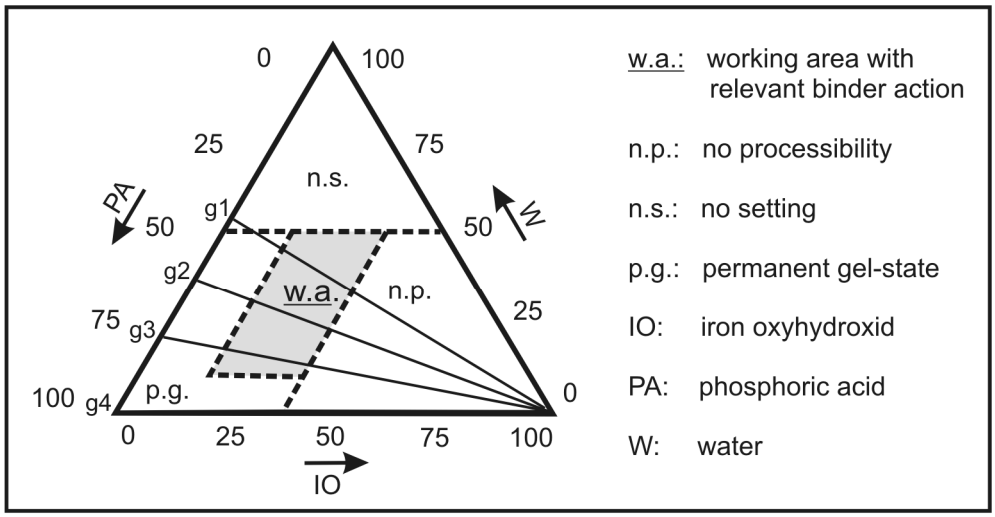

Fig. 7: Investigated composition in ternary basis system IO-PA-W

In the working area (w.a.) the setting time as the time limit for workability of the mixture (casting or forming) depends perceptively on the composition of the mixture and ranges from 15 min to 36 h. Already, the start viscosity varies from "aqueous consistency" to viscoplastic (g1 → g4 and 15 → 30 wt.% IO, respectively). This strong dependence of the setting behaviour on the ratio

IO/PA (which corresponds to the ratio intermediate product/activator, see Fig. 1) seems to be caused the fact that the phosphoric acid (PA) as a direct component is installed in the iron-phosphate network by polycondensation, indicated by Eq.1. For comparison in the case of the alkaline activation of metaclays by NaOH the chemical action of the activator shows more a dissolving character.

Furthermore, the structure of the iron-phosphate networks depend remarkably on the PA/W ratio realized in the preparation. In Fig. 8 the diffractograms from X-ray investigations of 4 solidified binders with the high IO-content of 30 wt.% are shown. The networks with mass ratios PA/W of 0.89 (g1) and 1.8 (g2) demonstrate an amorphous structure and the networks, formed with a lower water content or without additional water (PA/W=4.7 and ∞), prove to be clear crystalline. The identified crystalline phases are ortho-phosphate hydrates (preferably $Fe_3H_9(PO_4)_6 * 6H_2O$ (PDF 44-812)and traces of $Ca(H_2PO_4)_2 * 2H_2O$ (PDF 01-070-0090) from calcite of IO, see Tab.3).

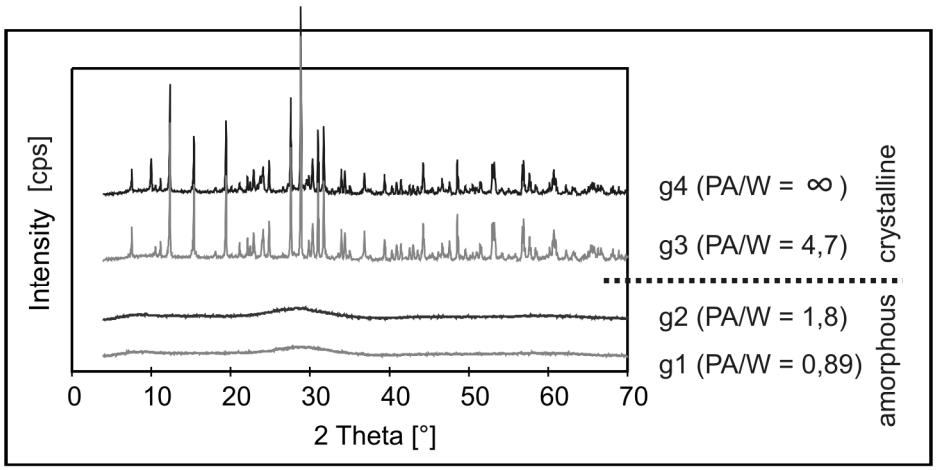

Fig. 8: X-ray diffractograms of iron-phosphate networks (30wt.%IO) in dependence on water content

Obviously, a sufficient high water content of the mixture favours a sol-gel transition while maintaining of the amorphous structure comparable with the formation of aluminosilicate geopolymers at room temperature. During the setting process the iron-phosphate materials retain the acidic character and the pH-values rises slightly about 3. That is why these binders show a good resistance against acidic attack; however the water stability is not full sufficient for practical applications. To optimize the materials properties, the addition of fine grains of metallic iron and different mineral powders to the fresh mixtures was tested.

Influence of additions on setting behaviour and materials properties. For the preparation of iron-phosphate ceramics the addition of elemental iron is recommended to intensify the solution process of iron(III)-oxide in phosphoric acid [9].
Corresponding to Eq. 2 the stochiometric reaction is linked to a formation of hydrogen.

$$Fe^0 + Fe^{3+} + H_3PO_4 \rightarrow 2Fe^{2+} + H_2PO_4^- + 0.5H_2 \qquad (2)$$

Furthermore, the oxidation potential of the air affects this redox-reaction. The Fe^0-addition was studied with two levels of conditions: substochiometric addition ($Fe^0/Fe^{3+} < 1$) and stochiometric addition ($Fe^0/Fe^{3+} = 1$). In the case of substoichiometrie addition of iron the increasing amount of Fe^0 leads to amorphous networks represented by the diffractograms in Fig. 9 (left).

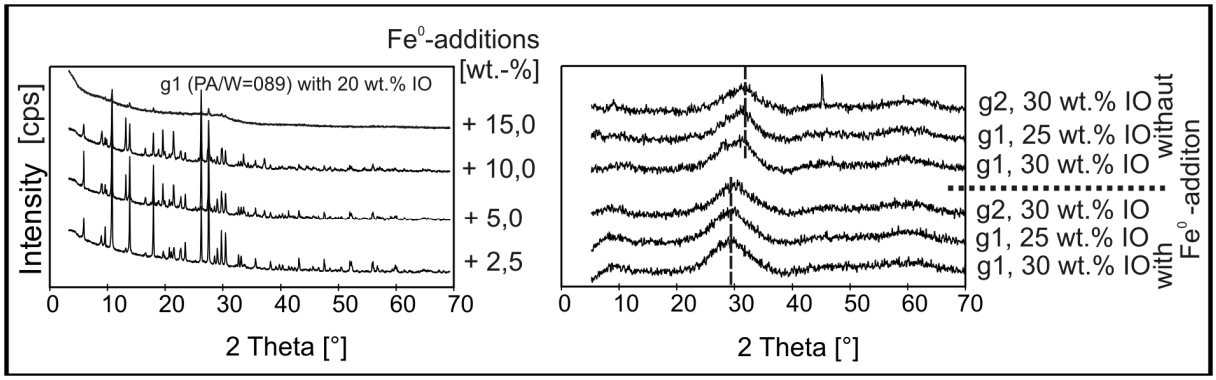

Fig. 9: X-ray diffractograms of iron-phosphate networks with Fe^0 -additions

A shortening of the setting time is also observed in the mixtures, prepared with increasing Fe^0-contents. The stochiometric Fe^0-addition to fresh mixtures, forming amorphous networks (typical g1 and g2 with 25-30 wt.% IO), allows the maintenance of the non-crystalline structure (Fig.9, right). Remarkably, the *amorphous humps* (2 $Theta_{max}$) show comparable shifts to smaller Theta-values, corresponding to a slight expansion of the atomic arrangement of the amorphous networks (d = Lamda/2sin (Theta) from 0.28 nm to 0.31 nm) by the remarkable introduction of iron (comp. aluminosilicate networks [10].

For further improving the application properties of the iron-phosphate binders, an addition of Basalt (B, d_{50} = 110 um) and Fly Ash (FA, d_{50} = 40 µm) powders to the fresh mixtures has been tested. The slight basic mineral powders increase the stability of the acidic iron-phosphate networks against water attack. Because of that, the prepared composite prisms (28d) demonstrate a good shape resistance in boiling water (2 h). In Fig. 10 the effect of the basic mineral powders on the materials strength is shown.

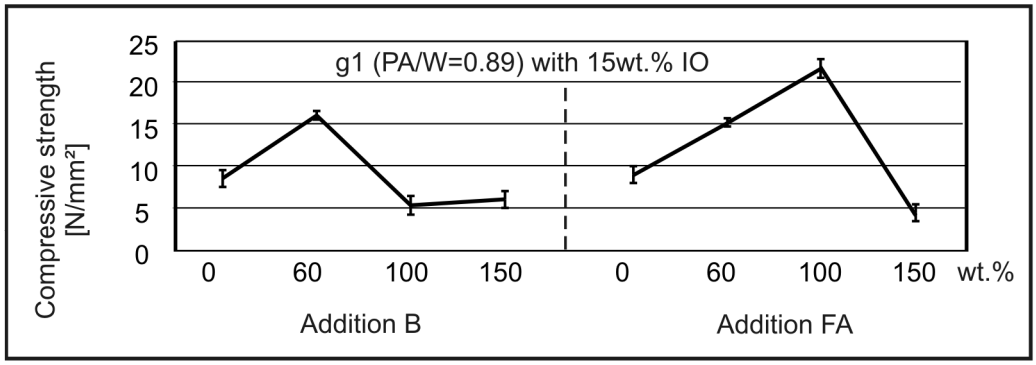

Fig. 10: Compressive strength of the iron-phosphate binder with additions of Basalt (B) and Flyh Ash (FA) powders

Both additives (60 wt.% B and 100 wt.% FA, resp.) increase the compressive strength of the composite materials by a factor of two. Obviously, the weak acid-base interaction promotes the cohesion of the network and mineral additives (compr. Al-phosphate networks [11]).

Summary

Geopolymer binders of an aluminosilicate basis have been studied for CO_2-poor composite cements using the smectitic/illitic clay Ndh (Nordhausen, Germany). The thermal activation was carried out at temperatures from 650 to 950°C in a direct and an indirect burning regime. The wet conditions of the indirect burning allow already at 750°C the formation of a sufficient amount of amorphous components from the three-layer clay minerals. The solubility tests with NaOH demonstrate for a period of 7 days an appropriate molar Si/Al ratio from 2 to 3 of the dissolved (free) silicate and aluminate species for these metaclays (750°C, indirect). The solubility behaviour of these metaclays

corresponds to a useful flexural strength ($\gtrsim$ 7 N/mm^2) of the networks generated by alkaline activations of the metaclays. The dry conditions of the direct burning realize only such favourable conditions at firing temperatures of 850°C. In every case, the optimal formation of strong geopolymers is limited, if the Si/Al-ratio exceeds values of about 5 in the first 3 days.

Geopolymeric iron-phosphate networks have been prepared for applications in an acidic environment. A technical precipitation product, consisting dominantly of an amorphous iron oxyhydroxide, was activates by phosphoric acid in an aqueous suspension. Appropriate mixtures with an increased water content lead to amorphous networks in the setting process. Low contents of water cause the formation of crystalline iron orthophosphates. The addition of elemental iron promotes the tendency for amorphous setting with a shortening of the setting time and the formation of slightly expanded networks. By the addition of basic mineral powders, the resistivity of the ceramic-like materials against water can be improved remarkably and the compressive strength will be doubled.

References

[1] J. L. Provis and J. S. J. Van Denventer: *Geopolymers, Structure Processing, Properties and Industrial Applications*, CRD Press, Woodhead Publ., Oxford, 2009, p. 3

[2] H.-M. Ludwig: *Herstellung und Anwendung von CO_2-armen Zementen*, 17. Int. Baustofftagung, Weimar, 2009, ed. by. J. Stark, FIB, p. 1-0057

[3] Ch. Kaps, M. Hohmann and A. Buchwald: *Geopolymers in Ceramic Building Materials*, ICC2, Proc., Verona, 2008, ed. by A. Bellosi and G. N. Babini, Faenza, Italy, p. 723

[4] P. V. Krivenko and G. Y. Kovalchuk: Journ. Mat. Science 42 (2007), p. 2944

[5] J. Thiery and P. Soukatchoff, U.S. Patent 4,994,114 (1991)

[6] J. Davidovits: *Geopolymer, Chemistry and Applications* (Institute Geopolymere, Saint-Quentin, France, 2008), p. 30

[7] W. D. Kingery: *Fundamental Study of Phosphate Bonding in Refractories: I – III,* Journ. Amer. Ceram. Soc. Vol. 33 (1950), p. 239

[8] I. Karpukhin, V. Vladimirov and S. Moizis: Refract. and Industrial Ceramics, Vol 46 (2005), p. 180

[9] A. S. Wagh: *Chemical Bonded Phosphate Ceramic* (Elsevier, 2004), p. 136

[10] J. Davidovits: *Structural Characterization of Geopolymeric Materials with X-Ray Diffractometry and MAS-NMR Spectroscopy*, Geopolymer ’88 Proceedings, p. 149

[11] D. S. Perera, J. V. Hanna, J. Davis, M. G. Blackford, B. A. Latella, J. Sasaki and E. R. Vane: J. Mat. Sci. 43 (2008), p. 6562

doi:10.4028/www.scientific.net/AST.69.41

Dissolution-reorientation-polycondensation process of metakaolin in alkaline solutions related to geopolymerization

Zhang Yunsheng[1], Sun Wei[1], Li Zongjin[2]

[1]Jiangsu Key laboratory for Construction Materials, Southeast University, Nanjing, 211189, P.R.China;

[2] Department of Civil Engineering, The Hong Kong University of Science and Technology, Clear water Bay, Kowloon, P.R.China)

Keywords: Geopolymer; Metakaolin; Dissolution; Reorientation; Polycondensation; Computational chemistry

Abstract: Geopolymer is a novel type of inorganic cementitious materials, which has become a hot topic across the world. Geopolymerization process of metakaolin in alkaline solutions shows important effects on final properties of hardened geopolymer. In this paper all the possible reaction pathways involved in the dissolution-reorientation-polycondensation process of metakaolin in alkaline solution were studied according to thermodynamic theory. The corresponding reaction energy of every possible pathway was also calculated using computation chemistry method-semi-empirical AM1 calculation. The optimum reaction pathway was analysized based on the energy-minimized principle. The calculation results showed that highly alkaline accelerated the dissolution of 6-membered tetrahedron rings of SiO4 or AlO4 tetrahedron representing the molecular structure of metakaolin during dissolution process. Si-Al hybrid reorientation should theoretically be primary reorientation pathway during reorientation process. Framework clusters should be primary polycondensation products during polycondensation process. The above studies enhanced our understanding of formation mechanisms of metakaolin in alkaline solutions related to geopolymerization.

1. Introduction

Geopolymer is a new type of aluminosilicate inorganic cementitious materials, which was developed by J.Davidovits in the later 1970s [1]. Geopolymer can be prepared by mixing reactive aluminosilicate materials with less or no CaO (such as metakaolin or fly ash) and highly alkaline solutions (such as LiOH, NaOH or KOH), then curing at 80°C or less. Under the action of highly alkaline solution, aluminosilicates are rapidly dissolved to form free SiO_4 and AlO_4 tetrahedrals. As geopolymerization process goes, mixing water is gradually split out and these SiO_4 and AlO_4 tetrahedrals are linked alternatively to yield polymeric chains (-SiO_4-AlO_4-,or -SiO_4-AlO_4-SiO_4-, or -SiO_4-AlO_4-SiO_4-SiO_4-) by sharing all oxygen atoms between two tetrahedrals, and finally forming rock-like geopolymer products [2]. Geopolymer made with reasonable mixture formulation can exhibit superior properties to Portland cement; lower calcining temperature (600 to 800 °C) and approximately 80% less CO_2 emission [3,4]; Rapid reaction rate and high early strength (70% of the final strength gain in the first 12 hours); low permeability [2,5,6], low shrinkage [2,9,10] and good fire and acid resistance [7-8]. In addition, excellent solidification of heavy metal ions is documented [2,5-14]. Thus, geopolymer has become perspective inorganic binders, which is extensively studied around the worlds. [15,16].

Formation process is of great importance for Geopolymer binder, since it directly determines the physical, mechanic and durability properties of matured Geopolymer. Although some efforts have been made on studies on formation process of Geopolymer, only a qualitative and describable

3-steps process of dissolution-reorientation-polycondensation involved in geopolymerisation reaction was proposed [17]. However, the setting and hardening of Geopolymer is so rapid that the 3-steps process almost occurs at the same time. Therefore, it is very difficult to separate and investigate each step by experimental method, therefore yielding no better understanding of the details of each step at present.

Quantum chemistry methods have proved to be a powerful tool to predicting molecular configuration and properties of silicates or alumino-silicate materials. With a great progress of computational power, it is possible to calculate the bonding, breaking and formation processes, in particular, the reaction pathways and energetics involving silicates or alumino-silicates from the atomic point of view [18-20]. In this paper, a semi-empirical quantum chemistry method based on the Hartree-Fock formalism is employed to study all the possible pathways involved in the formation process of metakaolin based Geopolymer.

2. Molecular representing model of metakaolin

When performing quantum calculation, a molecular model representing the structure of the main raw material should firstly postulated as input data. Metakaolin is one key reactive aluminosilicates to synthesis geopolymer binder [1-12]. When metakaolin (MK) contacts with highly alkaline solution, free Si and Al tetrahedras are dissolved from the surface of metaoline particles. These collusions among Si and Al tetrahedras inevitably occurs, resulting in orientation reaction. As more and more orientated clusters are released into solution, polycondensation process takes places and geopolymeric products forms. In this study, we firstly established a molecular model representing MK structure, and then study the dissolution, reorientation and polycondensation behaviors of the model using semi-empirical AM1 calculation. The calculation can be used to understand the foramtion process of MK in alkaline solutions.

MK is of sheet alumino-silicate materials. A few small molecular units [21] can reproduce the sheet structure periodically. Therefore, it is reasonable to use these small reproducible units to represent the structure of MK. In our studies, two 6-membered-rings molecular structural models were established in order to quantitatively analysis the formation process of geopolymer, as shown in Fig.1(a), and Fig.1(b).

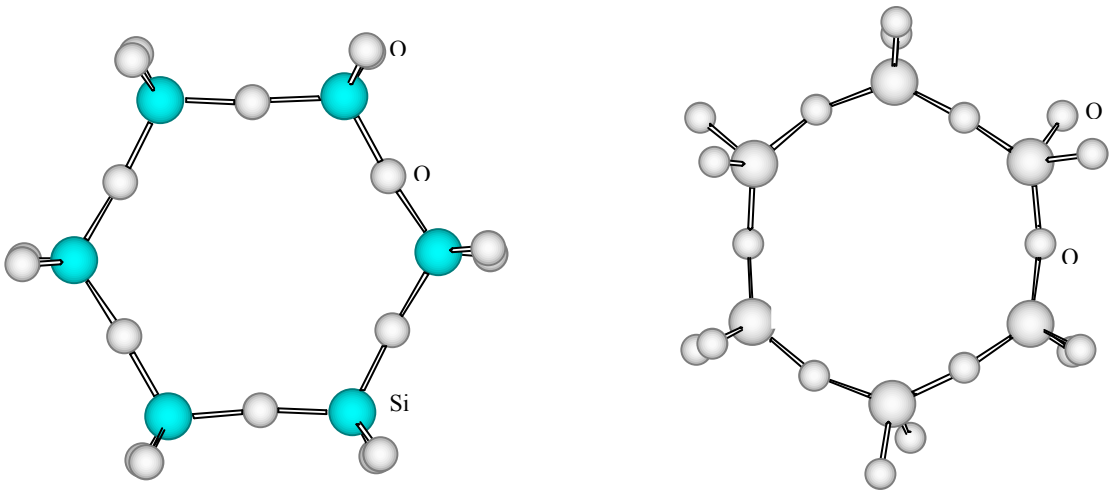

a. 6-member rings of SiO_4 tetrahedron b. 6-member rings of AlO_4 tetrahedron

Fig.1 Molecular representing model of metakaolin

3. Dissolution process

3.1 Dissolution pathways

On basis of the two 6-membered-rings models, all possible dissolution pathways of metakaolin in strongly alkaline solutions were investigated using semi-empirical AM1 method. The dissolution process of sing 6-membered ring can be divvied into 3 steps in strongly alkaline solutions, as shown from Eqs.(3) to Eqs.(10): (1) Ring breakage for releasing $HOSiO_3^{\equiv}$ or $HOAlO_3^{-IV}$ anion; (2) Formation of HO-Si(OM)$_3$ or HO-Al$^-$(OM)$_3$ species by ion-pairing reaction between $HOTO_3^{\equiv \text{ or } -IV}$ anion and M^+ cation; (3) Further interaction between the remaining broken ring cluster and MOH solutions. All possible pathways (equation 1 to equation 8) involved in the formation process of geopolymer were analyzed, and the enthalpies of each possible pathway were also calculated, and listed in table 1. As a result, the optimum pathways in geopolymerization process were determined according to energy minimization principle.

$(Si(OH)_2O)_6+3NaOH \Rightarrow (OH)_3Si\text{-}(Si(OH)_2O)_3\text{-}Si(OH)_3+HO\text{-}Si{\equiv}(ONa)_3+H_2O.$ $\Delta E3 \ldots (1)$

$(Si(OH)_2O)_6+3KOH \Rightarrow (OH)_3Si\text{-}(Si(OH)_2O)_3\text{-}Si(OH)_3+HO\text{-}Si{\equiv}(OK)_3+H_2O.$ $\Delta E4 \ldots (2)$

$Si(OH)_2O)_6+4NaOH \Rightarrow (OH)_3Si\text{-}(Si(OH)_2O)_3\text{-}Si(OH)_2\text{-}ONa+HO\text{-}Si{\equiv}(ONa)_3+2H_2O.$ $\Delta E5 \ldots (3)$

$Si(OH)_2O)_6+4KOH \Rightarrow (OH)_3Si\text{-}(Si(OH)_2O)_3\text{-}Si(OH)_2\text{-}OK+HO\text{-}Si{\equiv}(OK)_3+2H_2O$. $\Delta E6 \ldots (4)$

$(Al^-(OH)_2O)_6+3NaOH \Rightarrow (OH)_3Al^-\text{-}(Al^-(OH)_2O)_3\text{-}Al^-(OH)_3+HO\text{-}Al^-{\equiv}(ONa)_3+H_2O.$ $\Delta E7 \ldots (5)$

$(Al^-(OH)_2O)_6+3KOH \Rightarrow (OH)_3Al^-\text{-}(Al^-(OH)_2O)_3\text{-}Al^-(OH)_3+HO\text{-}Al^-{\equiv}(OK)_3+H_2O.$ $\Delta E8 \ldots (6)$

$(Al^-(OH)_2O)_6+4NaOH \Rightarrow (OH)_3Al^-\text{-}(Al^-(OH)_2O)_3\text{-}Al^-(OH)_2\text{-}ONa+HO\text{-}Al^-{\equiv}(ONa)_3+ 2H_2O.$ $\Delta E9 \ldots (7)$

$(Al^-(OH)_2O)_6+4KOH \Rightarrow (OH)_3Al^-\text{-}(Al^-(OH)_2O)_3\text{-}Al^-(OH)_2\text{-}OK+HO\text{-}Al^-{\equiv}(OK)_3+ 2H_2O.$ $\Delta E10 \ldots (8)$

Eqs.(1) and (2), (5) and (6) represent the ring breakage as well as formation of HOT(OM)$_3$ species in strongly alkaline environment. Eqs.(3) and (4), (7) and (8) include not only the ring breakage and formation of HOT(OM)$_3$ species, as in the case of Eqs.(1) and (2), (5) and (6), but also further interaction between the remaining broken ring cluster and MOH solutions. Therefore, the values of (ΔE3-ΔE1), (ΔE4-ΔE2), (ΔE7-ΔE5) and (ΔE8-ΔE6) actually represent the further interaction energies between MOH solutions and the remaining broken ring clusters.

3.2 Reaction energies of various dissolution pathways

Fig.2 and Fig.3 show the molecular models of HOT(OM)$_3$ and the remaining broken ring clusters. Table1 lists the reaction energies for Eqs.(1)-(8) using semi-empirical AM1calculations. The bond length and angle of the remaining broken 6-membered SiO_4 and AlO_4 tetrahedron ring models are also calculated using AM1 method in this paper. The changes in bond length and angle of the 6-membered rings models before and after dissolution in strongly alkaline solution are shown in Fig.4 and Fig.5. As can be seen, the bonds on boundary (Si-O_{br}) and bonds on ring (Si-O_{nbr}) are both stretched, while the angles on ring (O_{br}-Si-O_{br}) are reduced and the angles (Si-O_{br}-Si) are increased after the releasing of $Si(OH)_4$ cluster regarding single 6-membered SiO_4 tetrahedron ring model. This suggests that single 6-membered SiO_4 tetrahedron ring model contracts inwards after dissolution in strong alkaline environment, which can seen clearly in Fig.3(a,b).

For single 6-membered AlO_4 tetrahedron ring model, the reduction in the bonds on boundary

($Al\text{-}O_{nbr}$) and increase in the bond on ring ($Al\text{-}O_{br}$) are found after the releasing of $Al(OH)_4^-$ cluster. The angles on ring ($O_{nbr}\text{-}Al\text{-}O_{br}$) and ($Al\text{-}O_{br}\text{-}Al$) show a diminishing trend. This indicates that single 6-membered AlO_4 tetrahedron ring model expands outwards after dissolution in strong alkaline environment, which can be seen in Fig.3(c,d).

Based on the above analysis, we know that the single 6-membered ring models are readjusted after dissolution, resulting in some changes in bond length and angle.

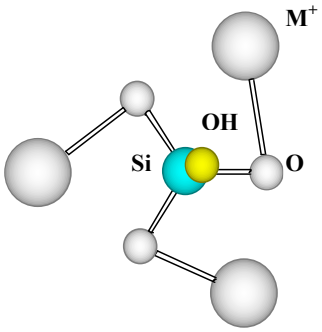

a. Molecular structure of $HO\text{-}Si(OM)_3$

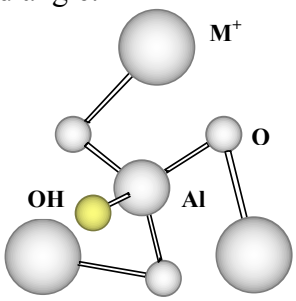

b. Molecular structure of $HO\text{-}Al^-(OM)_3$

Fig.2 Optimized molecular structure model of $HO\text{-}T(OM)_3$ (T represents Si or Al)

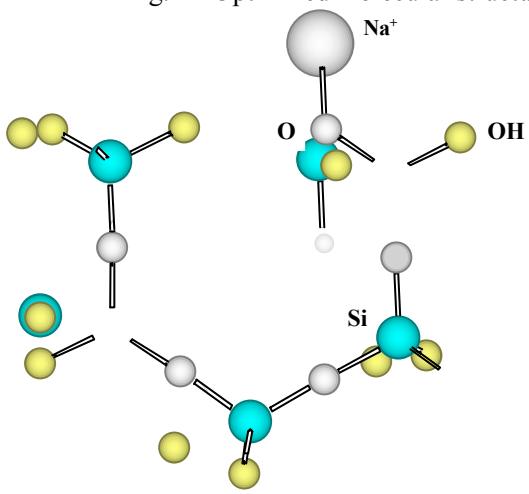

a. Molecular structure of $(OH)_3Si\text{-}(Si(OH)_2O)_3\text{-}Si(OH)_2\text{-}ONa$

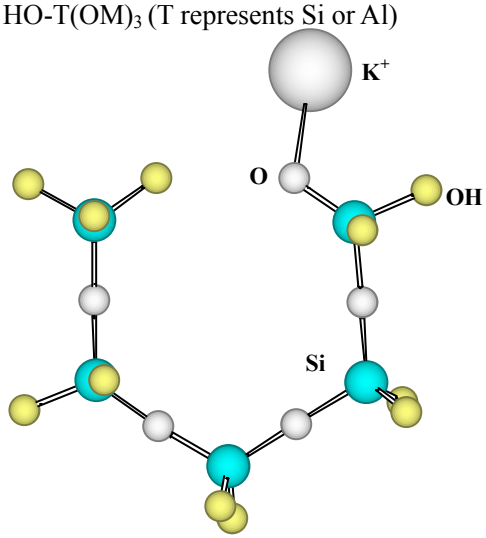

b. Molecular structure of $(OH)_3Si\text{-}(Si(OH)_2O)_3\text{-}Si(OH)_2\text{-}OK$

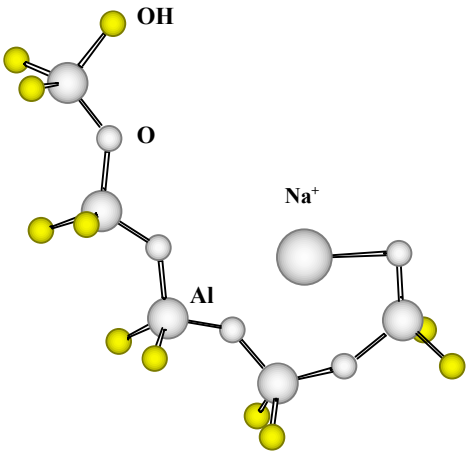

c. Molecular structure of $(OH)_3Al^-\text{-}(Al^-(OH)_2O)_3\text{-}Al^-(OH)_2\text{-}ONa$

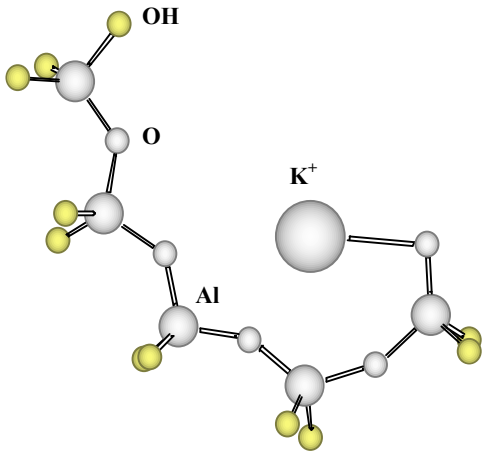

d. Molecular structure of $(OH)_3Al^-\text{-}(Al^-(OH)_2O)_3\text{-}Al^-(OH)_2\text{-}OK$

Fig.3 Optimized molecular structure of the remaining broken ring after dissolution

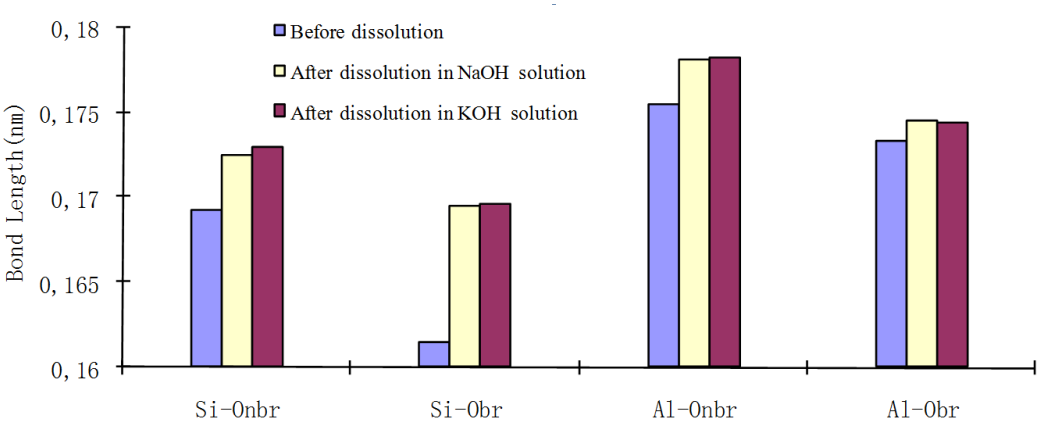

Fig.4 Bond length change of single 6-membered rings models before and after dissolution in strongly alkaline solution

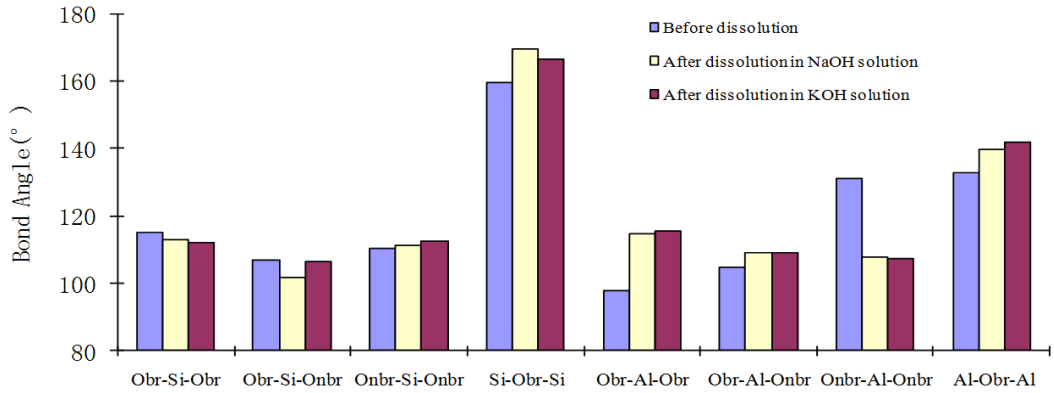

Fig.5 Bond angle change of single 6-membered rings models before and after dissolution in strongly alkaline solution

Table 1 Reaction heat of single 6-membered rings in strongly alkaline solution (KJ/mol)

ΔE1	ΔE2	ΔE3	ΔE4	ΔE5	ΔE6	ΔE7	ΔE8
-60.89	12.79	-227.43	-156.30	-1292.28	-1066.31	-1342.31	-1059.24

From table 1, it can be seen that alkaline environment significantly accelerate the dissolution process of single 6-membered ring models with much higher exothermal energies than neutral water environment ((ΔE=77.43KJ/mol). It is also found that dissolution in NaOH exhibit higher heat releasing than that in KOH (|ΔE1|>-ΔE2, |ΔE3|>|ΔE4|, |ΔE5|>|ΔE6|, |ΔE7|>|ΔE8|), which means that NaOH favors the dissolution of MK. This result has been verified by our experimental results.

As can be seen from comparison of Eqs.(1) and Eqs.(2), both of them include the releasing of $HOT_3^{\equiv}$ anion, and ion-pairing reaction between $HOT_3^{\equiv}$ anion and M^+ cation. The only difference between Eqs.(1) and Eqs.(2) is that ion-pairing reaction in Eqs.(1) is between $HOSiO_3^{\equiv}$ anion and Na^+ cation, while ion-pairing reaction in Eqs.(2) is between $HOSiO_3^{\equiv}$ anion and K^+ cation. Therefore, |ΔE1|>-ΔE2 indicates that ion-pairing reaction between $HOSiO_3^{\equiv}$ anion and Na^+ cation is stronger than that between $HOSiO_3^{\equiv}$ anion and K^+ cation. Similarly, |ΔE1|<|ΔE5|, -ΔE2<|ΔE6| also show Na^+ has stronger ion-pairing capacity with $HOAl^-O_3^{\equiv}$ than K^+. By using MAS-NMR techniques, McCormick et. al [22-24] and Swaddle et. al [25] also found that alkali metal cation of smaller size favor ion-pairing reaction with silicate monomer species in alkaline solution, which is consistent with our calculated result.

$|\Delta E1|<|\Delta E5|$, $-\Delta E2<|\Delta E6|$ show ion-pairing reaction between $HOAl^{-}O_3^{\equiv}$ and M^+ is stronger than that between $HOSiO_3^{\equiv}$ and M^+ in the same strongly alkaline solution.

The difference in reaction energy between $|\Delta E7|$ and $|\Delta E8|$ is 283.07 KJ/mol, which is the sum of 225.97 KJ/mol ($|\Delta E5|-|\Delta E6|$) and 57.10 KJ/mol ($|\Delta E7|-|\Delta E5|$)-($|\Delta E8|-|\Delta E6|$). In other words, 20.20% of the difference in the dissolution energy for T(Al) center dissolved in NaOH and KOH solution is contributed by stronger ion-pairing reaction, while 79.80% comes from further interaction between the remaining broken ring clusters and alkaline solution.

For single 6-membered AlO_4 tetrahedral ring model, the further interaction energy between the remaining broken ring clusters and NaOH ($|\Delta E7|-|\Delta E5|$=50.03 KJ/mol) is less than that between the remaining broken ring clusters and KOH ($|\Delta E8|-|\Delta E6|$=-7.07 KJ/mol). For single 6-membered SiO_4 tetrahedral ring model, the similar trends is also shown ($|\Delta E3|-|\Delta E1|$=166.54 KJ/mol, $|\Delta E4|-|\Delta E2|$=143.51 KJ/mol). This means that both Na^+ and K^+ can stabilize the remaining broken ring clusters with K^+ being slightly better.

4. Reorientation pathways of ion clusters

4.1 Reorientation pathways

In this study the reorientation reaction among two or three ion clusters $HOT(OM)_3$ (T represents Al^- or Si, M represents Na or K) was taken as an example to investigate the possible reorientation pathways and the structural configuration of the reorientation products. From the thermodynamic point of view, three types of reorientation pathways can possibly take part in the reorientation process of two ion clusters as modeled in equations (9) to (11). The Lowenstein aluminum avoidance principle sates that, whenever two tetrahedral are linked by one oxygen bridge, only one can be occupied by Al and there can hence be no Al-O-Al bridges [26]. Therefore, the reaction described in equation (11) impossibly proceeds, i.e., only equations (9) and (10) pathways can possibly take place for two ion clusters reorientation. Similarly, four possible pathways for three ion clusters reorientation as shown in equations (12) to (15). The corresponding energy-optimized geometries of the various reorientation clusters are also depicted in Fig. 6.

1) Two ion clusters reorientation:

$HO\text{-}Si(OM)_3+HO\text{-}Si(OM)_3 \Rightarrow OH\text{-}Si(OM)_2\text{-}O\text{-}Si(OM)_3+MOH.$ $\Delta E1\ldots\ldots(9)$

$HO\text{-}Si(OM)_3+HO\text{-}Al^{-}(OM)_3 \Rightarrow OH\text{-}Si(OM)_2\text{-}O\text{-}Al^{-}(OM)_3+MOH.$ $\Delta E2\ldots\ldots(10)$

$HO\text{-}Al^{-}(OM)_3+HO\text{-}Al^{-}(OM)_3 \Rightarrow OH\text{-}Al^{-}(OM)_2\text{-}O\text{-}Al^{-}(OM)_3+MOH.$ $\Delta E3\ldots\ldots(11)$

2) Three ion clusters reorientation:

$3HO\text{-}Si(OM)_3 \Rightarrow OH\text{-}Si(OM)_2\text{-}O\text{-}Si(OM)_2\text{-}O\text{-}Si(OM)_3+2MOH.$ $\Delta E4\ldots\ldots(12)$

$2HO\text{-}Si(OM)_3+HO\text{-}Al^{-}(OM)_3 \Rightarrow OH\text{-}Al^{-}(OM)_2\text{-}O\text{-}Si(OM)_2\text{-}O\text{-}Si(OM)_3+2MOH.$ $\Delta E5\ldots\ldots(13)$

$HO\text{-}Si(OM)_3+2HO\text{-}Al^{-}(OM)_3 \Rightarrow OH\text{-}Al^{-}(OM)_2\text{-}O\text{-}Si(OM)_2\text{-}O\text{-}Al^{-}(OM)_3+2MOH.$ $\Delta E6\ldots\ldots(14)$

$2HO\text{-}Si(OM)_3+HO\text{-}Al^{-}(OM)_3 \Rightarrow OH\text{-}Si(OM)_2\text{-}O\text{-}Al^{-}(OM)_2\text{-}O\text{-}Si(OM)_3+2MOH.$ $\Delta E7\ldots\ldots(15)$

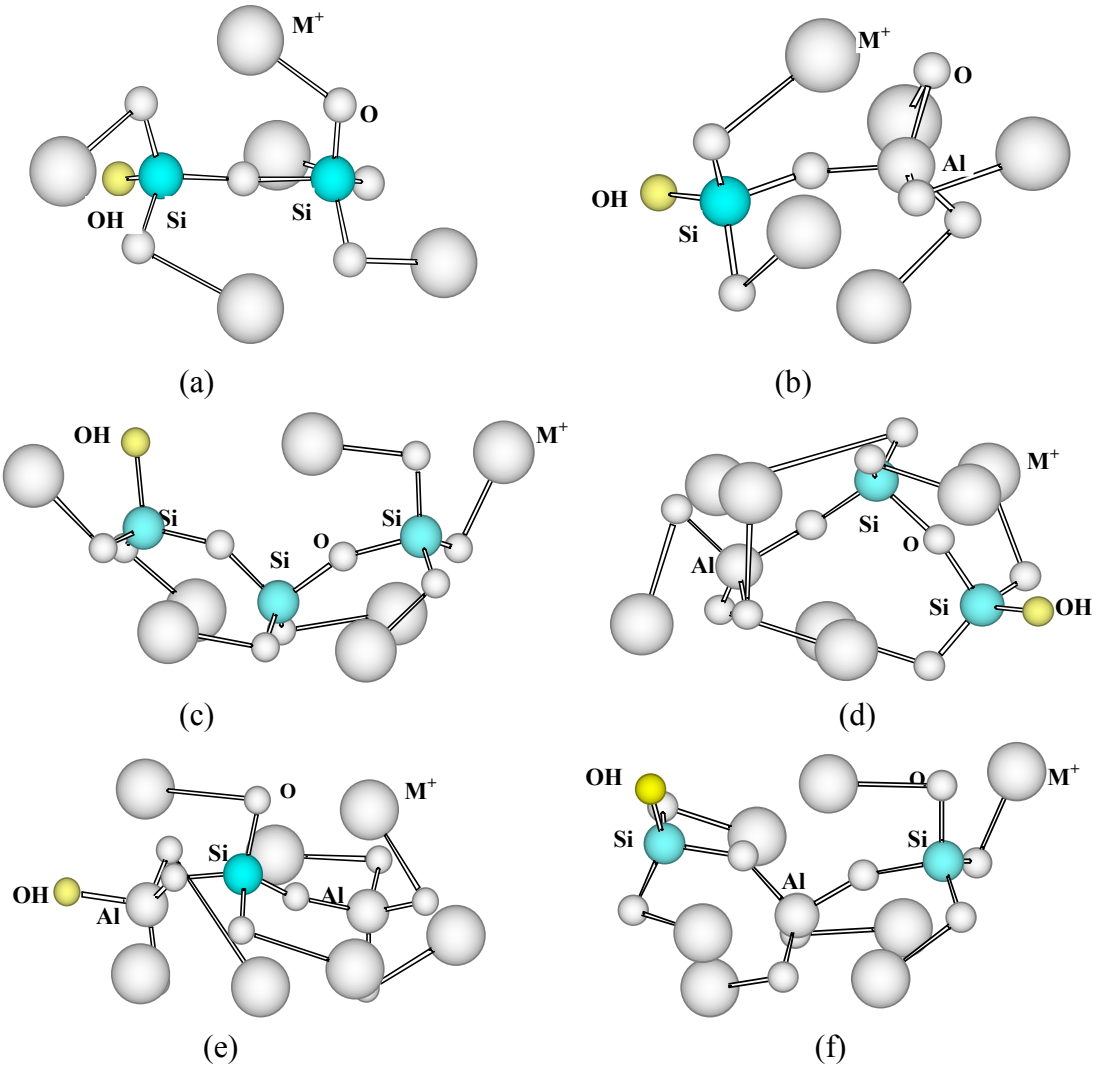

Fig. 6. Energy-optimised geometries of various reorientation clusters: (a) Si-Si reorientation; (b) Si-Al reorientation; (c) Si-Si-Si reorientation; (d) Al-Si-Si reorientation; (e) Al-Si-Al reorientation; (f) Si-Al-Si reorientation

4.2 Reaction energies of various Reorientation pathways

The reaction energies of all the possible orientation pathways (equations (9), (10), (12) to (15)) are calculated using Semi-empirical AM1 restricted Hatree–Fock method. The values are listed in Table 2.

As can be seen from Table 2, in NaOH solution the reaction energy of the hybrid reorientation reaction between $HOAl^{-}(OM)_3$ and $HOSi(OM)_3$ was lower than that of the homologue reorientation pathways between $HOSi(OM)_3$ and $HOSi(OM)_3$ apart from $\Delta E14_{(Na)}$ ($\Delta E10_{Na}<\Delta E9_{Na}$, $\Delta E13_{Na}<\Delta E12_{Na}$, $\Delta E15_{Na}<\Delta E12_{Na}$). This indicates that Si-Al hybrid reorientation process should theoretically be the easiest one among all the possible process and be the primary reorientation pathway. As a result, the Si-Al hybrid configuration should be the predominant molecular structure of the reorientation clusters. It is worth noting that Al-Si-Si reorientation reaction ($\Delta E135_{(Na)}$=-47.499 kJ/mol) exhibits the lowest reaction energy in all reorientation pathways of three ion clusters in NaOH solution, which implies that Al-Si-Si reorientation reaction should be primary reorientation pathways. In KOH solution, Si-Al homologue reorientation also exhibits lower reaction energies than Si-Si hybrid reorientation apart from $\Delta E10_K$ and $\Delta E14_K$ ($\Delta E10_K<\Delta E9_K$, $\Delta E15_K<\Delta E12_K$). This indicates that Si-Al homologue reorientation process should theoretically be primary reorientation pathway in KOH solution. It is important to point out that equation (14)

reaction energy ($\Delta E14$) was positive in various alkaline solutions ($\Delta E14_{Na}$=17.149 kcal/mol, $\Delta E14_K$=23.742 kcal/mol), which implies that the Al-Si-Al reorientation reaction should not occur spontaneously without an exterior heat resource. In addition, it was observed that the reorientation reaction energies in NaOH solution were lower than those in KOH solution ($E9_{Na}<\Delta E9_K$, $E10_{Na}<\Delta E10_K$, $E12_{Na}<\Delta E12_K$, $E13_{Na}<\Delta E13_K$, $E14_{Na}<\Delta E14_K$, $E15_{Na}<\Delta E15_K$), This suggests that the reorientation reaction is easier and stronger in NaOH solution than in KOH solution.

Table 2 Reaction energies of various reorientation pathways

$\Delta E9_{Na}$	$\Delta E9_K$	$\Delta E10_{Na}$	$\Delta E10_K$	$\Delta E12_{Na}$	$\Delta E12_K$	$\Delta E13_{Na}$	$\Delta E13_K$	$\Delta E14_{Na}$	$\Delta E14_K$	$\Delta E15_{Na}$	$\Delta E15_K$
-60.541	-19.634	-60.895	-13.435	-30.217	-26.630	-47.499	-31.988	17.149	23.742	-36.217	-27.220

5. Polycondensation process

Polycondensation pathways

In this paper polycondensation reaction among five ion clusters $(HO)_3SiOM$ is taken for example to investigate the possible polycondensation pathways and the structural configuration of the resultant products. From the thermodynamic point of view, only three types of polycondensation pathways possibly take place in the polycondensation proces: (1) Chain polycondensation; (2) Sheet polycondensation; (3) Framework polycondensation, as are modeled in Eq. (16) to Eq. (18). The corresponding energy-optimized geometries of the various polycondensation clusters are also depicted in Fig.7

(1) Chain $5(HO)_3SiOM \Rightarrow MO\text{-}Si(OH)_2\text{-}(OSi(OH)_2)_3\text{-}O\text{-}Si(OH)_3+4MOH$. $\Delta E1\ldots(16)$

(2)Sheet $5(HO)_2Si(OM)_2 \Rightarrow (O(OH)Si\text{-}(OM))_5+5MOH$. $\Delta E2\ldots(17)$

(3) Framework $5(HO)Si(OM)_3 \Rightarrow ((MO)_3Si)_2O_2SiO_2(Si(OM))_3)_2+3MOH+H_2O$. $\Delta E3\ldots(18)$

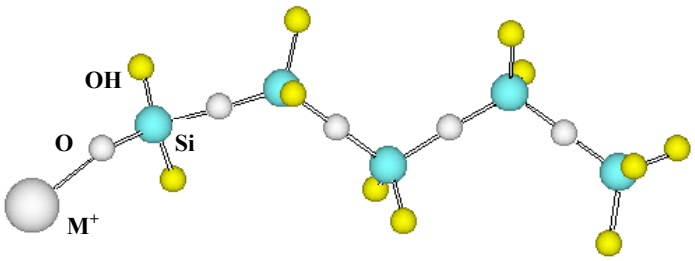

a. Chain

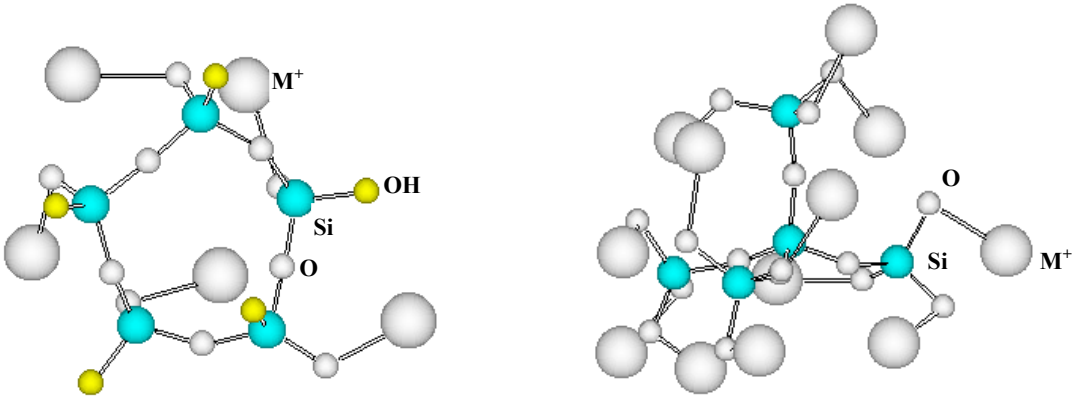

b. Sheet c. Framework

Fig.7 Energy-optimized geometries of three types of polycondensation clusters

5.2 Reaction energies of various polycondensation pathways

Semi-empirical AM1 restricted Hatree-Fock calculations are conducted on all the possible polycondensation pathways, as shown in Eq. (16) to Eq. (18). The calculated reaction energies for various pathways are listed in table 3.

Table 3 Reaction energies of various polycondensation pathways

$\Delta E16_{Na}$	$\Delta E16_{K}$	$\Delta E17_{Na}$	$\Delta E17_{K}$	$\Delta E18_{Na}$	$\Delta E18_{K}$
72.20467	81.29332	-11.2528	-12.3821	-60.0110	-22.1364

As can be seen from table 3, reaction energy of framework polycondensation reaction is lower than that of the other two types of polycondensation pathways in the same alkaline solution ($\Delta E18_{(K)} < \Delta E17_{(K)} << \Delta E16_{(K)}$, $\Delta E18_{(Na)} < \Delta E17_{(Na)} << \Delta E16_{(Na)}$). This indicates that framework polycondensation process should theoretically be the easiest one amongst all the possible process and be the primary polycondensation pathway. As a result, the framework structural products should be the predominant molecular structure in the resultant geopolymeric products. It is also observed that sheet polycondensation reaction energy ($\Delta E17$) is negative values in various alkaline solution ($\Delta E17_{(Na)}$= -11.2528kcal/mol, $\Delta E17_{(K)}$ =-12.3821kcal/mol), which implies that sheet polycondensation reaction can also take place spontaneously without exterior heat resource. Therefore, it is possible for sheet structural products to exist in the resultant geopolymeric products in theory. It is worth nothing that the chain polycondensation reaction is of endothermic reaction with $\Delta E>0$, indicating that the chain reaction can not undergo spontaneously without exterior heat resource.

In addition, it is observed that the framework polycondensation reaction energies in NaOH solution is lower than that in KOH ($E18_{(Na)} < \Delta E18_{(K)}$), while the opposite one is found for sheet polycondensation ($E17_{(Na)} > \Delta E17_{(K)}$). This suggests that the geopolymeric products synthesized in KOH solution contains more sheet molecular structure than NaOH solution.

6. Conclusion

Semi-empirical AM1 calculations have been conducted on optimized geometries of 6-membered AlO_4 and SiO_4 tetrahedral ring models in order to better understand the formation process of Metakaolin in alkaline solutions. Based on the calculated results, the following conclusions can be drawn:

(1) Dissolution process of geopolymer consists of ring breakage for releasing $HOTO_3^{\equiv}$ anion, formation of $HO\text{-}T(OM)_3$ by ion-pairing reaction between $HOTO_3^{\equiv}$ anion and M^+ cation, and further interaction between the remaining broken ring cluster and MOH solutions. A contracting inwards is observed when single 6-membered SiO_4 tetrahedron ring model subjected to strong alkaline action, while a moving outwards trend is found in single 6-membered AlO_4 tetrahedron ring model. 6-membered rings model of AlO_4 tetrahedron compared with 6-membered rings model of SiO_4 tetrahedron is more reactive and is easily broken to release $HOTO_3^{\equiv}$ anion in alkaline environment. Na^+ cation show stronger ring breakage and ion-pairing interaction than K^+ cation. The further reaction between the remaining broken ring cluster and strongly alkaline solution depended on the types of the remaining broken ring cluster and alkaline solution. KOH has slightly better in stabilizing the remaining broken ring clusters than NaOH. Therefore, NaOH solution compared with KOH is expected to give a higher dissolution extent of metakaolin and a faster formation of geopolymeric products.

(2) Si-Al hybrid reorientation should be primary reorientation pathway of Geopolymer made with NaOH or KOH activated metakaolin. NaOH solution had stronger capability in reorientation reaction than KOH solution.

(3) Framework clusters may be primary polycondensation products of Geopolymer made with NaOH or KOH activated metakaolin. It was also possible to the existence of sheet polycondensation clusters, the amount of which depended on the types of alkaline solution

Acknowledgements

Authors gratefully acknowledge the financial support from key projects in the national science & technology pillar program during the eleventh five-year plan period (2006BAJ04A10), 973 Program (2009CB623200), Program for New Century Excellent Talents in University(NCET-08-0116)

References

[1] J. Davidovits: J. Therm. Anal. Vol 35 (1989), p. 429-441.
[2] J. Davidovits, in: *Proceedings of the First European Conference on Soft Mineralog*, edtied by J. Davidovits and J. Orlinsl,Vol.1, The Geopolymer Institute, France, Compiegne, (1988), p. 25-48.
[3] J. Davidovits, in: *Ceramic Transactions, Cement-based materials: present, future, and environmental aspects*, edited by M. Moukwa, S.L. Sarkar, K. Luke and M.W. Grutzeck, American Ceramic Society, America, (1993), p. 165-182.
[4] R. Nowak: The New Sci. Vol 197 (2008), p.28-29
[5] J. Davidovits, C. D. Comrie, J.H. Paterson and D.J. Ritcey: Concr. Int. Des. & Constr. Vol 12 (1990), p.30-40.
[6] J.G.S. Van Jaarsveld, J.S.J. Van Deventer: Miner. Eng. Vol 10 (1997), p.659-669.
[7] R.E. Lyon, A. P.N. Foden, Balaguru, M. Davidovits, J. Davidovits: J. Fire Mater. Vol 21 (1997), p.67-73.
[8] A. Palomo, M.T. Blanco-Varela, M.L. Granizo: Cem. Concr. Res. Vol 29 (1999), p.997-1004.
[9] M. Sofi, J.S.J. van Deventer, P.A. Mendis: Cem. Concr. Res. Vol 37 (2007), p.251-257
[10] W. Hongling, L. Haihong and Y. Fengyuan: Coll. Surf. A Vol 268 (2005), p.1-6
[11] J.G.S. Van Jaarsveld, J.S.J. Van Deventer and A. Schwartzman: Miner. Eng. Vol 12 (1999), p. 75-91.
[12] J. Davidovits: Concr. Int. Vol 16 (1994), p.53-58.
[13] J.G.S. Van Jaarsveld, J.S.J. Van Deventer, L. Lorenzen: Metall. Mater. Trans. B Vol 29 (1998), p. 283-291.
[14] X. Hua, J.S.J. Van Deventer: Int. J. Miner. Process Vol 59 (2000), p.247-266.
[15] J. Davidovits, in: *Concrete technology, past, present, and future*, edited by P.K. Mehta, American Concrete Institute, Detroit, (1994), p. 383-397.
[16] A. Palomo, M.W. Grutzeck, M.T. Blanco: Cem. Concr. Res. Vol 29 (1999), p.1323-1329.
[17] J. Davidovits, in: *Proceedings of Geopolymere '99*, edited by J. Davidovits, Saint-Quentin, France, (1994), p. 83-96.
[18] Z. Yunsheng, S. Wei, L. Zongjin: J. Mater. Sci. Vol 42 (2007), p.3015-3023.
[19] Z. Yunsheng, J Yatao, S. Wei, L. Zongjin: Cem. Concr. Res. Vol 39 (2009), p.1174-1179.
[20] Z. Yunsheng, S. Wei, L. Zongjin: Adv. Cem. Res. Vol 21 (2009), p.67-73
[21] F.Liebau: *Structural Chemistry of Silicates：Structure, Bonding Formation and Classification*. (Springer, Berlin 1985).
[22] A.V. McComick, A.T. Bell, C.J. Raddke: J. Phys. Chem. Vol 93(1989), p.1733-1737
[23] A.V. McComick, A.T. Bell, C.J. Raddke: J. Phys. Chem. Vol 93(1989), p.1737-1741
[24] A.V. McComick, A.T. Bell, C.J. Raddke: J. Phys. Chem. Vol 93(1989), p.1747-1744.
[25] T.W. Swaddle, J. Salerno, P.A. Tregloan: Chem. Soc. Rev. Vol 23 (1994), p.319-325.
[26] W. Loewenstein: Amer. Miner. Vol 39 (1954), p.92-96.

doi:10.4028/www.scientific.net/AST.69.51

Understanding Study of Silicate based Gel formed during the Setting Ceramic Materials

Monique Tohoué Tognonvi[1,a], Sylvie Rossignol[1,b], Jean-Pierre Bonnet[1,c]

[1]GEMH-ENSCI, 47-73 Avenue Albert Thomas, 87065 Limoges, France

[a]tohoue.tognonvi@etu.unilim.fr, [b]sylvie.rossignol@unilim.fr,

[c]jean-pierre_bonnet@orange.fr

Keywords: concentrated sodium silicate solution, gelation in an alkaline medium, soluble and insoluble solid, dissolution/precipitation.

Abstract. Consolidation of cementitious and geopolymeric materials involves silicate-based gel formation. This in situ mechanism is difficult to identify because it occurs in a complex and developing system representing only a minority phase. A study based on the behaviour of acidified sodium silicate solutions in alkaline medium, was therefore initiated in order to define the conditions of irreversible setting. A concentrated sodium silicate solution ([Si]=7 mol/l, pH=11.56, Si/Na=1.71) was used as starting solution. ^{29}Si NMR spectroscopy, SAXS and elementary chemical analyses (ICP-AES) were used to characterize the various solutions.

Acidification of initial solution, leads in a range of relatively low pH and silicon concentration to various gels formation: (i) reversible transparent gels made up of aggregates of particles ($Si_7O_{18}H_4Na_4$) and which do not change over time, (ii) soluble white gels that lead to gradual formation of a soluble solid consisting of colloid composition of $NaSi_{1.87}O_{4.24}$, (iii) “irreversible” gels which provide a syneresis phenomenon leading to formation of a strongly consolidated solid made up of soluble phase rich in sodium similar to white gels ($NaSi_{1.87}O_{4.24}$) and an insoluble phase type silica of composition $NaSi_{12.66}O_{25.82}$.

Introduction

Concretes are composite materials obtained from a mixture of mineral binder, granular and water. The most commonly used binder is the cement which is a hydraulic binder (consolidation also occurs in water). The presence of water in the system causes first the partial dissolution of phases and then the "precipitation" of hydrates. These silicon-rich hydrates form a gel that would consolidate the materials. The gel is made up of solid particles with a composition of $(CaO)_x(SiO_2)(H_2O)_y$ where the values of x and y depend on the calcium and silicate content in the aqueous phase [1]. The attack of siliceous products (amorphous silica) or silico-aluminate (metakaolin) by alkaline lime-rich solutions leads also to the formation of these CSH gels. This reaction called pozzolanic reaction is now widely used as a substitute for the use of Portland clinker.

During last few years, new mineral binders, in particular geopolymers, generate great interest [2,3]. These materials are the result of the attack of siliceous products or silico-aluminate powders (metakaolin, fly ash, ...) by strongly alkaline solutions (KOH, NaOH, ...) at temperatures close to room temperature.

These binders have in common, the formation of a silicate-based gel. The formation mechanism is hard to identify because it occurs in-situ in a complex and evolving system in which it constitutes only a minor phase. To avoid this difficulty, the aim of this work is based on relation between composition of the liquid and the nature of the formed gels was carried out on alkali silicate solutions in a basic medium.

Experimental part

A concentrated sodium silicate solution from VWR Prolabo was used as starting solution. Its chemical composition determined by emission spectrometry (ICP-AES) is $3.41SiO_2.Na_2O.21H_2O$ ([Si] = 7.01 mol/l, Si/Na = 1.71, density = 1.32 and pH = 11.56). Dilute hydrochloric acid solutions ($0.5 < [H^+] < 2$ mol/l) were also used. These solutions are prepared from a commercial solution (Norma Prolabo) with 37 wt% by adding distilled water.

Gels were obtained by gradual addition of hydrochloric acid into the sodium silicate solution ($0.2 <$ [Si] < 6 mol/l and $9 <$ pH < 11.20) under magnetic stirring at room temperature (Fig. 1). The point of gelation was taken as the earliest moment at which the gel broke away from the wall instead of flowing as a liquid when the beaker was tilted [4,5].

During ripening of gels, a liquid phase and a solid appear. The liquid was separated carefully from the solid one to avoid any solid residue passing in the liquid. The liquid and the solid were both characterized by various technical methods. Some of final products that are stable in water were washed with distilled water several times until no reaction for Cl^- in the washing water with respect to Ag^+ was observed. And finally, they were rinsed and dried at 70 or 110°C. Drying step included also soluble samples that cannot be washed.

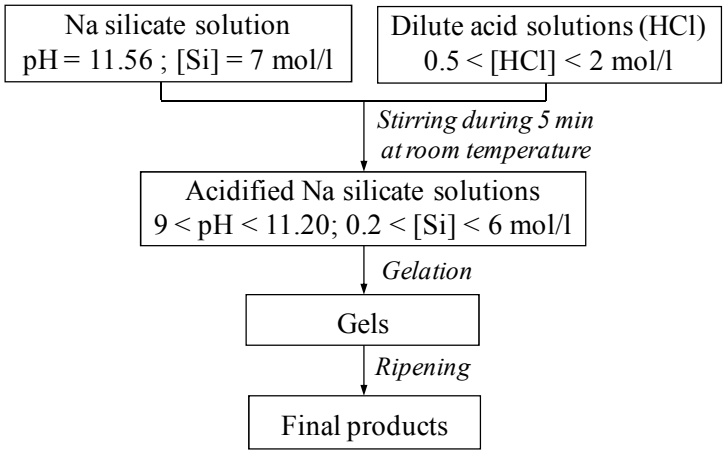

Fig. 1: Experimental protocol of gels formation

Characterization techniques

Composition of Na and Si elements available in the solid phase and in the supernatant were determined by means of elementary analysis. Measurements were carried out with a Thermo Jarrell Ash Corporation IRIS spectrometer (ICP-AES).

The surface area of the xerogels was determined by nitrogen adsorption–desorption isotherms after dehydration at 200°C for 2 hours. A mass of around 11 mg of xerogels was used for the experiment. The measurements were carried out in a Micromeritics Flow Sorb II 2300.

Results

i) Gelation process

The acidification of a sodium silicate solution by hydrochloric acid solution leads to various gels according to silicon concentration and pH value (Fig. 2). Three types of gels can be obtained: (i) transparent reversible gels (gels B) are obtained for [Si] > 4.14 mol/l and $11 <$ pH < 11.2, (ii) white soluble gels (gels C) can be observed for $4.14 \leq$ [Si] < 2.9 mol/l and $10.67 <$ pH < 11 and (iii) irreversible gels (gels D) are obtained for [Si] ≤ 2.9 and pH < 10.75. Gelation time was studied as a function of silicon concentration and pH value. One can observe that for all gels, gelation time increases when pH value increases and silicon concentration decreases. For gels B, gelation time increases slightly and is too long (t > 4 days). The increase of gelation time with pH value would be related to the increase of silica solubility when the pH increases [5]. Actually, when the pH increases, there would be competition between gelation and dissolution of particles, gelation

process would prevail but would be slowed by the dissolution hence the long gelation time. We can observe presence of both gels C and D at pH 10.67 and 10.75, consequently, these two types of gels would have similar behavior. Transparent reversible gel (gel B) has a single behavior.

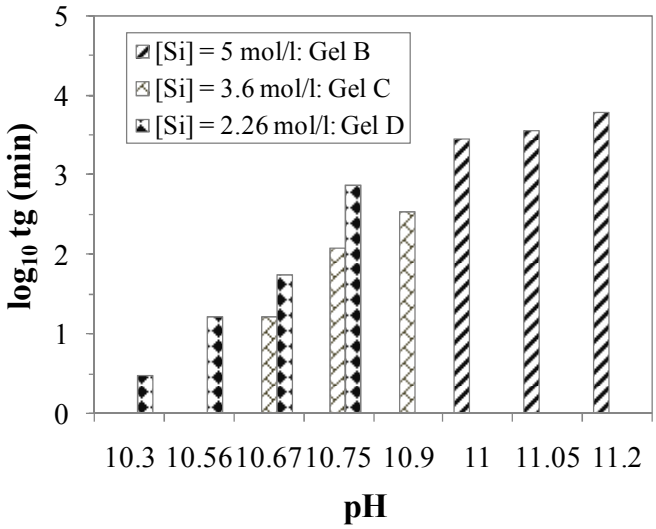

Fig. 2: Gelation time versus pH value and silicon concentration

ii) Ripening

Evolution of gels was followed during ripening at room temperature (Fig. 3). Gels B, appear at room temperature after a relatively long time (≥ 4 days). They do not show any detectable change with time (Fig. 3a). However, they are destroyed by the increase in temperature, by mechanical stirring and are entirely dissolved in water. They are reversible.

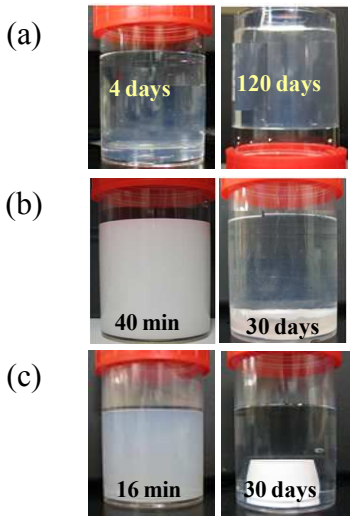

Fig. 3: Photography of various gels showing their evolution during ripening at room temperature: (a) a transparent reversible gel, (b) a soluble white gel and (c) an "irreversible" gel.

Ripening of white soluble gels leads to slow formation of a white solid that tends to retract gradually with time with an anisotropic effect. A supernatant can be detectable 30 minutes after gelation. Fig. 3b shows changes observed during ripening of a gel C obtained from a solution of silicon concentration equal to 3 mol/l and pH 10.67. This change is quite representative of that observed in all solutions where gel C appears. A low consolidated solid which is soluble in water can be obtained at the end of ripening. Consequently, the final solid could be constituted of lowly linked grains.

Evolution of volumic fraction of solid phase was followed during ripening as a function of pH value and silicon concentration of the initial mixture (Fig. 4). At constant pH value (pH 10.90) (Fig. 4a), correlation between the volumic fraction at the end of the process and the silicon content of the solution before gelation is obvious. Actually, the available silicon content in the system before gelation, increases with $(V_T-V_{sur})/V_T$. Decrease in volumic fraction of the final solid when silicon concentration decreases is in accordance with the silicon content of the initial solution. When silicon concentration decreases, solution becomes poor in silica. For constant silicon concentration ([Si] = 3.6 mol/l) (Fig. 4b), increase of pH leads to decrease of $(V_T-V_{sur})/V_T$ at the end of ripening. This observation could be explained by increase of silica solubility with pH. When pH increases, as silica solubility increases, the solid amount could decrease [5]. This is in agreement with the increase of the silicon content in the liquid phase when pH increases (Table 1).

Table 1: Evolution during ripening of the concentration of Si and Na in the supernatant for two systems of initial concentration: a) [Si] = 3.6 mol/l and [Na] = 2.11 mol/l at pH 10.90 and 10.75.

	Ripening time (days)	2	9	90
pH = 10.90	$[Si]_{sur}$ (mol/l)	2.15	2.48	2.49
	$[Na]_{sur}$ (mol/l)	1.31	1.51	1.52
	$(Si/Na)_{sur}$	1.64	1.64	1.63
pH = 10.75	$[Si]_{sur}$ (mol/l)	1.67	2.30	2.31
	$[Na]_{sur}$ (mol/l)	1.04	1.43	1.43
	$(Si/Na)_{sur}$	1.61	1.61	1.62

Composition of the solid skeleton was determined. The $(Si/Na)_S$ atomic ratio of solid skeleton obtained for [Si] = 3.6 and 4.14 mol/l (pH 10.75) is equal to 1.80, 1.88 and 1.87 at respectively 2, 9 and 90 days after ripening. Whatever the initial composition, the $(Si/Na)_S$ atomic ratio tends to increase slightly during ripening. It is interesting to mention that the values related to the end of ripening are all close to 1.87. The atomic ratio of the whole systems obtained from gels C is 1.87 [6]. Consequently, composition of the solid would be $NaSi_{1.87}O_{4.24}$.

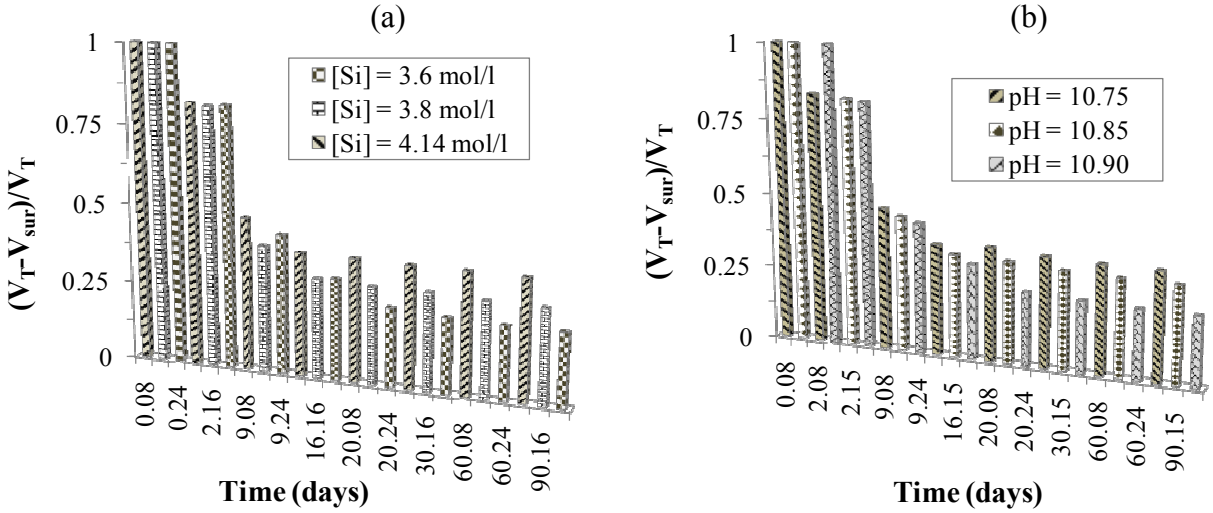

Fig. 4: Variation of the apparent volume of solid phase of gel C during ripening as a function of time for: (a) silicon concentration at pH = 10.90 and (b) pH value for [Si] = 3.6 mol/l.

After formation of "irreversible" gels, a syneresis phenomenon is always observed. This isotropic contraction of the gels D is followed by a clear liquid discharge. It is detectable several hours after the gel formation (about 1 hour for systems which gelation time is shorter and up to 4 days for

systems which gelation time is longer). Fig. 3c shows characteristics of evolution of behavior observed during this type of gel ripening.
Initial gel and solid resulting from syneresis, is not destroyed by the increase of temperature or by gradual dilution. At the end of syneresis, the obtained solid is monolithic, strongly consolidated and amorphous by XRD analysis [6].
Evolution during ripening of volumic fraction ($(V_T-V_{sur})/V_T$) of gels D, is shown in Fig. 5 for various silicon concentration and pH values. When syneresis is rapid and significant, it leads to a consolidated solid. The influence of silicon concentration on the kinetics of syneresis is extremely marked at constant pH value (Fig. 5a). The initial solutions most concentrated in silicon lead to the shortest gelation time and to the fastest syneresis. For [Si] = 1.76 and 2.26 mol/l, the behavior observed at 150 days after gelation can be considered as characteristic of the end of syneresis. It is also good to mention that volumic fraction occupied by the solid (gel + interstitial liquid) decreases when initial silicon concentration increases. This could be due to the slow-down of syneresis in dilute system, i.e. when silicon concentration decreases.

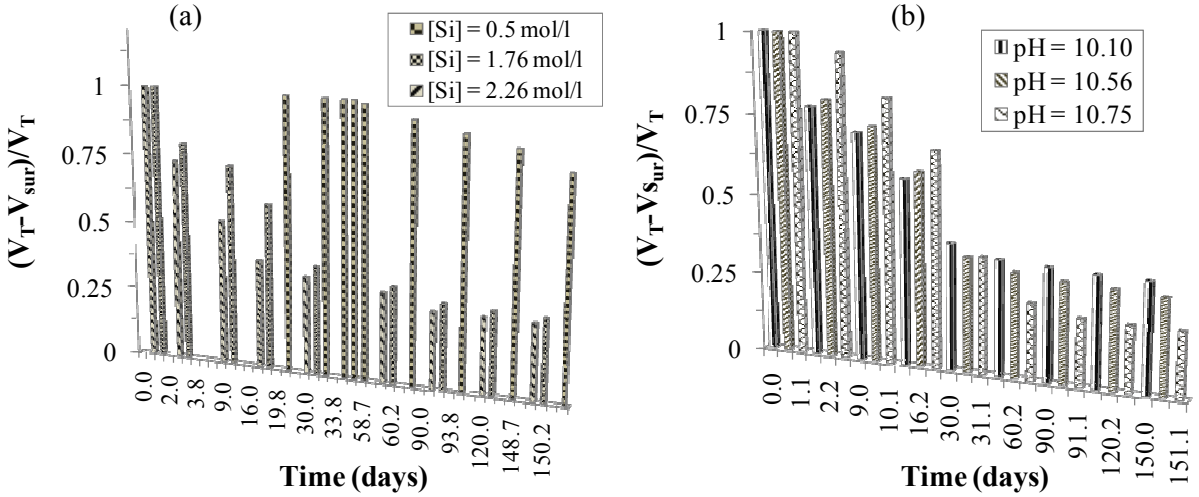

Fig. 5: Variation of the apparent volume of solid phase of gel D during ripening as a function of time for: (a) silicon concentration at pH = 10.56 and (b) pH value for [Si] = 1.76 mol/l.

At constant silicon concentration ([Si] =1.76 mol/l), the kinetics of syneresis is little pH-dependent even if it is longer for higher pH (Fig. 5b). When the pH decreases, the volumic fraction of solid, at the end of ripening process, increases. This observation can be attributed to the silica solubility at high pH [5] leading to increase of the silicon concentration in the supernatant (Table 2). Furthermore, these gels have the same behavior as a function of pH as gels C.

Table 2: Evolution during ripening of concentration of Si, and Na in the supernatant for two systems of initial concentration: a) [Si] = 1.76 mol/l and [Na] = 1.03 mol/l at pH 10.75 and 10.56.

	Ripening time (days)	2	9	150
pH =10.75	$[Si]_{liq}$ (mol/l)	1.03	1.04	1.07
	$[Na]_{liq}$ (mol/l)	0.80	0.80	0.83
	$(Si/Na)_{liq}$	1.29	1.29	1.29
pH =10.56	$[Si]_{liq}$ (mol/l)	0.88	0.89	0.90
	$[Na]_{liq}$ (mol/l)	0.82	0.82	0.83
	$(Si/Na)_{liq}$	1.07	1.08	1.08

Due to irreversibility of solids obtained from the ripening of gels D, they are washed with distilled water for several times in order to determine the composition of solid phase by ICP analysis. Each

sample has been washed for 70 times before analysis. Analysis of leach has shown presence of silicon and sodium elements [6]. These observations suggest that the consolidated solid obtained from ripening of gels D included two phases: a soluble phase which dissolves during washing step and an insoluble phase. Considering similarity of gels C and D, the soluble solid would be similar to that of gels C. The insoluble phases obtained from three systems of initial silicon concentration equal to 1.76, 2.26 and 2.81 mol/l were analysed. The $(Si/Na)_S$ atomic ration of these concentrations is respectively equal to 13.56, 12.46 and 11.91. The composition of washed products is very poor in sodium. These three solid provide a molar composition of $NaSi_{12.66}O_{25.82}$. This insoluble solid, under washing conditions, has a composition very close to silica.
Surface area of these washed solids by the BET method was respectively 291, 282 and 276 m^2/g. These results are very close to the values (~ 280 m^2/g) generally observed for xerogels of silica [7,8].

Summary

Acidification of sodium silicate solution with silicon and sodium concentrations, respectively, equal to 7 and 4.1 mol/l, leads to several situations in a range of relatively low pH and concentrations. For slightly lower silicon concentrations and pH value, a transparent gel made up of $Si_7O_{18}H_{4+n}Na_{4-n}$ aggregates is formed. For $10.67 < pH < 10.90$ and $2.9 < [Si] \leq 4.14$ mol/l, a soluble white gel appears which contracts gradually during ripening. The formed solid has a chemical composition consistent with the formula $NaSi_{1.87}O_{4.24}$. When the pH and [Si] become inferior, respectively to 10.75 and 3 mol/l, at least a part of formed gel is irreversible. It is not destroyed by adding water, raising temperature or mechanical stirring. These "irreversible" gels present a syneresis phenomenon during ripening leading to a strongly consolidated solid. The final solid included of two phases, one which is soluble in pure water could have $NaSi_{1.87}O_{4.24}$ as composition, and the other would be made up of nanometric particles of an insoluble product which composition has been estimated as $NaSi_{12.66}O_{25.82}$.

References

[1] H. Viallis-Terrisse, in: *Interaction des Silicates de Calcium Hydratés, principaux constituants du ciment, avec les chlorures d'alcalins. Analogie avec les argiles*. PhD thesis, University of Bourgogne, France, (2000).

[2] J. Davidovits and M.Davidovics, Patent n° EP 0 815 064 B1, vol. 1, (1996).

[3] J.W. Phair and J.S.J. Van Deventer: *Characterisation of fly ash-based Geopolymers activated with sodium aluminate*. Ind. Eng. Chem. Res. vol. 41 (2002), p. 4242.

[4] R.C. Merrill and R.W. Spencer: The Gelation of Sodium Silicate. Effect of Sulfuric Acid, Hydrochloric Acid, Ammonium Sulfate, and Sodium Aluminate. J. Phys. Chem. vol. 806 (1950), p. 806.

[5] R.K. Iler, in: *The Chemistry of Silica*, edited by John Wiley and Sons, New York (1979).

[6] M.T. Tognonvi, in: *Physico-chimie de la gélification du silicate de sodium en milieu basique.* PhD thesis, University of Limoges, France, (2009).

[7] B.P.W.J.G. Wijnen, T.P.M. Beelen, K.P.J. Rummens, H.C.P.L. Saeijs, R.A. Van Santen, Silica gel from water glass: a SAXS study of the formation and ageing of fractal aggregates. J. Appl. Cryst., vol. 24 (1991), p. 759.

[8] A.A. Christy: *Quantitative determination of surface area of silica gel particles by near infrared spectroscopy and chemometrics*. Colloids and Surfaces A: Physicochem. Eng. Aspects, vol. 322 (2008), p. 248.

doi:10.4028/www.scientific.net/AST.69.57

Use of sodium silicate gel as precursor of binder for cold consolidated materials

Monique Tohoué Tognonvi[1,a], Séka Simplice Kouassi[1,b], Toyotaka Maeda[2,c], Julien Soro[1,d], Sylvie Rossignol[1,e], Jean-Pierre Bonnet[1,f]

[1]GEMH-ENSCI, 47-73 Avenue Albert Thomas, 87065 Limoges, France

[2]Department of Material science and Engineering, Nagoya Institute of Technology, Showa, Nagoya, 466-8555, Japan

[a]tohoue.tognonvi@etu.unilim.fr, [b]seka-simplice.kouassi@etu.unilim.fr

[c]toyo0925@yahoo.co.jp, [d]julien.soro@unilim.fr,

[e]sylvie.rossignol@unilim.fr, [f]jean-pierre_bonnet@orange.fr

Keywords: concentrated sodium silicate solution, ternary diagram, dissolution/precipitation, consolidated materials and shrinkage.

Abstract. Consolidation of cements and geopolymers can be explained by the formation of alkali silicate or alumino-silicate gels formed in situ during materials setting. To control such a system, a study concerning the use of sodium silicate gel as binder was initiated to manufacture consolidated materials with different size distribution of silica. The gels used as precursor of binder were synthesised by acidifying with hydrochloric acid, a concentrated sodium silicate. Consolidated materials were obtained by mixing the previous solution before gelation with granular materials (fine silica powder and sands).

The existence domain of consolidated materials depends on the size distribution of sand. Consolidation of material is strong when the amount of silica is high. This result suggests a dissolution / precipitation reaction between gel and silica. Therefore, consolidation could be explained by the dissolution of small particles of silica and their precipitation into the grain boundary of sand. Mechanical properties are closed to those of cement materials.

Introduction

Sodium silicate solutions, also called water glass, are widely used in industry, for example as sealants, binders, deflocculant, emulsifiers and buffers in abrasive and casting industries. Those solutions are also used as reactant during formation of geoplymers [1,2]. The most commonly application is its use as inorganic binder [3]. Actually, sodium silicate binder is very successful, used for agglomeration processes that combine or consolidate fines or small particles into larger units [4,5]. Consolidation by sodium silicate solution is a physical-chemistry process where silicate reacts with particles surface. This dehydration by a drying or setting process involves bridges between particles. However, such a consolidation leads generally to the formation of water-soluble material for pH values above 11 at room temperature. In order to define conditions of irreversible gelation of sodium silicate solution, a study based on behavior of this solution was previously carried out in an alkaline medium [6]. Various types of gels were obtained: reversible transparent gels, white soluble gels and irreversible gels. Irreversible gels contract through a syneresis phenomenon and were stable in water. The aim of this study is to use characteristics of irreversible gels, which gelation time is equal to 55 min, to consolidate granular systems such as fine silica (D_{50} = 10μm) and large scale of size distribution of sand.

Experimental part

A concentrated sodium silicate solution ([Si] = 7.01 mol/l, Si/Na = 1.71, ρ = 1.32, pH = 11.56) from VWR Prolabo was used as starting solution. Dilute hydrochloric acid solution ($[H^+]$ = 0.5 mol/l) which was prepared from a commercial solution (Norma Prolabo) with 37 wt% by adding distilled water was also used.
Silica powder (ground sand C400, D_{50} = 10 µm) from SIFRACO was used. It is made up of 99.8 wt% in SiO_2. Three types of sand, S and F with 90 and 360 µm as average diameter of grains and standard sand, were used as granular systems. Sand S and F are provided by SIBELCO and are both made up of 99.6 wt% in SiO_2. Standard sand (Sd) is from SOCIETE NOUVELLE DU LITTORAL (EN 196-1) and is composed of grains size from 10 µm to 2 mm.
Materials were consolidated by an acidified sodium silicate solution with silicon concentration equal to 2.26 mol/l and pH value equal to 10.75. This acidified solution leads generally to irreversible gel formation. The mixture of acidified solution and silica is first realized and then sand was added according to the desired composition before gelation (Fig. 2). Fresh samples, after mixture, were placed into a sealed box and the humidity was maintained constant and was equal to 11.3 % with LiCl salt. Weight loss and shrinkage of materials were followed during drying process. Shrinkage was measured according to diameter and height of samples. Final materials after drying were characterized by three points bending tests. Consolidated materials are identified as $G_a s_x M_y$, where G, s and M are respectively gel, silica powder, sand of 90 µm (S), sand of 560 µm (F) and standard sand (Sd). a, x and y represent the mass composition of different compounds. As example $G_{33}s_{33}S_{33}$ is a consolidated material with 33 wt% in gel, silica and sand.

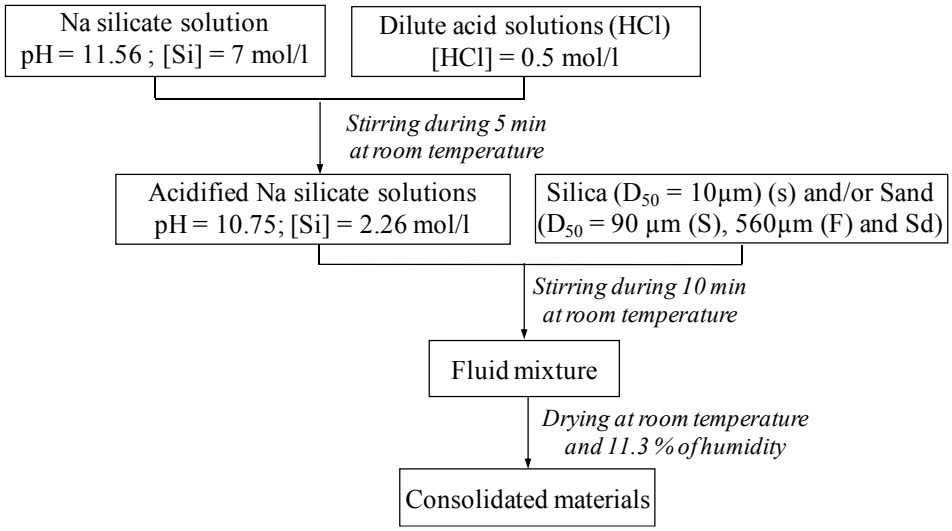

Fig 1: Experimental process of consolidated materials formation.

Mechanical properties were characterized using three points bending tests. Flexural stress of the samples was determined on parallelepiped specimens with respectively 40x40x160 mm^3 in size. Tests were performed using an apparatus JJ LLOYD (Ref. EZ20) material testing machine in a three-point flexural bending configuration at room temperature. Strain rate used for the bending experiments was 0.1 $mm.min^{-1}$.

Results

i) Effect of sand size distribution on consolidated materials

In order to determine the existence domain of consolidated materials, three types of silica with different size were used: a fine silica powder (D_{50} = 10 µm), two sands S and F constituted of particles of 90 and 560 µm as average diameter respectively. The various consolidated materials

obtained were gathered on the s-G-S/F ternary (Fig. 2). The possibility to obtain consolidated materials is very restricted. In presence of high amount of solution, samples display a flocculation of granular involving an heterogeneous samples. In the same way, in presence of low amount of acidified solution, the liquid is not able to completely soak granular involving the non feasibility of samples. The same phenomenon appears to the binary system. However, materials obtained in the binary gel-silica show a strong consolidation suggesting a possible reaction between SiO_2 particles and acidified silicate solution during the setting [7,8,9]. Actually, the choice of this solution is due to its gelation time which is adequate to realize the mixture (gelation time of 55 min) and thus sufficient to provoke reaction between silicate species in solution and silica particles. Then the process of syneresis can be undergone. Consequently, these materials (gel-silica mixture) present also a strong shrinkage due to the absorbent power of fine silica and to the syneresis phenomenon. As a result, fine silica-based materials can only be obtained for silica content ranges from 50 to 60 wt%. Materials obtained in the binary gel-sand present poor consolidation and very low shrinkage. This suggests that there is very low reaction between acidified solution and grains of sand due to the low reactivity surface of these large grains. In function of this remark, the mixture of the three materials (gel-silica-sand) displays range depending on the size distribution of sand. We can observe a shift of this domain towards high particle size of sand in relation to reactive surface accessible by the solution. One can also mention that the existence domain decreases when the particles of sand increases. Indeed, the domain of sand S with particles size equal to 90 µm is large than that of sand F which particles size is 560 µm.

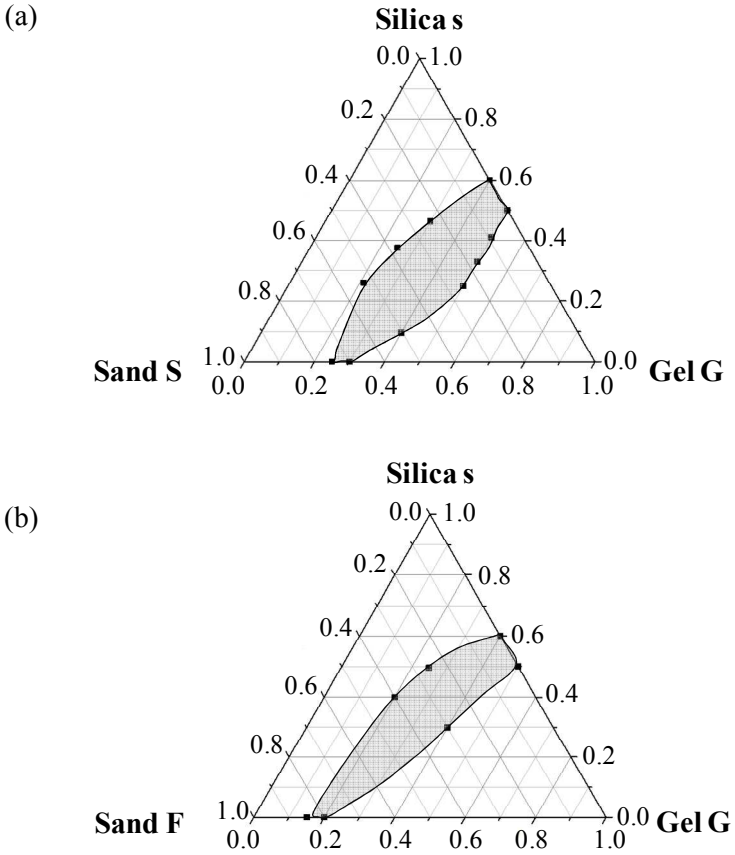

Fig. 2: Ternary diagram of consolidated materials formation with sand of: (a) 90 µm and (b) 560 µm.

To follow the ageing of samples, we proceed to gravimetric monitoring in terms of time. Weight loss values of consolidated materials were given as a function of y/(x+y) mass ratio (where x and y are silica and sand contents respectively) and gel content during drying at room temperature (11.3 % of humidity) (Fig 3). The weight loss of $G_{30}S_xS_y$ as a function of y/(x+y) mass ratio (silica and sand composition) remains constant (~ 5 wt%) after 10 days of drying (Fig. 3a). For a drying time

above 10 days, the weight loss decreases slowly when the y/(x+y) mass ratio increases. This could be due to the strong reactivity of fine particles of silica compared to low reactivity of large grains of sand (S) in basic middle [10,11]. Evolution of weight loss of consolidated materials (Fig. 3b) as a function of gel content during drying process shows a long time of drying. This is certainly due to the reaction of all components in presence which is carrying out in a basic middle and depending on experimental conditions (T = 25 °C, 11.3% humidity in a closed box). Actually, samples continue to dry after 100 days. We can also observe that for time below 10 days, samples show same behavior during drying, but when time becomes above 10 days, the weight loss decreases with increasing gel content. This is in accordance with water content introduced during samples preparation.

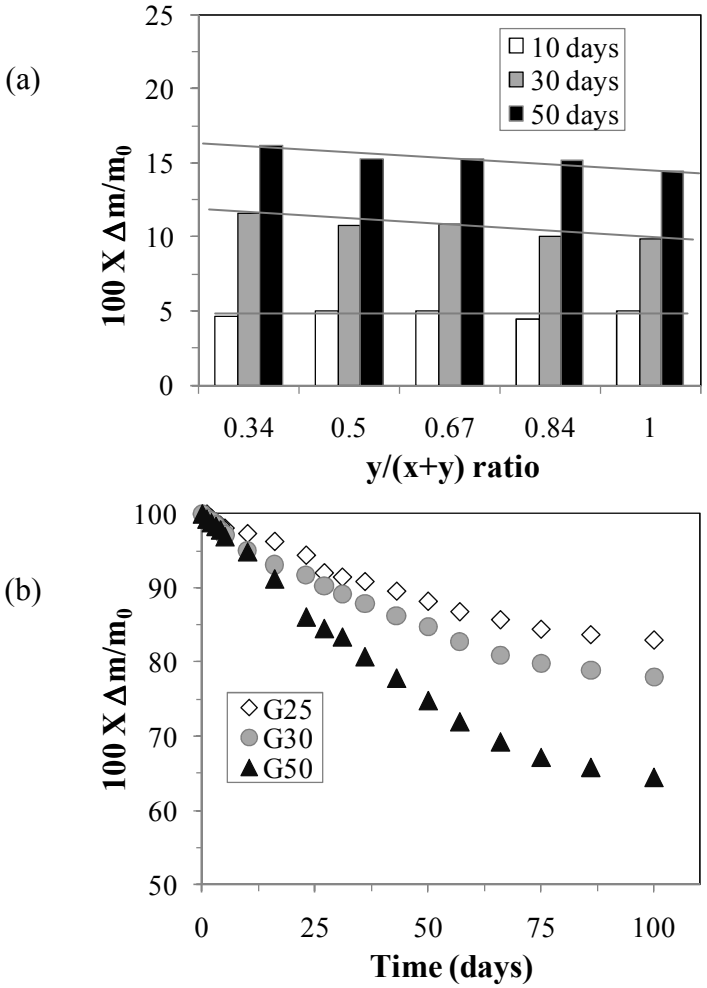

Fig. 3: Variation of weight loss of consolidated materials as a function of: (a) y/(x+y) mass ratio for $G_{30}s_xS_y$ and (b) gel content for y/(x+y) = 0.5.

ii) Mechanical properties of standard sand-based materials

In order to characterize mechanical properties of samples, three points bending tests were carried out on $G_{33}s_{33}Sd_{33}$ during drying (Fig. 4a). Bending stress increases from 2 MPa after 15 days to 5.6 MPa after 45 days. This result suggests that mechanical properties of samples increase with time. The effect of silica content was also studied after 28 days of drying for samples having constant gel content ($G_{33}s_xSd_y$) (Fig. 4b). We observe that bending stress increases with increasing silica content. Actually, in sample where there is no silica (only gel and sand), the bending stress is equal to 0.5 MPa and when silica content is equal to 51 wt%, the bending stress becomes 5 MPa. Consequently, addition of fine silica leads to strong consolidation and best mechanical properties.

This suggests a possible reaction between silica and gel. As reaction occurs in an alkaline medium and as silica solubility increases in basic medium, this reaction could be a dissolution / precipitation reaction. Therefore, consolidation could be explained by the dissolution of small particles of silica and their precipitation into grain boundary of large grains of sand. In these conditions, mixture of silica and gel could be considered as a mineral binder.

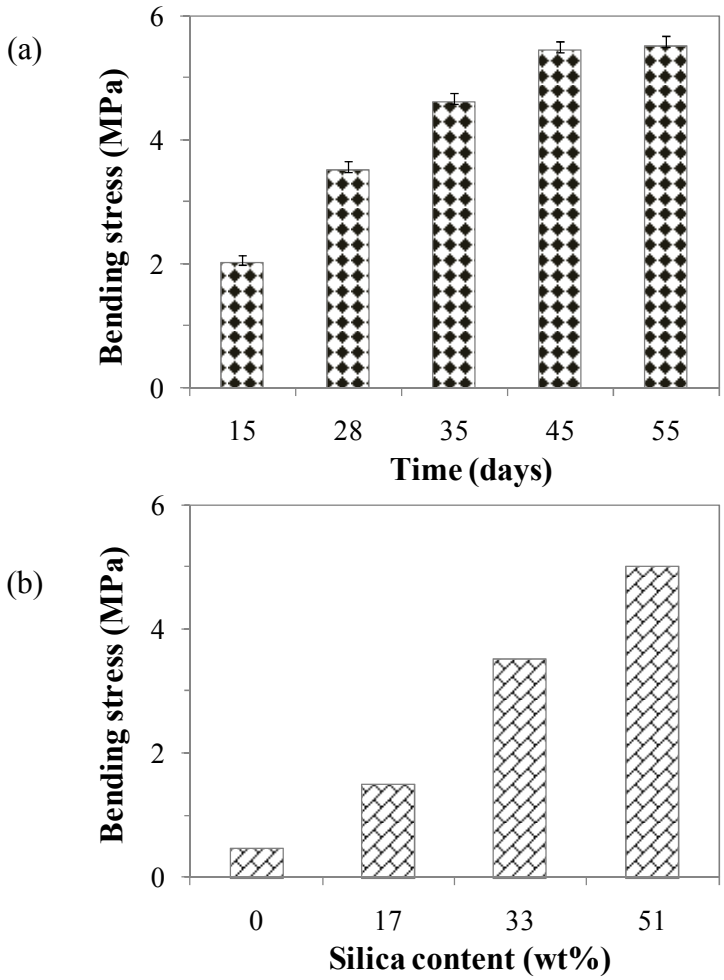

Fig. 4: (a) Variation of bending stress of $G_{33}S_{33}Sd_{33}$ as a function of time, (b) effect of silica content after 28 days of drying.

Summary

The gels used as precursor of binder were synthesised by adding hydrochloric acid into a concentrated sodium silicate. Consolidated materials were obtained by mixing the previous solution before gelation with granular materials (fine silica powder and sands). Therefore, consolidated materials were obtained through sodium silicate gelation in an alkaline medium. The use of gel with granular such as fine silica powder and sands permits to limit a range of existence. This existence range was determined as a function of size distribution and shows a shift to higher particle size of

sand. Strong consolidation and high bending stress values can be obtained when silica content increases. This suggests possible dissolution / precipitation reaction of silica leading to consolidate large grains of sand. Therefore, the mixture of gel and fine silica could be considered as a mineral binder for setting at room temperature.

References

[1] J.W. Phair and J.S.J. Van Deventer: *Characterisation of fly ash-based Geopolymers activated with sodium aluminate*. Ind. Eng. Chem. Res., vol. 41 (2002), p. 4242.

[2] J.W. Phair, J.S.J. Van Deventer and J.D. Smith: *Mechanism of polysialation in the incorporation of zirconia into fly ash-based geopolymers*. Ind. Eng. Chem. Res., vol. 39 (2000), p. 2925.

[3] H.E. Bergna and W.O. Roberts: *in Colloidal silica: fundamentals and applications*, edited by CRC Press Taylor and Francis Group, Wilmington (2006).

[4] K. Yamada, T. Hashimoto and Y. Furumi, Ceramics, vol. 11 (1976), p.785.

[5] K. Sangwal, B. Wiktorowska and T. Sokolowski in: *Elementary Crystal Growth*, edited by Saan Pub., Lublin (1994).

[6] M.T. Tognonvi, in: *Physico-chimie de la gélification du silicate de sodium en milieu basique.* PhD thesis, University of Limoges, France, (2009).

[7] R.K. Iler, in: *The Chemistry of Silica*, edited by John Wiley and Sons, New York (1979).

[8] K.G. Knauss and T.J. Wolery: *The dissolution kinetics of quartz as a function of pH at 70°C*. Geochem. Cosmochim. Acta, vol. 52 (1987), p. 43.

[9] J.H. Henderson, J.K. Syers, M.L. Jackson, "Quartz dissolution as influenced by pH and the presence of a disturbed layer". Israel J. Chem., vol. 8 (1970), p. 357.

[10] M. Mgaidi, F. Jendoubi, D. Oulahna, M. El Maaoui and J.A. Dodds: *Kinetics of the dissolution of sand into alkaline solutions: application of a modified shrinking core model*. Hydrometallurgy, vol. 71 (2004), p. 435.

[11] J.A. Van Lier, P.L. De Bruyn and J.Th.G. Overbeek: *The solubility of quartz*. J. Phys. Chem., vol. 64 (1960), p. 1675.

doi:10.4028/www.scientific.net/AST.69.63

Geopolymer Development by Powders of Metakaolin and Wastes in Thailand

Chayanee Tippayasam[1, a], Sansanee Boonsalee[3,b], Suvimol Sajjavanich[2,a], Chiara Ponzoni[4,c], Elie Kamseu[4,d] and Duangrudee Chaysuwan[1,a]

[1]Department of Materials Engineering, Faculty of Engineering, Kasetsart University, Bangkok, Thailand

[2]Department of Civil Engineering, Faculty of Engineering, Kasetsart University, Bangkok, Thailand

[3]Department of Science Service, Ministry of Science and Technology, Bangkok, Thailand

[4]Department of Materials and Environmental Engineering, University of Modena and Reggio Emilia, Italy

fengddc@ku.ac.th[a], ssansanee@dss.go.th[b], chiara.ponzoni@gmail.com[c] and kamseuelie2001@yahoo.fr[d]

Keywords: Geopolymer; Fly ash; Bagasse ash; Rice husk ash; Metakaolin

Abstract

Geopolymer has been developed as an alternative material to Portland cement. Geopolymer is based on the polymerization of alkaline activation and oxide of silicon and aluminium. These oxides can be found in many pozzolanic materials such as metakaolin and the wastes from industries and agricultures in Thailand, e.g., fly ash, bagasse ash and rice husk ash.

Pozzolanic materials were selected as source materials for making geopolymers into 4 different types. Sodium hydroxide concentration of 10 Molar (10MNaOH) and sodium silicate (Na_2SiO_3) solutions were used as alkaline activators by the mass ratio of Na_2SiO_3/NaOH at 1.5. The mixtures were cast in 25×25×25 mm. cubes. After casting, the geopolymers were cured at 80°C for 24 hrs. in an oven and then at room temperature for 7 days. The pozzolanic materials effects, the Si/Al molar ratio and the Na/Al molar ratio were studied and characterized.

An X-ray fluorescence (XRF) was chosen to determine the percentages of silica and alumina in order to verify the proper ratio of the fly ash, Rice husk ash, Bagasse ash and Metakaolin.The study also included the impact on mechanical and physical properties such as compressive strength, water absorption, density and porosity.

1.Introduction

Geopolmer was first originated by Davidovits (1979) to designate a new class of three dimensional silico-aluminate materials[1]. The geopolymer is produced by totally replacing the ordinary Portland cement. Hence, the use of geopolymer concrete to replace the cement is to reduce the CO_2 emissions by the cement industries [2]. Geopolymerization can be applied to utilize solid wastes and by-products containing silica and alumina which are called 'Pozzolans'. A geopolymer is environmentally friendly [3] which is attractive to increase attention in various research fields as a construction material[4]. Pozzolans from industrial and agricultural by-products such as fly ash, bagasse ash and rice husk ash were used to produce geopolymers in this research.

An industrial by-product, from power plants, which is now being used quite extensively as a pozzolan for replacing cement is fly ash. Bagasse ash is a by-product from sugar refinery whereas rice husk is a by-product from rice mill. When they are burnt both bagasse ash and rice husk ash contain around 80% of silica, silica in amorphous form suitable for use as a pozzolan[5]. Furthermore, the geopolymerization can be reacted with metakaolin, obtained by burning kaolin from Ranong province in Thailand, normally, at temperature higher than 600°C[6].

The main alkali solutions activated with pozzolans were sodium silicate and sodium hydroxide. In this research, the fly ash, bagasse ash, rice husk ash and metakaolin were used as the starting materials. They were studied the effects of pozzolanic materials, the Si/Al molar ratio, the Na/Al molar ratio and Na/Si molar ratio for mechanical and physical properties such as compressive strength, water absorption, density and porosity.

2. Experimental

2.1. Characterization of initial materials

Fly ash (FA) was lignite fly ash from Mae Moh power plant in the northern part of Thailand. Rice husk ash (RHA) was obtained from rice mill in the central part of Thailand. Bagasse ash (BA) was a by-product from sugar refinery at Kaset Thai Co., Ltd., in Nakhon Sawan province. Washed kaolin was obtained from Mineral Resources Development Co., Ltd., Ranong province in southern part of Thailand. FA, RHA and BA were ground by a ball mill until the mass of the fine particles retained on sieve size No.325 (aperture of 45 μm) was 1-3%. Metakaolin (MK) was subsequently produced by burning kaolin clay at 1000°C, for 6 hr. Table.1 shows the chemical compositions of FA, RHA, BA and MK as determined by X-ray fluorescence (XRF) analysis. X-ray diffraction (XRD) pattern of MK, in Fig.1, present mainly MK composed of α-quartz, metakaolinite and silicon oxide.

Tables 1 Chemical compositions of FA, RHA, BA and MK as determined by XRF (mass%)

Chemical composition (%)	SiO_2	Al_2O_3	Fe_2O_3	CaO	MgO	Na_2O	K_2O	SO_3
FA	39.88	22.36	13.22	12.85	2.56	1.72	3.09	2.97
RHA	94.25	0.52	0.22	0.70	0.40	0.05	2.26	0.82
BA	75.39	5.44	3.42	7.89	1.50	0.30	3.32	0.39
MK	53.48	44.08	0.63				1.65	

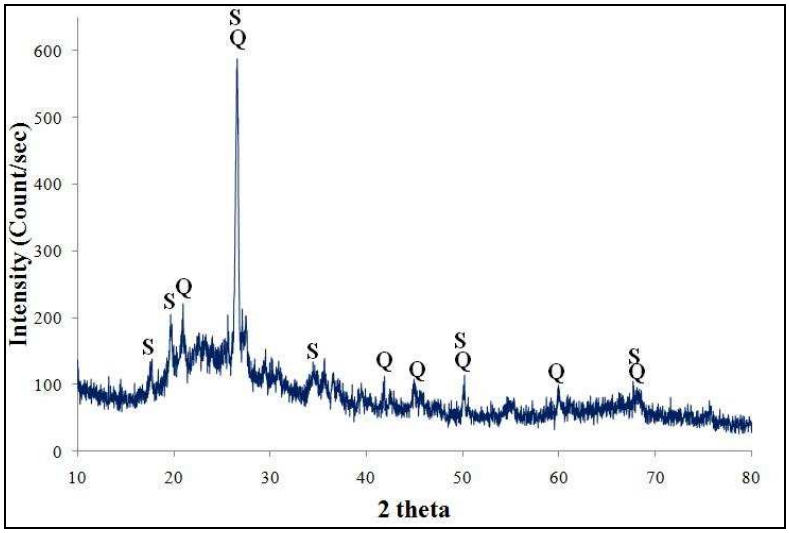

Fig. 1 XRD pattern of Metakaolin. Q = Quartz and S = Silicon oxide.

2.2. Alkali activators

Sodium silicate solutions (Na_2SiO_3) (13.8%Na_2O, 32.2% SiO_2 and 54.0%H_2O) and 10M NaOH solutions (commercial grade) were used as the alkali activators.

2.3. Methodology

2.3.1. Mixed proportions of geopolymer paste

FA, RHA, BA and MK were individually pre-mixed in a beaker. The mixed proportions of FA to RHA, FA to BA and FA to MK were prepared by variation to five ratios as; 0:100, 20:80, 50:50, 80:20 and 100:0 by weight. The ratios of solid to liquid (Na_2SiO_3 and 10MNaOH) were 80:20, 70:30, 60:40 and 50:50 by weight as geopolymer pastes. These proportions have difference of the Si/Al and Na/Al as shown in Table 2 and Fig.3

2.3.2. Mixing of geopolymer paste

The solution of Na_2SiO_3 and 10M NaOH were prepared at least 1 day prior to its use. The solution was poured into a beaker and mixed with solid homogeneously. Consequently, the pastes were poured into 25 × 25 × 25 mm^3 acrylic moulds. The specimens were wrapped with plastic film and then cured at room temperature for 24 hrs, further removing the mold and, finally, the specimens were cured at room temperature for 7 days.

2.4. Test of specimens

2.4.1. Compressive strength

The test was done in according to the ASTM C 618. The reported results are the average of four samples at 8 days age.

2.4.2. Water absorption, Density and Porosity

In order to determine the water absorption, density and porosity of mortar specimens, 7 days age of four cubes from each series were oven dried at a temperature of 85°C for 24 hrs and their weight were determined as the initial weight (W_d). A sample was then immersed in water for 24 hrs and weighed the sample in water as W_w. Finally, the saturated weight was weighed in air as W_a.

The water absorption was calculated using Eq.1

$$\%\text{Water absorption} = (W_a\text{-}W_d)/(W_a) \times 100 \quad (1)$$

The density was calculated using Eq.2

$$\text{Density} = (W_d)/(W_a\text{-}\ W_w) \times 100 \quad (2)$$

And the porosity was calculated using Eq.3

$$\rho = (W_a\text{-}W_d)/(W_a\text{-}\ W_w) \times 100 \quad (3)$$

where

ρ is vacuum saturated porosity (%),
W_a is weight in air of saturated sample (g),
W_d is dry weight after 24 hrs in oven at 85 ± 5 °C (g) and
W_w is weight in water of saturated sample (g)

The reported results are the average of four samples.

3. Results and Discussion

3.1. Effect of quantity of alkali liquid on compressive strength

The compressive strength of geopolymer specimens curing at room temperature and 8 days age were shown in Fig.2.

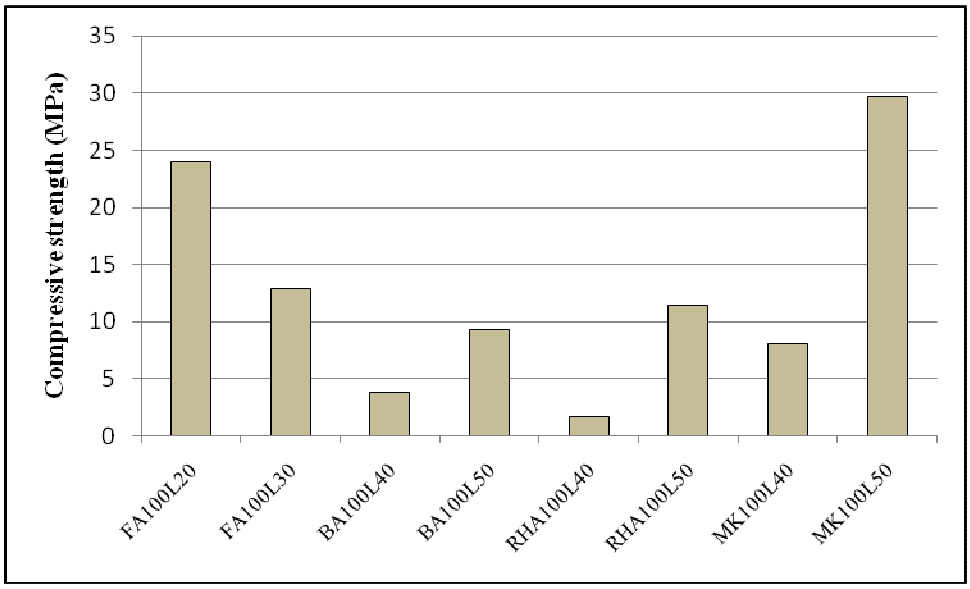

Fig. 2 Compressive strength vs. quantity of liquid alkali

From Fig. 2, the maximum compressive strength (31.57 MPa) was obtained from the specimens of MK100L50 (100% metakaolin and 50% liquid alkali) while the minimum strength (1.66 MPa) was from RHA100L40 (100% rice husk ash and 40% liquid alkali), therefore, the metakaolin would be focused in its activity. In additional, it was found that the compressive strength of geopolymer with FA obviously dropped when the percentage of alkali liquid exceeded 30%, whereas with BA, RHA and MK, the strength increased as the quantity of alkali liquid increased.

However, the 100% RHA and 100% BA were inappropriate to produce geopolymers because of their low compressive strength results. The reasons of low strength, probably, arise from the high Si/Al molar ratio as the percentage of SiO_2 contents of RHA and BA were 94.25 and 75.39, respectively, shown in Table 1. Therefore, it was thought to mix RHA and BA with FA in order to increase amount of Al_2O_3 which was brought from FA mainly and the Si/Al molar ratio would be implied to decrease. The percentage of alkali liquid for geopolymer was suitably used between 30-40%.

3.2. Effect of Si/Al molar ratio and Na/Al molar ratio on compressive strength

Table 2 Compressive strength, Si/Al molar ratio and Na/Al molar ratio

Formulae	Compressive strength (MPa)	Si/Al molar ratio	Na/Al molar ratio
FA20BA80L40	3.01	7.47	1.14
FA20RHA80L40	2.63	16.2	2.06
FA20MK80L40	25.09	1.27	0.25
FA50BA50L40	16.16	4.06	0.73
FA50RHA50L40	5.07	5.66	0.88
FA50MK50L40	31.89	1.41	0.30
FA80BA20L40	11.13	2.48	0.53
FA80RHA20L40	12.28	2.80	0.56
FA80MK20L40	21.37	1.62	0.38

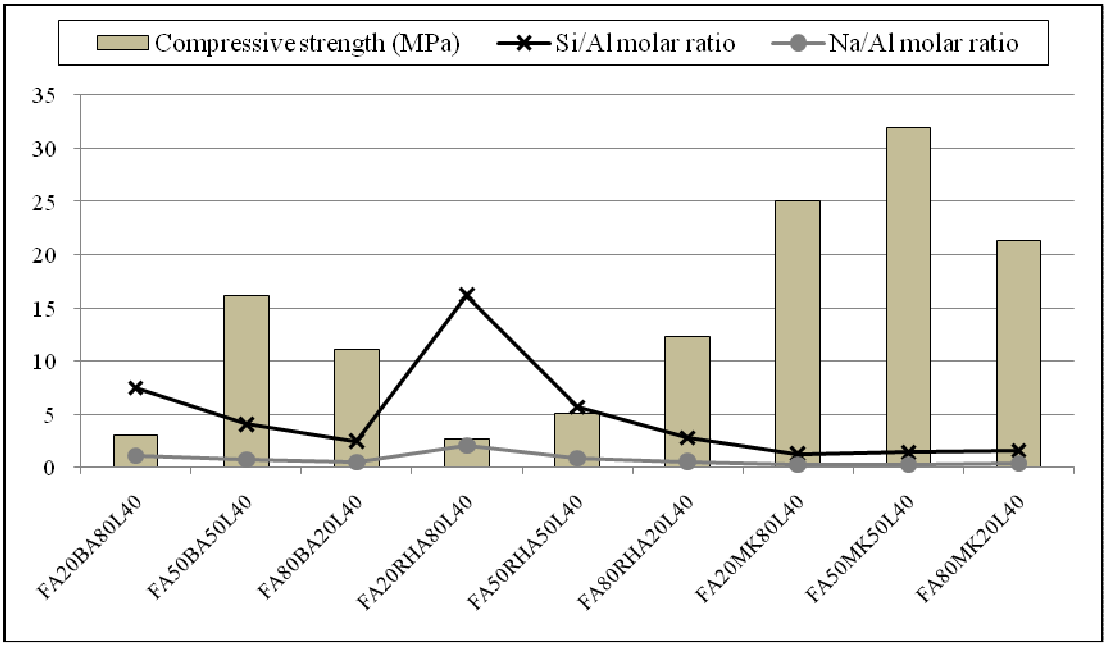

Fig. 3 Compressive strength vs. quantity of pozzolanic materials

The results of compressive strength of geopolymer specimens were shown in Fig. 3 at 40% alkali liquid and FA: other pozzolans (e.g. BA, RHA and MK) as 20:80, 50:50 and 80:20. The 50% FA-50% MK performed the maximum compressive strength (31.89 MPa) whereas the 20%FA-80%RHA performed the minimum (2.63 MPa). It was clearly found that the compressive strength of samples of BA and RHA mixed with FA, in Fig. 3, were much higher than those of only BA and RHA, in Fig. 2. For samples of MK mixed with FA and those of only MK, the compressive strength of them was similar because both materials have similar chemical compositions. It was interesting to consider the Si/Al molar ratio and Na/Al molar ratio with the compressive strength. In Fig. 3, the higher than 20 MPa compressive strength performed with the Si/Al molar ratio the value between 1 and 2 and Na/Al molar ratio less than 1.

3.3. Water absorption, density and porosity

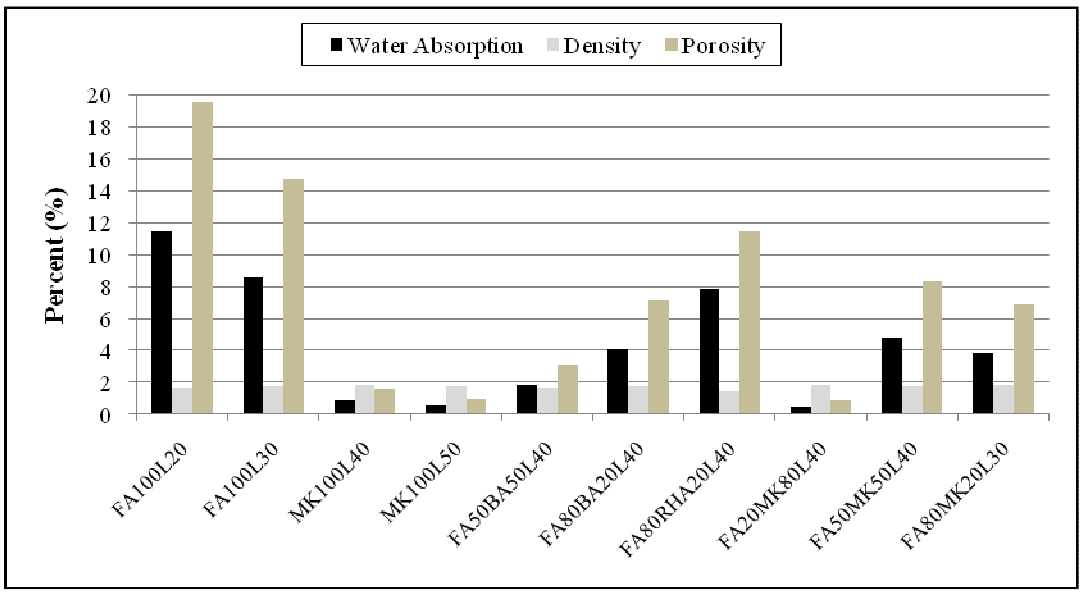

Fig.4 Water absorption, density and porosity

From Fig. 4, the maximum water absorption (11.43%) and porosity (19.52) were earned from FA100L20. The minimum water absorption (0.46%) and porosity (0.83) were received from FA20MK80L40. The water absorption of specimens was present in the same trend as the porosity. Each specimen has the comparable density. There were some specimens such as the 100% BA and 100% RHA not stable in water. The MK geopolymers present obviously low water absorption and porosity while FA geopolymers did oppositely. If these physical properties were compared with compressive strength, it was found that the lower water absorption and porosity, the higher compressive strength.

Conclusion

1. The compressive strength of geopolymers increased with the percentage of alkali liquid.
2. The Si/Al molar ratio of the value between 1 and 2 and Na/Al molar ratio of less than 1 were appropriate to produce geopolymers.
3. FA increased the amount of Al_2O_3 when mixed with BA and RHA and caused the Si/Al molar ratio to decrease.
4. The maximum compressive strength was gained from FA50MK50L40 specimens.
5. The minimum water absorption and porosity were received from FA20MK80L40 specimens.

Acknowledgement

The author would like to acknowledge the instrument and raw materials supports of Department of Science Service, Ministry of Science and Technology, Bangkok, Thailand and would like to thank Department of Materials and Environmental Engineering, University of Modena and Reggio Emilia, Modena, Italy for new and great experiences.

References

[1] Davidovits J. (2000), *Global Warming Impact on the Cement and Aggregates Industries*.

[2] McCaffrey R. (2002), Climate Change and the Cement Industry*, Global Cement and Lime Magazine*, (Environmental Special Issue), 2002, pp. 15-19.

[3] Hardjito D. and Rangan B.V. (2005). *Development and Properties of Low-calcium Fly ash based*
Geopolymer Concrete.

[4] Chen H.J., Ten T. and Chen K.H. (2003). *Use of Building Rubbles as Recycled Aggregates*. Cem Concr Res 2003; 33(1):pp.125–32.

[5] Chindaprasirt P., Kanchanda P., Sathonsaowaphak A. and Cao H.T. (2007). *Sulfate Resistance of BlendedCcements Containing Fly Ash and Rice Husk Ash*. Constructor Build Mater 2007; 21(6):1356–61.

[6] Shvarzman A., Kovlar K., Grader G.S. and Shter G.E. (2002). The Effect of Dehydroxylation/Amorphization Degree on Pozzolanic Activity of Kaolinite. Cement and Concrete Research 33 (2002) pp. 405-416.

[7] ASTM C 618, (2001). Standard specification for coal fly ash and raw or calcined natural pozzolan for use as a mineral admixture in concrete. Annual book of ASTM standards 04.0. pp. 310–313.

doi:10.4028/www.scientific.net/AST.69.69

Physical, Mechanical and Micro-structural Properties of F Type Fly-Ash Based Geopolymeric Bricks Produced by Pressure Forming Process

Omer Arioz[1, a], Kadir Kilinc[2, b], Mustafa Tuncan[2, c], Ahmet Tuncan[2, d], Taner Kavas[3, e]

[1]Cimsa, Ready-Mixed Concrete Company, Eskisehir, Turkey

[2]Department of Civil Engineering, Faculty of Engineering&Architecture, Anadolu University, Eskisehir 26555, Turkey

[3]Department of Materials Science&Engineering, Faculty of Engineering, Afyon Kocatepe University, Afyonkarahisar, Turkey

[a]oarioz@anadolu.edu.tr, [b]kadirkilinc@anadolu.edu.tr, [c]mtuncan@anadolu.edu.tr, [d]atuncan@anadolu.edu.tr, [e]tkavas@aku.edu.tr

Keywords: Geopolymer; Heat treatment temperature; Heat treatment duration; Geopolymeric brick; F-type fly ash; Sodium silicate; Sodium hydroxide solution; Compressive strength; Density; Microstructure.

Abstract

Geopolymer is a new class of three-dimensionally networked amorphous to semi-crystalline alumino-silicate materials, and first developed by Professor Joseph Davidovits in 1978. Geopolymers can be synthesized by mixing alumino–silicate reactive materials such as kaolin, metakaolin or pozzolans in strong alkaline solutions such as NaOH and KOH and then cured at room temperature. Heat treatment applied at higher temperatures may give better results. Depending on the mixture, the optimum temperature and duration vary 40-100 °C and 2-72 hours, respectively. The properties of geopolymeric paste depend on type of source material (fly ash, metakaolin, kaolin), type of activator (sodium silicate-sodium hydroxide, sodium silicate-potassium hydroxide), amount of activator, heat treatment temperature, and heat treatment duration. In this experimental investigation, geopolymeric bricks were produced by using F-type fly ash, sodium silicate, and sodium hydroxide solution. The bricks were treated at various temperatures for different hours. The compressive strength and density of F-type fly ash based geopolymeric bricks were determined at the ages of 7, 28 and 90 days. Test results have revealed that the compressive strength values of F-type fly ash based geobricks ranged between 5 and 60 MPa. It has been found that the effect of heat treatment temperature and heat treatment duration on the density of F-type fly ash based geobricks was not significant. It should be noted that the spherical particle size increased as the heat treatment temperature increased in the microstructure of F-type fly ash based geobricks treated in oven at the temperature of 60 °C for 24 hours.

Introduction

Fly ash is a waste material and it is utilized in cement and concrete production, and the stabilization of soil. Fly ash is obtained by collecting fine materials of chimney gases in coal burning thermal power plants in which 450 and 15 million tons of fly ash are collected each year in the world and Turkey, respectively [1, 2]. Fly ash is an important industrial by-product, in terms of its production quantity and its influence on environment [3]. The appropriate utilization of fly ashes reduces the air and environmental pollution [1, 2]. Worldwide millions of tons of fly ash are generated each year by coal-fired power plants satisfying the large demand for industrial and domestic energy. Only about 20-30% of the generated fly ash is used, mainly as additive in cement and concrete and as filling material, the rest is disposed of, landfilling is currently the processing technique used [4]. Particular emphasis has been placed on the waste materials with a view to developing geopolymers synthesised from the fly ash obtained as a by-product of coal combustion in power stations. Fly ash is extremely useful as it produces geopolymers with very high strengths [5]. From Van Deventer's research, fly ash has been found a suitable raw material for geopolymer, with the addition of metakaoline and under the activation of alkali and alkali-silicate solution [3]. Since fly ash contains a large amount of silica and alumina, it is a suitable source material for making geopolymers. The fly ash geopolymer is prepared by incorporating high alkaline solution and sodium silicate and is activated with temperature curing [6]. Fly ash-based geopolymerisation has only become the subject of intense research interest within the past decade; however there are currently a number of well-established academic and industrial research centres worldwide that are investing significantly in developments in this field [7].

When fly ash is utilised in bricks, the material is pressure formed and bricks are produced by pressure forming process [8]. Kaps et al. implements that clay minerals represent the starting materials with high importance for generation of both ceramics and geopolymer-containing products with the application in buildings. Geopolymer additions can work as a sinter assisting agent in the brick fabrication. The sintering process is accompanied by formation of crystalline alkali aluminosilicates. This effect becomes more significant for saving energy in an economized production technology [9]. Davidovits implements that Low Temperature Geopolymeric Setting (LTGS) takes place in alkaline conditions (NaOH, KOH) in concentrations from 1 to 5% by weight of the ceramic paste. At drying temperatures (50°C to 250°C), the kaolinite in clays is transformed by LTGS into a three dimensional compound of the Poly(sialate) Na-PS sodalite type or K-PS kaliophilite, stable to water and possessing high mechanical strength. Davidovits also states that LTGS may dramatically modernize the traditional ceramic industry [10].

Experimental Study

In this experimental investigation, semi-dry geopolymeric mixes were prepared and then shaped by pressure forming process applied at 30 MPa. In the production of geopolymeric mixes, F type fly ash, sodium silicate, and sodium hydroxide solution were used. Sodium hydroxide solution was prepared in one molarity such as 12 M. The prepared semi-dry geopolymeric pastes were formed by applying 30 MPa pressure and 190x90x50 mm bricks were produced. The production was carried out by using a special automatic mould and pressuring devices. The F-type fly ash based geopolymer bricks were treated at four different temperatures (40 °C, 60 °C, 80 °C, 100 °C) and six different durations (2, 4, 6, 24, 48, 72 hours). Both oven and steam treatments were applied and the effect of treatment type was determined. Thus, the effects of fly ash type, treatment type, treatment temperature and duration were extensively examined. The compressive strength and density properties of F-type fly ash based geopolymer bricks were determined at the ages of 7, 28 and 90 days according to recently published Turkish and European Standard TS EN 771-1 [11]. Micro-structural properties of F-type fly ash based geobricks were determined by using Scanning Electron Microscope (SEM).

Results and Discussions

Compressive strength of F-type fly ash based geopolymer bricks produced by sodium hydroxide solution: 7, 28 and 90-day compressive strength of F-type fly ash based geobricks produced by sodium hydroxide solution were shown in Fig. 1. It was observed that the effect of treatment temperature and duration on the 7,28, and 90-day compressive strength of oven and steam treated specimens was significant. The test results have shown that the compressive strength increased generally with increase in heat-treatment duration. According to the test results, the strength slightly increased with increase in age of the specimen (Fig. 1).

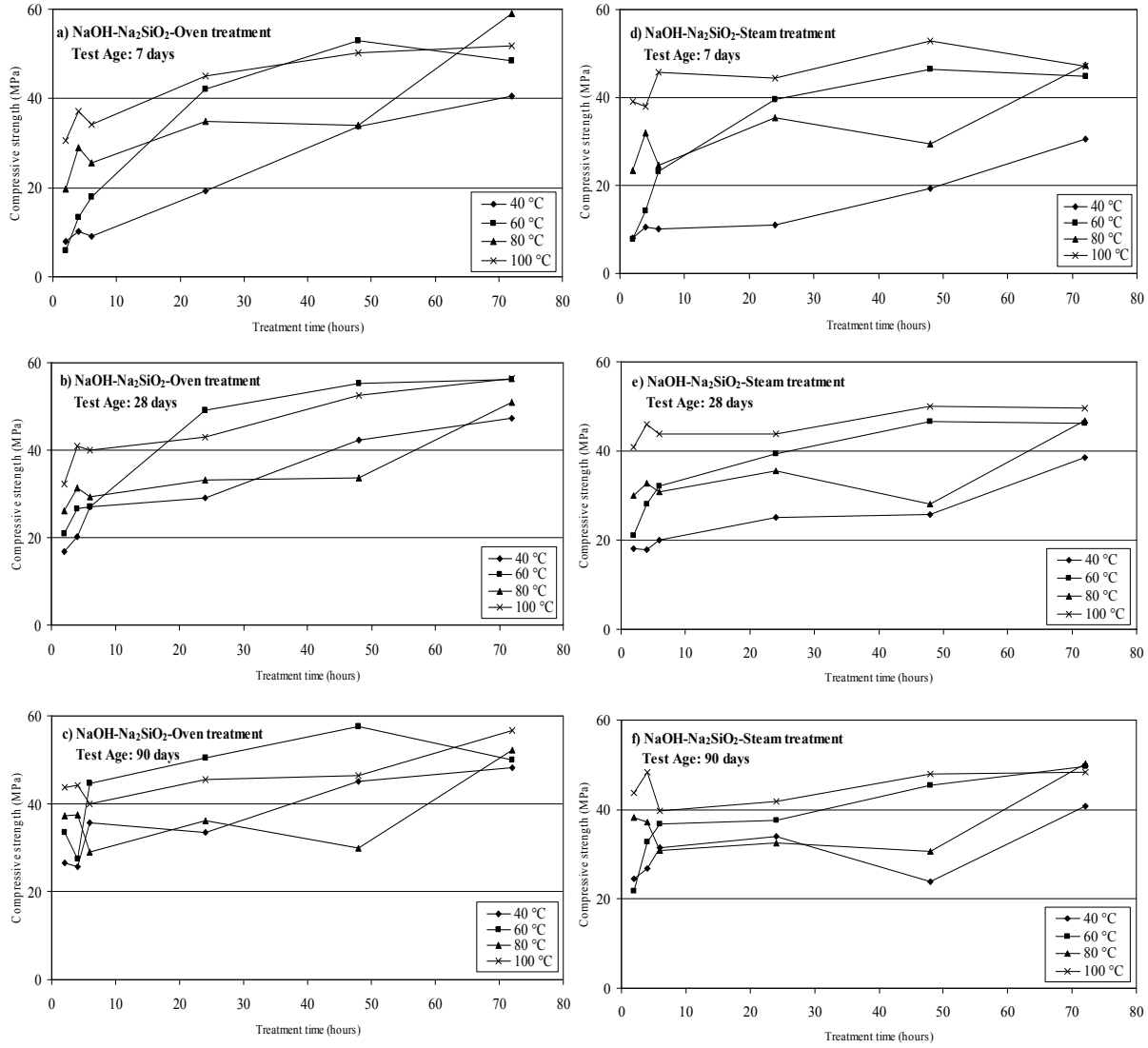

Fig. 1. Compressive strength of fly ash-sodium hydroxide-sodium silicate based geobricks

Density of F-type fly ash based geopolymer bricks produced by sodium hydroxide solution: 7, 28 and 90-day density of F-type fly ash based geobricks produced by sodium hydroxide solution were shown in Fig. 2. It was concluded that the effect of treatment temperature and duration on the 7, 28, and 90-day density of oven and steam treated geopolymeric bricks produced by sodium hydroxide solution can not be generalized (Fig. 2). The test results have shown that the effect of heat-treatment temperature on the density of geobricks was not remarkable. Similarly, the effect of heat-treatment duration on the density of geobricks was not remarkable. The densities of geobricks produced by steam-treatment were somewhat lower than those produced by oven-treatment. The effect of sample age on the density of geobricks was not pronounced (Fig. 2).

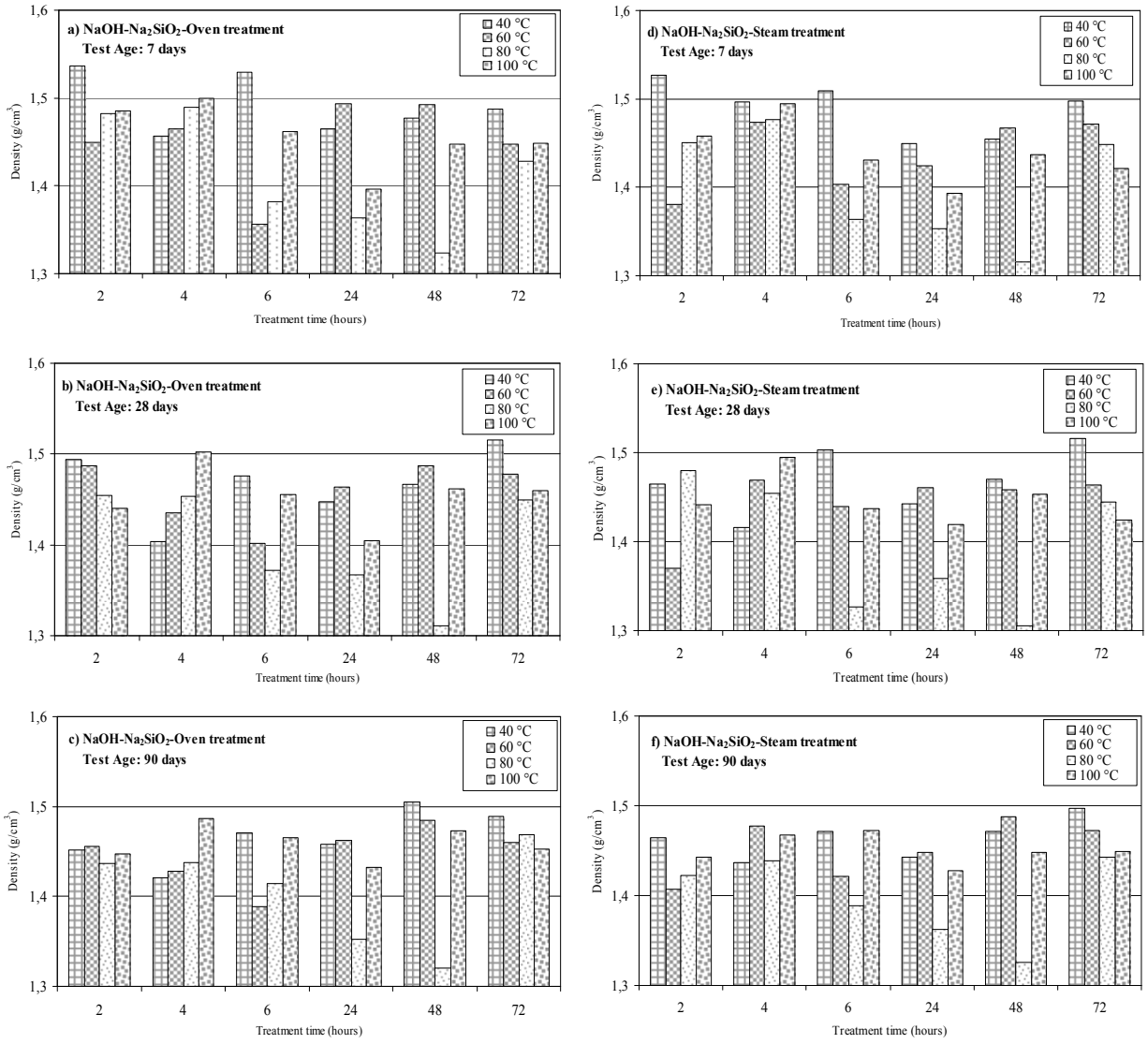

Fig. 2. Density of fly ash-sodium hydroxide-sodium silicate based geobricks

Micro-structural properties of F-type fly ash based geobricks: The micro-structural properties of 90-day F-type fly ash based geobricks oven-treated at the temperatures of 40 °C, 60 °C and 80 °C for 24 hours were summarised in Figure 3a, Figure 3b and Figure 3c, respectively. It should be noted that the spherical particle size increased as the heat treatment temperature increased in the microstructure of F-type fly ash based geobricks treated in oven at the temperature of 60 °C for 24 hours.

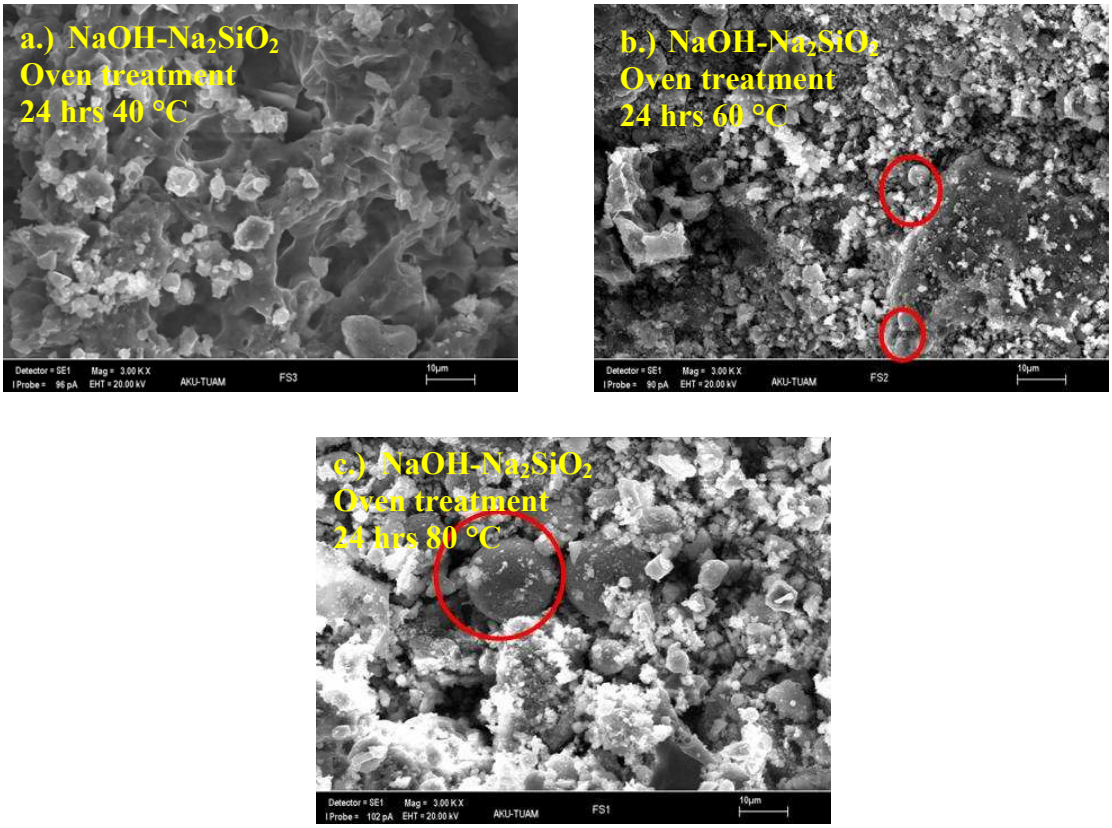

Fig. 3. The effect of heat-treatment temperature on the micro-structural properties of fly ash-sodium hydroxide-sodium silicate based geobricks

CONCLUSIONS

The following conclusions may be drawn from the present study;

1. The compressive strengths of F-type fly ash based geobricks ranged between 5 and 60 MPa. The strength increased with increase in heat treatment temperature especially for short durations such as 2, 4, and 6 hours.
2. The test results have shown that the compressive strength of F-type fly ash based geobricks increased generally with increase in heat-treatment duration.
3. It can be summarised that the required heat-treatment duration was found to be 6 hours to produce F-type fly ash based geobrick of 25 MPa strength at 40 °C.
4. The optimum heat-treatment temperature was 60 °C at which a F-type fly ash based geobrick of 42 MPa can be produced by applying a heat-treatment for 24 hours in an oven.
5. It was interesting that there were no remarkable difference between the strengths of oven and steam-treated specimens.
6. The effect of heat-treatment temperature on the density of F-type fly ash based geobricks was not remarkable.
8. The effect of heat-treatment duration on the density of F-type fly ash based geobricks was not remarkable.
9. It should be noted that the spherical particle size increased as the heat treatment temperature increased in the microstructure of F-type fly ash based geobricks treated in oven at the temperature of 60 °C for 24 hours.

ACKNOWLEDGMENTS

The authors wish to express their gratitude and sincere appreciation to the authority of Scientific and Technological Research Council of Turkey for financing this research work (Project no: 107M344).

REFERENCES

[1] T. Erdogan: *Concrete*: Publications of Middle East Technical University, Ankara (2003).

[2] H.Y. Aruntaş: *The using potential of fly ash in building area*: Journal of Gazi University Faculty of Engineering&Architecture Vol. 21 No.1 (2006), p. 193-203.

[3] P. Sun: *Fly Ash Based Inorganic Polymeric Building Material*: Dissertation, Doctor of Philosophy, Detroit, Michigan (2005).

[4] E.A. Ayuso, X. Querol, F. Plana, A. Alastuey, N. Moreno, M. Izquierdo, O. Font, T. Moreno, S. Diez, E. Vazquez, and M. Barra: *Environmental, physical and structural characterisation of geopolymer matrixes synthesised from coal (co-) combustion fly ashes*: Journal of Hazardous Materials Vol. 154 (2008), p. 175-183.

[5] C. Nicholson, R. Fletcher, N. Miller, C. Stirling, J. Morris, S. Hodges, K. MacKenzie, and M. Schmücker: *Building Innovation through Geopolymer Technology*: Chemistry in New Zealand, September (2005), p. 10-12.

[6] P. Chindaprasirt, C. Jaturapitakkul, W. Chalee, and U. Rattanasak:*Comparative study on the characteristics of fly ash and bottom ash geopolymers*: Waste Management, Article in Press, (2008).

[7] P. Duxson, J.L. Provis, G.C. Lukey, and J.S.J.V. Deventer: *The role of inorganic polymer technology in the development of green concrete*: Cement and Concrete Research Vol.37 (2007), p. 1590-1597.

[8] O. Arioz: *An Experimental Investigation on Fly Ash-FGD Gypsum-Lime Based Bricks*, Ms Thesis, Middle East Technical University, Ankara, 1997, p. 115.

[9] C. Kaps, M. Hohmann, A. Buchwald: *Geopolymers in Ceramic Building Materials*: Proc. of the ICC2 Global Roadmap for Ceramics, Verona, 29 June-4 July 2008, p. 723-734.

[10] J. Davidovits: *Road Map for Geopolymer Technologies*: Proc. of the ICC2 Global Roadmap for Ceramics, Verona, 29 June-4 July 2008, p. 689-702.

[11] TS EN 771-1: *Masonry Units-Properties-Part 1: Clay Masonry Units (Bricks)*, Turkish Standards Institute, Ankara (2005).

doi:10.4028/www.scientific.net/AST.69.75

Application of Micromechanics on Alkali-activated Materials

Vít Šmilauer[1,a], František Škvára[2,b], Jiří Němeček[1,c], Lubomír Kopecký[1,d], Petr Hlaváček[1,e]

[1]Czech Technical University in Prague, Faculty of Civil Engineering, Department of Mechanics, Thákurova 7, 166 29 Prague, Czech Republic

[2]Institute of Chemical Technology Prague, Department of Glass and Ceramics, Technická 5, 166 28 Prague, Czech Republic

[a]vit.smilauer@fsv.cvut.cz, [b]frantisek.skvara@vscht.cz, [c]jiri.nemecek@fsv.cvut.cz, [d]kopecky@fsv.cvut.cz, [e]petr.hlavacek.1@fsv.cvut.cz

Keywords: N-A-S-H gel, nanoindentation, alkali-activation, fly ash, metakaolin, micromechanics, elasticity, percolation, homogenization

Abstract. Research of alkali-activated materials has been a traditional domain of chemists. This paper exploits contribution of micromechanics to the subject. A new model for volumetric evolution of chemical phases is formulated. The first homogenization level identifies elasticity on the scale of N-A-S-H gel. Nanoindentation sensing technique yielded the intrinsic Young's modulus of N-A-S-H gel as ~18 GPa, which was further downscaled to the solid gel particles. Percolation theory had to be introduced to match an early-age elasticity. The second homogenization level takes into account an unreacted fly ash. Homogenization models match well the experimental elasticity and demonstrate stiffening of N-A-S-H gel, induced by increasing packing density of the solid gel particles. The percolation model explains a long setting time of alkali-activated materials.

Introduction

A group of alkali-activated aluminosilicate materials draws the attention of researchers worldwide; see [1,2] for a comprehensive review. In comparison with conventional Portland cement-based composites, these materials generally exhibit excellent durability, fire-resistance, but may suffer from efflorescence, shrinkage, cumbersome quality control or mastering the technology [3,4].

In the past, various raw materials (slag, fly ash, metakaolin, clay) were intermixed with strong alkaline solutions to synthesize a poorly crystallized inorganic gel binder [5]. Coined nomenclatures such as “soil cement” [6], “geopolymer” [7] or “inorganic polymer” [2] have characterized more or less similar dissolution-precipitation processes taking place in a strong alkaline environment. Here, the term N-A-S-H gel (aluminosilicate gel) will describe a binding matrix phase, embedding undissolved inclusions of a remaining raw material.

In the past, alkali-activated materials were characterized by a variety of experimental techniques including FTIR, ESEM, MAS-NMR, XRD, DTA or calorimetry [4,5]. The majority of experimental data were linked directly to the atomic scale and nanostructure of N-A-S-H gel. However, all the above-mentioned techniques suffer from data downscaling by several orders of magnitude to the nanostructure of N-A-S-H gel. In this sense, a traditional chemical description of alkali-activated materials may be enriched with micromechanics, as proven successfully for the description of Portland-based materials [8,9].

Micromechanical elastic analysis stems from the definition of intrinsic elastic properties of constituents. The constituent elasticity is assumed to remain independent on time; however, volume fraction of the constituent may evolve during the alkali-activation process. Nanoindentation sensing technique enables direct characterization of intrinsic mechanical properties on the micrometer and submicrometer scale. The response is obtained directly from a close vicinity of a small indent

without the interaction of a distant material. Nanoindentation has never been systematically performed in the field of alkali-activated materials, although a few attempts can be found [10].

This paper aims at interconnecting chemical and mechanical disciplines. First, intrinsic elastic properties are identified from alkali-activated fly ash (AAFA) and alkali-activated metakaolin (AAMK). Second, a new volumetric model of alkali activation is formulated. Third, two-scale elastic homogenization combined with percolation upscales the intrinsic properties to the macrospopic scale.

Materials, Alkali-activation and Curing

Raw fly ash (RFA) was produced in Chvaletice thermal electric power plant, Czech Republic, with the Blaine specific surface 210 m^2kg^{-1}. For nanoindentation, the RFA was ground in a small-scale ball mill in the quantity of 8 kg for 180 minutes. Cenospheres were crushed and facilitated a high packing density. Metakaolin originated from České lupkové závody a.s., Nové Strašecí, Czech Republic. Oxide compositions of both materials are summarized in Table 1.

Table 1. Chemical composition of fly ash and metakaolin, wt. %.

	SiO_2	Al_2O_3	Fe_2O_3	CaO	TiO_2	K_2O
Fly ash	51.9	32.8	6.3	2.7	1.89	2.12
Metakaolin	48.66	47.41	1.33	0.03	1.99	0.15

Alkali-activator was previously optimized to yield a high compressive strength while maintaining workability [4]. The activator was prepared by dissolving NaOH pellets in a tap water and by adding sodium waterglass. Table 2 summarizes the compositions of the mixtures. The final properties of the mixture can be controlled by three independent parameters, see Table 2. Metakaolin requires significantly more activator due to its higher surface area to maintain workability.

Table 2. Composition of alkaline activators and ratii to the activated material.

	Activator ratii		Activator to solid ratio
	Na_2O / SiO_2 (wt. %)	H_2O / Na_2O (wt. %)	
Ground fly ash	0.881	3.925	0.531
Metakaolin	1.669	2.743	1.416

Fly ash or metakaolin were mixed with the activator for 5 minutes, cast in plastic ampoules, 26 mm in diameter and 45 mm in height, gently vibrated for 5 minutes and sealed. Heat-cured fly ash or metakaolin samples were exposed to 80°C for 12 hours. Ambient-cured fly ash experienced ambient laboratory temperature, approx. 25°C, for the duration of six months prior to nanoindentation testing. Both materials are considered to be mature, although polymerization and hardening will never stop as known from C-S-H aging [11]. After a half-year from casting, the compressive strength of AAFA samples exceeded 70 MPa and 50 MPa of AAMK.

Methods

Nanoindentation. Activated samples were cut to parallel slices of approx. 10 mm in thickness, polished on fine emery papers and polishing cloth, and cleaned in an ultrasonic bath. Nanoindentation was carried out in a series of grids of 10 x 10 = 100 imprints in three representative areas. The distance between individual indents varied between 10 and 50 μm.

Nanoindentation measurements were performed in a load control regime using the CSM Nanohardness tester equipped with a Berkovich tip. The trapezoidal loading diagram was prescribed for all tests with a linear loading of 4 mN/min and lasting for 30 s, which produced the maximum load of 2 mN for all indents. Peak load of 2 mN led to maximum penetration depths ranging from 100 nm to 400 nm. Fig. 1 shows a typical force/penetration diagram for three identified material phases.

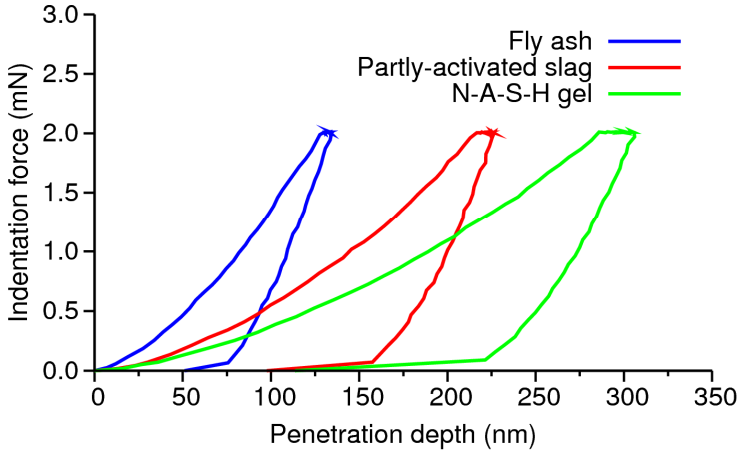

Figure 1. A typical nanoindentation diagram for alkali-activated fly ash.

The effective depth captured by the tip of the nanoindenter can be roughly estimated as three to four times of the penetration depth for the Berkovich indenter [12]. It yields the effective depth of around 1 μm from which the elasticity is obtained.

Determination of Open Porosity. Cylindrical samples (diameter 25 mm, thickness 5 mm) of a well-defined geometry were dried out in an oven at 105°C. Samples were remaining in the oven until the weight loss stabilized, which took from 3 to 6 days. A known skeletal density of fly ash from He pycnometry, a known skeletal density of activated fly ash and the known sample volume led to quantification of the open porosity. The open porosity was determined from three samples and the experiments were repeated during ambient curing of alkali-activated materials to access evolution of the open porosity.

Results and Discussion

Degree of Reaction. The degree of reaction, DoR, is defined as the amount of consumed fly ash during the alkali-activation process. Direct simulation of DoR from a known chemical composition is beyond capabilities of presented models, which do not include reaction kinetics. Instead, the evolution of DoR is taken from experimental data of Fernández-Jiménez et al. [13] who measured the DoR progress on AAFA samples activated with 8 M NaOH solution and cured at 85°C. The extent of DoR was determined by an acid attack with HCl 1:20. Similar results were observed on calorimetric data, revealing that the ratio activator/fly ash is insignificant for the DoR and that a maximum reaction rate occurs at 8-10 minutes after the contact, substantially reduced after 2 hours at elevated temperatures [14].

Arrhenius equation is utilized to recalculate DoR for various curing temperatures. For example, the time scaling from 60°C to 20°C means a slow down 70-times. The Arrhenius equation reads

$$\tau(T_{20}) = \tau(T_{60}) \exp\left[\frac{E_a}{R}\left(\frac{1}{T_{20}} - \frac{1}{T_{60}}\right)\right], \quad (1)$$

where the activation energy was found as 86.2 kJ/mol [4]. The transition from 85°C to 25°C predicts the scaling factor 340. Fig. 2 shows the DoR evolution at 25°C, recalculated from data presented in [13].

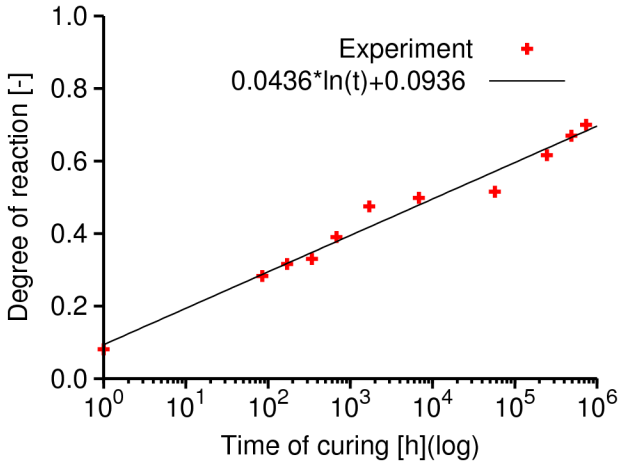

Figure 2. Progress of DoR for alkali-activated fly ash by 8M NaOH. Here, the evolution of DoR is showed for a reference temperature of 25°C. Original data [13] were gathered at 85°C.

Porosity and ESEM. AAFA and AAMK samples were crushed to the size of a few millimeters, dried at 105°C for 6 hours and intruded by mercury (MIP, Autopore III Micromeritics) or by He-pycnometry (Micromeritics AccuPyc 1330). The combination of MIP and He pycnometry allowed estimating the "total" porosity from bulk and skeletal densities. The porosity spans the range from a helium atom (d=0.062 nm) to the upper limit of MIP (d=120 μm). The pore size distribution obtained from MIP and He pycnometry is depicted in Fig. 3; for ordinary Portland cement paste and for alkali-activated samples.

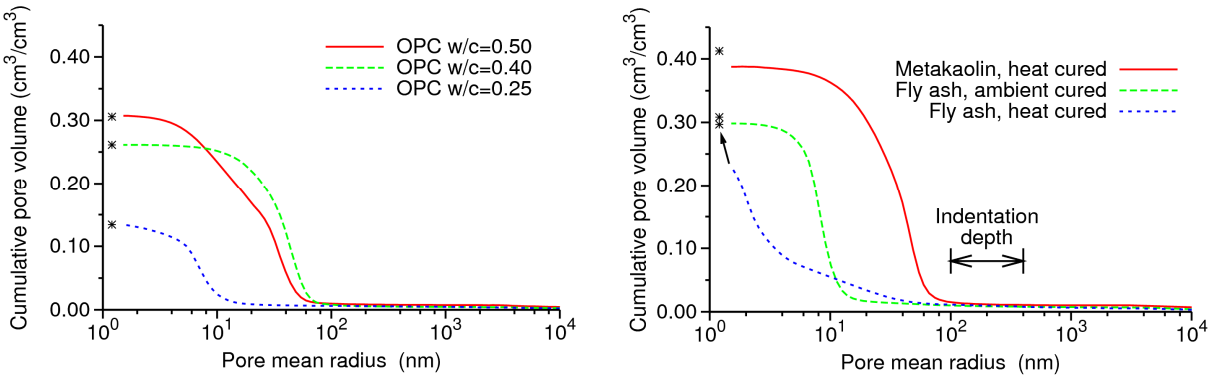

Figure 3. Cumulative pore volume by MIP and He pycnometry. OPC paste cured at 60°C for three months (left) and alkali-activated materials (right). An asterisk denotes the total volume.

In addition, Fig. 4 shows BSE images of AAFA cured under ambient and heat conditions.

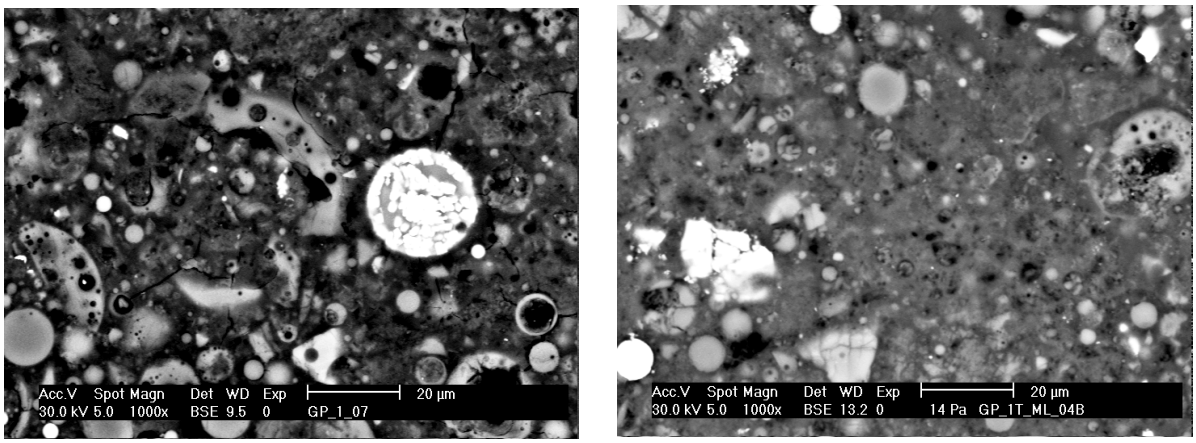

Figure 4. BSE images of AAFA cured under ambient conditions (left) and cured at 80°C for 12 hours (right).

Identification of N-A-S-H Gel Elastic Properties and Introducing Solid Gel Particles. Indentation moduli from 700 locations were gathered and recalculated to Young's moduli. The moduli were processed statistically to a histogram. Fig. 5 shows the histogram with a deconvolution to four Gaussian distributions. Deconvolution is generally an ill-posed problem and many solutions exist, however, the peak for N-A-S-H is clearly and unambiguously defined. Other phases are hypothesized to present partly activated slag and unreacted material.

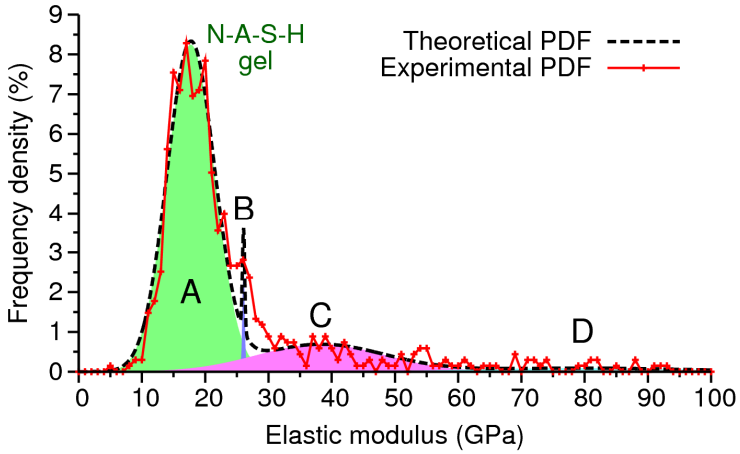

Figure 5. Overall experimental and theoretical probability density functions with segmented four phases in ambient-cured AAFA samples. Peaks are hypothesized to represent A - N-A-S-H gel, B - Partly-activated slag, C - Nonactivated slag, D - Nonactivated compact glass.

Deconvolution for heat-cured AAFA and AAMK samples yielded similar Young's moduli for the N-A-S-H gel. Table 3 summarizes N-A-S-H gel moduli together with corresponding volume fraction from the histogram. Volume fraction of N-A-S-H gel in the heat-cured AAFA is lower due to significant presence of peak B (not showed). Coincidence of the same moduli among different alkali-activated materials and curing procedures proves the same intrinsic elastic properties of N-A-S-H gel, irrespective of its origin.

Table 3. Elastic moduli of N-A-S-H gel synthesized from different precursors.

	Ambient-cured AAFA	Heat-cured AAFA	Heat-cured AAMK
Young's modulus of N-A-S-H gel	17.72 ± 3.75 GPa	17.03 ± 3.48 GPa	17.72 ± 4.43 GPa
Volume fraction from histogram	77.50 %	50.70 %	97.20 %

The histogram in Fig. 5 shows no porosity, which should be at least 30 % according to Fig. 3. As evident from Fig. 3, the nanoindentation imprint is much larger than a fine porosity, which is scattered within the sample. A minor part of porosity is apparently present in the fly ash (cenospheres, plerospheres) and the major part inside the N-A-S-H gel.

Any sol-gel system consists of solid particles dispersed in a liquid [15]. Sol-gel is far from equilibrium and solid particles may aggregate into clusters. If condensation reaction in the system exists and is irreversible, more and more solid particles appear in the system and grow into fractals [15]. Linking of clusters continues until they reach a percolation threshold signalized by a sudden change of many properties such as elasticity.

C-S-H is not a true gel but a precipitate, signalized by the presence of capillary pores. Reversible condensation reaction dominates C-S-H solidification [15]. Another consequence of reversibility is a constant 28 % porosity of the C-S-H gel, irrespective of an origin [16]. The constant porosity allowed considering the C-S-H gel as one phase from a micromechanical point of view; building block intermixed with the porosity at the constant fraction.

N-A-S-H is a true gel, which fills out all available volume around. Gel syneresis has been observed many times in alkali-activated materials; excessive shrinkage accompanied with strong sample disintegration might have occurred under sealed conditions. Due to a true gel nature, no constant gel porosity, as in the case of C-S-H, exists and the micromechanical response needs to be determined from the solid gel particles. The intrinsic elastic properties of the particles are obtained from a downscaling process. Knowing the elasticity of the N-A-S-H gel and the amount of porosity, one may determine unknown intrinsic elasticity of the solid gel particles.

Volumetric Model for Alkali-activation. Volumetric model for alkali-activation presents a stepping-stone for the micromechanical analysis. Much inspiration has been gathered from Portland cement, starting from maturity method [17] and continuing through a famous research carried out by Powers and Brownyard [16]. Fig. 6 shows the volumetric plots for both Portland cement and alkali-activated fly ash. Four chemically and mechanically distinctive phases needed to be identified and quantified in evolving AAFA.

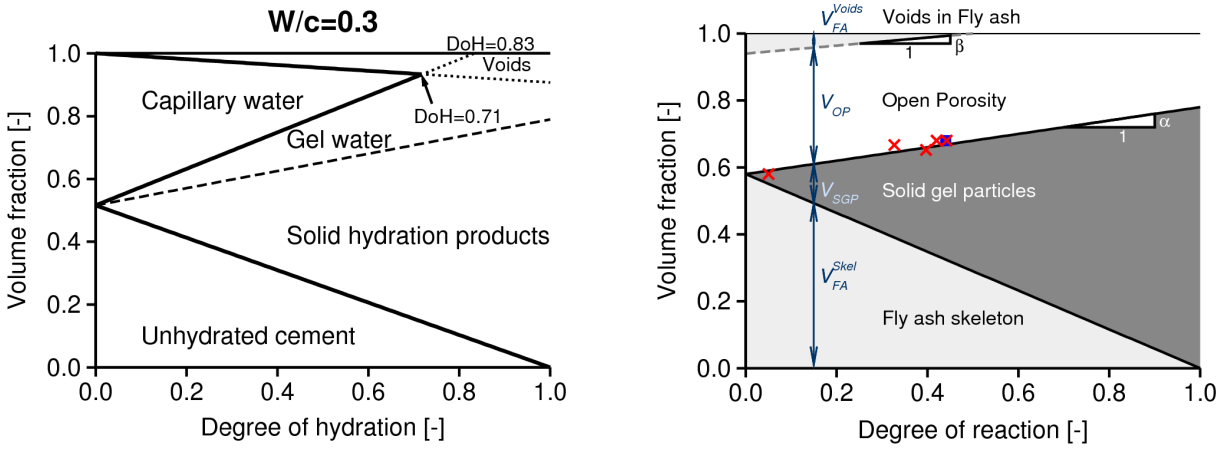

Figure 6. Comparison between Powers' model for ordinary cement and a new model for alkali activation of fly ash.

Referring to Fig. 6, V_{FA}^{Skel} represents the volume fraction fly ash skeleton. Voids persisting in the fly ash after the mixing are quantified with V_{FA}^{Voids}. It must be noted that within a few minutes of mixing, the activator efficiently destroys a thin shell of plerospheres and opens their porosity.

This is manifested by a partial loss of workability and the heat release in isothermal calorimetry. Voids in the fly ash were quantified from the combination of known skeletal density of fly ash, density of activating solution and measured volume and weight of mixture immediately after the mixing process.

V_{SGP} is the volume fraction of solid gel particles. The term 'N-A-S-H gel' is intentionally unused due to no characteristic porosity. The gel is treated as a combination of a liquid plus the solid gel particles. Volume of open porosity, V_{OP}, describes conveniently a part of accessible porosity by external water. The activator fills up the major part of the open porosity.

Degree of reaction (DoR) presents a microstructural parameter, which describes the alkali-activation progress. Expressing all reactions in terms of DoR is more convenient against time for two reasons:

- Circumventing a logarithmic time scale, needed for a proper time-plot of chemical phases.
- Mutual comparison for samples cured at various temperatures can be carried out.

The DoR=0.0 means no activation of fly ash, while a complete activation occurs at DoR=1.0. To build a simple conceptual model describing basic phenomena, several assumptions of the volumetric model were made:

- The whole activator is treated in the form of evaporable water, disregarding a small solid part remaining after drying. Under saturation, open porosity is completely filled with evaporable water.
- No chemical shrinkage/expansion occurs so that the volumetric balance of all liquid and solid phases is maintained during the activation progress.
- All reactions are time-independent and depend only on DoR. Such simplification neglects separate contribution of dissolution, precipitation and aging of N-A-S-H gel.

The volumetric model is expressed by a set of linear equations

$$V_{FA}^{Skel}(\mathrm{DoR}) = V_{FA}^{Skel}(0)\,[1-\mathrm{DoR}]\,, \tag{2}$$

$$V_{FA}^{Voids}(\mathrm{DoR}) = V_{FA}^{Voids}(0) - \beta\mathrm{DoR},\ V_{FA}^{Voids}(\mathrm{DoR}) \geq 0, \tag{3}$$

$$V_{SGP}(\mathrm{DoR}) = \left[V_{FA}^{Skel}(0) + \alpha\right]\mathrm{DoR}, \tag{4}$$

$$V_{OP}(\mathrm{DoR}) = 1 - V_{FA}^{Voids}(\mathrm{DoR}) - V_{FA}^{Skel}(0) - \alpha\mathrm{DoR}, \tag{5}$$

Parameters for Eq. 2 – Eq. 5 had to be obtained experimentally. The section Methods describes the assessment of the open porosity in the AAFA. V_{FA}^{Voids} disappear roughly at the DoR=0.5. This conclusion is supported with isooctane saturation of dried-out samples. The method was described previously in [18]. Table 4 summarizes fitted parameters for the volumetric model.

Table 4. Fitted parameters for the volumetric model of alkali-activation.

Parameter	Fitted value, see Fig. 6
$V_{FA}^{Skel}(0)$	0.58
$V_{FA}^{Voids}(0)$	0.06
$V_{OP}(0)$	0.36
α	0.2
β	0.12

Downscaling and Two-scale Homogenization. Elastic properties of the solid gel particles were obtained by means of a downscaling process. Characterization of N-A-S-H gel by nanoindentation was considered to occur at DoR=0.44, which gives the volume fractions summarized in Table 5.

Table 5. Volumetric fractions at DoR = 0.44 and elastic properties of constituents.

Parameter	Volume fraction [-]	Young's modulus [GPa]	Poisson's ratio [-]
$V_{FA}^{Skel}(0.44)$	0.324	104.0	0.20
$V_{FA}^{Voids}(0.44)$	0.001	0.001	0.001
$V_{OP}(0.44)$	0.325	0.001	0.499924
$V_{SGP}(0.44)$	0.350	38.2-**49.8**-59.5[a]	0.22-**0.23**-0.24[a]
Sum	1.000		

[a]) Three values stem from a standard deviation of N-A-S-H gel indentation moduli.

First, the solid gel particles and evaporable water were considered to form the N-A-S-H gel. Volumetric fractions of the above-mentioned phases are 0.5185 and 0.485, respectively. Mori-Tanaka scheme for an isotropic spherical inclusion [19] run with the reference phase of the gel particles and identified elastic properties of them, see Table 5. Standard deviation of indentation moduli for the N-A-S-H gel, 17.72 ± 3.75 GPa, see Table 3, led to the variation of elastic properties of the solid gel particles.

Second, elastic properties of AAFA constituents were connected with the volumetric model for alkali-activation. Two-level elastic homogenization seems to give reasonable results. At the first level, elastic properties of the N-A-S-H gel, composed from the solid gel particles and evaporable water in the open porosity, were obtained using the Mori-Tanaka method with the reference phase of the solid gel particles. The second level homogenized the gel, fly ash and voids in the fly ash, by repeating the Mori-Tanaka method with the reference phase of the N-A-S-H gel.

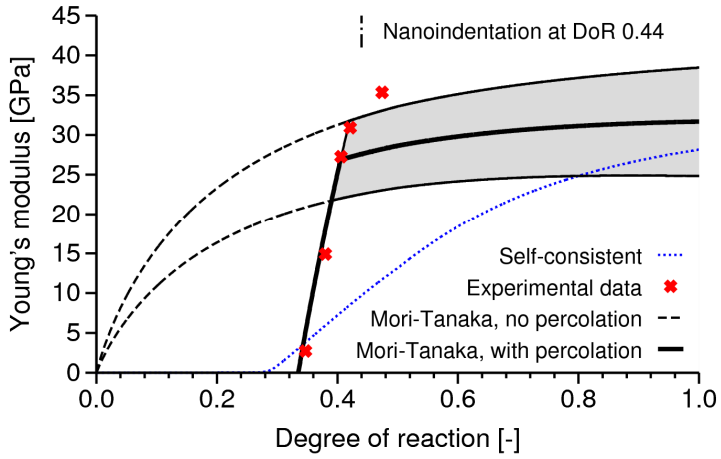

Figure 7. Homogenized elastic properties of alkali-activated fly ash combining the volumetric model, Mori-Tanaka homogenization method and the percolation theory.

Fig. 7 summarizes the results from two-scale homogenization at the level of AAFA. Experimental data came from a non-destructive measurement by a cyclic loading. The load level attained approximately 0.3 of the ultimate load. The force was applied uniaxially on prismatic samples 40 x 40 x 160 mm, equipped with a set of extensometers to control the bending.

Homogenization solely by Mori-Tanaka method shows a big discrepancy in the beginning of alkali-activation process. The reason lies in percolation properties of true N-A-S-H gel. Until a certain point called a percolation threshold, the solid gel particles are mutually separated although the volumetric model predicts their presence. The assumption of perfect bonding, on which the homogenization methods are based, is violated at this stage. Percolation problems are known to occur in early ages of hydration in the system of Portland cement paste [9]. Introducing the percolation function in the form

$$p = (DoR - DoR_p), \tag{6}$$

allowed to capture the percolation threshold, DoR_p, from which the N-A-S-H gel modulus becomes non-zero. The Young modulus from the N-A-S-H gel is multiplied with the Eq. 6. Calibration to the experimental data yielded DoR_p=0.335 and also set the upper limit at DoR = 0.405, above which percolation plays no role and Eq. 6 yields p=1.

The thick line in Fig. 7 shows the elastic prediction in terms of average AAFA's modulus. Introducing the scatter in the solid gel particles leads to widening the range of validity and seems to cover almost all experimental points. In addition, the self-consistent scheme in Fig. 7 demonstrates that intrinsic percolation threshold associated with the scheme is in reasonable correlation with experimental data. However, later elastic properties via the self-consistent scheme would be seriously underestimated, which denies its application.

Fig. 8 shows elastic results from the first level of N-A-S-H gel. The percolation function gives a negligible elasticity when DoR_p<0.335. At the percolation threshold, the volume fraction of the solid gel particles are V_{SGP}=0.2613 and that of the open porosity V_{OP}=0.3332. It means that the percolation threshold occurs when the solid gel particles have the relative volume 0.4395. Rintoul and Torquato [20] performed an extensive numerical study in the system of identical (monodisperse) overlapping spheres, resulting in the percolation threshold 0.2895±0.0005. The percolation threshold changes when a particle size distribution is taken into account. Two distinct sphere diameters were found to have the percolation threshold as high as 0.70 [21].

Note that the N-A-S-H gel is still stiffening due to increasing fraction of solid gel particles. The presented model, based on a packing density of the solid gel particles, does not address changes within the particle, which may polymerize on the atomistic scale.

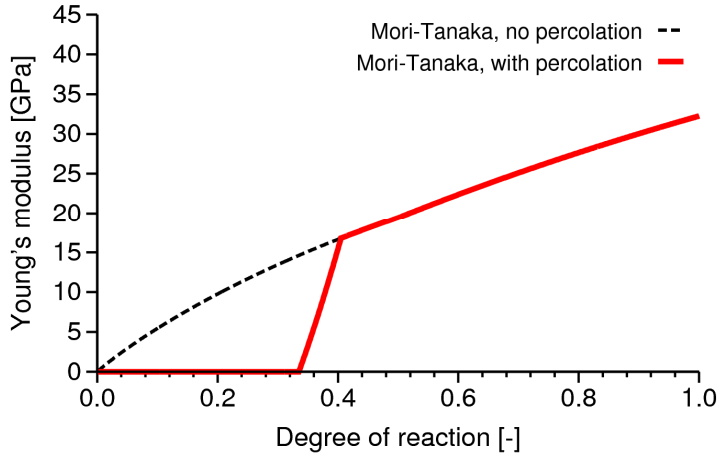

Figure 8. Evolution of Young's modulus within the N-A-S-H gel. Results from the volumetric model, Mori-Tanaka homogenization method and percolation theory.

Conclusions

The combination of nanoindentation, micromechanical modeling and volumetric model provides a different point of view on alkali-activated materials, particularly those made from the fly ash. The N-A-S-H gel is a true gel and the early elastic behavior can be conveniently described using the percolation theory. The models explain several phenomena occurring during the hardening and clarify why the hardening occurs within many days at ambient curing temperature and why the initial and final setting times lay so much far apart. Heat-curing process seems to be a necessity for the production of these materials on a large scale.

The Young modulus of the N-A-S-H gel (~18 GPa) is quite similar to C-S-H gels (21.7-29.4 GPa) [12]. Beyond the point of chemical compatibility, these gels can also coexist well together from the micromechanical match of the elastic moduli.

Acknowledgement

The authors gratefully acknowledge the financial support from the Czech Science Foundation, grant 103/08/1639 “Microstructure of inorganic aluminosilicate polymers”.

References

[1] F. Pacheco-Torgal, J. Castro-Gomes, S. Jalali: Alkali-activated binders: A review: Part 1. Historical background, terminology, reaction mechanisms and hydration products, Construction and Building Materials Vol. 22 (2008), p. 1305 – 1314.

[2] P. Duxson et al.: Geopolymer technology: the current state of the art, Journal of Materials Science Vol. 42 (2007), p. 2917 – 2933.

[3] C. Shi, P. V. Krivenko, D. Roy: *Alkali-activated cements and concrete* (Taylor & Francis, 2006).

[4] F. Škvára et al.: Material and structural characterization of alkali activated low-calcium brown coal fly ash, Journal of Hazardous Materials Vol. 168 (2009), p. 711-720.

[5] A. Fernández-Jiménez et al.: Immobilization of cesium in alkaline activated fly ash matrix, Journal of Nuclear Materials Vol. 346 (2005), p. 185-193.

[6] V. D. Glukhovsky: *Soil Silicates (Gruntosilikaty)* (Kiev, Budivelnik publisher, USSR 1959).

[7] J. Davidovits: Synthesis of new high-temperature geo-polymers for reinforced plastics/composites, in Proceedings of PACTEC'79, Society of Plastic Engineers (1979), p. 151-154.

[8] O. Bernard, F.-J. Ulm, and E. Lemarchand: A multiscale micromechanics-hydration model for the early-age elastic properties of cement-based materials, Cem. Concr. Res. Vol. 33 (2003), p. 1293-1309.

[9] V. Šmilauer, Z. Bittnar: Microstructure-based micromechanical prediction of elastic properties in hydrating cement paste, Cem. Concr. Res. Vol. 36 (2006), p. 1708-1718.

[10] I. Beleňa, W. Zhu: Nanoindentation Study of Na-Geopolymers Exposed to High Temperatures, in Proceedings of the Nanotechnology in Construction 3, edited by Z. Bittnar et al. (Springer, 2009), p. 169 – 174.

[11] F. Lea, *Lea's Chemistry of Cement and Concrete* (Elsevier 2004).

[12] G. Constantinides et al.: Grid indentation analysis of composite microstructure and mechanics: Principles and validation, Materials Science and Engineering A (2006), p. 189-202.

[13] A. Fernández-Jiménez, A. Palomo, and M. Criado: Microstructure development of alkali-activated fly ash cement: a descriptive model, Cem. Concr. Res. Vol. 35 (2004), p. 1204-1209.

[14] A. Palomo, M. W. Grutzeck, and M. T. Blanco, Alkali-activated fly ashes. A cement for the future, Cem. Concr. Res. Vol. 29 (1999), p. 1323-1329.

[15] G. W. Scherer: Structure and properties of gels, Cement and Concrete Research Vol. 29 (1999), p. 1149 – 1157.

[16] T. C. Powers and T. L. Brownyards: *Studies of physical properties of hardened Portland cement paste*, Bulletin 22 (Chicago: Research Laboratories of the Portland Cement Association 1948).

[17] N. J. Carino and H. S. Lew: *The maturity method: from theory to application* (NIST, 2001).

[18] D. S. Perera: Influence of curing schedule on the integrity of geopolymers, Journal of Materials Science Vol. 42 (2007), p. 3099-3106.

[19] T. Mori and K. Tanaka: Average stress in matrix and average elastic energy of materials with misfitting inclusions, Acta Metallurgica Vol. 21 (1973), p. 1605-1609.

[20] M. D. Rintoul and S. Torquato: Precise determination of the critical threshold and exponents in a three-dimensional continuum percolation model, J. Phys. A: Math. Gen. Vol. 30 (1997), p. 585-592.

[21] S. Torquato: *Random Heterogeneous Materials. Microstructure and Macroscopic Properties* (Springer-Verlag New York, 2001).

doi:10.4028/www.scientific.net/AST.69.86

Evaluation of the stability of waste-based geopolymeric artificial aggregates for wastewater treatment processes under different curing conditions

Isabel Castanheira e Silva[1,a]; João Castro-Gomes[2,b]; António Albuquerque[3,c]

[1] Castelo Branco Polytechnic Institute and Centre of Materials and Building Technologies, University of Beira Interior, 6201-001 Covilhã, Portugal, Tel: +351 275329981, Fax: +351 275329969

[2, 3] Centre of Materials and Building Technologies, University of Beira Interior, 6201-001 Covilhã, Portugal, Tel: +351 275329990, Fax: +351 275329969

[a] icastanheira@esa.ipcb.pt [b] castro.gomes@ubi.pt , [C] ajca@ubi.pt

Keywords: Artificial aggregates; compressive strength; geopolymers, wastewater treatment

Abstract. Waste geopolymeric artificial aggregates (WGA) with different atomic ratios of mining waste mud/Na_2SiO (4 to 5) and Na_2SiO/NaOH (1.25 to 5) were produced using curing temperatures of 20ºC and 130ºC and its structural stability and pH variation after immersion in water was observed during 3 months. Results showed that WGA with mud/Na_2SiO and Na_2SiO/NaOH of 5 and 4, respectively, cured at 20ºC presented good stability in water and pH decreased from 10 to 7 in 24 days. Compressive strength was determined in additional samples cured at 20ºC and 80ºC in dry conditions, for 13 curing ages and 15 water immersion periods (up to 14 weeks). Results of this second stage showed that increasing temperature to 80ºC accelerated compressive strength gain but only during the first 3 weeks (up to 15.4 MPa). After 24 h in water compressive strength decreased to half of the initial values determined in dry conditions in all samples and, therefore, the increase of temperature did not bring benefits to WGA strength in water. Regardless the curing temperature and the dry curing age comprehensive strength stabilizes between 1 MPa and 2 MPa after 4 weeks immersion in water, which are values that makes WGA suitable to be used as bed material for wastewater treatment processes.

1. Introduction

Some artificial materials (*e.g.* light-expanded clay aggregates (LECA) and thermoplastics) have shown to be more efficient and cost-effective competitive over conventional natural materials (*e.g.* gravel and sand) for wastewater treatment processes (WWTP) [1,2]. Bed materials frequently present clogging problems whose causes are related to the variation of its properties (*e.g.* compressive strength, specific surface area, void fraction and porosity), the release of fine material, excess of particulate matter and suspended solids and the development of precipitates [1] leading to resistance to flow and, therefore, to the decrease in treatment.

The use of hazardous materials or sub-products of combustion to produce artificial bed material for WWTP (namely to produce potential value of zeolitic materials) is a new area of research and a few studies have already been performed using coal fly ash [4] and agricultural by-products [3] for the removal of heavy metal, ammonia, residual organics and chlorine. The use of LECA is considered a good alternative solution compared with granite gravel to minimize the clogging problem and to increase the treatment capability [2,4]. LECA is a material with high porosity and water absorption capacity and good specific surface area, void fraction and adsorption capacity, which gives good conditions to remove pollutants through chemical and biological pathways. However, for some WWTP (*e.g.* biological packed bed and constructed wetlands) it is too light and did not fix easily as bed support.

Geopolymers are materials produced by reaction of aluminosilicate raw materials in alkaline environments and its production depends on chemical and mineralogical composition of the precursor materials (*e.g.* waste mud, fly ash, slag and clay), curing temperature, curing age, water content and type and concentration of the alkaline compounds [6,12,17,21]. It is a potential material for WWTP due to its high strength, good durability, low shrinkage, sulphate and acid resisting properties. It should also present appropriate porosity, void fraction and specific surface area and not change the characteristics of the water (*i.e.* not changing the pH or releasing hazardous materials into the water). Previous studies have demonstrated that alumino-silicate waste mud from a tungsten local mining exploration has very good reactivity with alkaline activators (sodium silicate and sodium hydroxide) after a thermal calcination (800ºC to 950ºC) to produce very resistant (10 to 90 MPa) waste geopolymeric artificial aggregates (WGA) [5].

Therefore, this work studies the influence of curing conditions (temperature and dry age) in the mechanical resistance of WGA produced with different atomic ratios of mining waste mud/Na_2SiO (4 to 5) and Na_2SiO/NaOH (1.25 to 5) in dry conditions and after immersion in water. The pH variation after immersion was also measured. Compressive strength gain/loss was evaluated on the most stable mixture for curing temperatures of 20ºC and 80ºC and different dry curing ages, as well as for additional different water immersion periods.

2. Materials and Methods

WGA was obtained using waste mud (*precursor* - P) from a local tungsten mine, after a thermal treatment for 2 hours at 800ºC as suggested by [7]. The chemical composition of the waste mud was determined by energy dispersive spectrometry (EDS, Rontech, Germany) as follows: 68.54% (SiO_2), 1.14% (Na_2O), 18.27% (Al_2O_3), 5.64% (Fe_2O_3), 5.24% (K_2O) and 1.17% (TiO_2). NaOH 10M solution (H) and a Na_2SiO L60 solution (S) were used as *alkaline activators*. The specific surface of the precursor (7.9 m^2/g) was calculated through the air permeability Blaine method using an EN 196-6 equipment (Acmel Labo, France).

In a first stage four mixtures of WGA having different atomic ratios of R(P/S) and R(S/H) were produced as presented in Table 1. Samples with 2x3 cm size and having an approximate shape of natural aggregates were left to cure at 20ºC for approximately 48 hours (16 samples per mixture). Half of samples were cured at 20ºC while the other half was cured at 130ºC. For the curing ages of 7, 14, 21 and 28 days, two samples of each mixture, for each curing temperature, were placed in vessels containing 1 L of water as described in [6]. The time of beginning of sample defragmentation and the daily pH were registered. Water in vessels were replaced each 24 h. pH observations were stopped once the values reached 7.

Table 1. Geopolymeric mixture composition and mass ratios R(S/H) and R(P/S)

Mixture	Na_2SiO_3 (g) Solution	NaOH (g) Solution	Precursor (g)	R(S/H)	R(P/S)
M1	187.5	150	750	1.25	4
M2	187.5	62.5	750	3	4
M3	187.5	46.9	750	4	4
M5	150	37.5	750	4	5

In a second stage, the mixture with more stable behaviour was selected for testing compressive strength in dry and wet conditions. Samples with 40x40x40 mm^3 were produced in a total of 352 cubes. The samples were first submitted to an initial dry curing period of 7 days at 20ºC and approximately 40% relative humidity and afterwards 144 units were kept at 20ºC while the other 208 units were cured at 80ºC followed by different periods of immersion in water. In Phase I, the 144 samples (cured at 20ºC) were immersed in water after 35, 42, 49, 56, 63, 70, 77, 84 and 91 days dry curing ages (9 Series of experiments, each one including 16 samples for testing). In Phase II, the 208 samples cured at 20ºC (during an initial period of 7 days in moulds) and 80ºC (after removal

from moulds) were immersed in water for the same dry curing ages (13 Series of experiments, each one including 16 samples for testing).

After each dry curing age, a set of 15 samples of each Series in each Phase was selected for water immersion in separate vessels containing approximately 1 L of water during 24 hours, 7, 14, 21, 28, 35, 42, 49, 56, 63, 70, 77, 84, 91 and 98 days (*i.e.* from 1 to 14 weeks of immersion period). During the immersion period the water in the vessels was changed every two days. A dry sample of each Series was tested to evaluate the compressive strength in dry conditions. After each immersion period, samples were removed and submitted to compressive strength (*i.e.* compressive strength was carried out for dry conditions and for 24hours, 7, 14, 21, 28, 35, 42, 49, 56, 63, 70, 77, 84, 91 and 98 days after immersion in water in each Series of both Phases). Compressive strength was determined according to ASTM C 109 for testing hardened concrete.

3. Results and Discussion

The first stage have shown that the average time necessary to get a pH of 7 varied as follows: 58±19 days (M1), 50±7 days (M2), 63±7 days (M3) and 24±7 days (M4). The mixture 7 had the lowest pH of the maximum observed in each experiment after the first day of immersion. For mixtures M1, M2 and M3, only the samples cured at 130ºC maintained the stability whilst, for mixture M4, there were samples cured at 20ºC that maintained the stability along the 3 months. In terms of structural stability in water and pH stabilization in a short period of time, mixture M4 (cured at 20ºC during 28 days) seems to present good potential for application in WWTP.

Previously studies [6] have shown that a minimal of 35 days was required for total activation of WGA at 20ºC. Therefore, the mixture M4 cured during 35 days at 20ºC was selected for the second stage of experiments. As presented in Figure 1, WGA showed different tendency (gain or loss) in evolution of strength for both curing temperatures. Samples cured at 20ºC in dry conditions presented higher compressive strength at early curing ages (9.1 MPa for 42 and 49 days) that decreased and became more instable for curing ages over 56 days. The average compressive strength between 42 and 91 days curing time was 7.3 MPa. Results observed at 20ºC are in agreement with the ones observed by Torgal *et al*. [5] for NaOH 24M but three times lower, which reflects the effect of activator concentration in the strengthening of WGA.

In samples cured at 80ºC compressive strength was higher than the observed in samples cured at 20ºC except for older curing ages, reaching a maximum value of 15.4 MPa for 21 days. The higher curing temperature for more than 21 days does not seem to positively have affected the compressive strength (values ranged from 11 MPa and 13.6 MPa between 21 and 63 curing ages) and curing for more than 63 days decreased the strength rapidly. Strength decline may be explained by the prolonged curing period at high temperature that breaks down the gelular structure of the geopolymer synthesis mixture, resulting in dehydration and excessive shrinkage as observed by [12]. WGA has shown high strength when cured at 80ºC even at early dry curing ages confirming the extreme reactivity of mine waste mud when activated with a highly alkaline solution. Similar results were observed by [9] that reported strength increase with curing temperature for alkali-activated fly ash. Therefore, the reason for gain and loss of strength could be explained by the occurrence of two parallel processes: further geopolymerisation of the unreacted waste mud and/or sintering process (strength increase); breakdown of the geopolymer structure due to exposition to prolonged high temperature (strength decrease). These two opposing processes may have occurred simultaneously in the WGA cured at 80ºC and whether the strength increases or decreases is dependent on the dominant process.

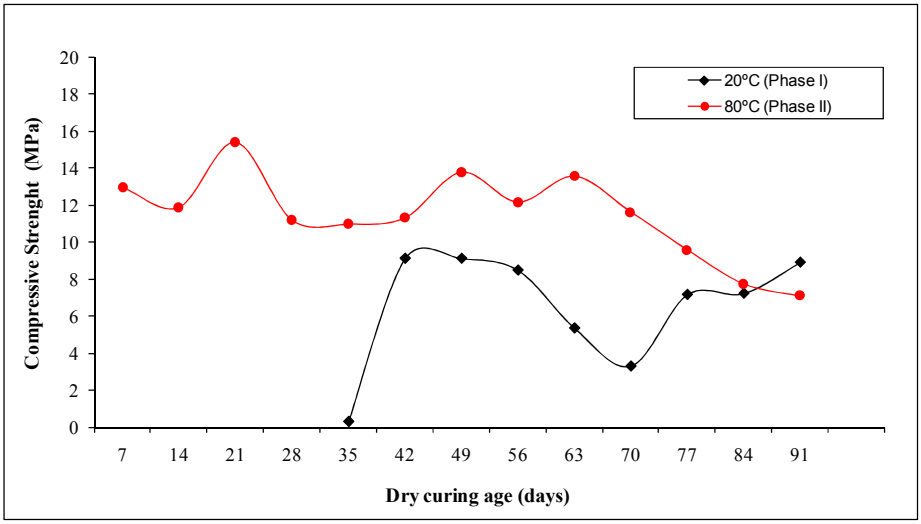

Figure 1. Compressive strength variation over dry curing ages for 20ºC and 80ºC curing temperatures (mixture M4)

Regardless the curing temperature and curing age, compressive strength reduced to approximately half of initial values (dry conditions) after 24 hours of water immersion (Figures 2 and 3). The decrease in strength continued during the first 4 weeks of immersion, stabilizing most of samples after that time between 1 MPa and 2 MPa. In samples cured at 20ºC for longer dry curing ages (91 days) the values stabilized between 2 MPa and 3 MPa after 6 weeks of immersion. These results show that water curing leads to a strength decrease of WGA as also observed by [10] for alkali-activated metakaolin. Water in excess seems to have affected the hydrolysis species and, therefore, hinders polycondensation kinetics, leading to molecular destabilization of the geopolymer matrix. Additionally, alkali ions have leached out from surfaces of geopolymers leading to pH rising, which may have contributed for a slow compressive strength development.

Regardless the ratios of P/S and S/H, all samples cured at 20ºC during less than 35 days disintegrated or dissolved in water between 1 day and 2 weeks. This behaviour might be related to the stage of geopolymer activation and mixture composition, which may have changed after contact with water. It is believed that increasing R(P/S) might result in higher Si and Al dissolution resulting in better geopolymerisation and consequently a stronger geopolymer structure. According to [7], the final SiO_2/Al_2O_3 atomic ratio in the hardened binder depends mainly on the reactivity of Al–Si because not all the silica and alumina are reactive. Admitting that Al and Si have synchro-dissolution behaviour in alkaline solution they could be dissolved from the mineral in some linked form and, therefore, the Si/Al ratio was not the same in the final hydration product.

For Si/Al of 1.9 [7] good results in strength were obtained with Al/Na equal to 1 and H_2O/Na_2O equal to 11. It was also found that Na^+ cation play a role in order to balance the deficit of electrical charges of the aluminium atom, and so the ratio Na/Al should be close to 1 for all bonds Si-O-Al to be established. However, the increased resistance is not only due to the strength of connections but also to the improvement of the microstructure. The molar ratios of the WGA used in this study were as follows: $Na_2O/SiO_2 = 0.053$, $Na_2O/Al_2O_3 = 0.36$, $SiO_2/Al_2O_3 = 6.852$ and $H_2O/Na_2O = 14.129$. The Na_2O/SiO_2 and Na_2O/Al_2O_3 ratios are too low and SiO_2/Al_2O_3 ratio is too high when compared with [27] results, namely $4.86 < SiO_2/Al_2O_3 < 5.9$, $0.31 < Na_2O/SiO_2 < 0.41$ and $1.50 < Na_2O/Al_2O_3 < 2.42$. On the other hand, the ratio of H_2O/Na_2O is also too high when compared with [27] results and could have lead to lower compressive resistance values, as found by [7].

The compressive strength after immersion stabilized around 1-2 MPa similar to the values presented by LECA (1.7 MPa), which needs high temperatures to be produced, but lower than the ones presented by granite gravel (up to 120 MPa), which is extracted from earth. The advantage of this WGA over that two materials is that it is produced from an hazardous material (*i.e.* promotes the reuse and encapsulation of waste mud from mine activities) at 20ºC, presents good stability in

water, does not change significantly the characteristics of water, is durable and, therefore, may have the same effectiveness of other materials for pollutant removal from wastewaters.

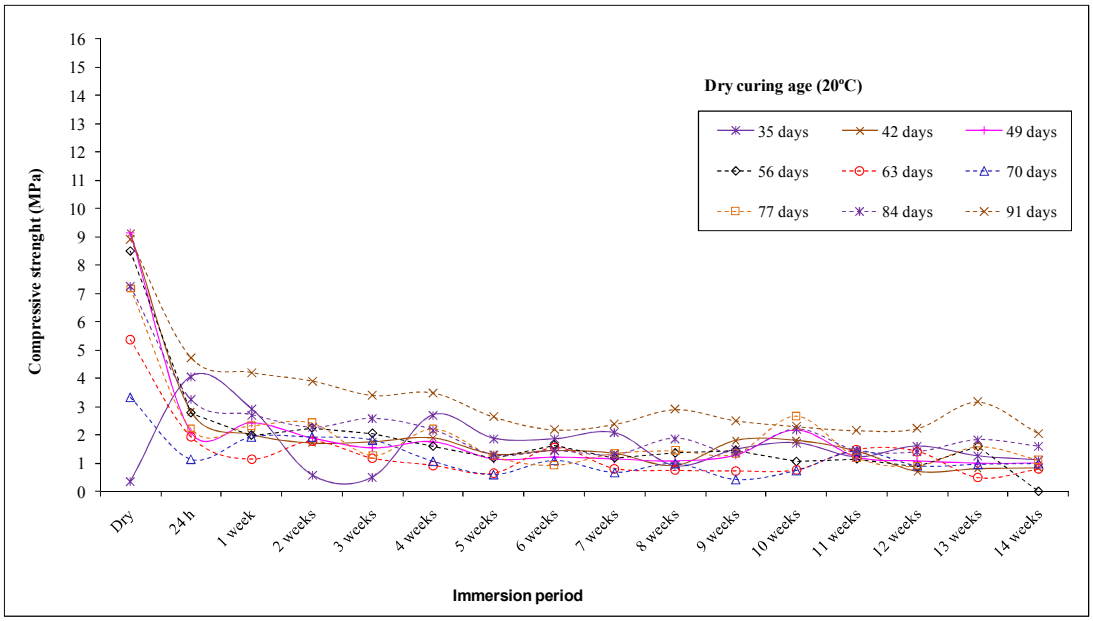

Figure 2. Compressive strength over water immersion period for curing temperature of 20ºC (Mixture M4 - Phase I)

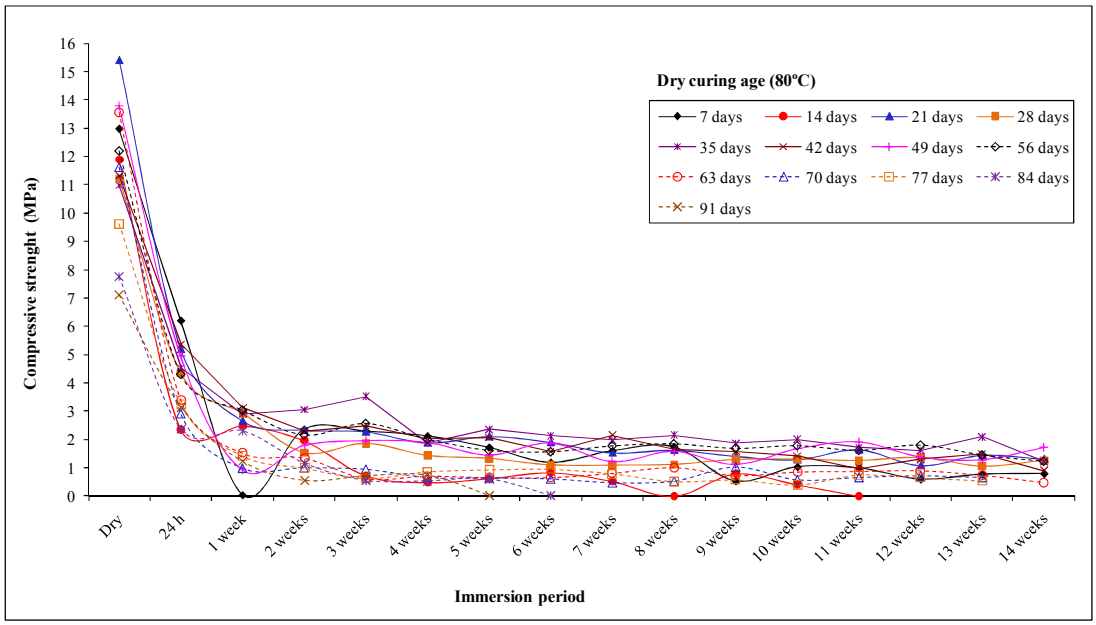

Figure 3. Compressive strength over water immersion period for curing temperature of 80ºC (Mixture M4 - Phase II)

4. Conclusions

The mixture M4 was found to be structurally stabled in water for a period of 6 months and having pH stabilization around 7 in the shortest period of time (24 days). Results obtained on mixture M4 for different curing conditions showed that compressive strength increased with curing temperature but not with curing age. Regardless of the curing temperature and curing age, compressive strength reduced to approximately half of initial values (dry conditions) after 24 hours of water immersion, stabilizing between 1 MPa and 2 MPa after 4 weeks immersion. As compressive strength after longer periods of water immersion was equivalent in samples cured at 20ºC and 80ºC, WGA cured at room temperatures presents both environmental and economical production advantages.

Therefore, WGA produced for ratios R(P/S)=5 and R(S/H)=4, cured at 20ºC and with a minimal curing age of 35 days, it appears as a potential bed material to be used in WWTP.

Acknowledgments

Authors acknowledge FCT by the partial finance through the PTDC/AMB/73081/2006 project.

References

[1] Metcalf and Eddy, Wastewater Engineering: Treatment, Disposal and Reuse. Fourth edition. McGraw-Hill, New York, USA, 2002, 1848 p.

[2] A. Albuquerque, J. Oliveira, S. Semitela, l. Amaral, Influence of bed media characteristics on ammonia and nitrate removal in shallow horizontal subsurface flow constructed wetlands, *Bioresource Technology*, 100 (2009), 6269-6277.

[3] D. Mohan, K. Singh, V. Singh, Wastewater treatment using low cost activated carbons derived from agricultural byproducts—a case study, *J. Hazardous Materials*, 152 (2008), 3, 1045-1053.

[4] R. van Deun, M. van Dyck, Expanded clay and lava rock as potential filter media for nutrient removal in vertical subsurface flow constructed wetlands, Proc. Society of Wetland Scientists European Chapter Meeting, SWS, Kuressaare, Saaremaa, Estonia, 23 p., 2008.

[5] F. Pacheco-Torgal, J. Castro-Gomes, S Jalali, Investigations on mix design of tungsten mine waste geopolymeric binder, *Construction and Building Materials*, 22 (2008), 9, 1939-1949.

[6] Silva I., Castro-Gomes J., Albuquerque A., Mineral wastes geopolymeric artificial (WGA) aggregates as alternative materials for wastewater treatment processes – study of structural stability and pH variation in water, Proc. of the *International Conference on Sustainable Building Affordable to All (SB10)*, Vila Moura, Portugal, 10 pp, 17-19 March 2010.

[7] F. Pacheco-Torgal, Development of alkali-activated binders using waste mud from Panasqueira mine, PhD thesis, University of Beira Interior, 2007 [in Portuguese].

[8] S. Wang, K. Scrivener, P. Pratt, Factors affecting the strength of alkali-activated slag, *Cem. Concr. Res*., 24 (1994), 1033-1043.

[9] A. Katz, Microscopic study of alkali-activation fly ash, *Cem. Concr. Re*s., 28 (1998), 197–208.

[10] A. Kirschner, H. Harmuth, Investigation of geopolymer binders with respect to their application for building materials. *Ceram. Silic*., 48 (2004), 117–20.

[11] P. Duxson, J. Provis, G. Lukey, S. Mallicoat, W. Kriven, J. van Deventer, Understanding the relationship between geopolymer composition microstructure and mechanical properties, *Colloids and Surfaces A: Physicochem. Eng. Aspects*, 269 (2005),47-58.

[12] J. van Jaarsveld, J. van Deventer, G. Lukey, The effect of composition and temperature on the properties of fly ash- and kaolinite-based geopolymers. *Chem. Eng. J*., 89 (2002), 63-73.

doi:10.4028/www.scientific.net/AST.69.92

Durability of Geopolymer Concrete upon Seawater Exposure

ASTUTININGSIH Sotya[1, a], NURJAYA Dwi Marta[1], ASHADI Henki Wibowo[2] and SWASTIKA Niken[1]

[1]Department of Metallurgy and Materials Engineering, Faculty of Engineering, University of Indonesia, Kampus UI, Depok 16424, Indonesia

[2]Department of Civil Engineering, Faculty of Engineering, University of Indonesia, Kampus UI, Depok 16424, Indonesia

[a]sotya.astutiningsih@ui.ac.id

Keywords: Geopolymer concrete, ASTM seawater, Fly ash, Dehydroxylated kaolin, Compressive strength

Abstract. Geopolymers are claimed to be resistant to chemical attack due to the absence of calcium. Geopolymer concrete with designed strength of 40 Mpa has been mixed from coarse aggregates, sands and geopolymer pastes. Two kinds of pastes are synthesized from different precursors, i.e. fly ash and dehydroxylated kaolin, using sodium silicate solution as the activator. Compression test pieces of 15x15x15 cm^3 of both geopolymer and ordinary Portland cement (OPC) concretes (ASTM C39) have been cast and cured. Curing was done at room temperature for 1 day while Portland cement concretes were immersed in water for 28 days to provide complete hydration. After curing, the samples were immersed in ASTM seawater (ASTM D1141-90) for 7, 28, 56 and 90 days. It is found that geopolymer concretes were in general more durable upon seawater immersion than OPC concrete, This is indicated by the compressive strength retained after immersion. Dehydroxylated kaolin geopolymers show the best performance whose strength did not decrease with time of immersion. The strength of fly ash geopolymers decreased by about 20% during 56-day immersion but did not decrease further. Calcium content is suspected to cause the decrease in strength upon immersion. Kaolin geopolymers containing no calcium showed the best performance, while OPC which consist mostly of calcium silicate hydrates as the strength contributor, showed consistent decrease in strength. It is also found from the experiment that room temperature curing of fly ash geopolymer was slow but continued to progress until 28 days both under dry condition (not immersed) and immersed in water.

Introduction

Indonesia, an archipelagic country with 17,504 islands stretching along the equator, has the second longest coastal line in the world, i.e. 8100 km. Marine infrastructure which requires special precaution is thus important in the country with 5.8 million km^2 of marine area. The presence of aggressive Cl and SO_4 ions in seawater decrease the durability of conventional Portland cement concrete which is the dominant material used for construction. On the other hand, geopolymer cement is claimed to be more resistant to chemical attack than OPC [1-3]. Study on mortars made from dehydroxylated kaolin immersed in aggresive solutions (deionized water, ASTM seawater, sodium sulphate and sulphuric acid) proved the durability of these materials [1]. Other investigation on geopolymer pastes made from fly ash and combinations of sodium silicate, sodium and potassium hydroxide as the activators found that in general geopolymers performed better in mechanical strength than ordinary Portland cement upon exposure to acids. However significant degradation was observed in geopolymers with certain type of activator due to depolymerisation [2]. On the contrary, durability of fly ash geopolymer mortars showed that these materiasl are more durable than OPC mortars regardless of the type of activator [3].This paper presents the effect of seawater immersion on the compressive strength of two kinds of geopolymer concretes made from fly ash and dehydroxylated kaolin compared with the OPC concretes.

Experiments

Geopolymer concrete with designed strength of 40 MPa has been mixed from coarse aggregates, sands and geopolymer pastes using the conventional mix design for OPC. Two kinds of pastes have been synthesized from different precursors, i.e. fly ash and dehydroxylated kaolin, using technical sodium silicate solution as the activator. Fly ash used was suppplied from Suralaya power plant, Northwest Java, while kaolin was originated from the island of Sumatra. The chemical compositions of both precursors, analysed using x-ray fluorescence spectrometry, are shown in Table 1 and 2. Molar ratios, using denomination proposed by Rahier et al [4], of fly ash paste and dehydroxylated kaolin paste are presented inTable 3 and 4 respectively. For comparison, conventional Portland cement concrete with the same designated strength was made. Compression test pieces of 15x15x15 cm^3 of both geopolymer and Portland cement concretes (ASTM C39) were cast and cured. Geopolymer concretes casted in sealed moulds were left for 1 day at room temperature to harden and then removed from the molds and left for another 14 days to allow curing, while Portland cement concretes were immersed in water for 28 days to provide complete hydration. After complete curing or hydration, these samples were immersed in ASTM seawater (ASTM D1141-90) for 7, 28, 56 and 90 days. Compressive strength of both kinds of concretes after immersion will be compared with the as-cured samples. Each compressive strength value presented was the average value of three measurements.

Table 1 Chemical composition of fly ash

Compound	Al_2O_3	SiO_2	S	K_2O	CaO	TiO_2	MnO	Fe_2O_3	SrO_2	MgO
Wt%	25.2600	47.2992	0.2969	0.7009	5.1482	1.7579	0.1238	16.5277	0.1743	2.7074

Table 2 Chemical composition of kaolin

Compounds	Al_2O_3	SiO_2	K_2O	TiO_2	V_2O_3	Fe_2O_3
Wt%	42.3029	55.1546	1.2419	0.2068	0.0037	1.0902

Table 3 Molar ratios of fly-ash - geopolymer paste

	Na / Al	Si / Al	H_2O / Na_2O	SiO_2 / Na_2O
Molar ratio	0.5908	2.3331	9.3840	1.7840

Table 4 Molar ratios of dehydroxylated kaolin - geopolymer paste

	Na / Al	Si / Al	H_2O / Na_2O	SiO_2 / Na_2O
Molar ratio	1.2103	1.7414	8.5648	1.0383

Results and Discussions

Fig. 1 shows the effect of seawater immersion on the compressive strength of (a) fly ash geopolymer, (b) dehydroxylated kaolin geopolymer and (c) Portland cement concretes. The strength of fly ash-based geopolymer concreest (Fig 1a), whether in dry condition or immersed in seawater increase with age, up to 28 days. In other words, at room temperature, the target strength of 40 MPa was achieved only after 2 weeks plus 28 days, whether in dry condition or immersed in

seawater. Previous unpublished experiments showed that the target strength of 40 MPa could be achieved in only 24 hours if cured at higher temperature. This agrees with other experiments that for the same period of time, higher curing time resulted in higher compressive strength [5]. Effect of seawater was seen after 28 day immersion in which the strength of the concretes decreased, while the one in dry condition (not immersed) remained.

On the contrary, the target strength could not be achieved by dehydroxylated kaolin geopolymer concretes even until 90 days (Fig 1b) although the maximum strength was achieved earlier than that of fly ash geopolymer concretes. It was suspected that curing could not be optimized due to incomplete dehydroxylation of the kaolin. However, the fact that seawater immersion did not decrease strength suggestsg that kaolin geopolymers were resistant to seawater.

Compressive strength of Portland cement concretes, on the other hand, consistently decreased with time of seawater immersion (Fig 1c). Similar phenomena were also observed where OPC pastes had been immersed in acetic and sulphuric acids [2].

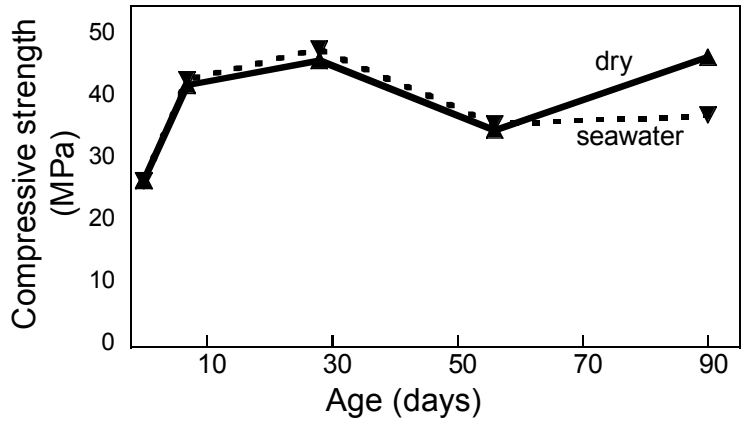

(a)

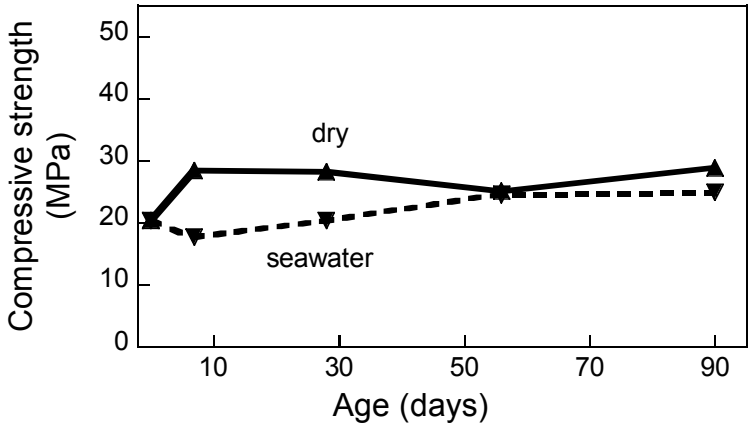

(b)

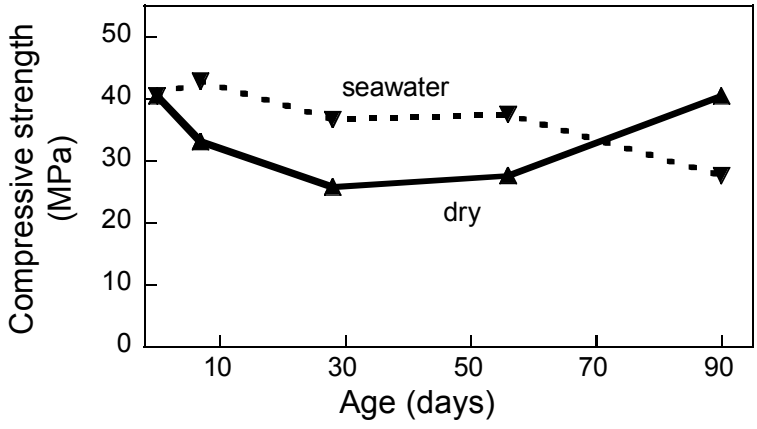

(c)

Fig. 1 Effect of seawater immersion on the compressive strength of (a) fly ash geopolymer concretes (b) dehydroxylated kaolin geopolymer concretes and (c) Portland cement concretes

Compared to Portland cement concretes, geopolymer concretes were more durable if exposed to seawater immersion in a way that mechanical strength did not decrease with time of seawater immersion, as shown in Fig. 2. Although kaolin geopolymers had the lowest strength, which might be due to incomplete dehydroxylation, there was no tendency that strength decreased with time of immersion. The resistance to seawater exposure may relate to the presence of Ca compounds. In dehydroxylated kaolin geopolymers where Ca is absent, mechanical strength was not affected by seawater immersion. Geopolymers synthesized from fly ash, which in this experiment contained 5% Ca oxide, showed a decrease in strength at 56 days but did not decrease further afterwards. Observation of the mechanical strength of the concretes immersed in seawater more than 90 days will provide better information on durability of the concretes since previous study observed fluctuation in flexural strength of metakaolin geopolymer mortars between 7 and 90 days of ASTM seawater immersion which were considered to be due to dissolution-precipitation phenomenon which gave a negative influence on the strength development [1].

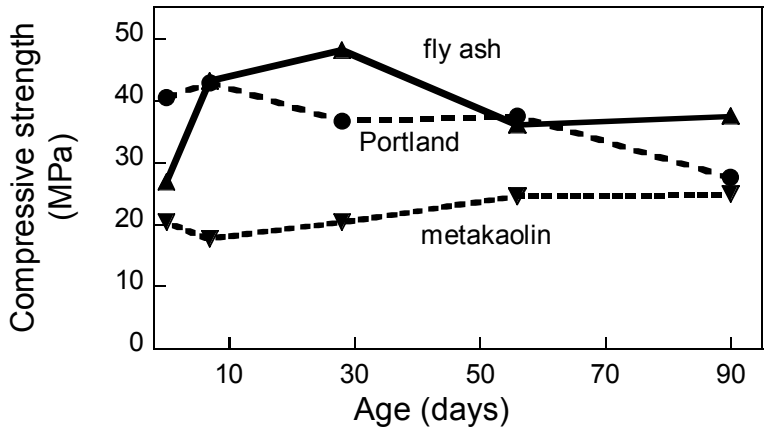

Fig. 2 Comparison of the behavior of fly ash, dehydroxylated kaolin and Portland cement concretes upon seawater immersion.

References

[1] A. Palomo, M.T. Blanco- Varela, M.L. Granizo, F. Puertas, T. Vazquez and M.W. Grutzeck: Cem. Con. Res. Vol. 29 (1999), p. 997

[2] T. Bakharev: Cem. Con. Res. Vol. 35 (2004), p. 658

[3] A. Fernandez-Jimenez, I. Garcia-Lodeiro and A.Palomo: J. Mater. Sci. Vol 42 (2007), p. 3055

[4] H. Rahier, B. Van Mele, J. Wastiels and X. Wu: J. Mater. Sci. Vol. 22 (1996), p. 71.

[5J.G.S. Van Jaarsveld, J.S.J. van Deventer and G.C. Lukey: Chem. Eng. Journal Vol. 89 (2002), p. 63

Summary

Geopolymer concretes, made in this experiment from fly ash and dehydroxylated kaolin, are in general more durable upon seawater immersion than Portland cement concretes. This is indicated by the compressive strength retained after immersion. Dehydroxylated kaolin geopolymer showed the best performance whose strength did not decrease with time of immersion. The strength of fly ash geopolymers decrease by about 20% during immersion of 56 days but do not decrease further. The decrease in strength is suspected to be related to calcium content, as OPC, being composed of mainly calcium silicate compounds, showed a consistent decrease in strength upon seawater immersion. On the other hand, kaolin geopolymers containing no calcium did not show a tendency to decrease in strength. It is also found from the experiment that room temperature curing of fly ash geopolymer is slow but continue to progress after 28 days both under dry condition (not immersed) and immersed in seawater.

doi:10.4028/www.scientific.net/AST.69.97

ROLE OF ALKALINE CATIONS ON GEOMATERIAL FOAMS

E PRUD'HOMME[1], P. MICHAUD[1], E. JOUSSEIN[2], C. PEYRATOUT[1], A. SMITH[1] AND S. ROSSIGNOL[1]

[1] Groupe d'Etude des Matériaux Hétérogènes (GEMH-ENSCI) Ecole Nationale Supérieure de Céramique Industrielle, 47-73 Avenue Albert Thomas, 87065 Limoges
[2] GRESE, EA 3040, 123 avenue Albert Thomas, 87060 Limoges
corresponding author - sylvie.rossignol@unilim.fr – tel.: 33 5 55 45 22 24

Keywords: Potassium, Metakaolin, Porosity, Silica fume, Foam.

Abstract

The synthesis of geopolymers based on alkaline polysialate, was achieved at slightly elevated temperature, by alkaline activation of raw minerals and industrial waste. The materials were prepared from a solution containing dehydroxylated kaolinite and alkaline hydroxide pellets dissolved in potassium or sodium silicate. Then the mixture was transferred to a polyethylene mould sealed with a top and placed in an oven at 70°C during 24 hours. The addition of an industrial waste, silica fume, leads to the formation of an in-situ inorganic foam. Whatever the alkaline cation, foam formation occurs. The properties depend on the viscosity of silicate precursors due to the amount of water and to the size of alkaline.

Introduction

Geopolymers are amorphous three-dimensional alumino-silicate binder materials, which were first introduced to the inorganic cementitious world by Davidovits in 1978 [1]. Geopolymers may be synthesized or slightly elevated temperature by alkaline activation of alumino-silicates obtained from industrial wastes, calcined clays, natural minerals or mixtures of two or more of these materials. In a strong alkaline solution, alumino-silicate reactive materials are rapidly dissolved into solution to form free SiO_4 and AlO_4 tetrahedral units [2, 3]. During the reaction of polycondensation the tetrahedral units are linked in an alternate manner to yield amorphous geopolymers. Geopolymer concretes are based on compounds that are generally produced from one or more solid components (binders) and one or more liquid components (activators), which react together to form strong, durable materials. Some binders have been used like PVA fibers or fly ash by technical extrusion but not in large-scale batch preparation like concrete [4]. Furthermore little work has been devoted to the feasibility of making geopolymer synthesized foam without organic additives [5, 6]. However, some ceramic foam synthesized to mechanical properties is prepared by addition of H_2O_2 and aluminum powders [7]. The aluminum was also used to the production of light weight refractory based on raw minerals [8]. In the same way, glass foams were obtained using sheet glass cullet with dolomite or calcite as foaming agent and displayed efficient compressive strength [9].

Amongst the different families of geopolymers, those based on potassium present modified thermal and mechanical properties due to the larger size of the potassium ion compared to sodium [10].

The aim of this work was to understand the role on the composition of foams based on alkaline species from raw minerals depending on the alkaline hydroxide added base. The kind of the polycondensation reaction of the various samples was determined by in-situ ATR, XRD and by thermal analysis coupled by mass spectrometer.

Experimental Part

Samples preparations

The initial geo-material was prepared from a solution containing dehydrated kaolinite supplied by AGS France and KOH pellets (85.7% of purity) or NaOH pellets (99% of purity) dissolved in potassium silicate or sodium silicate (Si/Na=1.7, density 1.33, 59% of water)11 as described in Figure 1. Two kinds of potassium silicate have been used: SiK_1 with Si/K=1.7, a density equal to 1.33 and 66% of water, and SiK_2 with Si/K=1.7, a density equal to 1.20 and 76% of water. The reactive mixture was then placed in a polystyrene sealed mould in an oven at 70°C during 4hrs so that the polycondensation reaction was complete. Then the material was removed from the mould and placed in an oven at 70°C during 24h for drying. In order to improve thermal properties by industrial waste, silica fume (0.7%wt of free silicon, 97.5%wt of silica, 0.275%wt of carbon) was added to the reactive mixture and placed in oven at 70°C in an open mold for 24hrs.

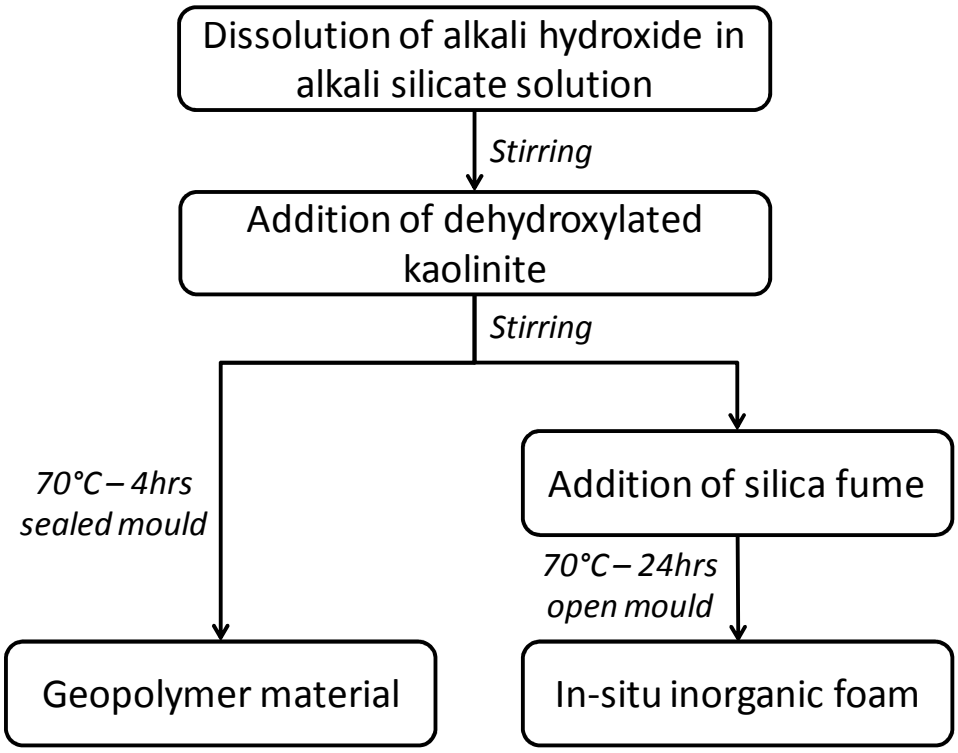

Figure 1: Synthesis protocol of geo-material and in situ inorganic foam.

To compare the influence of the nature of alkaline cation, some foam has been synthesized with the quasi same amount of alkaline using potassium or sodium silicate and potassium or sodium hydroxide (Table I). Samples 11K13Na and 23K0Na were synthesized with SiK_2, instead of 12K12Na and 24K0Na which were synthesized with SiK_1 and contained less water.

Table 1. Composition of various samples

ratio	n_{Al}/n_{Si}	$(n_K+n_{Na})/n_{Al}$	$(n_K+n_{Na})/n_{Si}$
Geopolymer	0.64	0.78	0.50
0K22Na	0.27	1.51	0.40
12K12Na (SiK_1)	0.27	1.51	0.40
11K13Na (SiK_2)	0.28	1.41	0.39
24K0Na (SiK_1)	0.27	1.51	0.41
23K0Na (SiK_2)	0.29	1.31	0.38

Characterization

FTIR spectra were obtained from a ThermoFischer scientific 380 infrared spectrometer (Nicolet) using the attenuated total reflection (ATR) method. The IR spectra were gathered between 500 and 4000 cm^{-1} with a resolution of 4 cm^{-1}. OMNIC (Nicolet Instruments), the commercial software, was used for data acquisition and spectral analysis.

X-ray patterns were acquired via X-ray diffraction (XRD) experiments on a Brucker-AXS D 5005 powder diffractometer using $Cu_{K\alpha}$ radiation ($\lambda_{K\alpha}$ = 0.154186 nm) and a graphite back-monochromator. XRD patterns were obtained using the following conditions: dwell time: 2 s; step: 0.04°. Crystalline phases were identified by comparison with PDF standards (Powder Diffraction Files) from ICDD.

Differential thermal analysis (DTA) and thermogravimetric analysis (TGA) were performed to characterize the solids. TDA–TGA experiments were carried out in a Pt crucible between 25 and 1200°C using a Setaram Setsys evolution. The samples were heated at 10°C.min^{-1} in dry airflow. Thermogravimetric analysis coupled with mass spectrometry (TGA-MS) was performed on a SDT Q600 apparatus from TA Instruments coupled by a heated capillary column with a Prisma QMS 200 mass spectrometer from Balzers. To measure the amount of H_2 formed, the samples were heated to 70°C (heating rate: 5°C/min) and maintained at this temperature during 2 hours under a dry air flow (100 mL/min). The fresh foam thermal analysis was performed up to 800°C (heating rate: 5°C/min) under Ar (100 mL/min).

The morphologies of the final products were determined using a Cambridge Stereoscan S260 scanning electron microscope (SEM). Prior to their analysis, a carbon layer was deposited on the samples.

RESULTS

1. Volumic expansion and microstructure

To increase the thermal resistance by creating porosity in the first synthesized geo-material, corresponding to the formulation $K^{+}_{0.10}[(SiO_2)_{1.63}AlO_2]_{0.10}$, 0.67 H_2O, addition of silica fume has been investigated. The addition of silica fume to the solution of SiO_2, K_2O and KOH in the same conditions as previously used11, gave a very reactant mixture involving the formation of in-situ inorganic foam. This new compound can be considered as a geo-material since the XRD pattern is characteristic of an amorphous material (Figure 2). Effectively, the maximum of diffracted intensity was positioned at similar 2θ values for both the original geo-material and inorganic foam. Moreover, since the XRD peak of the silica fume has disappeared in the foam XRD pattern, the formation of this compound involved dissolution or transformation of the small local order of silica fume. Another process could also appear, based on the presence of the diffraction peak attributed to the $KAlSi_3O_8$ compound. The same mechanism could be observed on the others XRD patterns corresponding to the various exchanges between sodium or potassium elements. From these data, it was very difficult to get information about the nature of alkaline cations since it appears that in SEM photos the microstructure is quite similar (Figure 3).

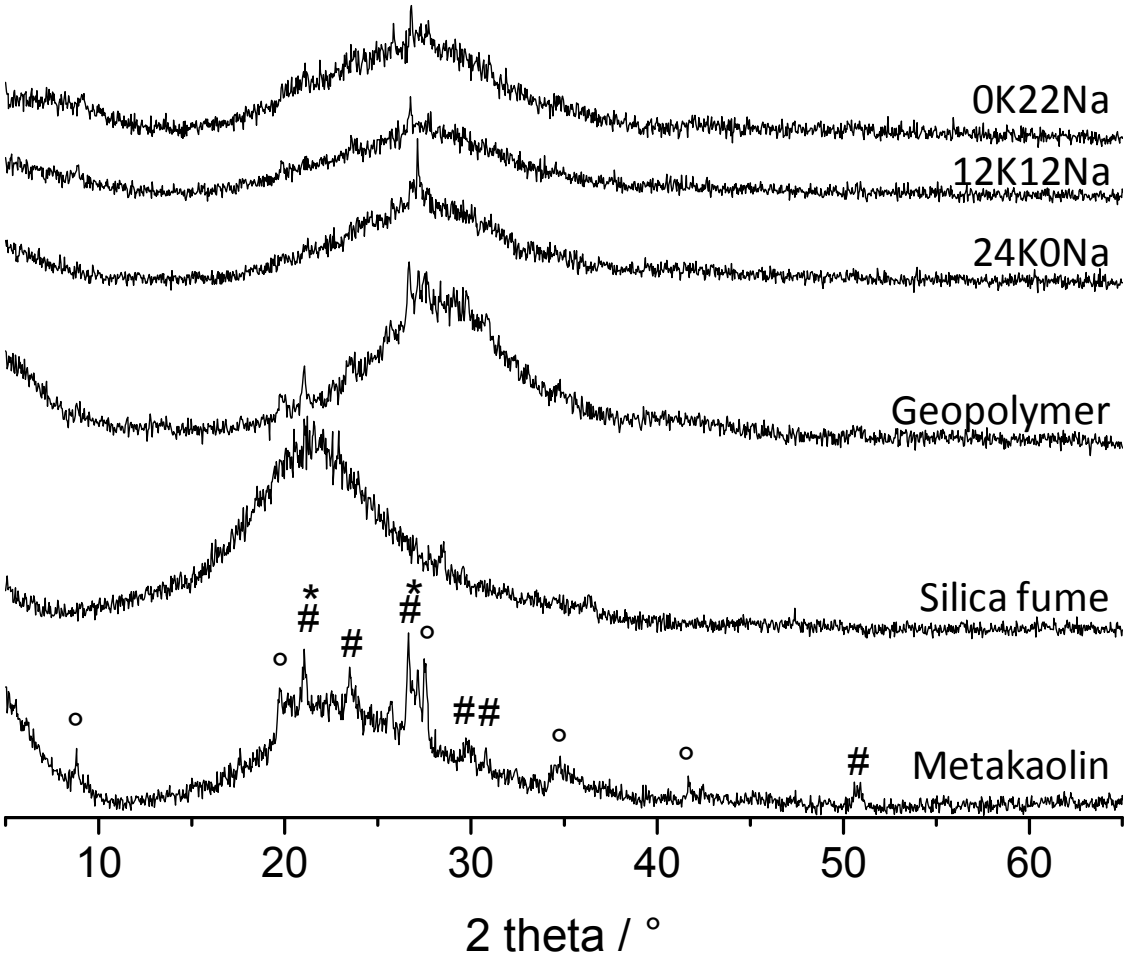

Figure 2. X-ray patterns of metakaolin, silica fume and of various foam compositions. (PDF files: * $KAl_4Si_2O_9(OH)_3$ 01-070-3754; ° Illite 00-002-0056,o; $KAlSi_3O_8$ 00-025-0618

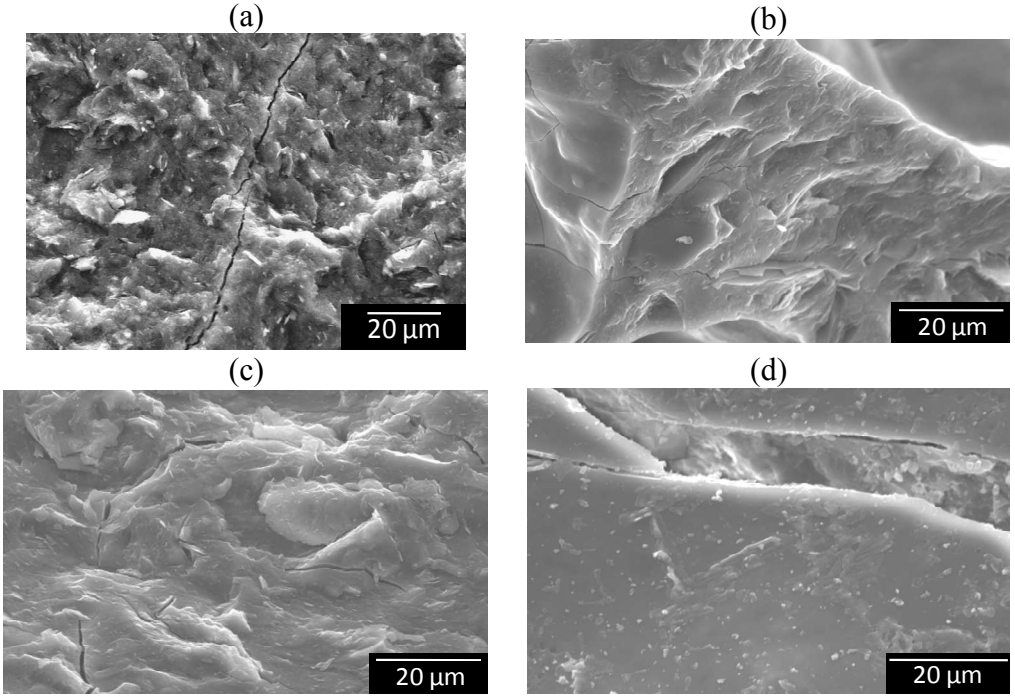

Figure 3. SEM observations of (a) geopolymer, (b) 0K22Na, (c) 12K12Na, (d) 24K0Na.

The inorganic in-situ foam formation can be explained on (i) a production of a gas, (ii) an increase of the viscosity and (iii) a consolidation of material. The generation of porosity was probably due to the H_2 production produced by water reduction and by the oxidation of free silicon in an basic environment ensuring to the formation of $Si(OH)_4$ species. To complete theses hypothesis, some experiments were based on the variation of water content containing in the silicate precursors. The results of volumic expansion correlated to water content are reported in Figure 4.

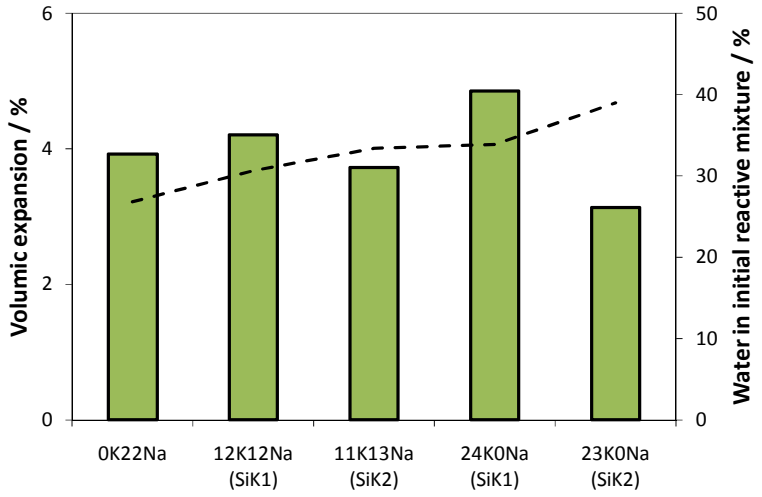

Figure 4. Evolution of ▭ volumic expansion and ▪▪▪ water rate in the initial reactive mixture as a function of various samples.

The water amount of alkaline silicate, as well as the nature of alkaline, induces variations on volume expansion. The comparison between 12K12Na and 11K13Na, and between 24K0Na and 23K0Na samples reveals that an increase of water in silicate involves a decrease of volumic expansion. Effectively, during the foam formation, there is a competition between the viscosity of mixture and the dihydrogen bubbles migration. When the viscosity increases, the gas diffusion is slowed involving a better volume expansion than in a fluid mixture where the bubbles can move. Moreover, the decrease of water content would be inducing a control of the porosity distribution. The substitution of sodium by potassium results in a decrease of volume expansion even if it is difficult to compare since the amount of water is different. However, the higher size of potassium relative to sodium leads to a lattice gel more disordered promoting an easier migration of dihydrogen responsible of the loss of volume expansion.

2. Amount of water and hydrogen: DTA-SM measurements

To complete this observation, experiments based on thermal analysis coupled by mass spectrometry were performed during the foam formation at 70°C (Figure 5). Whatever the samples, the endothermic peaks can be attributed to water loss during foam formation in relation with the ion current given to a mass of eighteen (H_2O). The difference of detected water can be explained by the amount of potassium silicate solution added to the various mixtures. In the case of foam the dihydrogen produced by free silicon can be observed.

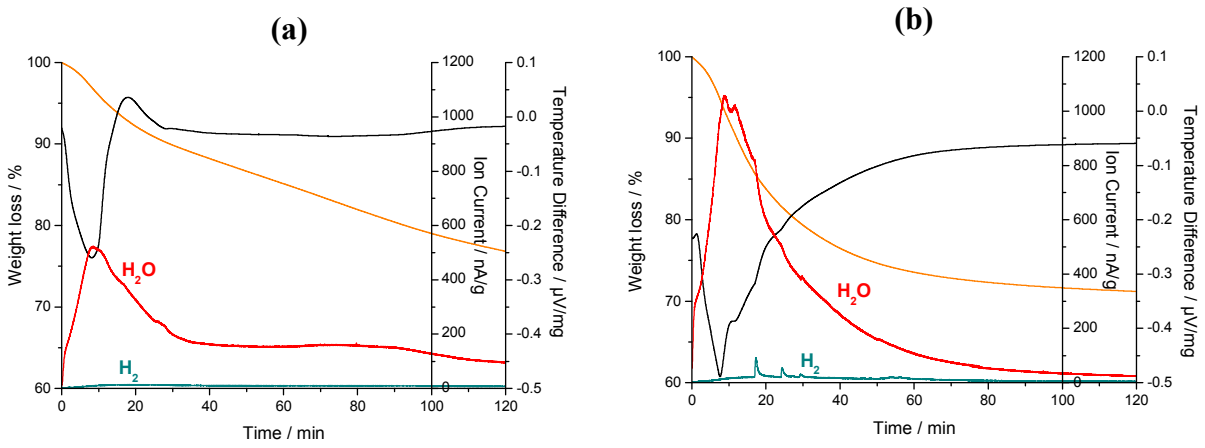

Figure 5. Thermal analysis coupled with SM measurements during formation at 70°C of the (a) geopolymer and (b) 24K0Na.

3. Monitoring of geopolymerisation by FTIR measurements

Since the formation of this material was due to a geopolymerization reaction involving the restructuration of material, therefore an ATR spectroscopy has been realised. A drop of reactant mixture was put on the diamond crystal protected by a cover, which prevented the water evaporation from the mixture at room temperature. These conditions were necessary to promote the polycondensation in closed environment [12]. The figure 6 shows the spectra of $K^{+}_{0.10}[(SiO_2)_{1.63}AlO_2]_{0.10}$, 0.67 H_2O of the first synthesized geo-material recorded as a function of time. The bands on the spectra at t=0h, respectively at 3255 and 1620 cm^{-1}, were attributed to Si-O-H bond and to water. Their intensity gradually diminished with time13. The bands due to Si-O-M bonds [14, 15] (M=Si, Al or K) were located in the 1100-950 cm^{-1} range and their precise positions depended on the length and bending of the Si-O-M bond as given in Table II. The decrease of OH bands compared to the Si-O-Al bands was due to the increase of the polycondensation time and was characteristic of the formation of geo-material. Furthermore, the Si-O-M^{+} [16] shift from 979 to 946 cm^{-1}, also in agreement with the literature data, gives evidence for dissolution of the metakaolin species by the basic environment [17]. This experiment as a function of time proved that, at room temperature, a time of 6h was sufficient to achieve a consolidated geo-material. To find evidence of the disorder in the silica fume lattice, the synthesis of the various foams, based on potassium or sodium, was studied by ATR spectroscopy (Figure 6, b, c, d). The main bands detected for the geo-material were observed on the various foams spectra and in fact the decrease of the OH and Si-O-M bands was faster. The polycondensation reaction in the foam seemed to be finished after 1h30 compared to 6h for geo-material. However, new bands also appeared and were located respectively at 1110, 914, 880, 800 and 670 cm^{-1} corresponding respectively to Si-O-T [17], Al-OH, Si-O-Si [18], Si-O-Al [16], and O-Si-O [14]. First, the decrease of the band at 1110 cm^{-1} linked to amorphous silica confirmed the loss of short range order of the silica fume always seen in the XRD pattern.

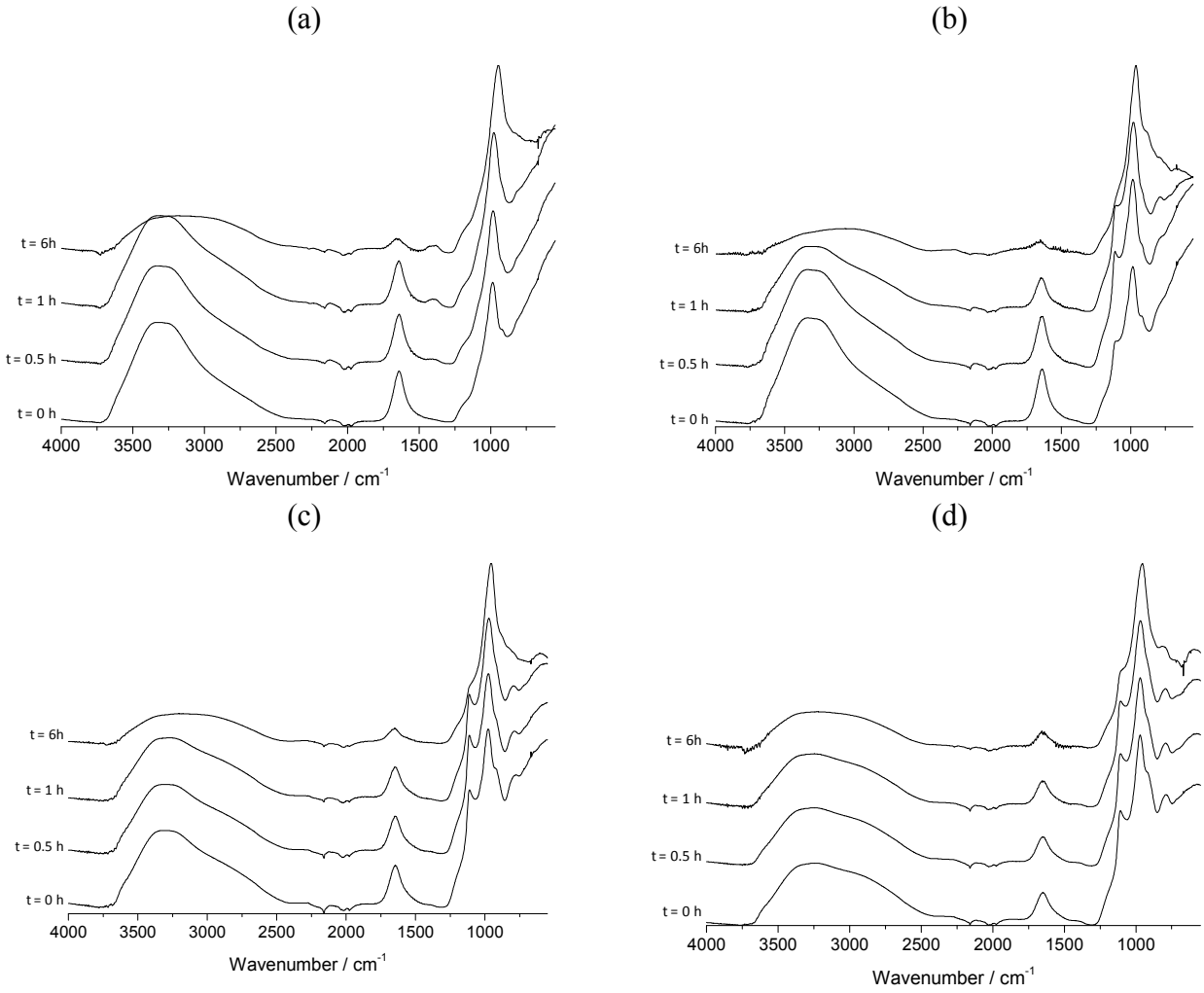

Figure 6. Infrared spectroscopy measurements during foam formation for sample (a) Geopolymer, (b) 24K0Na, (c) 12K12Na, (d) 0K22Na

To confirm this hypothesis, the variation of the band relative to silica fume at 1113 cm^{-1} in function of time for the three foams is showed Figure 7A. Whatever foams, the fast decrease observed reveals the existence of a strong reactant mixture due to the basic middle (pH=14). The difference noted between sodium or potassium can be linked to the nature of alkaline. The fact than the mixture containing the sodium is more viscous than in the case of potassium induces a slowdown of the kinetic reaction. The weak viscosity (24K0Na) involves a mixture very reactant with a high disorder promoting a faster dissolution mechanism.

At the same time, the band at 880 cm^{-1} due to stretching vibration of Si-OH increased revealing the consummation of water involving non bridging oxygen atoms. Similarly, the bands located at 914 and 800 cm^{-1} showed the attack of Al-O species during the geopolymerisation, which was not clearly observed for the geo-material. Another band at 670 cm^{-1} could be attributed to zeolite species and must be verified. These experiments proved the almost complete dissolution of raw materials to create the in-situ inorganic foam.

The differences induced by the use of potassium or sodium take place on the decreases of the band at 1100 cm^{-1} and the shift of the band at 970 cm^{-1}. These bands are respectively characteristic of Si-O-T in amorphous silica more Si-O-R^+ stretching (R=K or Na). To understand this shift, the range of displacement in function of the sample is represented in figure 7B. The position of this initial band (Si-O-R^+) is linked to the nature of alkaline cation as described by Yi Jialiang [19]. The intermediate position corresponding to the 12K12Na sample is in agreement with the mixture with

the same amount of sodium or potassium. Whatever the foam, the range of displacement is weaker than for the geopolymer composition. In presence of the geopolymer composition, the reactant mixture trends to give a stable state composition with an amorphous feature (Figure 2) inducing a decrease in the band position. On the contrary, in presence of the high reactant mixture (production of dihydrogen and dissolution of precursors), the strong metastable state resulting could be becoming fixed. The variation of the scale 24 and 17 cm^{-1}, for respectively 24K0Na and 0K22Na, can be due to a disorder induces by the alkaline element size. Taking into account the viscosity of the mixture in relation with the amount of water is currently in investigation.

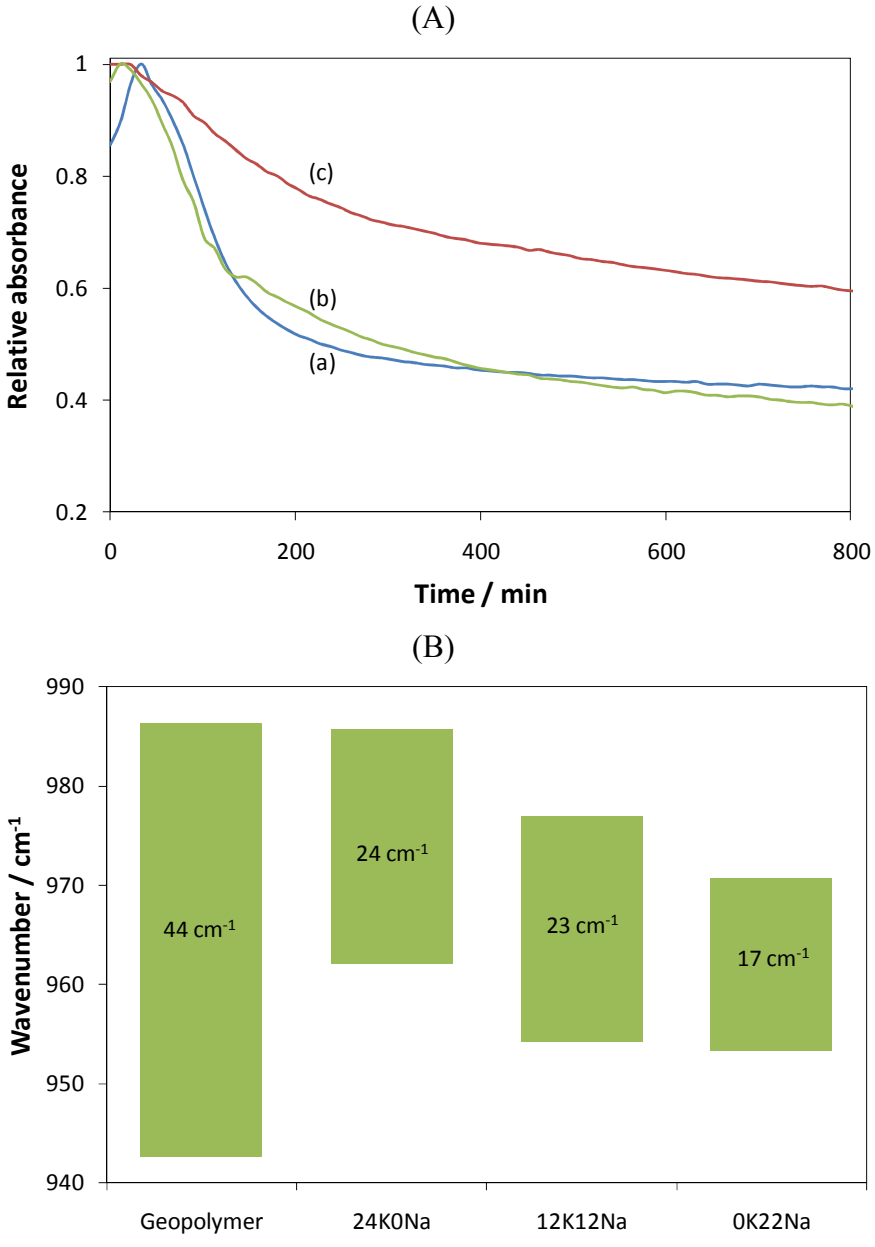

Figure 7. (A) Evolution of band absorbance relative to silica fume at 1113 cm^{-1} as a function of time in the case of (a) 24K0Na, (b) 12K12Na and (c) 0K22Na and (B) range of displacement of the band relative geopolymerisation (Si-O-R^+ vibrations).

CONCLUSION

The synthesis of various consolidated materials (geopolymer, in-situ inorganic foam) prepared from a mixture containing potassium silicate, potassium hydroxide, dehydroxylated kaolinite and

additive like silica fume was succefully achieved. This additive to the geo-material has involved modifications in terms of chemistry and porosity of the sample.

Whatever the alkaline Na or K element, the microstruture and the amorphous feature of the foam appear similar. However, the reactivity of the mixture depending on the viscosity and on the rate of water induces differences such as thermal behavior or silica fume kinetic dissolution.

The synthesized inorganic foam was characteristic of a porous material where the structure can be controlled by the nature of the alkaline cation. This demonstrates the importance of the potassium element. Furthermore, this in-situ inorganic foam is characteristic as an insulating material.

REFERENCES

[1] J. Davidovits, Chemistry and Applications, 19-36 (2008).

[2] H. Xu, Geopolymerisation of Aluminosilicate Minerals, *PhD Thesis*, Department of Chemical Engineering, University of Melbourne, Australia, (2001).

[3] M.W. Grutzeck and D.D Siemer, Zeolithes Synthesised from Class F Fly Ash and Sodium Aluminate Slurry, *J. Am. Ceram. Soc.*, **80 (9)**, 2449-2458, (1997).

[4] Z. Li, Y. Zhang and X. Zhou, Short Fiber Reinforced Geopolymer Composites Manufactured by Extrusion, *Journal Materials in Civil Engineering*, vol **17(6),** 624-631, (2005).

[5] J. P. Wu, A.R. Boccaccini, P.D. Lee and R.D. Rawlings, Thermal and Mechanical Properties of a Foamed Glass Ceramic Material Produced from Silicate Waste, *Eur. J. Glass Sci. Technol. A*, **48 (3)**, 133-141, (2007).

[6] V. Barbosa and K. Mackensie, Synthesis and Thermal Behaviour of Potassium Sialate, *Mater. Letters*, **57**, 1477-1482, (2003)

[7] J.L. Bell and W.M. Kriven, Preparation of ceramic foams from metakaolin-based geopolymer gels, *Ceramic Engineering and Science Proceedings,* **29 (10),** 97-112, (2009)

[8] T. Jettner, H. Moertel, V. Svinka and R. Svinka, Structure of kaoline-alumina based foam for high temperature applications, *J. of European Ceram. Soc*., **27**, 1435-1441, (2007)

[9] H.R. Fernandes, D.U. Tulyaganov, J.M.F. Ferreira, Preparation and characterization of foams from sheet glass and fly ash using carbonates as foaming agents, *Ceram. Inter*., **35**, 229-235, (2009).

[10] P. Duxson, G. C. Lukey, and S. J. Van Deventer, Thermal Conductivity of Metakaolin Geopolymers Used as a First Approximation for Determining Gel Interconnectivity, *Ind. Eng. Chem. Res.*, **45**, 7781-7788, (2006).

[11] E. Prud'homme, P. Michaud, E. Joussein, C. Peyratout, A. Smith, S. Arri-Clacens, J.M. Clacens, S. Rossignol, Silica fume as porogent agent in geo-materials at low temperature, *Journal of the European Ceramic Society*, **30**, 1641-1648 (2010).

[12] J. Davidovits, Synthetic Mineral Polymer Compound of the Silicoaluminates Family and Preparation Process, *US Patent, **4**, 472, 199*, (1984).

[13] P. Innocenzi, Infrared Spectroscopy of Sol-Gel Derived Silica-Based Films: a Spectra-Microstructure Overview, *Journal of non crystalline solids*, **316**, 309-319, (2003).

[14] M. Criado, A. Polomo and A. Fernandez-Jiménez, Alkali Activation of Fly Ashes, Part 1: Effect of Curing Conditions on the Carbonation of the Reaction Products, *Fuel,* **84**, 2048-2054, (2005).

[15] J. Davidovits, Scientific Tools, X-rays, FTIR, NMR, *Geopolymer: Chemistry and Applications*, 61-76, (2008).

[16] W. K. W. Lee and J. S. J. Van Deventer, Use of Infrared Spectroscopy to Study Geopolymerization of Heterogeneous Amorphous Aluminosilicate, *Langmuir*, **19**, 8726-8734, (2003).

[17] C. A. Rees, J. L. Provis, G. C. Luckey and J. S. J. Van Deventer, Attenuated Total Reflectance Fourier Transform Infrared Analysis of Fly Ash Geopolymer Gel Aging, *Langmuir*, **23**, 8170-8179, (2007).

[18] T. Uchino, T. Sakka, K. Hotta and M. Iwasaki, Attenuated Total Reflectance Fourier-Transform Infrared Spectra of a Hydrated Sodium Silicate Glass, *J. Am. Ceram. Soc.,* **72 (11)**, 2173-2175, (1989).
[19] Y.I. Jialiang, IR Studies of Alkali Silicate Glasses, *Journal of Non-Crystalline Solids*, **52**, 211-215 (1982)

doi:10.4028/www.scientific.net/AST.69.107

Comparative study of the consolidation process and properties of clay based geomaterials and “geomimetic” lateritic clay based materials

G.L. Lecomte[1,a], A. Wattiaux[2,b], and G. Lecomte[1,c],

[1]Groupe d’Etude des Matériaux Hétérogènes – ENSCI, 47 à 73 Avenue Albert Thomas, 87065 Limoges, France

[2]Institut de Chimie de la Matière Condensée de Bordeaux, 7 avenue du Docteur A. Schweitzer, 33608 Pessac, France

[a]gisele.lecomte@unilim.fr, [b]wattiaux@icmcb-bordeaux.cnrs.fr , [c]gylecomte@yahoo.fr

Keywords: ”geomimetic” materials, geomaterials, pozzolanic reaction, iron binding, clay platelets, hydraulic binding

Abstract

The present work focuses on the elaboration of low energy consuming materials and the correlation between their final properties and the fabrication route. For this purpose, geomaterials have been elaborate using a common raw clay material. Also an original route has been developed to elaborate “geomimetic” materials. The raw material consists of lateritic clay, whereas the main reactives are namely: nitric acid, fulvic acid, and calcium hydroxide in an aqueous medium. In both materials, the strengthening process and the final characteristics of the as-obtained products have been investigated. Namely: the characteristic compressive strength and the resistance to water seeping and wearing. The geomaterials exhibit a good resistance towards water seeping and wearing, but the products obtained using Portland cement present a greater characteristic compressive strength than with lime. “Geomimetic” materials are also water resistant. In fact, the products elaborated using nitric acid exhibit the best characteristic compressive strength, namely 20 MPa. While with fulvic acid, an environmental friendly organic acid, a characteristic compressive strength of 12 MPa is obtained. Thus the latter appears competitive towards usual stabilized earth and concrete building materials.

Introduction

Geomaterials are composites resulting from strengthening processes at low temperature (less than 200°C), which can involve a preliminary heat treatment (temperature less than 900°C) of some components in order to enhance their reactivity. These composites exhibit structural properties similar to those of concretes or ceramics with current good mechanical strength and / or good

durability. In developing countries (especially sub-Saharan Africa), common building materials are mainly concrete, fired clay and stabilized bricks.

The goal here is to develop high performance geomaterials from local widespread raw materials. The latter include lateritic clays (rich in aluminum and/or iron) as well as other various minerals such as pozzolan and marble. Also an original class of products, designated as "geomimetic" materials in relation with their similarities with naturally occurring lateritic concretions, has been worked out through an acid-base reaction.

In fact, the products developed herein aim to suit various criteria

- Economic Criteria related to reduced transport costs of materials, especially due to materials importation. Developing low-temperature bricks, thus low energy cost products.
- Service properties requirements namely, compressive strength (greater than 0.2 MPa) and resistance towards water erosion.

Experimental

The samples have been mechanically tested using a LLYOD EZ20 device, equipped with compressive, tensile and bending test units. The deflection rate is maintained at 0.5 mm/min. Tests are carried out on normalized cubic samples with sides of 40 mm which satisfy the requirements of standard building codes (EN 12390, EN 7721 and NF 1961). The characteristic maximum compressive strengths are mean values over six tests under the same conditions. The associated relative deviation is ±0.5 MPa.

X-ray powder diffraction (XRPD) analyses have been performed using the Cu $K_{\alpha 1}$ monochromatic radiation, on a Siemens D5000 Bragg–Brentanno type diffractometer. Data are collected in the range $3 \leq 2\theta \leq 60°$ in step scan mode with steps of 0.04° and counting time of 4.8 s/step.

The split resistance towards water of the elaborated samples is estimated through the observation of the behavior of these products, previously submitted to water current during 24 h. The other water resistance test performed consists in dripping water onto the samples during 24 h at a constant frequency.

Materials

Three raw materials from Cameroons were used in this studied, namely: two lateritic clays and a kaolinic clay. They are respectively labelled L1, L2 and K3. Their mineralogical and chemical compositions are given on Table 1. The latter shows that raw clay L2 is well-crystalline and contains more kaolinite than clay L1, while K3 mainly contains kaolinite and illite as predominant crystalline phases.

The binders or reagent used in this study are: nitric acid (HNO_3), fulvic acid, calcium hydroxide ($Ca(OH)_2$) and sodium hydroxide (NaOH). Also, an Ordinary Portland Cement (OPC), a pozzolan and a marble from Cameroon were used.

Geomaterials were elaborated following three predominant axes:

- NaOH interaction type samples using L1 and L2 as raw materials
- Hydraulic binding through Portland cement, the cement content being always 8 %wt.
- Pozzolanic binding using calcium hydroxide (lime) a natural pozzolan or a recomposed one (from marble and L1).

Table 1: chemical and mineralogical composition of the raw clays (L1, L2 and K3)

	Major chemical composition (%wt.)							**Major mineralogical components (%wt.)**			
	SiO_2	**Al_2O_3**	**K_2O**	**Na_2O**	**CaO**	**Fe_2O_3**	**LOI**	**kaolinite**	**illite**	**quartz**	**goetite**
L1	***46.1***	***27.1***	***0.2***	***0.2***	***1.1***	***23.4***	***11.2***	***55***	***nd***	***19***	***23***
L2	***56.2***	***24.1***	***0.4***	***0.6***	***0.6***	***10.2***	***9.5***	***62***	***nd***	***22.9***	***12***
K3	***50.7***	***30.9***	***3,5***	***1.3***	***0.4***	***1.5***	***12.7***	***80***	***17***	***2***	***nd***

The "geomimetic" materials result from an acid-base strengthening reaction of lateritic clays [1]. The manufacture of these products involves a 24 hours acid leaching of the lateritic clay, previous to the base neutralisation; afterwards, the strengthening is obtained after a 18 days curing under water saturated condition at 60°C (see Fig. 1 for the oversimplified process steps).

The compressive strength measurements of all samples are performed when curing is completed first without any other treatment and second after water dipping tests when possible.

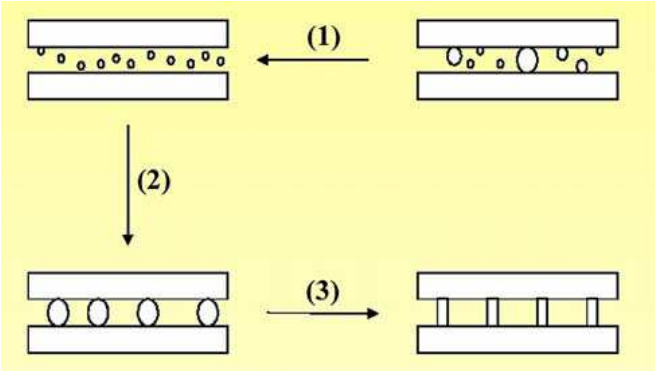

(1) Clay platelets washing
(2) Purified clay platelets binding
(3) Strengthening of the platelets binding

Figure 1: outline of the effect of acid and base treatments on the lateritic clay

Results and discussion

All the experiments were performed using raw materials crushed and screened under 200 μm. Tables 2 and 3 present respectively the composition of the various samples and the corresponding compressive strength.

It appears that the mean compressive strength of the silico-aluminates, consolidated in strongly basic media, is about 8 MPa. They also exhibit a good resistance to water seeping and wearing. In fact lateritic clay L1 leads to better characteristics than the kaolin-rich ones L2 and K3. This behavior results from the greater proportion of free reactive silica and alumina in L1 than in L2 and K3. It is consistent with their comparative mineralogical compositions and BET surface areas (see Table 4).

The related strengthening reaction can be considered in two main stages [2]:

- At first the dissolution of free silica and activated L1 occurs under basic conditions (pH value > 12). The stable species are $[SiO_2(OH)_2]^{2-}$ and $[Al(OH)_4]^-$, according to literature (see Fig. 2).
- Finally, since the saturation content of $[SiO_2(OH)_2]^{2-}$ (140 mg/L) is quickly reached, the polycondensation begins through the reaction of Si-OH with Al-OH and Si-OH. Actually, the oligo(sialate-silixo) precursor is form and the final poly(sialate-silixo) is obtained.

Table 2: summarized formulations of the studied samples (composition in %wt.)

	Labels	Clay	Cement	Pozzolan	Water or Water/binder ratio (*)	$Ca(OH)_2$	NaOH (10 mol/L)	Fulvic acid	Nitric acid
L1- based samples	S1	*60*			*15*		*25*		
	S2	*55*			*20*	*15*			*10*
	S3	*55*			*5*	*15*		*25*	
	S4	*55*			*20*		*15*		*10*
	S5	*55*			*5*		*15*	*25*	
	S6	*92*	*8*		*2 (*)*				
	S7	*92*			*2 (*)*	*8*			
	S8	*65*		*35*	*0.9(*)*				
L2-based samples	S9	*60*			*15*		*25*		
	S10	*55*			*20*	*15*			*10*
	S11	*55*			*5*	*15*		*25*	
	S12	*55*			*20*		*15*		*10*
	S13	*55*			*5*		*15*	*25*	
	S14	*92*	*8*		*2 (*)*				
	S15	*92*			*2 (*)*	*8*			
	S16	*65*		*35*	*0.9(*)*				
K3-based samples	S17	*60*			*15*		*25*		
	S18	*92*	*8*		*2 (*)*				
	S19	*92*			*2 (*)*	*8*			
	S20	*65*		*35*	*0.9(*)*				

Table 3: Summarized final properties of the studied samples

	Labels	Characteristic compressive strength (MPa)	Resistance to water seeping and wearing (Yes or No)
L1- based samples	S1	*8*	*Yes*
	S2	*20*	*Yes*
	S3	*12*	*Yes*
	S4	*No strengthening*	*No*
	S5	*-no strengthening*	*No*
	S6	*9*	*Yes*
	S7	*4*	*Yes*
	S8	*8*	*Yes*
L2-based samples	S9	*5*	*Yes*
	S10	*15*	*Yes*
	S11	*9*	*Yes*
	S12	*No strengthening*	*No*
	S13	*-no strengthening*	*No*
	S14	*7*	*Yes*
	S15	*3*	*Yes*
	S16	*7*	*Yes*
K3-based samples	S17	*3*	*Yes*
	S18	*8*	*Yes*
	S19	*3*	*Yes*
	S20	*7*	*Yes*

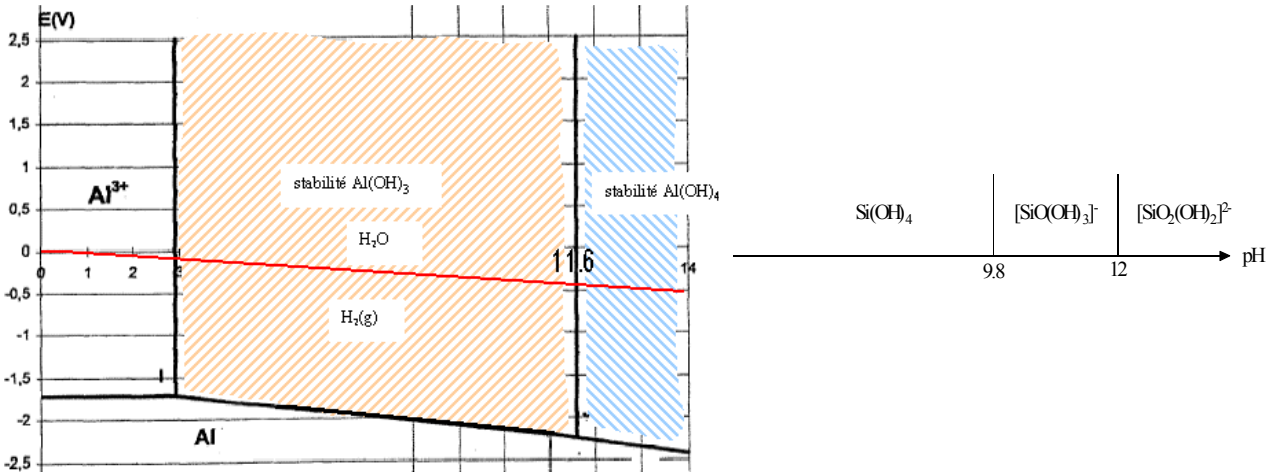

Figure 2: Stability domain of the (a) aluminium and (b) silicon complexes with respect to pH value

The activation of L1 through firing at 700°C prior to its use, enhance its reactivity with soda and thus final compressive strength of 10 MPa can be reached.. An immersion into water increases the final resistance to 16 MPa. This specific behavior is consistent with the ability of the products to incorporate a fraction of available water into their structures in order to proceed further hardening.

The « geomimetic » products obtained using nitric acid exhibits better mechanical strength than those involving the use of fulvic acid. No strengthening is obtained when using soda base, because of the high pH value of the medium (pH value > 12), the stable hydroxide ($[Fe(OH)_4]^-$ ions) does not precipitate [3,4]. As already mentioned in a previous study, the possible strengthening mechanisms involve an iron binding effect onto clay platelets with a concomitant pozzolanic binding through the reaction of excess lime with free silica and alumina.

It is obvious that the "geomimetic" products exhibit final characteristics similar to those obtained for geomaterials resulting from NaOH-activated L1. But the preferred option is the former due to two main points:

- With "geomimetic" materials, there is no need to perform a previous heat treatment for equivalent properties, thus energy saving;
- Also, the use of a more available and environmental friendly reagent, fulvic acid, is a promising feature for prospective development

Nevertheless, these arguments need complementary ageing study before any other assessment.

The cement stabilized materials exhibits a mean compressive strength of 8 MPa, which is comparatively lower than those obtained with geopolymer-like products and "geomimetic" materials. Indeed, it is very complex to achieve a homogeneous mixture with optimized cement-clay particles contact. Therefore, the main contribution in strengthening is the hydraulic hardening of the cement providing that the required water is readily available[5]. In contrast, when using lime as binder, the obtained products exhibit a low compressive strength (3 MPa) after a 28 days curing at

40°C under water-saturated atmosphere. Actually, the hydraulic binding of lime is less strong that with Portland cement since it also undergoes a competitive carbonation reaction with ambient atmosphere [6]. Also the pozzolanic reaction does not proceed effectively due to the high amount of crystalline phases in raw material, thus less free reactive silica and/or alumina. Nevertheless, more reactive clays are obtained after a thermal activation [7,8] at 700°C. Then the resulting geomaterials are resistant towards water wearing and have compressive strength of 10 MPa. Also, an increase of lime content to 20 %wt., leads to a higher compressive strength (25 MPa). This is consistent with the formation of great amount of binding hydrated calcium silicates (CSH) and/or calcium alunino-silicates (CSAH).

Three natural binders have been elaborated and used for L1 and L2 based geomaterials:

- A mixture of lime with natural pozzolan (CPL1) or/L1 fired at 700°C (CPL2);
- A mixture of marble and L1, fired at 750°C for 30 min (CPL3).

The final characteristics are presented in Fig. 3. It appears that the first recomposed cement fits our requirements. Chapelle's tests performed on these cements are in good correlation with the difference in the final compressive strength. The strengthening phases have been identified as hydrated CSH and CSAH gels which strongly coated and bridged clay platelets (see Fig. 4).

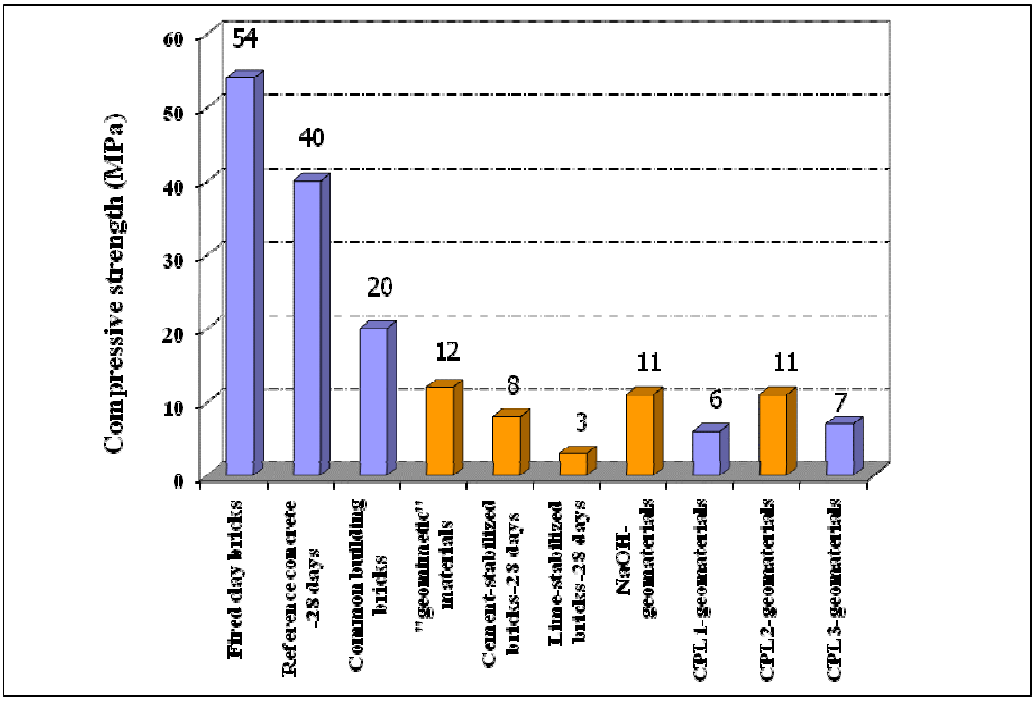

Figure 3: Comparative compressive strengths of some common materials for building purposes and those of our materials

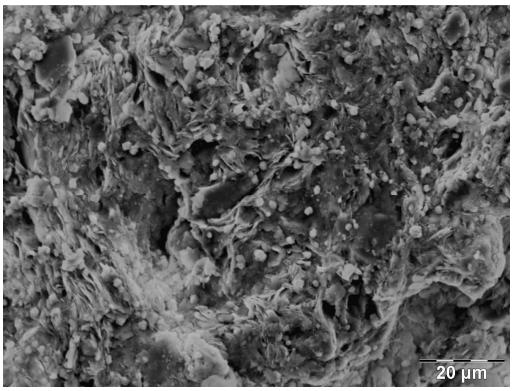

(a)

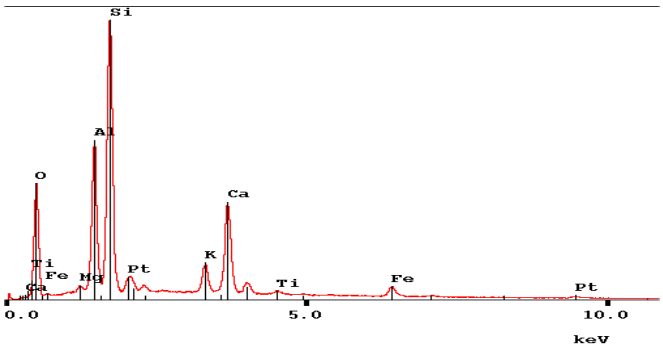

(b)

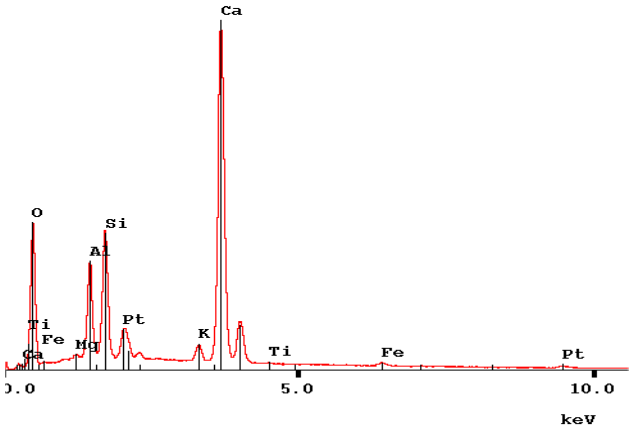

(c)

Figure 4: SEM images of pozzolanic binded geomaterials (a) and corresponding EDS spectra of (b) global composition and (c) local composition of the joining spheres evidenced on image (a) (white points)

Conclusion

The comparative study of some geomaterials and "geomimetic" materials has been performed with respect to their mechanical properties and their interactions with water. Indeed, geomaterials resulting from cement (8 %wt.) stabilized clays exhibit lower compressive strength than those obtained through a geopolymeric strengthening using NaOH. This behavior is justified by the difference in strengthening mechanisms. The use of lime instead of cement does not lead to better final properties; indeed, an improvement of the compressive strength (25 MPa) is only obtained when the lime content is increase up to 20 %wt. and /or the raw clay is thermally activated at 700°C. Therefore a great amount of binding hydrated calcium silicate and/or alumino-silicate gels is formed.

The attempt to use pozzolanic reaction as the main strengthening process, with natural or reconstituted pozzolans, leads to water resistant geomaterials with higher compressive strengths (up to 16 MPa). But these characteristics are reached providing a preliminary heat treatment at 700°C to activate the lateritic clay or at 750°C to achieve the marble-lateritic clay reaction. At last a good compromise is achieved through the elaboration of "geomimetic" materials using raw lateritic clay

and fulvic acid, an environmental friendly component. The as-obtained products exhibit a compressive strength of 12 MPa and an excellent stability towards water seeping and wearing.

References

[1] G.L. LECONTE, E. LESUEUR, J.P. BONNET and G. LECOMTE: Const. Build. Mater. 23 (2009), pp. 1126 - 1132

[2] C. BOUTTERIN & J. DAVIDOVITS: Geopolymère 88, vol 1, pp. 79-88

[3] J.P JOLIVET, in: "De la solution à l'oxyde, Condensation des cations en solution aqueuse, Chimie des surfaces des oxydes", InterEditions/CNRS Editions, 1994

[4] P. PASCAL, in: Nouveau traité de chimie minérale, TII pp. 970-986 and TVIII p. 152

[5] F. LASISI, EO. AJAYI and JA. OSUNADE:. Int J Cement Compos Lightweight Concrete 6 (1984), pp. 201 – 203.

[6] J. LIU, T. WANG and Y. TIAN: Cold region Science and Technology 61 (2010), pp. 29 - 33

[7] G. KAKALI, T. PERRAKI, S SIVILIS and E. BADOGIANNIS: "Applied Clay Science 20, pp. 73-80

[8] F.G. BELL: Engineering geology 42 (1996), , pp. 223 – 237

doi:10.4028/www.scientific.net/AST.69.117

New Geopolymers Based on Electric Arc Furnace Slag

M. C. Bignozzi[1, a], L. Barbieri[2,b] and I. Lancellotti[2,c]

[1] Dipartimento di Ingegneria Civile, Ambiente e dei Materiali Università di Bologna, Via Terracini 28, 40136 Bologna, Italy

[2] Dipartimento di Ingegneria dei Materiali e dell'Ambiente, Università di Modena e Reggio Emilia, Via Vignolese, 905/a, 41100 Modena, Italy

[a]mchiara.bignozzi@mail.ing.unibo.it, [b]luisa.barbieri@unimore.it, [c]isabella.lancellotti@unimore.it

Keywords: Geopolymer, Electric arc furnace slag, Industrial Waste, Waste management.

Abstract. Electric arc furnace slag (EAF-S), coming from a steel productive plant in Italy, has been used as new source for geopolymers synthesis. The slag has been geopolymerized alone and with different content of metakaolin (MK) with the aim to investigate if EAF-S content plays a role in geopolymerization process. Mechanical properties results and microstructure analysis highlight that the optimum weight ratio MK/EAF-S to be used as starting materials is 40/60, 30/70, 20/80. Moreover EAF-S, when used with MK, directly participates in the formation of calcium-rich alumino-silicate gels.

Introduction

Geopolymer systems are today largely investigated. Their structure, mainly amorphous, is usually obtained by alkali-activated polymerization of alumino-silicate sources such as calcined clays and feldspars [1,2]. Although the most part of studies has been addressed on metakaolin based geopolymers with the aim to well understand the reaction mechanism and operative conditions, recently geopolymer systems based on industrial waste have been developed. Indeed, several types of industrial waste are rich in silica and alumina thus fulfilling the first requirement necessary for geopolymeration.

Investigations on coal fly ash and blast furnace slag as unconventional sources of alumino-silicate are currently running highlighting that the geopolymerization process can successfully occur [3-5]. However, both coal fly ash and blast furnace slag are fruitfully used in special cement production (pozzolan and blast furnace cements); the possibility to find other industrial waste to be recycled for geopolymers production is definitely a challenging issue as it would involve a minor use of landfill disposal and a safeguard of not renewable raw materials [6].

Accordingly, in this research, the geopolymerization of electric arc furnace slag is reported and discussed. Electric arc furnace allows steel production mainly from steel scraps, with limited amounts of iron scrap, pig iron and direct reduced iron. This technology is widely used as it has a less severe impact on the environment than the one based on blast furnace [7].

Electric arc furnace usually produces two types of slag, which derive from the furnace and the refining process (also known as secondary metallurgy process) and differ by chemical composition. The slag coming from the ladle, where steel refining process occurs, has been here investigated as new geopolymer source and named as EAF-S. EAF-S represents about 1/3 of the total amount of slag usually produced in an electric arc furnace and its European production can be estimated about 4 millions ton/year [8].

Geopolymers based on metakaolin and EAF-S in different amount have been prepared and characterized from a mechanical and microstructure point of view. The results are discussed and compared with those obtained for geopolymers made of 100% metakaolin and 100% EAF-S, geopolymerized in the same experimental conditions.

Experimental Section

Materials. Metakaolin (MK) was obtained by calcination of a commercial kaolin (Argirec B24, AGS Mineraux, Clerac, France) at 700 °C for 5h. EAF-S was kindly supplied by Acciaieria di Rubiera SpA, Casalgrande, RE, Italy. A highly representative sample of EAF-S was directly collected in the steel productive plant. The slag is usually piled in a covered area of the industrial plant, before landfill disposal that usually occurs every 2-3 months. EAF-S is produced as fine powder, however the fraction > 0.105 mm was eliminated by sieving with the purpose to obtain a grain size distribution as much similar to that one of metakaolin. The grain size distribution curves of EAF-S and MK, determined by a laser particle-size analyzer (Master Sizer 2000, Malvern Instruments), are reported in Fig.1.

Chemical and mineralogical analysis was carried out on EAF-S and MK by X-Ray fluorescence spectrometer (XRF, PW 1414, Philips Thermo ARL (ADVANT'XP+)) for the main elements and by X-ray powder diffractometer with Ni-filtered Cu Kα (λ = 1.54 Å) radiation (PW 1840, Philips) in the 5-70° 2θ range. The crystalline phases were identified by comparison with tabulate data on the JCPDS files.

A sodium silicate solution with a weight ratio SiO_2/Na_2O = 1.99 was used and a NaOH 8M solution was prepared by dissolution of NaOH pellets (Fluka, 99.5%) in distilled water.

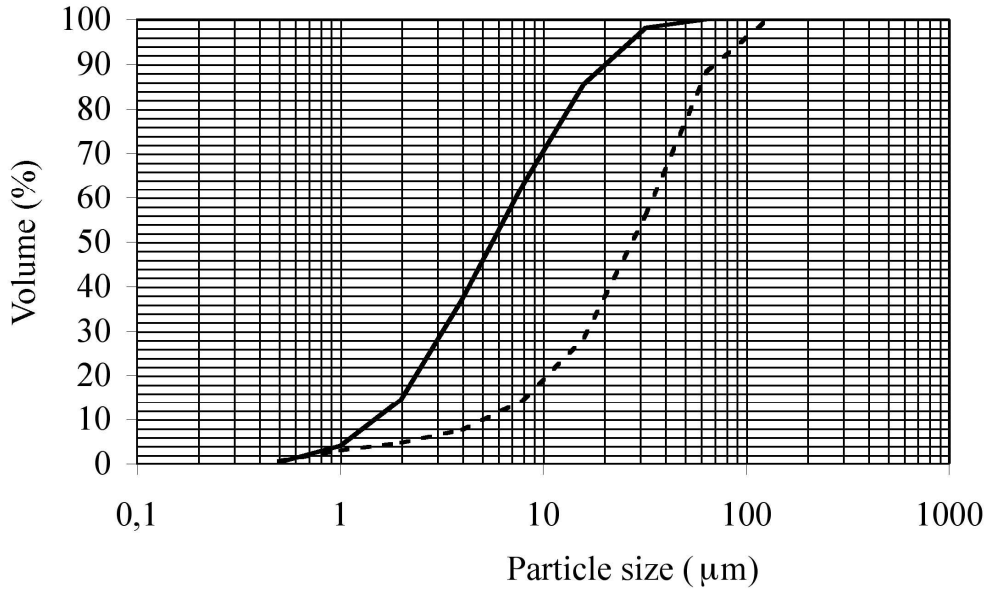

Fig.1 Grain size distribution of MK (full line) and EAF-S (dotted line).

Geopolymer samples preparation. Different amount of metakaolin (MK) and/or EAF-S were mechanically mixed in a planetary mixer according to the formulations reported in Table 1. After 10 min of mixing, sodium hydroxide and sodium silicate solutions were added forming homogenous slurry. However, for some samples distilled water addition was required to reach the target workability (30-50%). After 5 min of mechanical mixing, the slurry was transferred in a mould to form 3 prisms of 4x4x16 cm. During the filling procedure, the geopolymer mix was mechanically adjusted to remove the entrained air. Samples were cured for 24 h at room temperature and R.H. > 90%, then de-moulded and cured for 6 days at T = 20±2 °C and R.H. ≈ 55%.

Characterization. Sample workability was obtained by a flow table test according to the procedure usually adopted for cement mortar reported in UNI 7044. The workability (w%), determined measuring the average diameter (*d*) of the spread mixture obtained using a conical ring (d_{max}=100 mm, d_{min}=70 mm, h=60 mm), was calculated by the following equation: w%= 100*(*d*-

100)/100 with *d* in mm. Flexural and compressive strength of geopolymer samples was determined by an Amsler-Wolpert machine (100 kN) at a constant displacement rate of 50 mm/min. Water absorption test was carried out on geopolymer prism samples: samples were weighted after being immersed in water for 24 hours or up to reaching a constant mass (M_W), then they were weighted after being dried at 100°C for 24 or up to reaching a constant mass (M_D). Water absorption was calculated by the following equation: $WA\% = 100*(M_W-M_D)/M_D$.
Scanning electron microscopy (SEM) analysis was carried out by means of ESEM QUANTA200 - FEI instrument equipped with energy dispersion spectroscopy for chemical analysis (X-EDS Oxford INCA – 350) on fresh fractured samples previously coated with Au/Pd by vaporization under vacuum.

Table 1. Formulations of geopolymer samples

	MK [g]	EAF-S [g]	NaOH 8M [g]	Reoflux B [g]	Distilled water [g]	Workability [%]
MK100	1000	-	300	300	350	30
MK75S25	750	250	300	300	200	30
MK50S50	500	500	300	300	110	50
MK40S60	400	600	300	300	-	40
MK30S70	300	700	300	300	-	45
MK20S80	200	800	300	300	-	50
S100	-	1000	300	300	220	30

Results and discussion

Chemical composition is reported in Table 2 for MK and EAF-S. According to its origin, EAF-S shows a high content of CaO (54.5 %) and a certain amount of MgO (4.0 %), besides SiO_2 (16.4 %) and Al_2O_3 (11.1 %). As expected, MK is mainly constituted by SiO_2 (47.6%), Al_2O_3 (37.7%), and small contents of Fe_2O_3 (1.6 %) and TiO_2 (1.7 %). From a mineralogical point of view (X rays diffraction spectra are not reported for brevity sake), EAF-S exhibits the presence of Ca_2SiO_4 Olivine (γ–C_2S) (ICDD #180-941), $Ca_2(Al(AlSi)O_7)$ Ghelenite (ICDD #174-1607), $Ca_{12}Al_{14}O_{33}$ Mayenite, syn (ICDD #170-2144) and MgO Periclase (ICDD #45946). MK is mainly amorphous except for the presence of a minor crystalline impurity identified as (K,Na) $(Al,Mg,Fe)_2$ $(Si_{3.1}Al_{0.9})$ O_{10} $(OH)_2$ Muscovite-3T ((ICDD #07-0042).

Table 2. Chemical composition of MK and EAF-S by XRF (wt%).

	SiO_2	Al_2O_3	CaO	Fe_2O_3	TiO_2	MgO	K_2O	MnO	ZnO
MK	47.6	37.7	0.08	1.6	1.7	-	1.0	-	-
EAF-S	16.4	11.1	54.5	8.7	0.3	4.0	0.4	2.0	0.57

As reported in Table 1, geopolymer samples containing up to 50 wt% of MK have required the addition of different amount of distilled water to reach a suitable workability for relevant geopolymers preparation. However, such addition has a direct effect on the material mechanical properties as shown in Fig. 2 and 3.
Both flexural and compressive strength increases with EAF-S reaching the maximum values for EAF-S content ranging between 60 and 80 wt%. The investigated mechanical properties suddenly decrease for sample containing 100% EAF-S. Low mechanical performances of geopolymers MK100, MK75S25 and MK50S50 can be ascribed to the addition of water in the mix, however it is evident that EAF-S, when used in S100, is not able to reach a successful geopolymerization process.

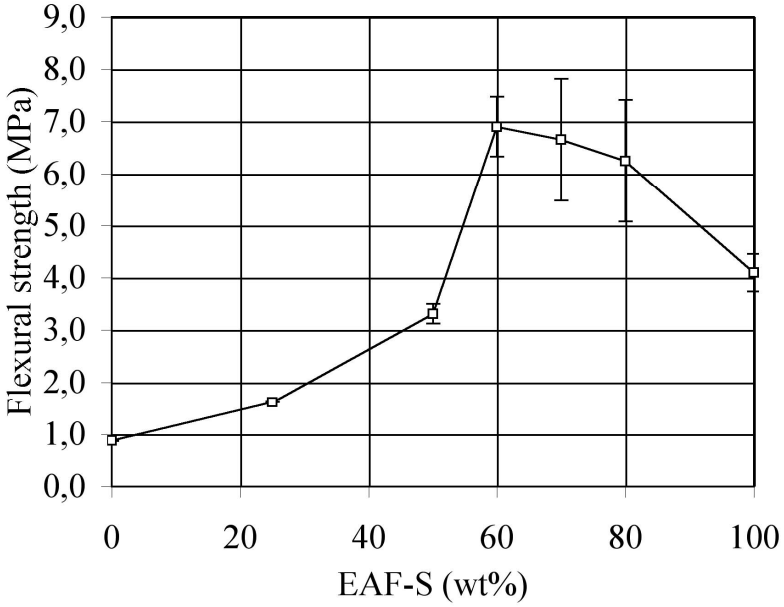

Fig.2 Flexural strength of geopolymer samples at 7 days of curing as function of EAF-S content (average of 3 measurements, standard deviation bar is also reported).

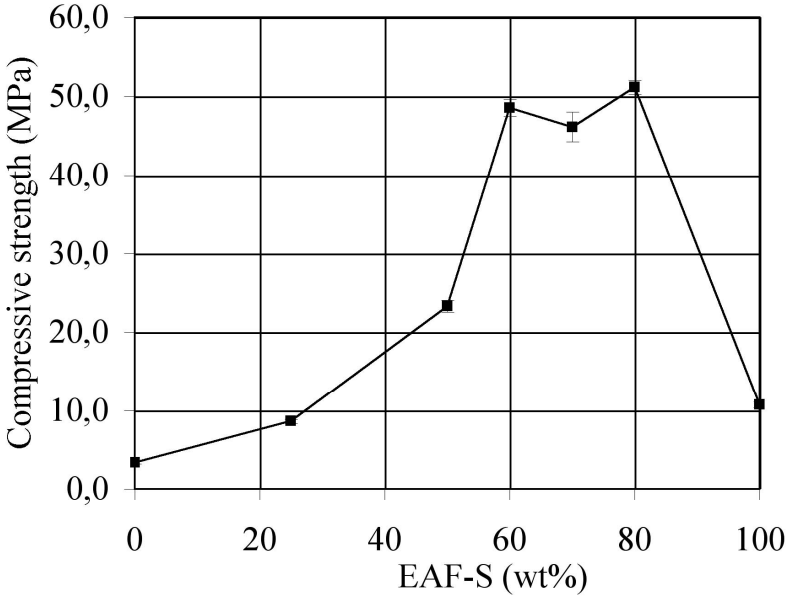

Fig.3 Compressive strength of geopolymer samples at 7 days of curing as function of EAF-S content (average of 5 measurements, standard deviation bar is also reported).

Geopolymers with optimized mechanical strength occur when MK and EAF-S are respectively combined with weight ratios equal to 40/60, 30/70 and 20/80. Water absorption results confirm the results above described. WA% decreases with the content of EAF-S reaching the minimum values for the EAF-S% ranging between 60 and 80, then WA% increases in correspondence of 100% EAF-S content (Fig. 4). Microstructure investigation has been carried out by SEM and EDS with the aim to find a relationship between physical-mechanical properties of geopolymer samples and MK/EAF-S ratio. Micrographs, reported in Fig. 5, clearly show modifications in gel formation as function of EAF-S content. MK100 shows a homogeneous structure, whereas in S100 an amorphous structure enriched in Ca is evident together with needle crystals rich in Na and Si (Table 3), thus confirming that the EAF-S geopolymerization is not completed. Such results agree with the low mechanical properties previously detected for this formulation. Indeed, needle crystals are absent in M50S50. In this sample calcium ion leads to the formation of different calcium-alumino-silicate amorphous gels

with a chemical composition characterized by different Si/Ca and Si/Al ratios (Table 3). A previous investigation [9] highlighted that the presence of calcium silicate source as starting material and the formation of soluble calcium species in the alkaline environment can interfere in geopolymerization process reacting with the dissolved silicate and aluminate species, thus confirming our findings.

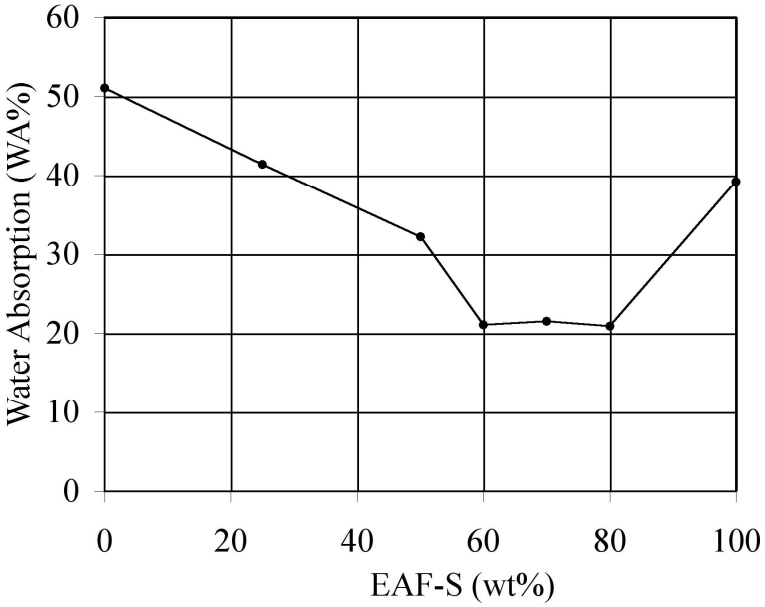

Fig.4 Water absorption of geopolymer samples at 7 days of curing as function of EAF-S content.

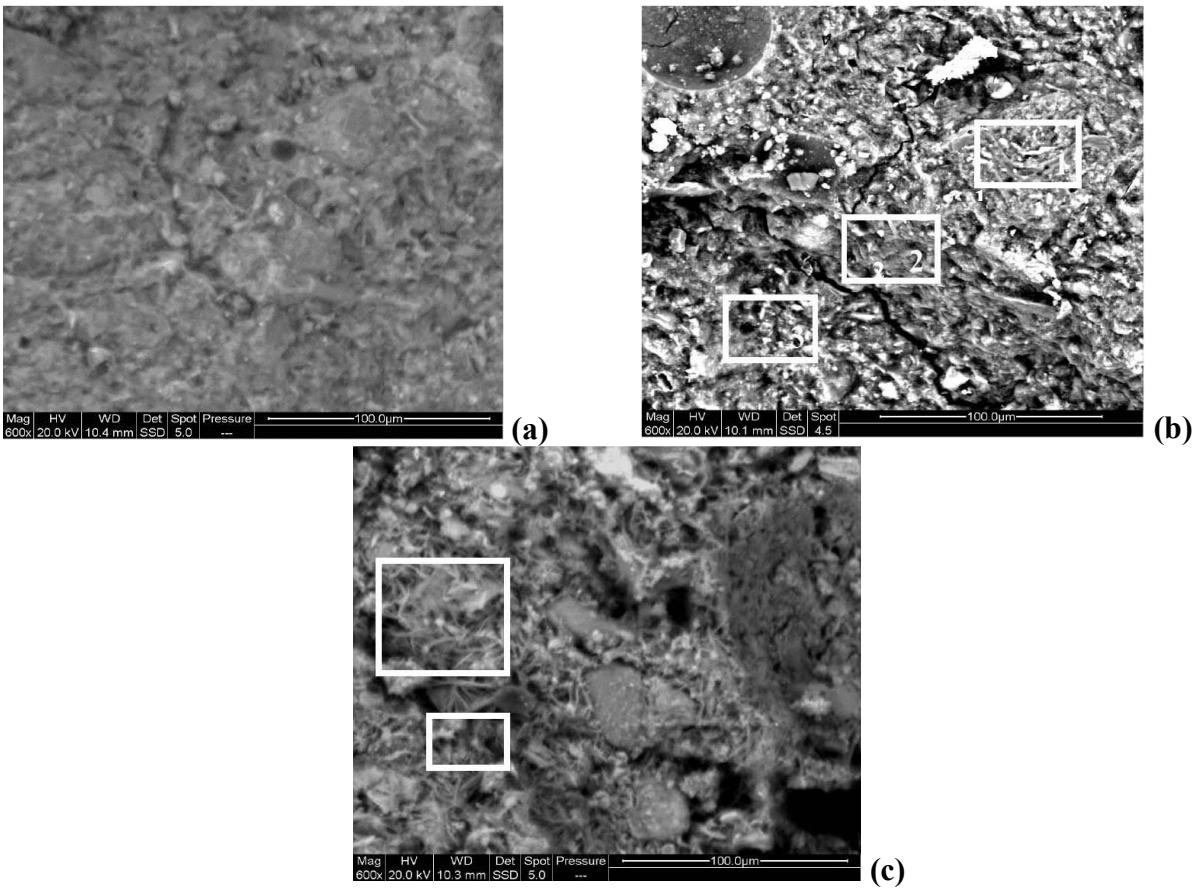

Fig. 5 SEM micrographs of MK100 (a), MK50S50 (b) and S100 (c).

Conclusions

The investigated electric arc furnace slag seems suitable to be geopolymerized with sodium hydroxide and sodium silicate solutions, however the combination with MK (up to 40%) is strongly recommended if appreciable mechanical properties and compact microstructure are desired features for the samples. EAF-S directly participate in the formation of calcium-rich alumino-silicate gels when MK is present, whereas the evidence of crystalline phases with needle morphology indicates that geopolymerization process is incomplete for sample S100.

Table 3. Chemical composition of different areas by EDS in geopolymer samples (wt%).

Element	S100 gel	S100 needle crystals	MK50S50 gel-area 1	MK50S50 gel-area 2	MK50S50 gel-area 3
C	9.76	8.39	9.91	-	-
Na	8.32	6.61	2.74	8.46	10.4
Mg	0.79	0.44	-	-	-
Al	3.93	7.49	4.26	13.1	14.7
Si	6.51	16.24	15.2	21.6	23.2
S	0.26	-	-	-	-
K	0.20	0.40	-	-	-
Ca	18.9	6.51	13.8	12.6	6.08
Mn	0.42	-	-	-	-
Fe	1.88	0.90	-	-	-
Si/Ca	0.3	-	1.1	1.7	3.8
Si/Al	1.6	-	3.6	1.6	1.6

References

[1] H. Xu and J. S. J. Van Deventer: International Journal of Mineral Processing, Vol. 59 (2000), p. 247.

[2] K. Komnitsas, D. Zaharaki: Minerals Engineering, Vol. 20 (2007), p. 1261.

[3] W.K.W. Lee and J.S.J. van Deventer: Colloid Surf. A, Vol. 211 (2002), p. 49.

[4] C.K. Yip and J.S.J. van Deventer: J. Mater. Sci. Vol. 38 (2003), p. 3851.

[5] M. Izquierdo, X. Querol, J. Davidovits, D. Antenucci, H. Nugteren and C. Fernández-Pereira: Journal of Hazardous Materials, Vol.166 (2009) p. 561.

[6] I. Lancellotti, E. Kamseu, M. Michelazzi, L. Barbieri, A. Corradi and C. Leonelli: Waste Management, Vol. 30 (2010), p. 673.

[7] P. Crompton: Resources Policy, Vol. 27 (2001) p. 87.

[8] S. Kourounis, S. Tsivilis, P.E. Tsakiridis, G.D.Papadimitriou and Z. Tsibouki: Cement and Concrete Research, Vol. 37 (2007), p. 815.

[9] C. K. Yip, G. C. Lukey, J. L. Provis, J. S.J. van Deventer: Cement and Concrete Research, Vol.38 (2008) p. 554.

doi:10.4028/www.scientific.net/AST.69.123

Characterization of geopolymer materials containing MSWI fly ash and coal fly ash

Salvatore Andini[1,a], Raffaele Cioffi[2,b], Francesco Colangelo[2,c], Claudio Ferone[2,d],Fabio Montagnaro[1,e], Luciano Santoro[1,f]

[1] Dipartimento di Chimica, Università di Napoli Federico II, Complesso Universitario di Monte Sant'Angelo, 80126 Napoli (Italy)

[2] Dipartimento per le Tecnologie, Università di Napoli Parthenope, Centro Direzionale Is. C4, 80143 Napoli (Italy)

[a]salvatore.andini@unina.it, [b]raffaele.cioffi@uniparthenope.it, [c]colangelo@uniparthenope.it, [d]claudio.ferone@uniparthenope.it, [e]fabio.montagnaro@unina.it, [f]luciano.santoro@unina.it

Keywords. Geopolymer, Coal fly ash, Municipal solid waste incinerator ash.

Abstract. In this work three samples of MSWI ash have been stabilized in systems containing coal fly ash and able to give geopolymers through a polycondensation reaction. Monolithic products were obtained with both MSWI ashes as received and after chloride partial removal by water washing. The polycondensation products have been characterized qualitatively by means of FT-IR spectroscopy and scanning electron microscopy (SEM) and quantitatively through the determination of the amount of reacted water and silicate. Differently from traditional cement based stabilization systems, those based on geopolymerization show a chemical behaviour almost insensitive to the presence of chlorides and sulphates in the MSWI ash. On the other hand, the microstructure is strongly affected by the content of soluble salts.

Introduction

Geopolymers are also referred to as alkali-activated alumino-silicate binders and comprise three classes of inorganic polymers that, depending on the silica/alumina ratio, are based on the following three different monomeric units: (─Si─O─Al─O─), polysialate (PS), SiO_2/Al_2O_3=2; (─Si─O─Al─O─Si─O─), polysialatesiloxo (PSS), SiO_2/Al_2O_3=4; (─Si─O─Al─O─Si─O─Si─O─), polysialatedisiloxo (PSDS), SiO_2/Al_2O_3=6.

The synthesis of geopolymers takes place by polycondensation and can start from metakaolinite by reaction with alkali metal (Na or K) silicate [1,2]. Alternatively, geopolymers can be obtained starting from many raw silico-aluminates and alumino-silicates, including coal fly ash [3-5]. Also in this case the polycondensation takes place by reaction with alkali metal silicate.

Whatever the case, the synthesis of geopolymers relies on the same reaction mechanism; when in contact with the high pH alkaline solution, the starting materials dissolve and the geopolymers are precipitated.

Amorphous geopolymers are obtained at condensation temperatures ranging from 20 to 90°C, while crystalline ones are formed in autoclave at 150-200°C. The structure of crystalline geopolymers resembles that of zeolite A [1].

Geopolymeric materials are attractive because excellent mechanical properties and durability can be achieved [6]. Thermal stability and resistance to acid attack are equally excellent [7]. Furthermore, due to much lower Ca content, geopolymer-based materials are much more resistant to acid attack than Portland cement-based ones [8].

Great interest also derives from the reduced energy requirement for the manufacture of new materials based on geopolymers. In fact, the reaction pathway requires either metakaolinite, obtained by calcining kaolinite at temperatures of 600-700°C, or raw silico-aluminates and alumino-silicates. This also implies that, in comparison to traditional cement-based materials, green house gas emission can be strongly reduced.

The applications of geopolymer-based materials range within the fields of new ceramics, cements, matrices for hazardous waste stabilization, fire-resistant materials, asbestos-free materials and high-tech materials [1,9,10].

In this work, coal fly ash has been used for the synthesis of geopolymeric matrices able to incorporate and stabilize three samples of ash from municipal solid wastes incinerators (MSWI). The different MSWI ash samples have been used not only as received, but also after washing to reduce their chloride content. The products obtained in the different experimental conditions have been characterized from the qualitative point of view by means of FT-IR and SEM and from the quantitative point of view through the measurement of the amounts of silicate and water reacted upon polycondensation.

Materials and methods

The three MSWI ash samples come from plants located in southern, central and northern Italy. These samples, coming from the incinerators REA located in Dalmine (BG), Mobil located in Colleferro (RM) and Tecnitalia located in Brindisi, were labelled as DAL, MOB and TMT respectively. The three samples have been submitted to chemical analysis and the results are shown in Table 1.

Table 1. Chemical composition of MSWI fly ashes, mg/kg

Components	Samples		
	MOB	TMT	DAL
Al	12000	27000	14000
As	4.2	5.9	2.1
Ba	112	227	185
Cd	65	217	88
Ca	230000	270000	165000
Cr tot	85	270	412
Fe	12000	10700	9450
Mg	8500	7500	1240
Hg	< 0.1	27	5
Ni	130	163	117
Pb	8950	17110	6580
Cu	815	6220	4114
Zn	9100	6230	8400
Si	110000	130000	97000
Na	15000	28000	119000
K	11300	17000	24000
Cl^-	113000	49000	75000
SO_4^{2-}	29000	68000	34000

The coal fly ash used for the synthesis of the geopolymers was supplied by the Italian electricity board (ENEL) and comes from the power plant located in Brindisi (Southern Italy). Its characterization by means of traditional chemical analysis gave the following chemical composition: SiO_2, 44.3%; Al_2O_3, 20.2%; Fe_2O_3, 10.5%; K_2O, 8.1%; CaO, 0.5%; Na_2O, 0.3%; loss on ignition at 1050°C, 11.35%. Alkali activation, necessary to promote polycondensation, was carried out by adding NaOH and sodium silicate solutions of proper concentration.

As already pointed out, the geopolymers produced from coal fly ash were used as stabilizing matrices of three different MSWI ash samples.

The three samples of MSWI ash were submitted to the stabilization treatment both as received and

after partial soluble salts removal (mainly chlorides and sulphates) carried out by water washing in a 2/1 liquid to solid ratio. The compositions of the systems tested were assessed by fixing at 20/6.5 the ratio MSWI ash/coal fly ash and after some trial tests in which the effects of the concentration and amount of sodium silicate and hydroxide solutions were evaluated in relation to the formation of monolithic products. The complete set of experimental compositions is reported in Table 2.

Table 2: Compositions of the systems tested

System	Type of MSWI ash	MSWI ash [g]	Coal fly ash [g]	Sodium silicate solution (1.15 M) [g]	Sodium hydroxide solution [g]
MOB_{AR}	MOB as received	20	6.5	7.5	7.5 (10 M)
MOB_{W}	MOB washed	20	6.5	6	6 (10 M)
TMT_{AR}	TMT as received	20	6.5	4	4 (10 M)
TMT_{W}	TMT washed	20	6.5	3.5	3.5 (10 M)
DAL_{AR}	DAL as received	20	6.5	5.5	5.5 (17 M)
DAL_{W}	DAL washed	20	6.5	5	5 (17 M)

The components of all the systems listed in Table 2 were carefully mixed and the resulting mixtures were kept in small polyethylene cylinders. The polycondensation reaction was carried out at 25°C for times equal to 1, 3, 7, 14 and 28 days.

The specimens obtained at any polycondensation time were characterized by means of a Nicolet Nexus FT-IR spectrometer and a FEI Quanta 200 FEG scanning electron microscope. The same specimens were used for the quantitative determination of water and sodium silicate consumed during the polycondensation reaction. The amounts of reacted sodium silicate and water at any polycondensation time were determined as follows. Each specimen was ground under acetone, filtered and washed with diethyl ether to remove all the residual aqueous phase. Finally, heating in oven at 40°C was carried out to ensure the loss of any residual fraction of the liquids previously used. The cumulative amount of reacted sodium silicate and water was obtained by weight difference between the solid recovered after the above treatments and the ashes initially employed. The amount of reacted water was determined by the excess loss on ignition of the recovered solid over that of the initial ashes.

Results and discussion

Infrared spectroscopy is a useful tool for revealing the formation of geopolymers. In fact, in FT-IR traces of raw silicates and silico-aluminates, the Si─O asymmetric stretching in tetrahedra is responsible for an absorption band centred at about 1000 cm^{-1} [11,12]. When geopolymers are formed, this band is shifted to lower wavenumbers as a consequence of polycondensation with alternating Si─O and Al─O bonds. This phenomenon can be clearly seen in Fig. 1, where the results of FT-IR characterization are reported for system TMT_{AR} at some selected polycondensation times. The band originally present at 1032 cm^{-1} in the trace relative to TMT ash as received shifts to 977 cm^{-1} after a polycondensation time of 28 d. In addition, the intensity of this band increases with time, indicating a corresponding increase of polycondensation degree.

Fig. 2 shows the micrographs of the three systems investigated after 14 days curing. The three systems contain the ashes DAL (a), MOB (b) and TMT(c) as received, that is without partial soluble salts removal. Despite the results of FT-IR investigation show that polycondensation takes place in all the systems, the morphology of the cured samples containing the ash as received does not appear so compact to favour the development of good physico-mechanical properties. This observation holds for all the ashes, even if the content of soluble salts is quite different from case to case.

Fig. 3 shows the micrographs of the system containing ash MOB previously washed and cured 14 days, the same time as the systems of Fig. 2. In this case the specimens morphology looks much more compact (Fig. 3a), able to favour much higher physico-mechanical performance. Furthermore,

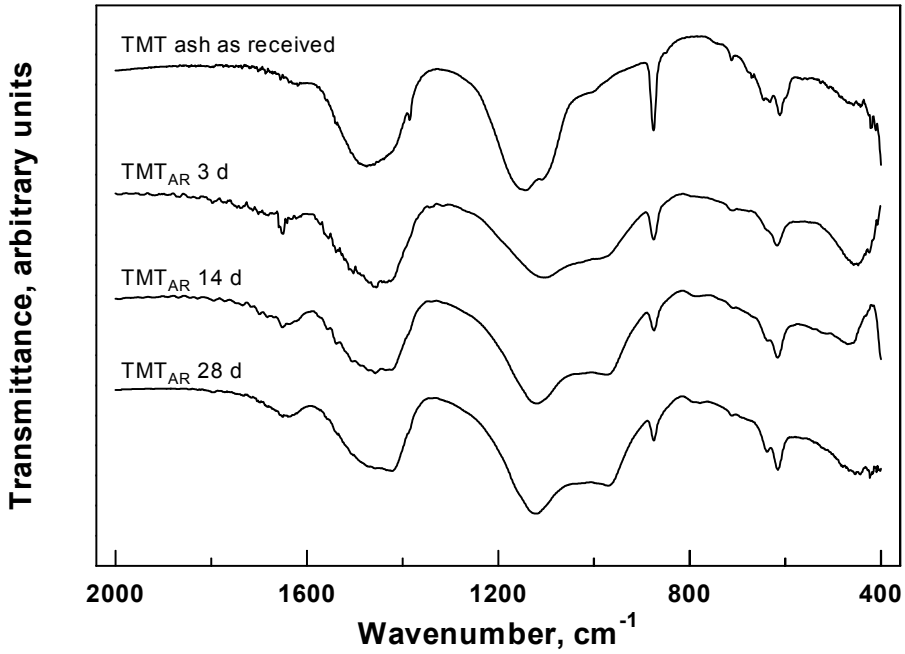

Fig. 3b shows that polycondensation takes place by virtue of a topochemical reaction mechanism in which the products grow on the reactive particles.

Figure 1: Results of FT-IR characterization of selected specimens of system TMT$_{AR}$.

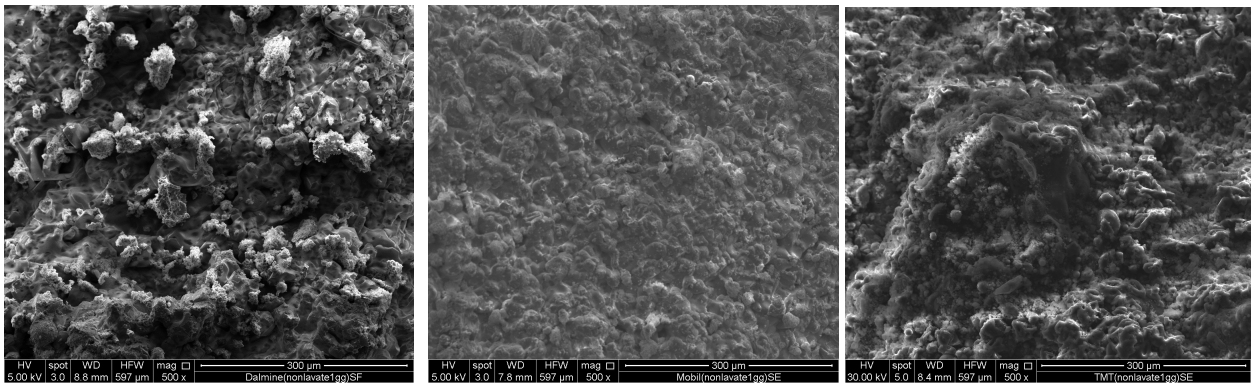

(a) (b) (c)

Figure 2: SEM Micrographs of systems DAL (a), MOB (b) and TMT (c).

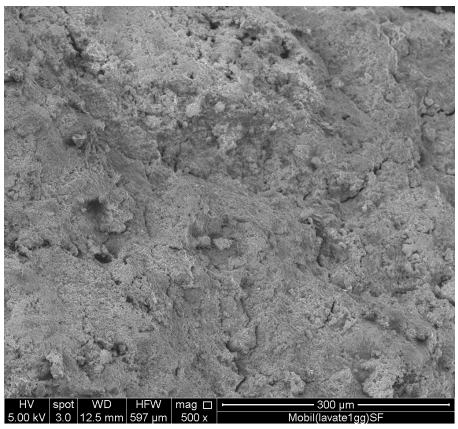

(a)

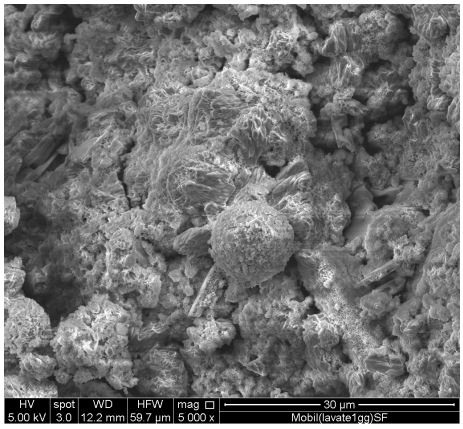

(b)

Figure 3: SEM Micrographs of system MOB, 500X (a) and 5000X (b)

The quantitative data of reacted water and silicate are reported in Tables 3 and 4 for all the systems studied at all the polycondensation times investigated. The data of Table 3 show that the amount of water bonded to the geopolymers decreases as the polycondensation time increases. This is a direct consequence of the reaction mechanism: initially, the starting materials dissolve in the highly alkaline reaction medium giving rise to the formation of geopolymer precursors in which several hydroxyl groups are present; then, crosslinking of these precursors takes place and the polycondensation occurs with water expulsion [13].

Table 3: Amount of reacted water in grams per gram of initial ashes

System	Polycondensation time [d]				
	1	3	7	14	28
MOB_{AR}	0.0656	0.0513	0.0517	0.0499	0.0379
MOB_{W}	0.0838	0.0597	0.0466	0.0435	0.0365
TMT_{AR}	0.0723	0.0413	0.0517	0.0099	0.0007
TMT_{W}	0.0598	0.0597	0.0466	0.0325	0.0245
DAL_{AR}	0.1795	0.0413	0.0213	0.0199	0.0123
DAL_{W}	0.1084	0.0637	0.0546	0.0625	0.0645

The data of Table 4 show that, despite a few exceptions, the amount of reacted silicate increases with reaction time. Some differences are seen in relation to MSWI ash origin, but in all the cases the degree of polycondensation was high enough to get monolithic products. Reducing the content of chlorides by washing has a minor effect, if any. This is particularly relevant in relation to MSWI ash stabilization, as it is well known that the effectiveness of traditional cement-based matrices can be severely compromised by high chloride content.

Table 4: Amount of reacted silicate in grams per gram of initial ashes.

System	Polycondensation time [d]				
	1	3	7	14	28
MOB_{AR}	0.0918	0.1092	0.1052	0.1119	0.1208
MOB_{W}	0.0923	0.0988	0.1048	0.1128	0.1139
TMT_{AR}	0.0474	0.0682	0.0702	0.0789	0.1008
TMT_{W}	0.0693	0.0698	0.0748	0.0828	0.0829
DAL_{AR}	0.0474	0.0692	0.0302	0.0789	0.0508
DAL_{W}	0.0893	0.1304	0.1007	0.1028	0.0659

Conclusions

This work has proved that geopolymer-based stabilizing matrices can be formed starting from mixtures containing coal fly ash and MSWI ash. Three different samples of MSWI ash were used and in all the cases the polycondensation took place with formation of monolithic products. Some of the experiments were carried out with MSWI ash in which the soluble salts content had been significantly lowered by water washing. The results of these experiments proved that the content of these salts plays a minor role on the quantitative aspects of polycondensation, but strongly affect the microstructure of the products formed. Then, it can be inferred that MSWI ashes washing can be very advantageous from the point of view of physico-mechanical properties development.

References

[1] J. Davidovits: Journal of Thermal Analysis Vol. 37 (1991), p. 1633.

[2] R. Cioffi, L. Maffucci, L. Santoro: Resources Conservation and Recycling Vol. 40 (2003), p. 27.

[3] J.G.S. van Jaarsveld and J.S.J. van Deventer: Industrial Engineering Chemistry Research Vol. 38 (1999) p. 3932.

[4] S. Andini, R. Cioffi, F. Colangelo, T. Grieco, F. Montagnaro, L. Santoro: Waste Management Vol. 28 (2008) p. 416.

[5] E.I. Diaz, E.N. Allouche, S. Eklund: Fuel Vol. 89 (2010) p. 992

[6] A. Palomo, A. Macias, M.T. Blanco, F. Puertas: Proceedings of the 9th International Congress on the Chemistry of Cement, New Delhi, India, Vol. 5 (1992), p. 505.

[7] M. Schmücker and K.J.D. MacKenzie: Ceramic International Vol. 31 (2005), p. 433.

[8] T. Bakharev: Cement and Concrete Research Vol. 35 (2005), p. 658.

[9] W.M. Kriven, J.L. Bell, M. Gordon: Ceramic Engineering and Science Proceedings Vol. 25 (2004), p. 57.

[10] I. Lancellotti, E. Kamseu, M. Michelazzi, L. Barbieri, A. Corradi, C. Leonelli: Waste Management Vol. 30 (2010), p. 673

[11] W.K.W. Lee and J.S.J. van Deventer: Colloids and Surfaces A: Physicochem. Eng. Aspects Vol. 211 (2002), p. 115.

[12] J.W. Phair and J.S.J. van Deventer: International Journal of Mineral Processing Vol. 66 (2002), p.121.

[13] H.Xu and J.S.J. van Deventer:International Journal of Mineral Processing Vol.59 (2000),p.247.

doi:10.4028/www.scientific.net/AST.69.129

Formation of tetra-coordinated aluminum in the low temperature ashes

Pavel Straka

Institute of Rock Structure and Mechanics, v.v.i, Academy of Sciences of the Czech Republic,
V Holešovičkách 41, Praha 8, Czech Republic
email: straka@irsm.cas.cz

Keywords: aluminum, complex, low temperature ashes

Abstract. Formation of tetra-coordinated aluminum in low temperature coal ashes was investigated. Coal samples were intensively air-oxidized at 350°C for 160 hours, then ^{27}Al MAS NMR spectra of obtained ashes were acquired and compared against those for initial coals, a reference ash and Al standards. It was found that chemical shift at 4 ppm with coals corresponds to that for triaquo-hydroxo-diphenoxido-aluminum(III) complex and the shift at 72 ppm with resulting coal ashes agrees with that for Al tetra-coordinated with oxygen. So, in the presence of coal organics the tetra-coordinated Al is formed under low temperature conditions. Formation of this form of Al can be elucidated as follows. Probably, Al in coal originates from kaolinite, as this mineral is very frequent in coal. Mentioned Al-complex was formed through the long-term reactions of kaolinitic hexa-coordinated Al with phenols/polyphenols as prevailing oxygen-contaning components in coal substance. During this process the octahedral structure of hexa-coordinated Al was retained, but ligands coordinated around the central Al atom changed. At first, delamination of a kaolinitic structure through the effect of coal organics proceeded and separation of the Al gibbsite octahedral and silica tetrahedral layers occurred. Then, two oxygens in the Al octahedron were substituted with two phenoxide groups while OH groups were preserved. As result, Al-tetrahydroxo-diphenoxide ion was formed, further stabilized in a water environment as $Al(H_2O)_3(OH)(C_6H_5O)_2$. During low temperature ashing this complex was transformed to Al tetra-coordinated with oxygen only at 350°C.

Introduction

As a result of enormous production of coal ashes, these substances are currently envisioned as a mineral resource rather than as a residual waste. Therefore, they are presently intensively studied both in terms of composition and use. As part of this effort is to study the low temperature ashes originating e.g. from the catalytic processes, certain combustion techniques, a coal mines dust thermal treatment etc. In our case, the low temperature ashes from different bituminous coals have been studied in terms of behavior of Al compounds in the temperature changes to 350°C. The aim of this study is to describe a formation of aluminum tetra-coordinated with oxygen during low temperature coal oxidation, as this structure is crucial for the further utilization of ashes.

Materials and Methods

For investigations, bituminous coals from the Czech Republic were chosen. Crushed (1–2 mm) and air-dried samples of the Paskov, the Staříč and the Lazy coals (the Czech part of the Upper Silesian Coal Basin) were used. Coal samples were intensively air-oxidized at 350°C for 160 hours in a muffle kiln [1]; then, ^{27}Al MAS NMR spectra of obtained ashes were acquired and compared to those with the original coals and standards. Following reference minerals and compounds were chosen for a) an evidence of sensitivity of ^{27}Al MAS NMR method to chemical environment of Al atom, b) identification of Al compounds in tested ashes and coals:

- α-Al_2O_3 (Korund Benátky, SRO, Czech Rep.); γ-$Al(OH)_3$, (Lachema Brno Comp., gibbsite, proven by the XRD method); kaolinite (Kaolin Sedlec IA Standard, Sedlecký kaolin AS, Czech Rep.); aluminum phenoxide (Sigma Aldrich), $Al(H_2O)_3(C_6H_5O)_3$ (elemental analysis is in Table 1); Al-catechin complex prepared according to [2]; further:

- triaquo-hydroxo-diphenoxido-aluminum(III) complex (THDA), with the formula $Al(H_2O)_3(OH)(C_6H_5O)_2$, prepared by a long-term reaction of gibbsite powder with phenol (1:1) in water as follows. 25g of gibbsite was blended with the same amount of phenol and 110 ml water. The suspension was kept in capped flasks at room temperature for 15 months; then conc. NaOH was added for the removal of the unreacted phenol. Then, the formed precipitate was washed and air-dried. Subsequently, 500 ml of ethanol was added for leaching; after the ethanol evaporation, a solid phase of leach was obtained as ruby/violet powder. The yield was 1-2 %. Elemental analysis of the complex is shown in Table 1;
- triaquo-trihydroxo-aluminum(III) complex (TTA), with the formula $Al(H_2O)_3(OH)_3$ prepared by a long-term hydrolysis (20 months) of $AlCl_3$ (25 g) in water (110 ml) at pH 5.5. After addition of small quantities of NaOH to increase pH a white precipitate was obtained. After drying the complex as a white powder was obtained, further purified by 1M HCl. The yield was about 20 %. Elemental analysis of this complex is shown in Table 1;

Table 1 Elemental analyses of the reference Al complexes [wt.%]

Complex	*C*	*H*	*O*	*Al*
Al phenoxide	56.56	6.25	29.02	8.17
THDA	49.68	5.70	35.16	9.46
TTA	0.00	6.55	74.57	18.88

- wood ash, prepared in an industrial incinerator with a recycling of unburned fuel at the temperature of 400–500°C. The main signal in ^{27}Al MAS NMR spectrum was 58 ppm.

For the organic elemental analyses of the reference compounds, the Flash 1112 EA analyzer (Thermo Finnigan, Rodano) was used and the analysis of the aluminum was carried out on an XRF spectrometer EDS Spectro X-Lab (SPECTRO Analytical Instruments, Kleve). The aluminum complexes/structures both in the mentioned coals/ashes and the reference compounds were analyzed by solid-state nuclear magnetic resonance measurements of ^{27}Al on a Bruker Avance 500 spectrometer (Bruker, Rheinstetten). FTIR spectra of THDA complex were acquired on a FTIR spectrometer Bruker IFS 66. A KBr pressed disk technique was applied. 64 scans were collected for each measurement over the spectral range of 400–4000 cm^{-1} with a resolution of 2 cm^{-1}. Spectra were deconvoluted using an Omnic 7,3 software (Thermo Electron Corporation).

Results and Discussion

Given the low concentration of Al complexes in coal, their isolation is very difficult. It is therefore feasible to use the solid-state ^{27}Al MAS NMR method, create a comparative scale of complexes and to identify complexes in question *in situ* on the basis of the same or similar chemical shifts (an allowable difference of +/- 1–2 ppm in the range of about 0–20 ppm). The same method can be used for ashes (an allowable difference of +/- 15 ppm in the range of 50–80 ppm). Firstly, signals in ^{27}Al MAS NMR spectra of the obtained ashes were evaluated. Generally, the signals in the range of 50–80 ppm belong to the Al tetra-coordinated with oxygen (further {4Al}). In all the cases a signal at 72 ppm was found (71.78 ppm at the Paskov, 71.74 ppm at the Staříč and 71.95 ppm at the Lazy coal ashes). These values correspond well to those found with the reference wood ash (Fig. 1). In Fig. 1, the main signal at 58 ppm (peak area 76.94%) proves that {4Al} is present. After deconvolution, the minor signals at 67.85 (4.42%), 61.89 (2.07%), and 50.98 (16.58%) ppm were detected. These signals can be attributed to different chemical environments of {4Al} in the wood ash. All these findings prove that the {4Al} structure was present in ashes in question. Further, the ^{27}Al MAS NMR signals of original coals were investigated. In all cases, the signal at 4 ppm was found: 3.96 ppm at the Paskov, 4.16 ppm at the Staříč and 4.98 ppm at the Lazy coals.

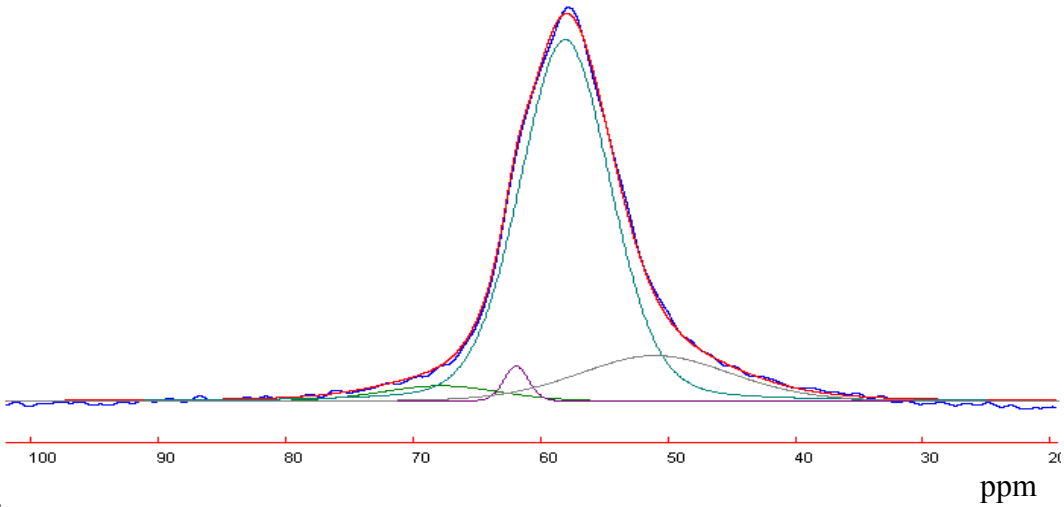

Fig. 1 ^{27}Al MAS NMR spectrum of the reference wood ash. Positions [ppm]: 67.85 (peak area 4.42%); 61.89 (2.07%); 58.05 (76.94%); 50.98 (16.58%).

These values were compared with those obtained at reference compounds (Table 2). From Table 2 it follows that the signal 4 ppm matches well with those found at THDA complex. Regarding the signal at 72 ppm at ashes this means that THDA existing in coals was during low temperature oxidation converted into {4Al}. In this connection, the oxidative altered coal from the Upper Silesian Coal Basin was tested (volatiles 30.8 wt.%, dry ash free basis; ash 3.8 wt.%, dry basis). This coal comes from the vicinity of red beds bodies (oxidative and thermally altered claystones, siltstones and sandstones); during its history it was naturally altered by oxidation under low temperature conditions at temperatures below 150°C [1,3]. Due to this, both the structures THDA and {4Al} were expected in the sample. As the acquired ^{27}Al MAS NMR spectrum shows (Fig. 2), two signals both at 72 ppm (23,65%) and 5 ppm (61,03%) were recorded, thus, the two structures were present, as expected. Therefore, under low temperature conditions the THDA complex changes into {4Al}. Moreover, after deconvolution of the spectra a signal at 16 ppm was discovered (Fig. 2), which is assigned to Al-catechin [4] or Al-catechin-like complex (Table 2). Probably, this complex is also changed into {4Al} during low temperature conversion. It seems that THDA

Table 2 ^{27}Al MAS NMR signals of reference minerals and complexes

Reference compounds	*[ppm]*	*Description*
Aluminum phenoxide	20.90	Al surrounded by 3 phenoxide anions and 3 water molecules.
α-Al_2O_3	14.16	Corundum – distorted octahedra.
Al-catechin complex	13.85	Al complex with irregularly arranged phenolic molecules.
γ-$Al(OH)_3$	8.86	Gibbsite – distorted octahedral.
kaolinite	4.82	Kaolinite – distorted octahedra.
$Al(H_2O)_3(OH)(C_6H_5O)_2$ (THDA)	4.15	Al complex with octahedral molecules.
$Al(OH)_3(H_2O)_3$	-1.10	Al complex with symmetrically arranged OH and water ligands.

complex originated from a gibbsite layer of kaolinite, which is very frequent in coals [5]. Firstly, the delamination of kaolinitic layers to octahedral gibbsite and tetrahedral silicate layers occurred due to long-term exposure of water and coal organics. Subsequently, reactions of gibbsite with phenols led to Al-tetrahydroxo-diphenoxide complex ion, further stabilized in a water environment (i.e. in a weakly acidic environment) as $Al(H_2O)_3(OH)(C_6H_5O)_2$ complex, (THDA). During low

temperature ashing this complex is transformed to {4Al} only at 350°C. This hypothesis was further tested.

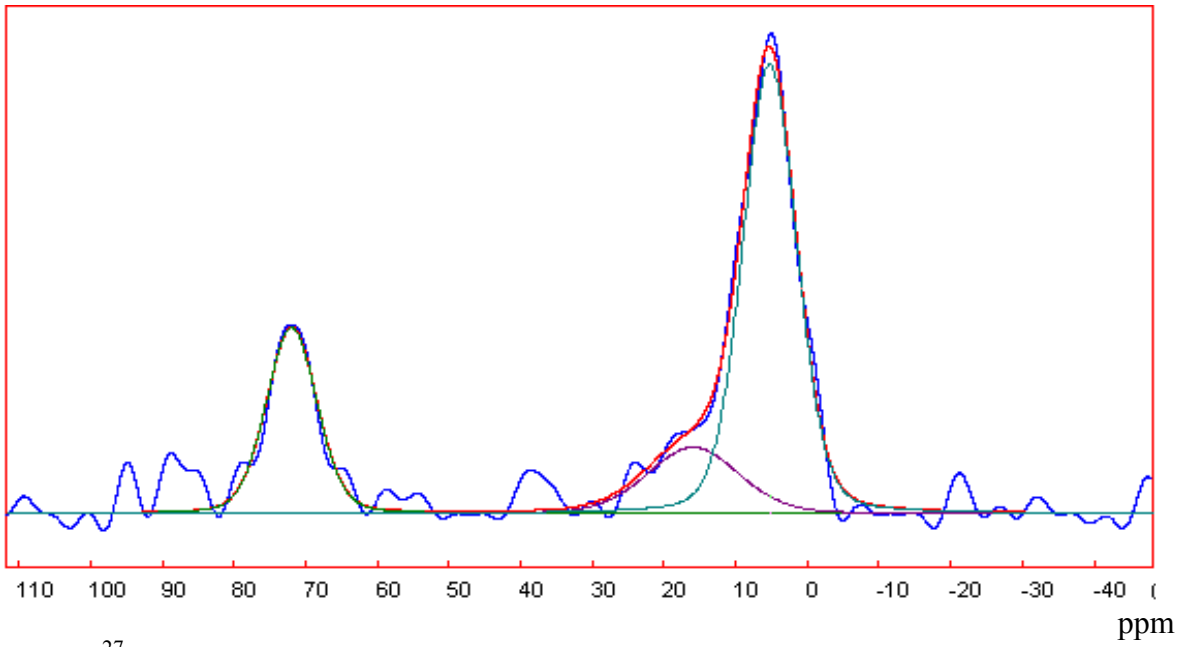

Fig. 2 ^{27}Al MAS NMR spectrum of bituminous coal altered through natural oxidation at temperature below 150°C. Positions [ppm]: 71.93 (peak area 23,65%); 15.94 (15,32%); 5.22 (61,03%).

In our considerations a key compound is complex THDA. Therefore, this complex was studied using FTIR spectroscopy. Obtained FTIR spectrum is pictured in Fig. 3. By referring to different previous spectral studies the major vibrational bands are assigned (peaks with very weak intensities at 2718, 2604, 2493 and 1776 cm^{-1} are not assigned). Figure 3 displays, beside peaks with medium intensities, three dominant bands: a broad strong band at 3433 cm^{-1}, a band with three maxima at 1624, 1607 and 1598 cm^{-1}, and a broad band at 1446 cm^{-1}; further, three regions of 1165-1024, 880-693 and 618-512 cm^{-1}.

The broad strong band at 3433 cm^{-1} is due to O–H stretching vibrations of H_2O and OH groups [6]. The band with mentioned three maxima is due to bending vibrations HOH (1624 cm^{-1}) [6] and aromatic in-ring C–C stretches (1607 and 1598 cm^{-1}) [7]. The broad peak at 1446 cm^{-1} probably reflects an important phenomenon of Al–O–C linkage (see later). Further vibrations, CCH bend (1385 cm^{-1}) [8], phenoxide CO stretches (1335 and 1242 cm^{-1}) and C–H out of plane bends (880-693 cm^{-1}) [7] again prove an aromatic part of complex. Finally, vibrations in two regions, 1165-1024 and 618-512 cm^{-1}, are assigned to the AlO–H vibrations (1165-1024 cm^{-1}) [9] and Al–O stretches (618-512 cm^{-1}) [6,9].

It seems that the mentioned broad band at 1446 cm^{-1} is composed of at least two components; an overlapping of both covalent Al–O–C and in-ring CC stretch vibrations is suggested. Probably, it reflects an important phenomenon of Al–O–C group predicted in the work [8]. Therefore, this high-intensity band and the above-mentioned band with three maxima at 1624, 1607 and 1598 cm^{-1} were further deconvoluted (Fig. 4). Deconvolution in Fig. 4 shows 7 main peaks at 1434, 1468, 1504, 1570, 1600, 1624 and 1645 cm^{-1}. These peaks are assigned to Al–O–C covalent linkages (1434 cm^{-1}), in-ring CC stretches (1468, 1504, 1570 and 1600 cm^{-1}), and HOH bends (1624 and 1645 cm^{-1}). On the whole, FTIR spectrum is consistent with the formula of THDA.

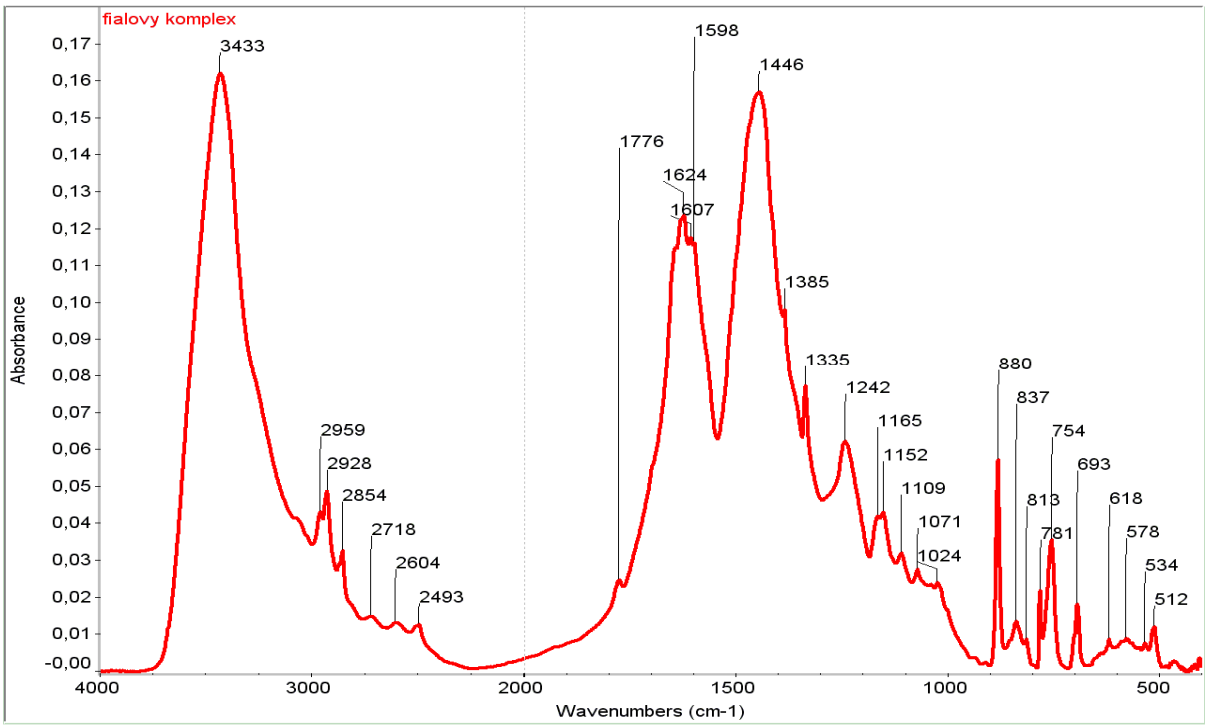

Fig. 3 FTIR spectrum of triaquo-hydroxo-diphenoxido-aluminum(III) complex (THDA).

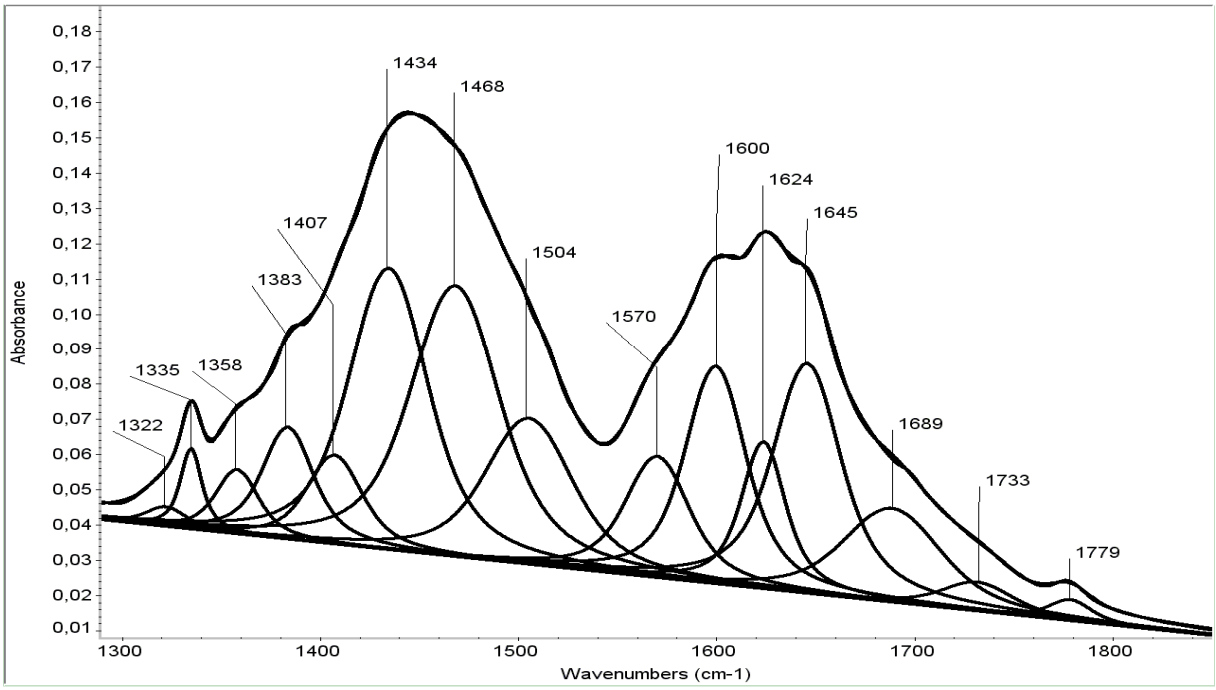

Fig. 4 Deconvolutions of the bands at 1624/1607/1598 cm^{-1} and 1446 cm^{-1} (see FTIR spectrum in Fig. 3).

From these data it follows that THDA will not be too thermally stable. Therefore, the behavior of this complex during heating in an inert atmosphere was followed by TG and DSC methods. It was found that THDA is thermally stable up to 150°C, rather less. Activation energy was very low: 3.12 kJ/mole. This means that the decomposition takes place quite easily and formation of structure {4Al} is thus easier than through usual thermal treatment of kaolinite at e.g.

600°C. Therefore, during low temperature coal ashing, THDA or its part is transformed to {4Al} only at 350°C.

Concluding remarks

Sensitivity of ^{27}Al MAS NMR to chemical environment of Al atom. A considerable sensitivity of ^{27}Al MAS NMR method to chemical environment of Al atom is evident from different chemical shifts of three Al minerals (Table 2, corundum, gibbsite and kaolinite). In corundum α-Al_2O_3, Al^{3+} ions are surrounded by their six nearest oxygen neighbors at 1.849 and 1.980 Å [10] (or at 1.855 and 1.972 Å [11]), and the four near nearest Al^{3+} neighbors at 2.65 and 2.79 Å [12], as a result of which, a distinct NMR signal is expected because of these Al–O distances. Since further reference compounds, gibbsite γ-$Al(OH)_3$, consist of octahedral layers with two Al sites with the Al–O distances spread over 1.832 to 1.947 Å [13], a different NMR signal than in corundum can be expected. The third reference mineral, kaolinite, has two Al sites like gibbsite, but the Al–O distances are between 1.880 and 1.969 Å [14] without a resolved mode. In kaolinite, a gibbsite-like layer is associated to a tetrahedral Si layer; therefore, a different NMR signal is expected again.

Decomposition of THDA. The decomposition temperature of triaquo-hydroxo-diphenoxido-aluminum(III) complex (below 150°C, as mentioned) is comparable to that of aluminium phenoxide (below 155°C, as found by TG/DSC). The reason is that the structure of both complexes is similar as Al phenoxide is in fact a triaquo-triphenoxido-aluminum(III)complex. This findings support the structure found by FTIR.

Complexes in coal substance. The THDA complex is present in the coal substance, i.e. in the organic mass of coal. In the case of thermally and oxidative altered coal, beside the THDA complex also the {4Al} structure was present in coal substance as ash content was only 3.8 wt.% (dry basis).

Ackowledgement. This work was supported by the Grant Agency of Academy of Sciences of the Czech Republic under the project No. IAA300460702.

References

[1] Z. Klika: Journal of the Czech Geological Society Vol. 44/3-4 (1999), p. 335.
[2] Y.M. Chen, M.K. Wang and P.M. Huang: J. Agric. Food Chem. Vol. 54 (2006), p.212.
[3] Z. Klika: Journal of the Czech Geological Society Vol. 44/3-4 (1999), p. 343.
[4] Nagata T., Hayatsu M. and Kosuge N.: Phytochemistry Vol. 31 (1992), p.1215.
[5] Thomas L.: Coal Geology, John Wiley & Sons Ltd., Chichester (2007).
[6] Beran A., Voll D. and Schneider H.: J. of the European Ceramic Society Vol. 21 (2001), p.2479.
[7] Silverstein R.M. and Webster F.X.: Spectrometric Identification of Organic Compounds, 6th ed., John Wiley and Sons, New York (1998).
[8] Kubicky J.D., Itoh M.J., Schroeter L.M. and Apitz S.E.: Environ. Sci. Technol. Vol. 31 (1997), p.1151.
[9] Sinkó K., Mezei R., Rohonczy J. and Fratzl P.: Langmuir Vol. 15 (1999), p.6631.
[10] Ildefonse P., Cabaret D., Sainctavit P., Galas G., Frank A-M. and Lagarde P.: Phys. Chem. Minerals Vol. 25 (1998), p.112.
[11] Lewis J. and Schwarzenbach D.: Acta Cryst. A Vol. 38 (1982), p.733.
[12] Newham R.E. and de Haan Y.M.: Z. Kristallogr. Vol. 117 (1962), p.235.
[13] Saalfeld H. and Wedde M.: Z. Krystallogr. Vol. 139 (1974), p.129.
[14] Bish D.L., von Dreele R.B.:. Clays Clay Miner. Vol. 37 (1989), p.289.

doi:10.4028/www.scientific.net/AST.69.135

Medium to long term engineering properties and performance of high-strength Geopolymers for structural applications

Kwesi Sagoe–Crentsil, Trevor Brown and Shiqin Yan
CSIRO Materials Science and Engineering
PO Box 56, Highett, Victoria 3190, Australia
Kwesi.Sagoe-Crentsil@csiro.au

Keywords: Geopolymer, fly ash, permeability, performance, concrete

Abstract. The medium to long term engineering performance of high-strength geopolymer concrete systems are largely dependent on fluid ingress and the transport phenomena that govern permeability of structural members exposed to aggressive environments. For the purpose of analysing durability performance, both high pressure water and gas permeability testing of fly-ash geopolymer(GP) concretes have been assessed for samples cured under ambient and steam exposure conditions at 65^{O}C. The observed mean permeability coefficient values for gas(k) and water(K_w) of steam-cured structural grade concrete was respectively 6.19E-17m^2 at 300kPa gas pressure and 1.52E-10m/s at 525kPa water pressure. While mean gas permeability values were comparable to reference steam-cured ordinary Portland cement(OPC) systems, the corresponding water permeability coefficient data for geopolymer concrete was ten-fold higher. The transport properties of OPC concrete systems are typically governed by water-to-cement ratio and the degree of hydration which is linked to the level of porosity and pore interconnectivity. However, corresponding permeability of geopolymer concrete appears to be dictated by an inherent mesoporous capillary pore network structure for which transport properties appear to be partly dependent on mode of concrete curing. The Paper examines global implications of increased permeability and key durability parameters such as chloride diffusion, carbonation rates and steel reinforcement corrosion on long-term engineering and durability performance.

Introduction

The durability and long-term engineering performance of ordinary Portland cement(OPC) concrete can be normally assessed by measurement of fluid transport parameters such as permeability and gas diffusion[1,2]. In general, such transport processes play a crucial role in the degradation mechanisms of concrete structures and are often controlled by pore size distribution and pore connectivity as well as overall concrete strength, system chemistry and the prevalence of cracks. Whereas permeability tends to be more influenced by pore connectivity, the elastic properties and strength of concrete are affected by the total volume of pores, in particular, the distribution of macropores which are sized greater than 50nm[3-4]. Corresponding studies investigating various aspects of mix composition, microstructure and durability issues relating to the family of geopolymer (GP) systems are now only beginning to emerge [5-9]. For instance, the work of Kriven et al[10] examined the pore network distribution of GP binders and observed that there exist several clusters of pore sizes and found them not too dissimilar to those characterising OPC systems.

The deterioration of OPC concrete arising from ingress of various ions, liquids and gases from the environment are well documented[11-12]. The key mechanisms involve diffusion of chlorides or carbon dioxide leading to depassivation of steel reinforcement, and, eventually, distress of structural members. Similarly, the ingress of chemicals, such as acids, alkalies and sulphates can induce chemical deterioration of concrete, much as the deterioration of concrete caused by freeze-thaw action.

While there are several published literature on the transport mechanisms, including test methods for permeability of Portland cement concretes [13], only very limited data currently exists on transport mechanisms of geopolymer binder systems. As such, the implications of long-term performance of geopolymer concrete in relation to gas and water permeability, concrete durability and overall structural performance are yet to be fully addressed. Other traditional factors known to enhance concrete durability including mix design parameters, chemical admixtures and optimal curing conditions need to also be assessed for GP systems. Thus, this paper examines aspects of the inter-relationships between strength and permeability of geopolymer concrete by examining the effects of cure condition on concrete water permeability and the mechanisms that control overall transport processes in GP concrete systems.

Experimental

Materials. Table 1 shows chemical composition of ASTM Type I ordinary Portland cement used for reference concrete mixtures and Class F fly ash used for the Geopolymer (GP) mixtures. Table 2 provides concrete mix proportions of the concrete formulations. River sand and local 9mm Hornfels coarse aggregate was used. Both the reference OPC and GP concrete mixes were designed to achieve target 28day strength of 40MPa.

The reference OPC concrete samples were prepared in a similar fashion as GP concrete and moulded according to standard requirements for compressive strength measurements. After casting, GP samples were either initially cured in the laboratory for 24hrs i.e., ambient-cured samples or placed in the steam curing chamber at 65^{O}C for 6hrs. Thereafter, all samples, including ambient cured specimens were stored at 23 ^{O}C and 100%RH. until required for testing. Standard concretes cylinders of 100x200mm diameter were used for compressive strength measurements. Table 3 provides data on measured fresh concrete properties.

Table 1. Chemical analysis of OPC and Fly ash

Oxide	OPC (wt %)	Fly Ash (wt %)
SiO_2	20.2	47.19
Al_2O_3	4.16	29.79
Fe_2O_3	5.30	13.93
CaO	64.8	3.29
MgO	1.29	1.38
Na_2O	0.22	0.24
K_2O	0.42	0.49
TiO_2	-	1.77
SO_3	2.67	0.13
LOI	1.34	1.3

Table 2. Concrete mix proportions

Material	OPC Concrete (Kg/m^3)	GP concrete (Kg/m^3)
Fly ash	-	269
Ordinary Portland Cement	346.0	-
Coarse aggregates (9mm)	1112.4	1163
Silicate Solution/NaOH	-	148
Dry Sand	753	784
Water	186.2	27

Table 3. Fresh concrete properties

Wet concrete property	GP concrete	OPC concrete
Mix Temp. (^{O}C)	25.5	15.7
Flow (mm)	260.0	-
Slump (mm)	160.0	120
Wet density (kg/m^3)	2430.0	2381

Compressive strength testing: Concrete cylinders for compression testing were tested in accordance with AS 1012.9(1999)-Standard Test Method for Compressive Strength of Cylindrical Concrete Specimens[14]. Specimens were capped using conventional sulphur capping method in accordance with the Australian Standard AS 1012.9 (1999) for concrete compressive strength tests at 1, 7 and 28 days. Tests were performed in a 2500 kN ELE Universal testing machine.

Water permeability: The coefficient of water permeability (K_w) was determined by measuring the amount of water passing through the specimen and calculated using Darcy's law [15]. The test determines rate of water absorption through the concrete surface. The experimental setup for the capillary absorption test is shown in Fig 1 for high water pressure testing. Prior to conducting permeability testing, 50mm sliced disc samples were cut from the concrete cylinders, and embedded in 25 mm thick epoxy resin to enable water-tight fit within the permeability cell. Test specimens were then loaded into the water pressure cell and a fixed 525kPa pressure head applied throughout the duration of the test.

Measurement on the manometer was initiated after a constant a constant rate flow rate was observed. Only sectioned samples from the middle of cylinders were used in permeability measurements. The permeability value was calculated from the sample geometry, fluid characteristics, measurement of flow rate and the applied pressure by standard methods based on Darcy's equation as shown in Equation 1 for steady state conditions. Table 4 provides test parameters used for permeability measurements.

$$K_w = \frac{QL}{A\Delta h} \qquad (1)$$

K_W = Permeability Coefficient
Q = Flow rate (m^3/s)
L = Thickness of concrete sample (m)
A = Cross-sectional area of concrete sample (m^2)
P = Absolute water pressure (Pa)
Δh = pressure head (m).

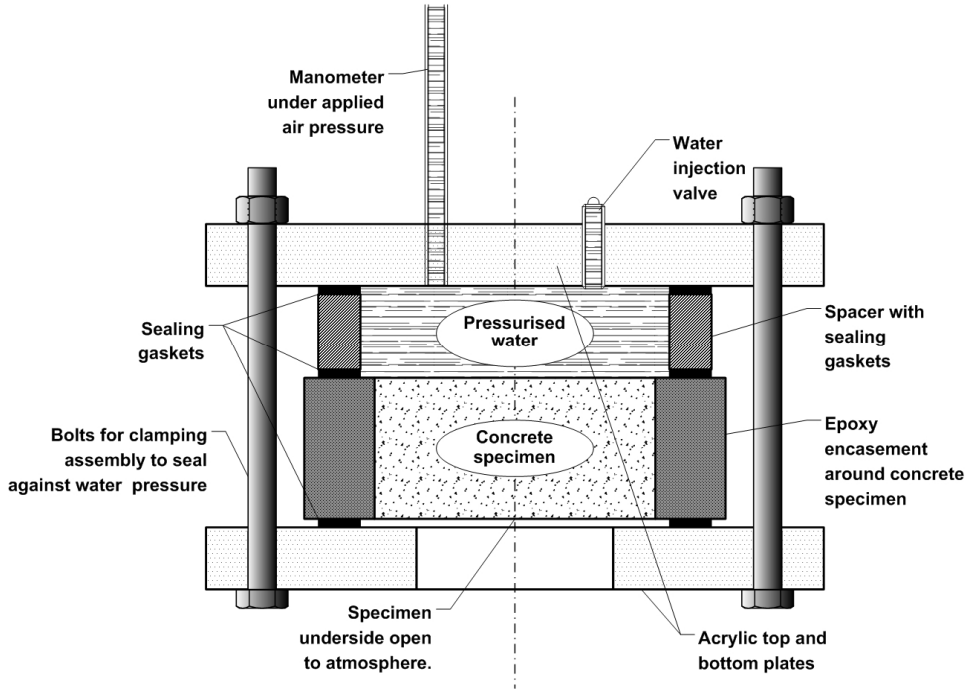

Fig. 1. High Pressure testing cell

Table 4. Test parameters used for permeability measurements

Parameter	Value
Sample Thickness(L)	0.05m
Sample X-sectional area (A)	0.00785398m^2
Pressure head (P)	5.00E+05Pa
Viscosity (υ)	1.00E-03Pa/s
P/Δh	9.80E+03Pa/m

Results and Discussion

Compressive strength: The mean compressive strength development of ambient and steam-cured OPC and GP concretes are shown in Table 5. The results of Table 5 show that steam-cured GP and OPC samples varied slightly from the target strengths of 40MPa at 28days. It is also observable, that the strength development under the two curing conditions, i.e. ambient and heat-cured concretes, up to 28days generally showed different strength development trends. A relatively rapid early age strength development trend was observed for ambient-cured OPC specimens compared to GP concrete. For fly ash GP concrete, it is expected that the rate of early strength increase can also be dependent on ambient temperature, with higher ambient curing temperatures resulting in marginally higher early compressive strength gains.

The observed compressive strength gain of the heat-cured GP concrete was minimal compared to the equivalent GP concrete. The heat-cured OPC specimens typically show greater strength development, achieving nearly 40% increase between 1 day and 28-days during fog-room storage. However, only a corresponding marginal increase in compressive strength of less than 5% is observed between one day and 28 days for the heat-cured GP samples. This strength increase is a result of residual polymerization reactions that occurs beyond the initial heat exposure. Only a relative modest strength increase occurring between 7d and 28d for GP concretes, which is typical of this class of materials, suggesting that significant polymerization reaction occurs during the initial heat curing regime compared to equivalent hydration reactions characterising OPC systems.

Table 5. Compressive strength development of ambient cured OPC and GP concretes

Compressive strength	GP Steam-cure (MPa)	GP Ambient-cure (MPa)	OPC Steam-cure(MPa)	OPC Ambient-cure (MPa)
1day	42.3	-	22.5	9.1
3day	-	2.0	-	-
7day	42,3	7.2	28.0	35.4
28day	44.0	35.5	38.1	43.7

Image analysis of pore distribution. Figure 2(a,b) show optical micrographs of 28day-GP samples alongside image analysis pore distribution maps. The relatively dense microstructures suggest possible good mechanical properties, partly attributable to the near-complete gelling characteristics of traditional silica geopolymer systems during heat-curing. The mean pore diameter of 5.78mm for the GP samples remain similar to the equivalent value of 5.76mm for the reference OPC value shown in Fig 3(a,b). The pore coverage of the two systems however differs with the GP registering 8.85% coverage compared to 8.43% value for OPC. The impact of the difference in pore coverage on fluid transport mechanisms is however not immediately obvious. It must be noted that, although the macropore distribution of the GP and OPC samples is relatively similar, fluid transport through the matrix may occur through capillary pores.

There is also some contribution to transport of liquids and gases arising from connected microscopic/gel pores. However in real structural systems the influence of cracks on transport mechanisms and, eventually, on system durability performance can become very significant depending on the nature and type of pore structures.

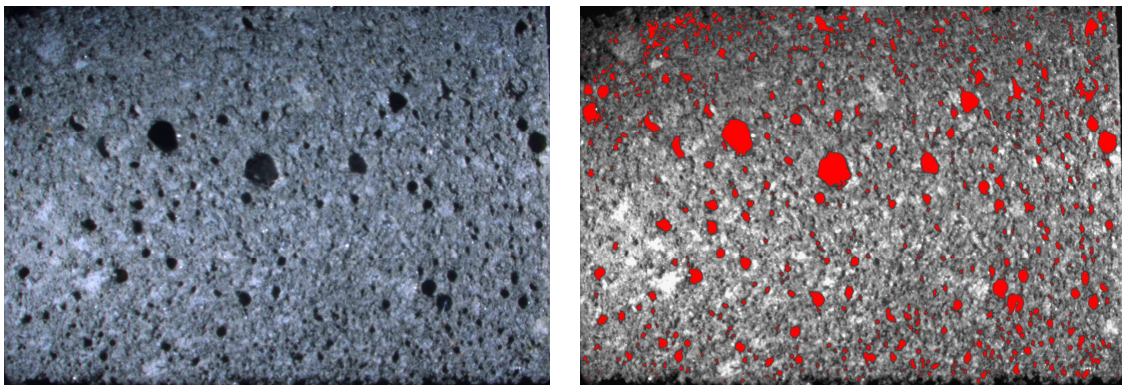

Fig 2: (a) Optical micrograph of GP concrete (b) Image analysis threshold image: registering 8.85% coverage of pores; mean pore diameter of 5.78mm

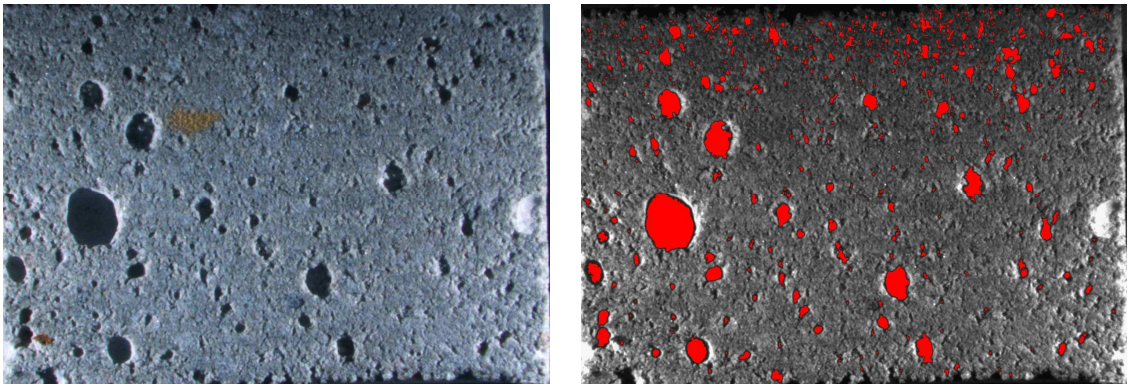

Fig 3 (a) Optical micrograph of OPC concrete (b) Image analysis threshold image: registering 8.43% coverage of pores; mean pore diameter of 5.76mm

Water permeability. Plots for steady state flow rates measured during water permeability tests for steam- cured OPC and GP concretes at 28 days are shown respectively Figs 4 and 5. The permeability results show significant differences between GP and OPC concretes. The effects of curing process and binder type significantly influence permeability of the concrete mixes from the mean water permeability coefficient values of all samples shown in Table 6. From Table 6, OPC concretes show reduced permeability values of nearly an order of magnitude for steam-cured samples and about two orders of magnitude for ambient-cured samples compared to the equivalent GP concretes. By comparison negligible difference was recorded for the air permeability measurements with corresponding values of GP and OPC samples respectively determined to be, 6.19E-17m^2 and 6.32E-17 m^2.

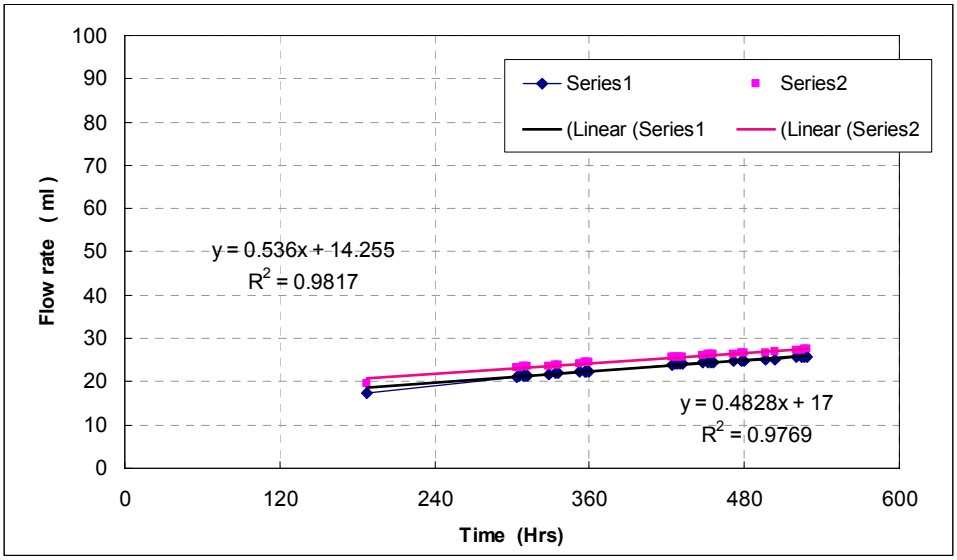

Fig 4. Flow rate measurement plot for 28day-steam cured OPC sample after

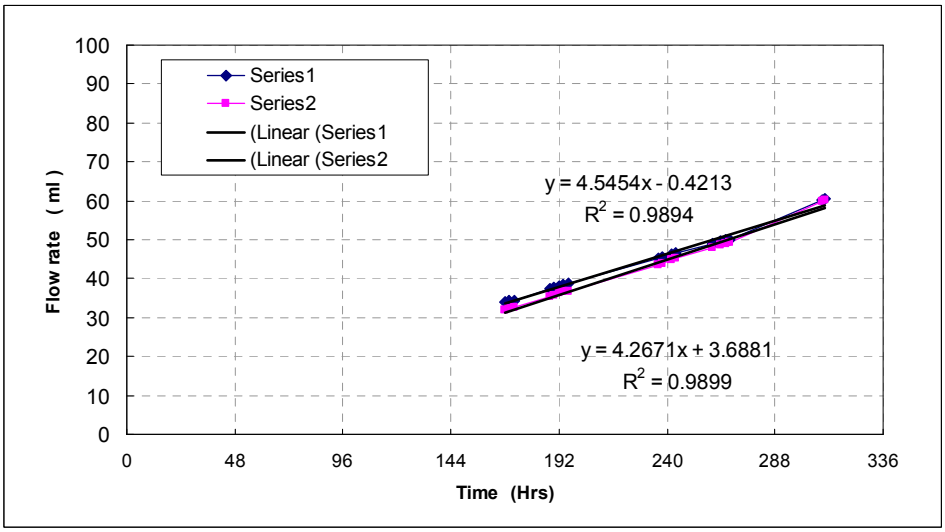

Fig 5. Flow rate measurement plot for 28day-steam cured GP sample after

The transport of fluids through concrete generally occurs through the network of continuous capillary and micropores which exist in the concrete's cementitious matrix, as well as the porosity that exist in the interfacial regions with the aggregate[4,13]. The mechanism of transport through the pore system can be by any combination of diffusion, permeation, capillary action and absorption processes [2].

The measured permeability of concrete may however be influenced by two primary factors, i.e. porosity and interconnectivity of pores in the cement paste or micro-cracks in concrete, especially at the paste/aggregate interface. For OPC concrete, the porosity and interconnectivity are controlled for most part by the w/c ratio, degree of hydration, and the degree of compaction.

Table 6. Mean water permeability coefficient values for OPC and GP concretes at 28days

Mix ID	**Steam-cure** Permeability(K_w m/s)	**Ambient-cure** Permeability(K_w m/s)
GP concrete at 28d	1.52E-10	7.21E-10
OPC concrete at 28d	1.73E-11	8.67E-12

Whereas the underpinning mechanistic parameters that control the movement of gases, liquids and ions through GP concrete may be expected to be similar to OPC systems, the interactions between transported fluids and chemical constituents of the binder matrix as well as the pore water often dictate the impact on concrete durability and performance[16]. For instance, when capillary pores are relatively dry, absorption dominates and when they are relatively saturated, diffusion becomes the dominant transport process. These mechanisms may act simultaneously or may prevail in sequence during consecutive periods of time.

The integrity of structural concrete, subjected to atmospheric gas transport, for instance can be significantly influenced by binder selection as well as concrete mix design to enhance its capacity to neutralise atmospheric CO_2. The use of different supplementary cementitious binders such as fly ash and blast furnace slag can also influence the rates of OPC concrete carbonation, and ultimately structural integrity[17, 18]. Thus, the mechanisms of deterioration can often be very complex, since in addition to the transported fluid, variables such as the nature and type of reaction products, degree of polymerization, system chemistry, humidity differentials, temperature and other secondary factors all contribute to concrete deterioration.

In the case of chloride diffusion it is generally recognised that a threshold concentration of the chloride ions must be exceeded for steel reinforcement corrosion to occur. This threshold arises from the capacity of free Cl ions to initiate corrosion, subject to alkaline pore solution chemistry and prevalence of certain aluminate of the cement matrix phases amongst other factors [19]. The corresponding risk factors associated with GP binder systems though likely to be similar to OPC systems, remain largely unclear.

Conclusions

1 For the purpose of analysing durability performance, both high pressure water and gas permeability testing of fly-ash based geopolymer concretes have been assessed for samples cured under ambient and steam exposure conditions at 65^{O}C.
2 The observed mean permeability coefficient values for gas(k) and water(K_w) of structural grade concrete was respectively 6.19E-17m^2 at 300kPa gas pressure and 1.52E-10m/s at 525kPa water pressure.
3 The gas permeability values of reference OPC systems were comparable to geopolymer concrete but the corresponding water permeability coefficient data for geopolymer systems were typically ten-fold higher.
4 The mechanism of fluid transport in geopolymer concrete appears to be dictated by an inherent mesoporous capillary pore network structure which is dependent on mode of concrete curing
5 General durability parameters and associated transport properties of governing geopolymer concrete material have been examined

References

[1] L, Basheer, J. Kropp, D. J. Cleland Assessment of the durability of concrete from its permeation properties: a review. Construction and Building Materials 15, 93-103(2001)
[2] E.J. Garboczi Permeability, diffusivity and micro-structural parameters. A critical review. Cement Concr Res, 20 pp, 990:591-601(1990)
[3] P.B Bamforth. The relationship between permeability coefficients for concrete obtained using liquid and gas. Mag Concr Res;39(138):3–10 (1987)
[4] J. Merchand, B Gerard. Microstructure-based models for predicting transport properties. In: Reinhardt HW, editor. RILEM report no. 16: penetration and permeability of concrete. E&FN Spon; (1997)
[5] J. Davidovits, Properties of geopolymer cements, in: P.V. Krivenko (Ed.), *Alkaline cements and concretes*, vol. 1, Vipol Stock, Kiev, Ukraine, pp. 131– 149. (1994)
[6] M. Criado., A Palomo., A Fernandez-Jimenez. Alkali activation of fly ashes. Part 1: Effect of curing conditions on the carbonation of the reaction products. Fuel 84 2048–2054(2005)
[7] H. Xu, J.S.J Van Deventer. The geopolymerisation of aluminosilicate minerals. Int J Miner Process;59 :247–66.(2000)
[8] J.M Miranda., A. Fernandez-Jimenez., J.A Gonzalez., A. Palomo. Corrosion resistance in activated fly ash mortars Cement and Concrete Research 35 1210– 1217(2005)
[9] P.V Krivenko,. Alkaline cements: terminology, classification aspects of durability, Proc. of 10th Int. Cong. Chem. Cem, pp. 4iv046– 4iv050. Goteborg (Sweden). (1997)
[10] W.M. Kriven, J. L Bell, S. W. Mallicoat, and M Gordon, ‘‘Intrinsic Microstructure and Properties of Metakaolin-Based Geopolymers’, pp. 71–86 in Int. Workshop on Geopolymer Binders, Interdependence of Composition, Structure and Properties. Edited by Bauhaus-Universitat¨ Weimar, Germany, (2006); W. M. Kriven, and J.L. Bell, Cer. Eng. and Sci. Proc., 25 [3-4] (2004)
[11] K K Aligizaki. Pore structure of cement-based materials: testing, interpretation and requirements. Taylor & Francis; (2006)
[12] J W Figg. Methods of measuring the air and water permeability of concrete. Mag Concr Res, Lond ;25(85):213-219 (1984)
[13] G. J. Verbeck. Pore structure significance of tests and properties of concrete and concrete making materials. ASTM Special Tech Publ; 169A:211-19(1982)
[14] AS 1012.9(1999)-Standard Test Method for Compressive Strength of Cylindrical Concrete Specimens(1999)
[15] R. P Khatri, V Sirivivatnanon, Methods for the determination of water permeability of concrete. ACI Mater J., 94 (3) 257-61(1997)
[16] P.A.M Basheer. A brief review of methods for measuring the permeation properties of concrete in-situ. Build Struct Inst Civil Eng 1993;99, 1.74-83.
[17] G.J Verbeck. Carbonation of hydrated Portland cement. Am Soc Test Mater; 17–36(1958).
[18] J Merchand, Gerard B. Microstructure-based models for predicting transport properties. In: Reinhardt HW, editor. RILEM report no. 16: penetration and permeability of concrete. E&FN Spon; (1997)
[19] L. O. Nilsson et al., Chloride penetration into concrete, State-of-the-art, transport processes, corrosion initiation, test methods and prediction models, The Report No. 53, Road Directorate, Copenhagen,: 151 pp.(1996)

doi:10.4028/www.scientific.net/AST.69.143

Bond Strengths of Geopolymer and Cement Concretes

Prabir Sarker

School of Civil and Mechanical Engineering, Curtin University of Technology, Perth, Western Australia

p.sarker@curtin.edu.au

Keywords: beam end specimen, bond strength, geopolymer concrete, pull-out test.

Abstract. Geopolymer is an inorganic alumino-silicate product that shows good bonding properties. Geopolymer binders are used together with aggregates to produce geopolymer concrete which is an ideal building material for infrastructures. A by-product material such as fly ash is mixed together with an alkali to produce geopolymer. Current research on geopolymer concrete has shown potential of the material for construction of reinforced concrete structures. Structural performance of reinforced concrete depends on the bond between concrete and the reinforcing steel. Design provisions of reinforced concrete as a composite material are based on the bond strength between concrete and steel. Since geopolymer binder is chemically different from Ordinary Portland Cement (OPC) binder, it is necessary to understand the bond strength between geopolymer concrete and steel reinforcement for its application to reinforced concrete structures. Pull out test is commonly used to evaluate the bond strength between concrete and reinforcing steel. This paper describes the results of the pull out tests carried out to investigate the bond strength between fly ash based geopolymer concrete and steel reinforcing bars. Beam end specimens in accordance with the ASTM Standard A944 were used for the tests. In the experimental program, 24 geopolymer concrete and 24 OPC concrete specimens were tested for pull out. The concrete compressive strength varied from 25 to 55 MPa. The other test parameters were concrete cover and bar diameter. The reinforcing steel was 500 MPa steel deformed bars of 20 mm and 24 mm diameter. The concrete cover to bar diameter ratio varied from 1.71 to 3.62. It was found from the test results that the failure occurred by splitting of concrete in the region bonded with the steel bar, in both geopolymer and OPC concrete specimens. Comparison of the test results shows that geopolymer concrete has higher bond strength than OPC concrete. This suggests that the existing design equations for bond strength of OPC concrete with steel reinforcing bars can be conservatively used for calculation of bond strength of geopolymer concrete.

Introduction

Concrete is the most widely used construction material in the world. Ordinary Portland Cement (OPC) has been traditionally used as the binding agent for concrete. The worldwide consumption of concrete is estimated to increase due to the increase of infrastructure in countries such as India and China [1]. About 1 ton of carbon dioxide is released to the atmosphere during the manufacture of 1 ton of cement. Globally, the cement production contributes about 7% of the world's carbon dioxide [1]. The worldwide annual cement production is estimated as 2 billion tons at present and is expected to increase to 4 billion tons in 30 years from now [2]. In order to control the effect of global warming, it is necessary to reduce the emission of CO_2 gas to the environment. The use of an alternative low-emission binding agent for concrete will help reduce the environmental impact of manufacturing of cement. Geopolymer is an alternative material that can act as a binding agent in concrete. The geopolymer binder contains no cement and thus will help enhance sustainability to construction industries.

Geopolymer Concrete. Geopolymer is a type of alumino-silicate product that shows good bonding properties. The geopolymer binders utilize a material such as fly ash or metakaolin as the

source of Silicon and Aluminium for reaction by an alkali. In fly ash-based geopolymer binder, fly ash is reacted with an alkaline solution to create an alumino-silicate binder. Geopolymer binders are used together with aggregates to produce geopolymer concrete. The basic ingredients of fly ash-based geopolymer concrete are fly ash, alkali, fine aggregates and coarse aggregates. However, water and superplasticizer can be added to improve workability of the concrete. Current research [3-6] has shown potential use of geopolymer concrete as a construction material. Geopolymer concrete has the properties of high compressive strength, very little drying shrinkage, low creep, and good resistance to acid and sulphate attack. It was also shown that the structural performance of geopolymer concrete beams and columns is similar to that of OPC concrete members [7, 8].

Bond Strength of Concrete. The knowledge of bond behaviour between reinforcing steel and concrete is critical to the design of reinforced concrete structures. Bond behaviour is the interaction of the reinforcing bar with the concrete. This is described as the transfer of forces from the reinforcement to the surrounding concrete by adhesion between the bar and concrete, frictional force at the interface and bearing of the ribs of deformed bars against the concrete. The adhesion depends on the bar surface condition and the type of concrete. Bond resistance is governed by several factors such as compressive and tensile strengths of concrete, the concrete cover to the bar, confinement due to transverse reinforcement, surface condition of the bar and bar geometry [9-11]. Structural performance of reinforced concrete members depends on the bond between concrete and the reinforcement. The design provisions of reinforced concrete as a composite material utilize the bond strength between the two materials. The commonly used steel reinforcing bars have been developed for use with OPC concrete. Since geopolymer binder is chemically different from OPC, it is necessary to understand the bond properties between geopolymer concrete and steel reinforcement. This paper studied the bond strength of fly ash-based geopolymer concrete by using pull-out tests. A comparison is made between the bond strengths of geopolymer and OPC concretes with reinforcing steel.

Experimental works

Test Specimens. Pull-out test using beam-end specimens is used to evaluate the bond strength of a material because the test is relatively simple to conduct and it simulates the state of stresses in a beam [12, 13]. Geopolymer and OPC concrete beam-end specimens were manufactured and tested for pull out in accordance with ASTM 944 [14] to study the bond between concrete and reinforcing bars. The overall dimensions of the specimens were 250 x 250 x 600 mm. The bars were de-bonded outside of the bonded length by using PVC pipes. The geometry of the specimens is shown in Fig. 1. The specific dimensions of each specimen of geopolymer and OPC concrete are given in Tables 1 and 2 respectively. In Tables 1 and 2, the specimens are designated by using the concrete batch used to cast them and a specimen number of that batch. For example, the designation of GPC2 S3 indicates that it is the specimen number 3 cast by using geopolymer concrete of batch 2.

In order to prevent the specimens from failing by flexure or shear, as opposed to a bond failure, N16 and N12 bars were used as longitudinal and shear reinforcements respectively. The shear reinforcement was configured as two separate legs as shown in Fig. 1. They were not used in the form of closed ties to minimise confinement effect on concrete against splitting of the concrete during the pull-out test. The pull-out bars were either N20 or N24.

Materials. Low-calcium fly ash was used as the base material for geopolymer concrete. Locally available aggregates comprising 10mm and 7mm crushed granite-type coarse aggregates and fine sand were used. The aggregates were prepared to saturated-surface-dry (SSD) condition before mixing the concrete. The alkaline liquid used was a combination of sodium hydroxide and sodium silicate solutions. The sodium hydroxide solution was made by dissolving commercial grade Na(OH) solids in distilled water. The concentration of the Na(OH) solution was 14 Molars and it

was prepared at least 24 hours prior to use. The sodium silicate solution had a chemical composition of 14.7% Na_2O, 29.4% SiO_2, and 55.9% water by mass. A commercially available naphthalene sulphonated super plasticizer and normal tap water were added to improve the workability of fresh geopolymer concrete.

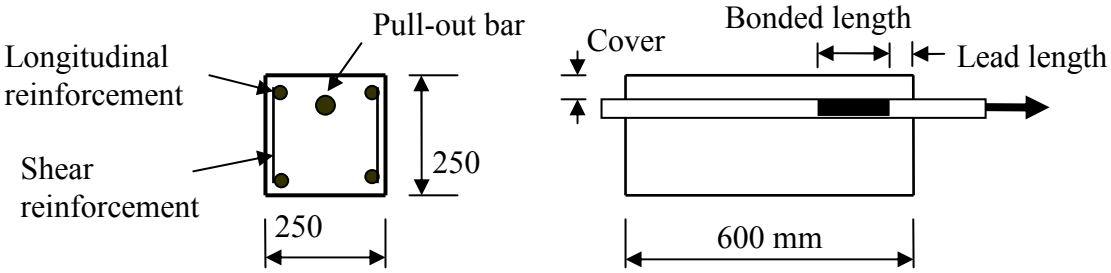

Fig. 1: Geometry of the beam-end specimens

Table 1: Specimen details and failure loads of geopolymer concrete specimens

Specimen	Compressive strength, f_c (MPa)	Bar diameter, d_b (mm)	Cover, c (mm)	c/d_b	Bonded length, l_d (mm)	Pull-out load, P (kN)	Bond strength, u (MPa)
GPC1 S1	25.5	24	42	1.75	100	80	10.61
GPC1 S2			44	1.83	110	108	13.02
GPC1 S3			44	1.83	100	82	10.88
GPC1 S4			65	2.71	120	125	13.82
GPC1 S5			66	2.75	125	105	11.14
GPC1 S6			64	2.67	110	123	14.83
GPC2 S1	29.7	20	45	2.25	100	90	14.32
GPC2 S2			45	2.25	100	82	13.05
GPC2 S3			41	2.05	95	79	13.23
GPC2 S4			64	3.20	110	105	15.19
GPC2 S5			64	3.20	105	85	12.88
GPC2 S6			66	3.30	115	80	11.07
GPC3 S1	32.5	24	44	1.83	100	92	12.20
GPC3 S2			45	1.88	100	110	14.59
GPC3 S3			41	1.71	100	98	13.00
GPC3 S4			63	2.63	100	111	14.72
GPC3 S5			66	2.75	100	133	17.64
GPC3 S6			62	2.58	100	130	17.24
GPC4 S1	39.5	20	42	2.10	100	94	14.96
GPC4 S2			42	2.10	100	95	15.12
GPC4 S3			46	2.30	100	105	16.71
GPC4 S4			68	3.40	100	122	19.42
GPC4 S5			68	3.40	100	88	14.01
GPC4 S6			64	3.20	100	100	15.92

The mixture proportions of the geopolymer and OPC concrete are given in Table 3. Specimens of batches GPC1 and GPC2 were cast using mixture 1 and specimens of batches GPC3 and GPC4 were cast using mixture 2. Mixtures 3, 4 and 5 were used to cast OPC specimens of batch OPC1, OPC2 and OPC3, and OPC4 respectively. Samples of steel bars were tested in the laboratory to obtain the actual yield and ultimate strengths. These results are given in Table 4.

Table 2: Specimen details and failure loads of OPC concrete specimens

Specimen	Compressive strength, f_c (MPa)	Bar diameter, d_b (mm)	Cover, c (mm)	c/d_b	Bonded length, l_d (mm)	Pull-out load, P (kN)	Bond strength, u (MPa)
OPC1 S1	42.3	20	45	2.25	100	98	15.60
OPC1 S2			42	2.10	95	75	12.56
OPC1 S2			65	3.25	100	115	18.30
OPC1 S2			63	3.15	100	95	15.12
OPC1 S2		24	45	1.88	95	88	12.29
OPC1 S2			65	2.71	145	115	10.52
OPC2 S1	37.2	20	45	2.25	100	64	10.25
OPC2 S2			45	2.25	100	63	10.03
OPC2 S3			45	2.25	100	66	10.48
OPC2 S4			65	3.25	100	60	9.55
OPC2 S5			65	3.25	100	72	11.50
OPC2 S6			65	3.25	100	89	14.09
OPC3 S1	34.0	24	45	1.88	100	82	10.85
OPC3 S2			45	1.88	100	86	11.43
OPC3 S3			45	1.88	100	64	8.46
OPC3 S4			65	2.71	100	83	10.99
OPC3 S5			65	2.71	100	90	11.95
OPC3 S6			65	2.71	100	87	11.56
OPC4 S1	55.3	24	65	3.25	100	92	14.60
OPC4 S2			45	1.88	100	93	12.31
OPC4 S3			45	1.88	100	86	11.35
OPC4 S4			65	2.71	100	106	14.05
OPC4 S5			65	2.71	100	90	11.89
OPC4 S6			65	2.71	100	84	11.13

Manufacturing and Testing of the Specimens. The manufacture and curing process of geopolymer concrete were based on earlier research [8]. The coarse aggregates (10mm and 7mm), sand and fly ash were first mixed dry in the laboratory pan mixer for about three minutes. At the end of this mixing, the alkaline liquid, together with the super plasticizer and the extra water were mixed together and added into the dry mixture. The mixing continued for another four minutes. After mixing, the fresh concrete was placed into the moulds.

The specimens were cast in a horizontal position and were vibrated with a standard mechanical vibrator. Standard 100mm x 200mm cylinders were cast for compressive strength tests of the concrete. The geopolymer concrete specimens were placed inside the steam curing chamber after

casting. The specimens were de-moulded after curing, and left in ambient conditions in the laboratory until the time of testing.

The beam-end specimens were tested for pull-out in accordance with the ASTM A944 Standard [14]. A schematic diagram of the load reaction configuration of the test rig is shown in Fig. 3. The specimens were loaded using a hydraulic jack until failure. The reinforcing bar in the specimen was pulled at a loading rate of 8 kN per minute. The specimens were tested within the ASTM A944 requirement that failure should not occur in the first three minutes.

Table 3: Mixture proportions of concrete (kg / m^3)

Ingredients	Geopolymer concrete		OPC concrete		
	Mixture 1	Mixture 2	Mixture 3	Mixture 4	Mixture 5
Cement	-	-	420	357	424
Fly Ash	408	408	-	-	-
20mm aggregate	-	-	560	-	-
10mm aggregate	555	555	540	458	456
7mm aggregate	647	647		549	547
Sand	647	647	740	760	697
Sodium hydroxide	41	41	-	-	-
Sodium silicate	103	103	-	-	-
Water	24.3	14.95	130	225	225
Superplasticiser	5.6	5.6	3	-	-

Table 4: Properties of steel reinforcement

Diameter (mm)	Nominal area (mm^2)	Yield strength (MPa)	Ultimate strength (MPa)
12	110	531	672
16	200	525	655
20	310	570	662
24	450	555	648

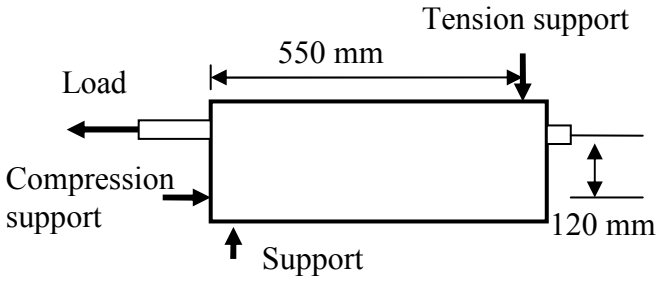

Fig. 2: Schematic diagram of test rig showing load-reaction configuration.

Test Results and discussions

All the specimens failed by splitting of the concrete in the region where the steel bar was bonded to the concrete as shown in Figs. 3 (a) and 3 (b). Concrete splitting crack patterns in the geopolymer concrete specimens were similar to those in the OPC concrete specimens. The failure occurred in a brittle manner in both types of concrete specimens. The pull-out load of each specimen is given in Tables 1 and 2.The test results in terms of bond strength and effect of different test parameters on bond strength are discussed in the following sections.

Fig. 3 (a) : Geopolymer concrete specimen

Fig. 3 (b) : OPC concrete specimen

Effect of parameters. The ultimate pull out failure load of each specimen was divided by the surface area of the bonded length of the bar to calculate the average bond strength. This bond strength is denoted by u and the values are given in Tables 1 and 2. Since bond strength varies with the test parameters, the bond strength of geopolymer concrete is compared with that of OPC concrete for the same test parameter. The test parameters in this study are concrete compressive strength, bar diameter and concrete cover to the pull-out bar. The bond strength of the specimens with similar parameters are combined together to obtain a mean value of the bond strength for a test variable. These values are then plotted against the variable to compare its effect on the bond strength of OPC and geopolymer concrete.

The effect of concrete cover on bond strength for 20 mm and 24 mm diameter bars are shown in Figs. 4 and 5 respectively. Since the concrete compressive strength of the specimens were different, the bond strengths were normalized with respect to $f_c^{0.5}$. It can be seen that the normalized bond strength increased with the increase in concrete cover for both 20 and 24 mm bars. The trend is similar in both types of concrete. It is observed from these graphs that geopolymer concrete has higher bond strength than OPC for the same bar diameter and concrete cover.

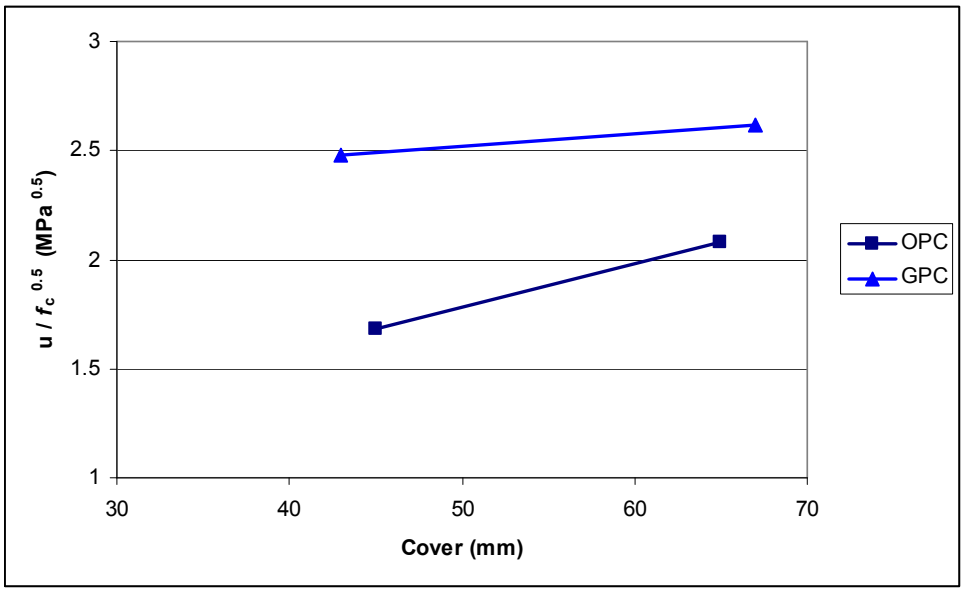

Fig. 4. Bond strength vs concrete cover for 20 mm bar

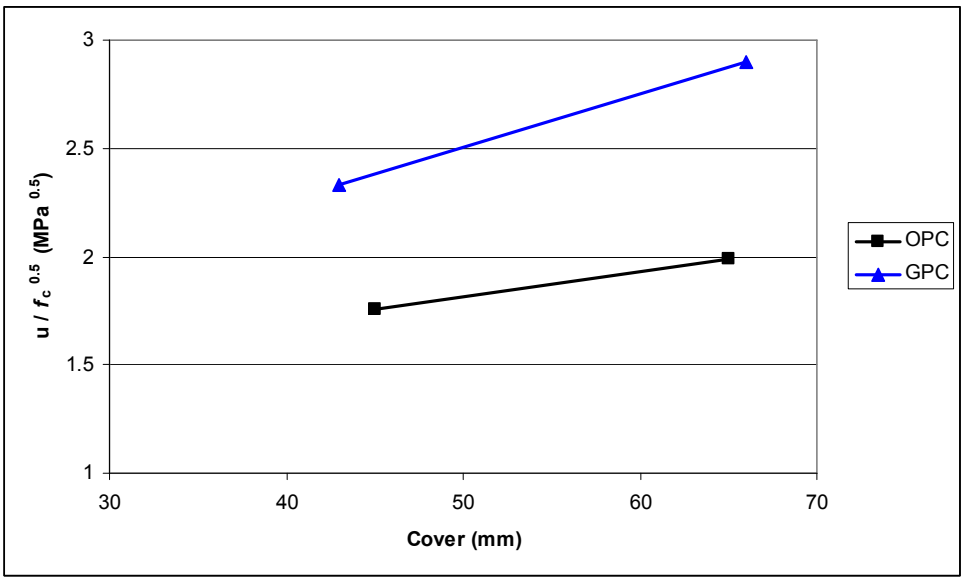

Fig. 5. Bond strength vs concrete cover for 24 mm bar

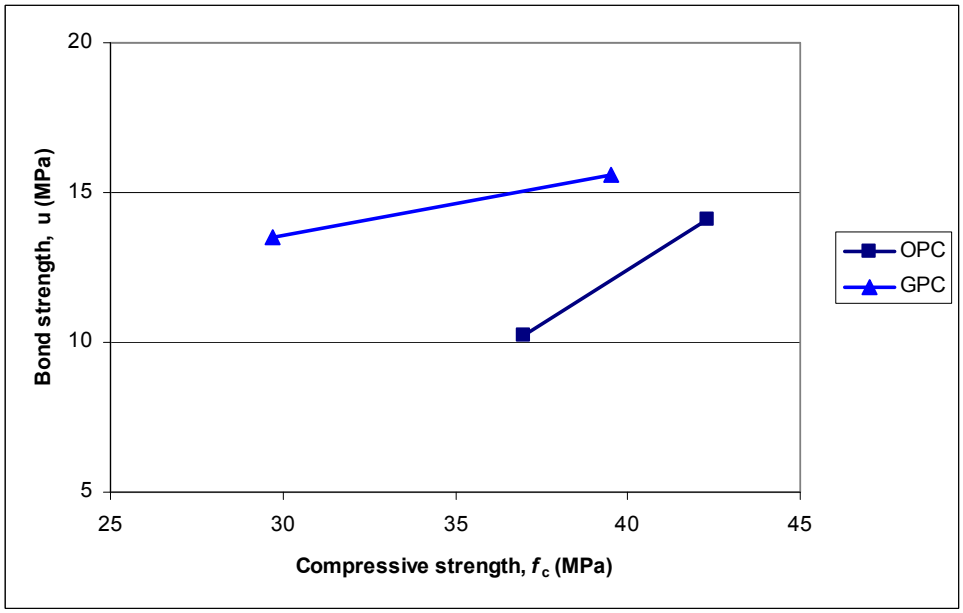

Fig. 6. Bond strength vs concrete compressive strength for 20 mm bar and 45 mm cover

Similarly, the effect of concrete compressive strength on bond strength of OPC and geopolymer concrete are shown in Figs. 6 and 7. Again, the specimens of similar compressive strength are combined together to obtain a mean value of the bond strength. It is seen from Figs. 6 and 7 that bond strength increased with the increase of compressive strength for both types of concrete. In both the figures, the trend line for geopolymer concrete is above the line for OPC concrete. This shows that the bond strength of geopolymer concrete is higher than that of OPC concrete for the same compressive strength.

Finally, the bond strength normalized with respect to $f_c^{0.5}$ are plotted against the concrete cover to bar diameter ratio (c/d_b) and shown in Fig. 8. All the test specimens of OPC and geopolymer concrete are used to obtain mean values of normalised bond strength and c/d_b ratio for this graph. It is seen from this graph that normalized bond strength increased with the increase of c/d_b ratio in both types of concrete. The trend line for geopolymer concrete is similar to that of OPC. However

the trend line of geopolymer concrete is above that of OPC concrete. Therefore, the test results show that bond strength of geopolymer concrete is generally higher than the line for OPC concrete. This suggests that the current bond strength equations [9, 10, 12] for OPC concrete can be used for conservative prediction of the bond strength of geopolymer concrete.

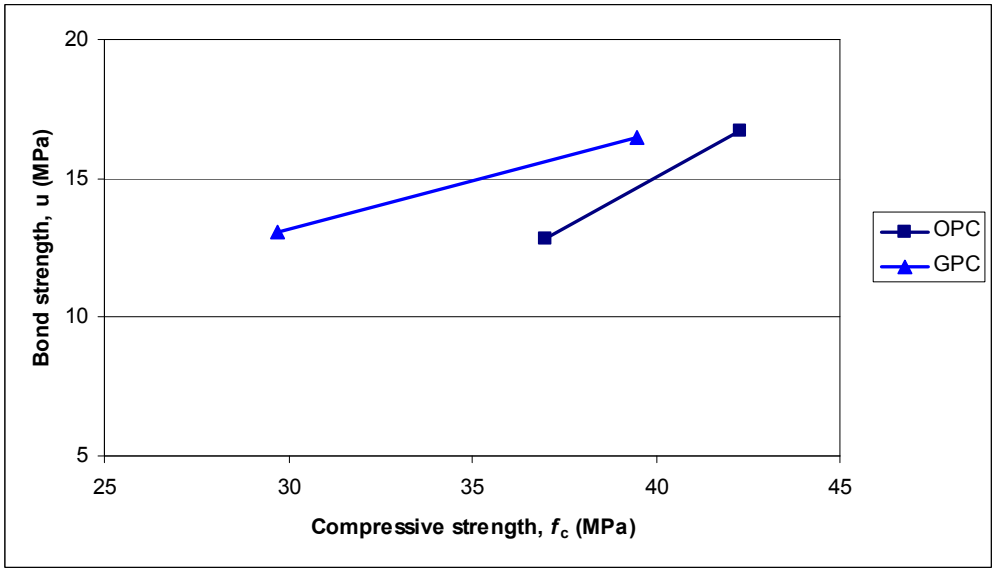

Fig. 7. Bond strength vs concrete compressive strength for 20 mm bar and 65 mm cover

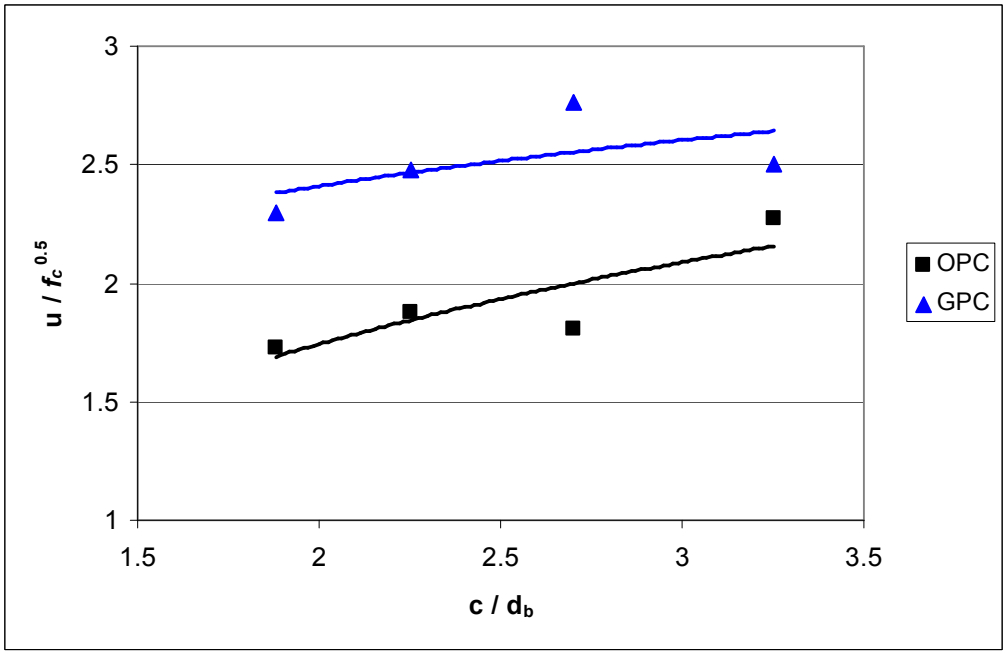

Fig. 8: Variation of bond strength with c/d_b ratios.

Conclusions

Twenty-four geopolymer and 24 OPC concrete beam-end specimens were manufactured and tested for pull out in accordance with the ASTM 944 Standard. The test results were used to compare the

bond strengths of geopolymer and OPC concretes with steel reinforcing bars. The following conclusions are drawn from the experimental results:

- Both geopolymer and OPC concrete specimens failed by splitting of concrete along the bonded length of the pull-out bar. Both types of concretes showed similar cracking patterns and brittle failure under the pull out load.
- In both types of concrete, bond strength increased with the increase of concrete cover and the concrete compressive strength.
- In both types of concrete, the bond strength normalized with respect to concrete compressive strength showed an increasing trend with the increase of concrete cover to bar diameter ratio.
- Generally, geopolymer concrete has higher bond strength than OPC concrete for the same test parameter. This suggests that the current bond strength equations for OPC concrete can be used for conservative prediction of the bond strength of geopolymer concrete.

Acknowledgements

The author gratefully acknowledges the contributions of Rocky Vasile, Aidan Grigg and the laboratory technicians of the Department of Civil Engineering, Curtin University of Technology to carry out the experimental works.

References

[1] P.K. Mehta: *Concrete International* Vol. 23, No. 6 (2001), p. 61-66.

[2] K. Sakai, in: *Proceedings of the 6th International Conference on Analytical Models and New Concepts in Concrete and Masonry Structures*, Lodz, Poland, (2008), p. 139-155.

[3] B.V. Rangan: *Indian Concrete Institute Journal* (2006) October – December, p. 9-17.

[4] A.M. Fernandez-Jimenez, A. Palomo and C. Lopez-Hombrados: *ACI Materials Journal* Vol.103 (2006), p. 106 – 112.

[5] D. Hardjito, S. E. Wallah, D.M.J. Sumajouw and B.V. Rangan: *ACI Materials Journal*, Vol. 101, (2004), p. 467-472.

[6] M. Sofi, J.S.J. van Deventer, P.A. Mendis and G.C. Lukey: *Journal of Materials Science*, Vol. 42 (2007), p. 3107-3116.

[7] P.K. Sarker: *Materials and Structures* Vol. 42 (2009), p. 715 – 724.

[8] D.M.J. Sumajouw, D. Hardjito, S.E. Wallah and B.V. Rangan: Journal of Material Science Vol. 42, No. 9 (2007), p. 3124-3130.

[9] M.R. Esfahani and B.V. Rangan: *ACI Structural Journal* Vol. 95, (1998). P. 272 – 280.

[10] C. O. Orangun, J. O. Jirsa and J. E. Breen: *ACI Journal* (1977) March, p. 114-122.

[11] D. Darwin, M.L. Tholen, E.K. Idun and J. Zuo: *ACI Structural Journal* Vol. 93 (1996), p. 347-359.

[12] ACI Committee 408: *Bond Development of Straight Reinforcing Bars in Tension (ACI 408R-03)* American Concrete Institute, Farmington Hills, USA(2003).

[13] T.M. Ahlborn and T. C. DenHartigh: *Journal of Transportation research Board* (2003), p. 88-95.

[14] ASTM A 944-99: *Standard Test Method for Comparing Bond Strength of Steel Reinforcing Bars to Concrete Beam-End Specimens*, American Society for Testing and Materials Standard, West Conshohocken, US (1999).

doi:10.4028/www.scientific.net/AST.69.152

Use of local raw materials for construction purposes

Hubert Rahier [1, a], Faten Slatyi[2,b], Islam Aldabsheh[2,c], Mazen Alshaaer[2,d] Hani Khoury[2,e], Muayad Esaifan[3,f] and Jan Wastiels[3,g].

[1]Dept. Physical Chemistry and polymer Science, Vrije Universiteit Brussel, Pleinlaan 2, Brussels, Belgium

[2] Dept. of Geology, Materials Research Laboratory, University of Jordan, Amman 11942 Jordan

[3] Dept. of Mechanics of materials and constructions, Vrije Universiteit Brussel, Pleinlaan 2, Brussels, Belgium

[a]hrahier@vub.ac.be, [b] fmastergeo@gmail.com, [c]islam.aldabsheh@gmail.com, [d] mazen72@yahoo.com, [e]khouryhn@ju.edu.jo, [f]isefan_muayed@yahoo.com, [g]jwastiel@vub.ac.be

Keywords: geopolymers, mechanical properties, XRD, TGA, durability

Abstract. A geopolymer produced from Jordanian kaolinite is described in this work. The aim is to produce low environmental impact materials from local raw materials. In this paper the emphasis is on the general characteristics of the material and on its durability. With the used kaolinite, specimens with compressive strength of 41 MPa under dry conditions and 23 MPa under immersed water conditions were obtained. The durability under environmental conditions was good.

Introduction

Since some years research is going on in Jordan to produce construction materials, starting from local raw materials [1,2]. Geopolymers have the benefit that they have a smaller environmental impact than concrete, but also the main raw material, for instance kaolinite, is often locally available. To minimize the production cost, the kaolinite will be used as such and thus not be dehydroxylated.

The aim of this research is to

-find out which local raw materials can be used (reactive and filler)
-optimize the production (composition, curing) of bricks, tiles,.
-find out how to do the production in the field
-make a water reservoir for water harvesting

The proposed raw materials are kaolinite, smectite rich clay, tripoli, calcareous porcelanite, diatomaceous clay, silica sand, granite, zeolitic tuff, scoria (tuff) and basalt. The reactivity of these materials was tested in the framework of the PhD of Islam Aldabsheh and Muayad Esaifan. No further details will be given in this text.

As kaolinite, a Hiswa clay, rich in kaolinite was chosen [3-5]. With the Hiswa kaolinite (JHK), specimens with compressive strength of 41 MPa under dry conditions and 23 MPa under immersed water conditions were obtained. Since the materials will be used for the construction of water ponds, the durability of these specimens was tested. These materials also exhibit good mechanical performance upon heating to 600 °C, opening a possibility for use under elevated temperatures. The work presented in this paper is part of the PhD of Faten Slaty [6].

Results and discussion

Optimization of the geopolymer preparation. First an optimization of the composition and reaction conditions was performed. The NaOH and sand (JSS) amount were varied with respect to the amount of kaolinite (JHK). In Table 1 the compressive strength as a function of the amount of NaOH is presented. The optimal amount is about 16wt% of NaOH compared to the raw kaolinite.

Table 1: The optimization for NaOH ratio in the JHK geopolymer mixture

JHK: JSS: NaOH: H_2O	Compressive strength [MPa]	Avg. strength [MPa]
100: 50 : 8: 22	13.2	13.0
	13.1	
	12.6	
100: 50: 12: 22	26.66	23.5
	20.7	
	23.1	
100: 50 : 14: 22	29.2	29.4
	30.4	
	28.6	
100: 50 : 16: 22	32.1	33.1
	34.2	
	32.9	
100: 50 : 18: 22	31.2	30.3
	31.0	
	28.6	
100: 50 : 20: 22	27.7	28.0
	27.3	
	28.8	

For sand an optimized ratio of about 0.5 to 1 sand/kaolinite was obtained.

The reaction product of the final geopolymer was studied with XRD (Fig 1). Na-zeolitic phases namely: phillipsite ($(Na,K,Ca)_{1\text{-}2}(Si,Al)_8O_{16}.6(H_2O)$) and natrolite ($Na_{16}Al_{16}Si_{24}O_{80}.16(H_2O)$) were identified. Hydroxysodalite ($Na_2Si_2Al_2O_5(H_2O)_6$) is also observed. Quartz occurs as a major phase in the specimen along with the remainings of kaolinite, muscovite/illite and hematite.

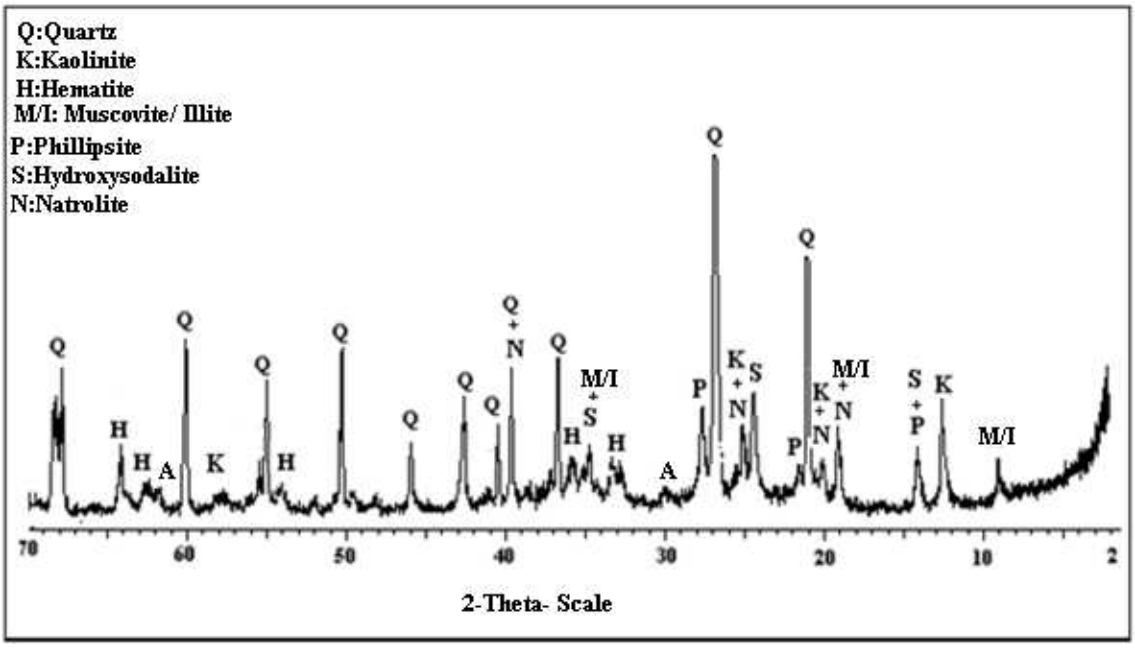

Figure 1: The XRD spectrum of the optimized geopolymer specimen

Durability. Geopolymer specimens were subjected to different types of durability tests namely: the drying shrinkage test, ambient conditions, de-ionized water conditions, wetting-drying cycles, and the aging tests under chemical conditions, which include the chemical attack, acid attack, and alkali-silica reaction. The samples proved to be stable under ambient and water conditions. Possibly a slow further hardening occurs improving the mechanical strength upon storage. The results for the wetting-drying cycles are shown in Table 2. The compressive strength varies between 18 and 30MPa without a trend. Even after 100 cycles no deterioration of the samples is observed.

Table 2: Mechanical strength for the geopolymers of JHK with sand (JHKS) under wetting-drying conditions

Cycles No.	5	10	25	50	100
Avg. Strength for mix. JHKS	21.7	25.5	25.3	21.5	24.6
JHKS 1	28.8	18.3	26.4	16.5	27.2
JHKS 2	18.3	31.4	19.1	26.0	21.4
JHKS 3	18.0	26.9	30.5	22.1	25.4

The specimens were also subjected to immersion in sea water and sodium sulfate solution. Again no negative impact on the samples was observed. The obtained compressive strength results during the acid attack (HCl, 0.1N) test are given in Table 3. According to these results, the compressive strength values decrease as a function of time. The average compressive strength has decreased already after 7 days to about 15MPa (starting from about 23) and decrease even further to 9 MPa after 90 days. The specimens are visually being attacked (weight loss) by the acid. The samples also do not withstand the alkali-silica reaction.

Table 3: Mechanical strength for the geopolymer specimens immersed in hydrochloric acid

Time	7	30	60	90
Avg. Strength mix JHKS	15.0	12.5	11.7	9.0
JHKS1	14.5	12.6	10.7	9.2
JHKS2	16.0	11.3	11.7	9.4
JHKS3	14.6	13.5	12.6	8.4

Conclusion

Geopolymer specimens were prepared from a local Jordanian Kaolinite (Hiswa Clay) and NaOH solution. An optimized composition of 100:100:16:22 kaolinite:sand:NaOH:water was obtained. The samples were shown to be stable under environmental conditions and to wet/dry cycles. Only acid and alkaline attack breaks down the material.
The Hiswa clay is thus suited to be used as a raw material for the production of bricks and tiles for the construction of water reservoirs.

References

[1] J. Gogo, “Geological and Geotechnical Evaluation of Latosols from Ghana, and their Improvement for Construction”, Ph.D. Thesis (1990), Vrije Universiteit of Brussel.
[2] M. AlShaaer, H. Cuypers, and J. Wastiels, “Stabilisation of kaolinitic soil for construction purposes by using mineral polymerisation technique”, in Proceedings of the 6th International Conference Technology for Developing Countries, (3), Jordan, Hole Musa Resheidat, (2002) p 1085-1092.
[3] H. Khoury and W. El-Sakka: Mineralogical and industrial characterization of the Batn El-Ghoul clay deposits.,Appl. Clay Sci., (1) (1986), p 321–351.
[4] H. Khoury: Clays and clay minerals in Jordan. Publications of the University of Jordan, Amman. (2002) 116pp.
[5] H. Khoury, (2006): Industrial rocks and minerals in Jordan (second edition). Publications of the University of Jordan, Amman. 361pp
[6] F. Slaty “Durability of Geopolymers Product from Jordanian Hiswa Clay” PhD dissertation (2010).

doi:10.4028/www.scientific.net/AST.69.156

Development of building materials through alkaline activation of construction and demolition waste (CDW) - Resistance to acid attack

Joana Gonçalves Rapazote [1,a], Cristóvão Laginhas [2,b], Amândio Teixeira-Pinto [3,c]

[1,2,3]Universidade de Trás-os-Montes e Alto Douro, Escola de Ciências e Tecnologia, Departamento de Engenharias, 5001-801Vila Real, Portugal

[a]jrapazote@utad.pt, [b]cristovaolg@yahoo.com, [c]yrache@utad.pt

Keywords: Construction and demolition waste recycling; alkaline activation; building materials; acid resistance

Abstract. Construction and demolition waste (CDW) is a by-product of construction and demolition activity. It consists mostly of inert and non-biodegradable material such as concrete, plaster, metal, wood, plastics etc. CDW is priority waste in the E.U. due to the increased quantities and volumes that are produced. While retrievable items such as brick, wood and metal wires are recycled, concrete, masonry tile and ceramic waste, accounting for more than 60% of CDW, are not being currently recycled.

The main objective of this study is to develop a process for obtaining new building materials from CDW using low temperature geopolymerisation in alkaline environment.

The two major fractions of the CDW which are not currently being recycled are concrete, mortars, masonry and rubbles for one side and ceramic tile, mosaic and bricks for the other. The major constituents of the first fraction are SiO_2 and CaO along with minor concentration of Al_2O_3 and Fe_2O_3, mostly crystalline. The major constituents of the latter are SiO_2 and Al_2O_3 and comprise crystalline as well as glassy constituents.

The aluminosilicate fraction of both fractions will actively participate in the reaction and for the obtaining of ASH gel (A= Al_2O_3, S = SiO_2, H = H_2O), which is the main binding phase. Any deficiency (quantity) in chemical constituents will be compensated by addition of suitable material, e.g., Al_2O_3 can be compensated with a source of alumina which will be added for alkaline activation reaction. The remaining non aluminosilicate portions such as iron oxide and others will act as filler material. The final product is a very hard ceramic like product. These products can be used for civil engineering applications such as pavement blocks, precast concrete blocks, retaining walls, in general the same use as plain concrete.

Introduction

European Environment Agency estimates a production of 500 kg per capita year of CDW [1] which approximately doubles the production of municipal solid waste [2]. Environmental impact associated with construction activity is relevant and society is concerned about that.

Construction activity needs to contribute for sustainable development and environmental protection and for that is necessary to improve practices considered environmental friendly including recycling of by-products, energy saving, decreasing of natural resources demand and diminishing of greenhouse emissions.

Use waste as prime material for building materials production directly presents significant advantages on decreasing needs of natural resources for construction industry and on reduction of landfill disposal of construction and demolition waste.

Scientific community concerned with environmental issues is looking for alternatives [3,4,5,6]. It is accepted that alkaline activated products or geopolymers have better environmental performance than Ordinary Portland Cement (OPC).

According to Komnitsas et al [7] geopolymers production is responsible for three times less CO_2 emissions and around 60% less energy consumption in comparison with OPC.

This work appears as a contribute to the challenge made by different researchers to new developments in alkaline activation technology namely using aluminosilicate mineral wastes [8,9,10] to get products with advanced properties and well established in construction and mineral industry [7].

So, this paper reports results achieved from a research project related to the development of a new building material obtained by alkaline activation of construction and demolition waste (CDW) and includes experiments to evaluate acid attack on the new materials.

Waste recycling by alkaline activation is cement free, raw materials for binder and aggregate compounds are exclusively made from CDW; additive used as a source of aluminium was obtained from water treatment plant sludge.

Researchers usually report the incorporation of waste in concrete production but it's uncommon to find studies dedicated to building materials produced exclusively from waste.

Methodology and Experimental work

CDW consists of two major fractions of (a) concrete products and stone masonry, (b) bricks, tiles and ceramic waste. They are the goal of this work because they are not being currently recycled; they are inert, they have aluminosilicates as major constituents and they appear in different times on construction site (so they can be easily separated and collected).

The first step on this research included the collecting and selecting the waste in three general categories according with their origin:

- A: Ceramic products (including bricks, roof and floor tiles and sanitary ware);
- B: Concrete products (mainly cement blocks);
- AB: Mixture of A and B.

Their classification according the European Waste Catalogue and Hazardous Waste List is shown in table below. Hazardous substances or contaminated material were excluded from the study.

Table 1: Classification of prime materials used according to European Waste Catalogue

Material	Code	Description of waste included in each category
-	17 00 00	Construction and demolition waste
-	17 01	Concrete, bricks tiles and ceramics
B	17 01 01	Concrete
A	17 01 02	Bricks
A	17 01 03	Tiles and ceramics
-	17 01 06(*)	Mixtures of, or separate fractions of concrete, bricks, tiles and ceramics containing dangerous substances
AB	17 01 07	Mixture of concrete, tiles, ceramics other than those mentioned in 17 01 06

Specimens were prepared exclusively from CDW and sludge (as an additive). The solids (binder and aggregates) were mixed with a liquid alkaline activator, conformed in 4x4x16cm^3 moulds, vibrated and cured. Finally samples were subjected to strength mechanical tests and durability experiments.

Samples of Ordinary Portland Cement 32,5 class were prepared and subjected to the same conditions than CDW probes to get comparable results.

Preparation of Binders and aggregates. Binders and aggregates were prepared from 800kg of raw materials A and B respectively after a set of operations that includes:

- Collection;
- Classification;
- Homogenization;
- Crushing by a jaw crusher,
- Milling with a metal ball mill RETSCH S100.
- Sieving
- Thermal treatment for 2 hours at 750ºC (only for B material).

First of all, aggregates were prepared from A, B or mix of both materials. They were ready to use after crushing in a jaw crusher and sieving below 4,75mm (according to the size of moulds).

To prepare binders, powders were collected from A and B materials after crushing and then milled and sieved below 250µm. Different conditions of milling and sieving were performed with no relevance to the optimisation of results.

A thermal treatment for 2 hours at 750ºC (from room temperature) was applied to material B to increase its reactivity for alkaline activation by dismantling its crystalline structure and increasing the amount of amorphous phases. The thermal history of ceramic products (A) favours the direct use without that treatment.

Specific weight of materials determined according to LNEC E64 – 1979 specification, was 2700 kg/m^3 for A and 2725 kg/m^3 for B, water was used for the determination with picnometer.

Sludge from water treatment plant, named herein L, was used as supplementary alumina source to binder A in accordance with Portuguese patent nº 104535 from 2009 [11], after being submitted to a thermal treatment of 2 hours at 750ºC and sieved below 250µm. After that the new material was named binder AL.

Binder ALB (after AL and B) was obtained by mixing 50% of each AL and B binders. That ratio was tested comparatively with different proportions (75/25 and 25/75). That ratio was chosen because the others didn't revealed advantages on mechanical strength.

Homogenization of the mixture of binders and additives was performed in ball mill for 1 hour to get the final binders AL and ALB (already with additive). Binder B, with no additive, was ready to use after manual homogenization.

The chemical compositions and loss of ignition of materials before and after preparation were determined by X-Ray fluorescence on Siemens SRS3000 equipment and presented in table 2.

Table 2: Chemical composition and loss of ignition of materials by XRF

Type	SiO_2	Al_2O_3	CaO	Fe_2O_3	K_2O	MgO	TiO_2	Na_2O	LOI
A	66,37	21,62	3,13	2,56	2,96	0,78	0,61	0,64	0,82
L	29,98	49,17	0,56	6,16	1,44	0,56	0,16	0,21	10,24
AL	52,76	31,92	2,57	4,78	2,31	0,69	0,46	0,46	3,16
B	41,88	1,74	34,18	0,41	0,45	0,29	0,02	0	20,39
ALB	47,21	16,77	18,66	2,46	1,37	0,49	0,23	0,14	11,98

Activator. Alkaline activator was obtained by mixing 1 part of sodium hydroxide solution (at 15 molal to binder AL and ALB and 12,5 molal to binder B) and 2 parts of sodium silicate solution (commercial brand Solvay D40), and was left to cool to ambient temperature before use. Solutions of sodium hydroxide were prepared from dissolution of pearls of NaOH with 99% of purity and then were left to cool to room temperature before mixing with sodium silicate.

Previous work to get the most appropriate activator was performed with sodium hydroxide in different concentrations and in different proportions with sodium silicate for each binder.

Compositions. Better compositions achieved for each category (ceramics waste, concrete waste and mixture of concrete and ceramics wastes) were performed according the information on table 3.

Table 3: Characteristics of optimal compositions achieved with CDW

Code	Materials	Binders (with additives)	Aggregates	Ratio*
17 01 02 and 17 01 03	A	0,7A+0,3L	2A	0,8
17 01 01	B	1B	2B	0,6
17 01 07	AB	0,35A + 0,5B+0,15L	1A+1B	0,7

* Activator/Binder

To evaluate and select the optimal compositions the influence of the following parameters was considered:

- Workability of pastes
- Needs of liquid phase (expressed on activator/binder ratio)
- Setting process
- Strength results

Mixing Process. The mixing order used to prepare the specimens was always the same. It began with activator followed by binder and finally the aggregate's incorporation occurred. The performed mixing order is accepted as the optimum for some authors [12, 13].

After the mixing process, the paste was conformed in 3 steel prismatic moulds of 4x4x16cm^3 and compacted on a vibration table. Samples were cured at 65ºC for 48 hours at 98% relative humidity. Thermal curing occurred at climatic chamber WEISS WK11340/40.

Mechanical strength. Mechanical strength tests were performed according to EN196-1:2006 in a Form-Test model Mega 10-250-15D hydraulic press equipment. Flexural strength was determined with centre point loading as is shown in figure 1 a) and b).

Fig.º1: a) and b) to flexural strength and c) to compressive strength tests

Durability. Experiments to evaluate durability of new materials, in this case resistance to acid attack, were performed, being the specimens subjected to mechanical tests after that. OPC mortar specimens were prepared and subjected to the same conditions to allow comparison of results.

The specimens tested, 3 for each material, A, AL and ALB (and OPC), were immersed on acid solutions for 30 days. Hydrochloric, nitric and sulphuric acid solutions at 5% (w/w), were prepared. The 3 specimens of each material were immersed in a volume of 3 litres of acid solution. Different containers were used for the AL, B, ALB and OPC probes. After that the specimens were left immersed for 30 days at room temperature. Finally they were dried at 40ºC until constant weight and subjected to compressive and flexural strength tests.

Results and discussion

Results achieved with waste materials are showed in comparison with OPC.

Mechanical results obtained after curing process (I) are very satisfactory for AL and ALB materials with 43,8MPa and 42,9 MPa and quite satisfactory for B material 20,6 MPa as is shown in figure 2.

The compressive resistance of AL and ALB still increased after cure. After 28 days (A28) materials AL and ALB reached respectively 50,4MPa and 52,6MPa, while B material shows a slight decreasing to 17,9MPa. The probes made with OPC got 40,6 MPa at 28 days.

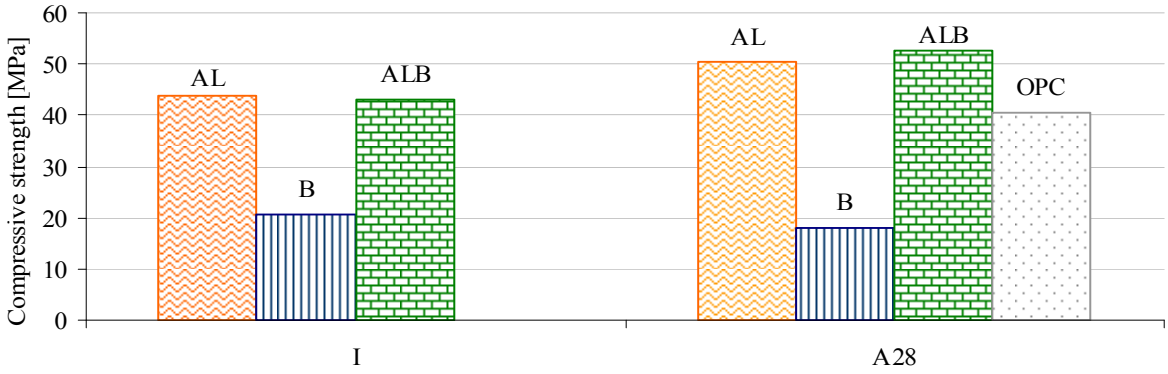

Fig.º2: Compressive strength of materials after curing process (I) and 28days later (A28)

Flexural strength results are showed in figure 3 and it is possible to observe a comparable behaviour to compressive results above announced, with a slightly change on AL and ALB positions.

AL and ALB got initially (I) flexural resistance of 6,7MPa and 6,6 MPa that increase after 28 days significantly to AL that reach 8,3 MPa, while ALB have similar resistance (6,6MPa). Material B shows a modest flexural resistance of 4,1MPa after curing (I) that decrease to 2,1 MPa 28 days later. OPC mortar shows 6 MPa of flexural strength after 28 days of curing.

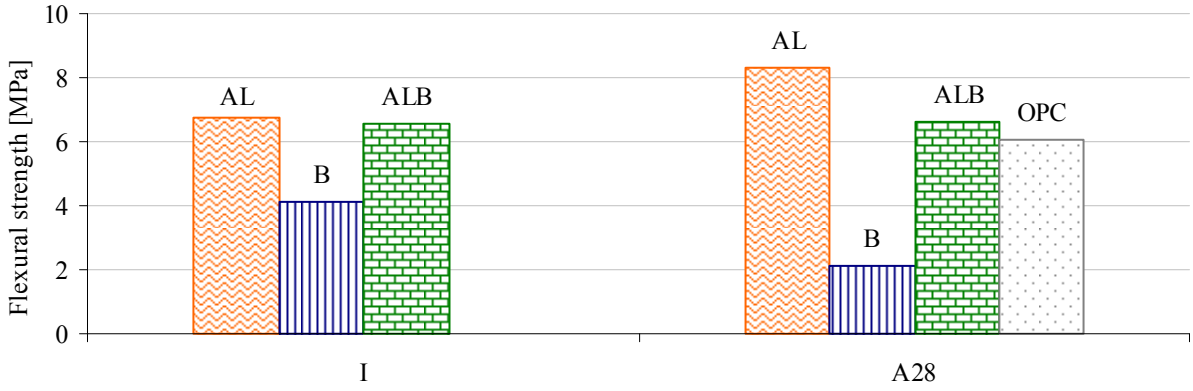

Fig.º3: Flexural strength of materials after curing process (I) and 28days later (A28)

Better mechanical performance is presented for AL and ALB material when compared with OPC mortar. Material B presents a mechanical performance lower than all of OPC, AL or ALB materials.

In figures 4 and 5 are represented the compressive and flexural resistance reached by AL, B, ALB an OPC after immersion on HCl, H_2SO_4 and HNO_3 solutions in comparison with reference results (control) above presented.

In general it is observed that immersion on acid solutions affects negatively the mechanical resistance of materials. AL is the exception once that presents a positive reaction to acid immersion with gain of compressive resistance in all acids.

It is remarkable that after nitric acid immersion compressive strength of AL increases almost 10MPa, reaching 52MPa, while in flexural got the biggest value of the study, 7,3MPa.

Similar behaviour for all acid solutions was observed for B material with final compressive resistances around 17,5MPa and flexural between 1,4MPa and 1,7MPa. Nevertheless, it should be

noted that if results for B after acid immersion are compared with those obtained at 28 days after curing, B material is not significantly affected by acid attack.

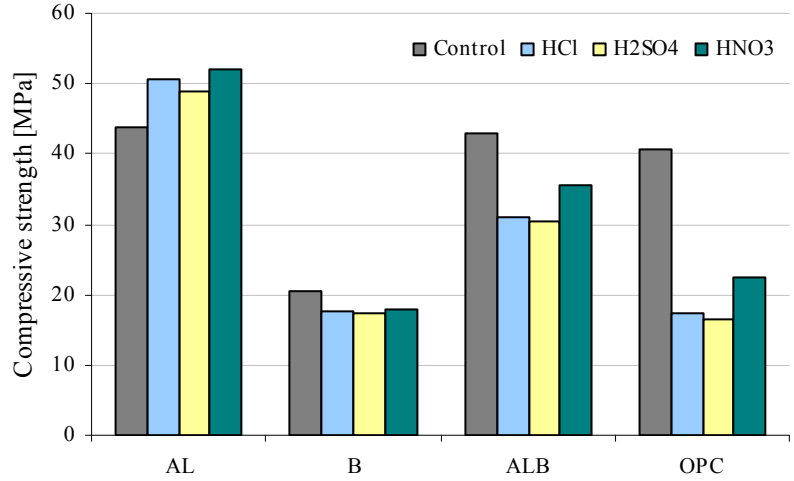

Fig.º4: Compressive strength of materials after acid attack

Material ALB presents a compressive strength between 30,3MPa to sulphuric acid and 35,6MPa to nitric acid. Flexural resistance, around 4,7MPa was achieved for ALB to all acids results.

Mechanical results achieved between 16,5MPa and 22,4MPa to compressive strength and between 2,9MPa and 3,4MPa to flexural strength after acid immersion means that *OPC reached the worst performance of the study* compared with the new materials AL, ALB and B (exception made to flexural resistance of B).

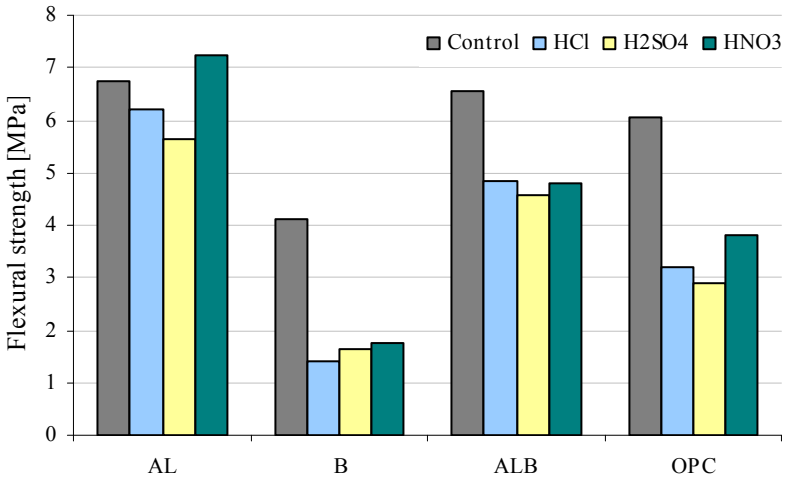

Fig.º5: Flexural strength of materials after acid attack

In figure 6 and 7 are shown for all materials the percentages of compressive and flexural resistance that remains after acid attack in comparison with the reference results for each one.

For all materials better results were achieved on nitric acid in comparison to hydrochloric and sulphuric acid solutions, while the worst performance was reached on sulphuric acid attack.

Material AL (made from ceramic waste) achieved better results for compressive strength after immersion on acid solutions (nitric, sulphuric and hydrochloric). This is supported by *an increasing of resistance of more than 10% to all acids and of almost 20% to nitric acid results when compared with reference,* as is shown on figure 6.

Hydrochloric and sulphuric acids affects in a similar way ALB, with around 28% of loss, while nitric acid cause 17 % of loss on compressive strength, corresponding to a final 35,6 MPa of resistance achieved for ALB as can be analysed in figure 6.

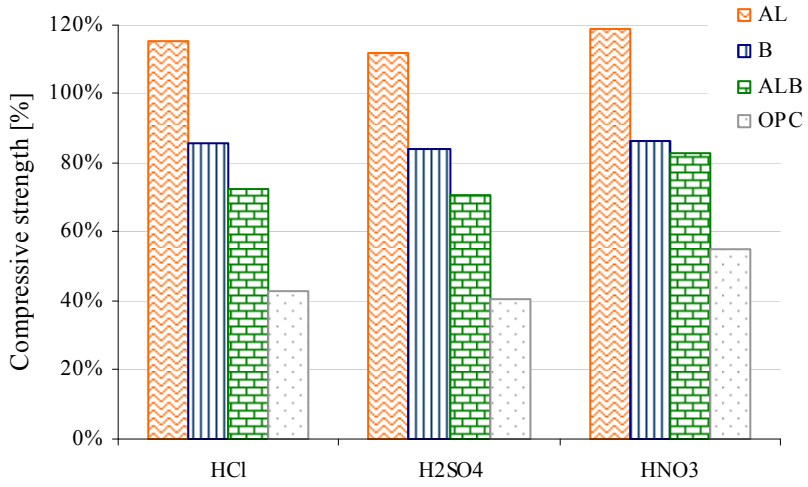

Fig.º6: Remaining compressive strength of AL, B and ALB and OPC after acid attack

Results for ALB shows a decrease on flexural performance to 70% of the initial with respect to sulphuric acid, while nitric and hydrochloric acids shows a loss that led to 74% of the initial which corresponds to a remaining 4,8MPa.

For B material the loss is about 15% on compressive strength and about 60 % on flexural strength which means that it is the highest differential on compressive/flexural performance on studied materials.

In general results to OPC indicate that the loss of strength is about 50% or more which is very significant. In nitric acid, the better one, remaining resistance to OPC is 55 % to compressive and 57% to flexural one, while in sulphuric acid the remaining flexural resistance is 48% and compressive is 41%.

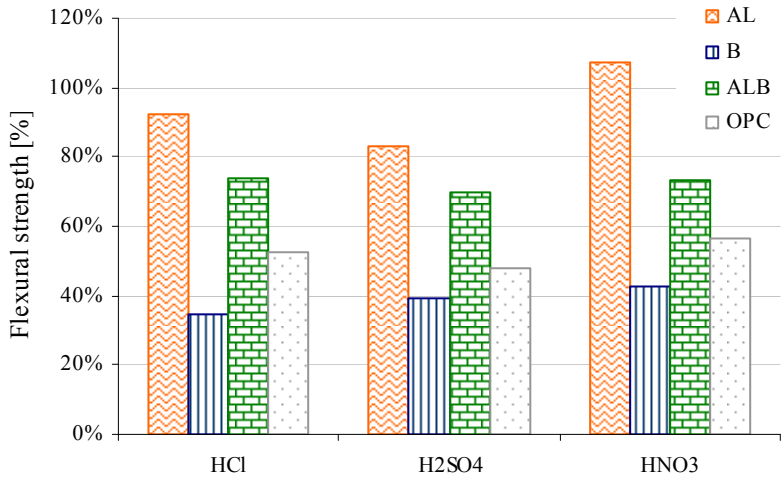

Fig.º7: Remaining flexural strength of AL, B and ALB and OPC after acid attack

Conclusions

Results achieved with AL, B and ALB binders indicate that real applications as building materials for demanding mechanical strength performance with construction and demolition waste should be more investigated. This is demonstrated by compressive resistances around 44 MPa for AL, 20 MPa for B and 43 MPa for ALB and by flexural resistance achieved around 6,6 MPa for AL and ALB and 4,1MPa for B.

Acid attack tests were performed to evaluate the behaviour of these new materials in aggressive conditions compared with normal ones. In this communication encouraging results are presented for acid attack that suggest that this technique can be considered as a solution for some of the problems placed by CDW, once that results achieved indicate higher durability to AL and ALB when compared to OPC.

All results in this research indicate that AL and ALB materials (made from waste), have a better performance than OPC mortar, while B material is not so satisfactory.

It is possible to conclude that alkaline activation of CDW is emerging also as an environmentally friendly technique of waste management with potential for wide-scale utilization in the construction industry.

References

[1] Symonds Group: *Construction and demolition waste, management practices and their economic impacts*, Report to DGXI – European Commission, (1999) 203p.

[2] European Environment Agency: Environment *Signals 2001 (Chapter Waste), Environmental Assessment Report Nº 8* (2001), p 99-104.

[3] P. Duxson, A. Fernández-Giménez ,J.L. Provis, G.C. Lukey , A. Palomo, J.SJ. van Deventer. Journal of Materials Science 42 (2007), p.2917-2933.

[4] J.W. Phair. Green Chemistry, Vol. 8 (2006), p. 763-780.

[5] P. Duxson, J.L: Provis, G.C. Lukey, J.S.J. van Deventer. Cement and Concrete Research Vol. 37 (2007) p. 1590-1597.

[6] A. Teixeira Pinto: *Novos sistemas ligantes obtidos por activação alcalina" in* Construção Magazine, nº 3, (2002).

[7] K. Komnitsas, D. Zaharaki. Minerals Engineering Vol. 20 (2007), p. 1261-1277.

[8] H. Xu, J.S.J. van Deventer. Minerals Engineering, Vol. 15, (2002), p.1131-1139.

[9] F. Pacheco-Torgal, J. Castro-Gomes, S. Jalali, Construction and Building Materials,Vol. 22, (2008), p. 1201-1211

[10] J. Rapazote, C. Laginhas, A Teixeira Pinto: *A Reciclagem da fracção inerte de RCD pelo processo de activação alcalina*, in 5ºCLME proceedings, Mozambique (2008), ref. 23A005.

[11] A. Teixeira-Pinto and P.Tavares. Portuguese Patent N.º 104535 (2009).

[12] F. Pacheco-Torgal, J. Castro-Gomes, S. Jalali. Construction and Building Materials, Vol. 22, (2008), p. 1315-1322.

[13] A. Teixeira Pinto, P. Fernandes, S. Jalali, Geopolymer Conference proceedings, Melbourne, Austrália (2002).

doi:10.4028/www.scientific.net/AST.69.164

Repairing of Damaged Stone in Monuments and Stone Buildings

Amândio Teixeira Pinto
Departamento de Engenharias
Escola de Ciências e Tecnologia
Universidade de Trás-os-Montes e Alto Douro
Quinta de Prados, 5001-801 Vila Real, Portugal
yrache@utad.pt

Keywords: Stone monuments; preservation; alkaline activation

Abstract - The main causes of rock degradation in stone buildings are discussed and the current methods of recovering damaged stones are summarized.
The Alkaline Activation seems to present a great potential to deal with particular cases of damaged stones resulting mainly from fracture incidents provoked by physical actions, where the global substitution of the stone itself is not considered.
A practical case of recovering granite on the windows frames of a beautiful chalet to be intended for the Municipal Archives at Vila Real is described, in what is considered to be the first experiment of this technique in recovering building stone.

Rocks and Main Causes of Their Degradation

Natural rocks are mono or polyphasic chemical systems, mainly composed by minerals that are in thermodynamic balance under specific conditions of temperature and pressure.

Considering their path one can find basically two types of systems: (a) endogenous systems, which develop below the terrestrial crust therefore out of action of free water and oxygen but under high temperatures (800 to 1200ºC) and pressures of several thousands of bares, and (b) exogenous systems, which are hydrated and oxygenated under normal atmospheric pressure and average temperatures of 20 to 25ºC.

By obvious reasons, rocks that Man normally uses in his accomplishments belong almost exclusively to the second system, those of the exogenous rocks, which present themselves well combined with oxygen at different steps of hydration.

It is interesting to notice that approximately half of the terrestrial crust weight is formed by oxygen and by the103 chemical elements of the Periodic Table. Of those, only 8 occur in significant quantities, representing 98.6% of the Crust. Table 1gives an idea of the partition of the principal constituents of the average 60 km thick surface layer of the planet.

Table 1. Main elements and minerals in the Terrestrial Crust

A			B	
Elements	% in weight	% in volume	Minerals	% in volume
Oxygen	46.60	92.0	Plagioclase	39
Silicon	27.72	0.8	Alkal. Feldspar	12
Aluminium	8.13	0.8	Quartz	12
Iron	5.00	0.7	Pyroxene	11
Calcium	3.63	1.4	Mica	5
Sodium	2.83	1.6	Amphiboles	5
Potassium	2.59	2.1	Olivine	3
Magnesium	2.09	0.6	Clayey Minerals	4.6

While the first three columns indicate data relative to the 8 main elements present on the Crust, the next two refer to the most abundant minerals. From these one can see that Plagioclase and Alkaline Feldspar (both belonging to the great group of Feldspars) represent in terms of volume more than half of the solid inorganic material of the first 60 km of the Earth. It is possible to conclude that all 8 categories of minerals belong to the silicate group, which accounts for 91.5% of the total volume [1].

Consequently it is easy to understand that the degradation processes affecting the majority of the rocks as time elapses, are associated with the modifications that the former minerals experiment under different conditions. These modifications are the result of chemical arrangements towards stability of the chemical elements that form them.

Basically, rocks can experiment modifications by a chemical reason or suffer alterations due to a physical cause. In the majority of cases rock stability is synergically affected by both situations. In fact, in many circumstances, there is a cyclic association of both factors, one acting as a catalyser of the other. It is the case of water freezing inside porous rocks, that develops a very strong stress gradient responsible for local ruptures that exposes the inside and sound part of the stones to the action of aggressive agents. It is expected that the degradation process speed up from that point on [2].

Sometimes, degradation occurs directly, or by an inductive form, from Man's action, when the stone is being submitted to conditions not in accordance with its real capacities. For example, the introduction of bolts or iron connectors, inside the stone, for fixing window frames that later experiment a significant increase in volume when becoming rusty. This old used process can install in the stone a level of tensions that easily overcomes the rupture state. These phenomena can also be developed with wooden connectors for the same purpose, during changes from the dry to the wet season. Both systems are quite common in old buildings or monuments.

Chemical actions, by their turn, can sometimes associate several types of situations, not only related with the normal degradation of the rock itself as a consequence of meteoric agents (mainly the rain water), but also due to the accumulation of dust and sediments of chemical nature as smoke particles or combustion gases from motor vehicles [1]. With time, some thick layers are formed where aggressive agents are in high concentrations. Fig. 1 documents a well-known case of deposits encrusted over the limestone of the Cathedral of Lisbon. The same picture shows also several zones of physical rupture, all along the edges and mainly on the right side of the lower frieze.

Also, it must be mentioned one of the most active factors of degenerative action on stones, the biological colonisation promoted by fungi, lichens and mosses. Faecal residues from pigeons, seagulls and other birds create acid environments, very aggressive, that jeopardize in a significant way the chemical stability of rocks.

Fig. 1 – Patina over limestone (Cathedral of Lisbon)

Generally speaking, the effects of the three principal types of decay: - chemical, physical and biological, mutually add, converge and reinforce themselves. Chemical phenomena may have physical effects, a physical transformation can develop chemical reactions and biological actions can rebound in chemical and physical modifications.

Repairing Approaches and Remedies

It is easily understood that within the frame of the possible interventions to solve stone degradation problems there is not a unique solution. Some of the known solutions (brushing, water pressure spraying, chemical cleaning and others) can cover a couple of aspects, while others are posing specific problems of rock integrity [1]. However, almost all of them may involve a prejudicial and deleterious effect on the stone itself, which must be considered and evaluated in advance. Therefore cautiousness and parsimony must be used in their application.

In a general sense, preservation solutions have the objective of impeding the evolution of certain degrading phenomena, but unfortunately their range of application is scarce and limited. The degradation state of the stone is sometimes so advanced that there is no support, at all, for stabilization procedures. And, as reversibility is impossible in practice, a great part of recovering solutions may involve the definitive removal and substitution of important parts of the stone itself.

As a consequence of the use of classical approaches for cleaning (application of abrasive agents, brushing or using of chemicals), more and more layers (no matter as thin they could be) of rock material are being removed, considering the fact that the natural binder that keeps the rock integrity is continuously weakening [2].
This type of solutions is time limited in its application, so big is the risk of vanishing the global sense of the structure where the stone is included.

By all appointed reasons, the only solutions that seem to be practicable not only in the frame of maintenance of architectonic forms and draft, but also in terms of the structural function affected to the stone blocks, are those that foresee the substitution of degradated stones. This type of intervention, sometimes seen as the only procedure of preserving indefinitely an architectonic patrimony, demands by one side the need to create and develop centres or schools where the art of carving stones can be studied and promoted, but also enhances the need for techniques that do not necessarily involve the substitution of damaged stones. As a matter of fact there are some problems where the degradation is quite limited or the substitution of the stone is so costly or implicates such degree of difficulties (in terms of structural sustainment, for example) that is not economically feasible to remove the stone and place a new one, unless the overall integrity of the building is threaten.

In this context, the Alkaline Activation technique can be a solution of great interest for the rebuilding and restoration of damaged stones in monuments, buildings and bridges.

The Alkaline Activation and the Repairing of Natural Stones

It is now well known that the Alkaline Activation is a chemical reaction that is processed in strong alkaline environment among the several oxides that are present in different alumino-silicates [3]. Taking granite as an example, we can summarize [4] the chemical phenomena that explain the alterations of feldspars (other granite components, as quartz and muscovite, do not suffer chemical degradation):

- progressive hydration of the aluminium environment
- subsequent modification of the coordination number of aluminium with oxygen (from 4 to 6)
- lixiviation of alkaline metals (sodium and potassium)
- reduction of silicic acid levels
- transformation of matrix structure (from 3D into 2D-clay particles)

This way the granitic rock is transformed into clay (the phenomenon is called kaolinization). The alkaline activation uses exactly the opposite processes enabling the reversibility of the chemical transformations experienced so far by the rock:

- previous dehydration of clay (by calcination)
- therefore modification of the coordination number from 6 to 4
- enrichment of sodium or potassium levels
- increase of the silicic acid level
- transformation of matrix structure (from 2D into 3D)

The dehydration treatment of clay (kaolin is the most used type of clay) is made in a furnace at 750ºC, giving place, as a consequence, to an amorphous material called *metakaolin* (MK). Due to calcination, this material is almost an amorphous product, presenting, therefore, a great potential for chemical combination [4].

Therefore a powder material like metakaolin can be transformed in very short time under alkaline conditions in solid and sound material hard and resistant to mechanical action. In fact its strength can be superior to that developed in hydraulic binding systems like ordinary Portland cement [5].

When properly mixed with a selected set of aggregates (mostly fine graded material) to obtain a certain pattern of texture, it is possible to restore granite, limestone, basalt and other types of

rocks. In such case, this cementitious system is well adapted to the repairing of stone damages whenever a substitution is not advisable or possible. Much work has been made by the majority of researchers in this field that put in evidence the main characteristics of this type of materials: - they present high mechanical capacity to withstand charges and crashes, high resistance to weathering conditions, repeated cycles of heat and humidity, freeze and thawing, low retraction and chemical stability.

Therefore, given that the main natural components of rocks are used, all conditions seem to be present to obtain a good and permanent solution for hazards in stone constructions.

Application Cases

The new Municipal Archive of the city of Vila Real, in Northern Portugal, is installed in a reformed building, from the XIX century, situated near by the main Railway Station. As it is common in Portuguese traditional architecture for this type of building, several parts are made in plain granite, in particular the windows and doors frames, the friezes and the floor-bases of balconies.

Due to the application of iron bolts to fix the windows and their consequent oxidation there were damages that have induced the rupture of the majority of the stone frames (Fig. 2).

Fig. 2 – Physical Rupture

The project team responsible for the building restoration decided to promote the replacement of a great number of frame stones, accepting anyway the possibility of restoring some of the remaining by the alkaline activation technique, which had been presented in a public conference at the University of Trás-os-Montes e Alto Douro.

Operative Conditions

Some granite from the replaced stone elements was selected for preparing an extended granulometry (0/9.5mm) to be used as aggregates. In sequence some experiments were made in laboratory (using two different colours of Metakaolin), to approach the true colour of natural stone (Fig.3).

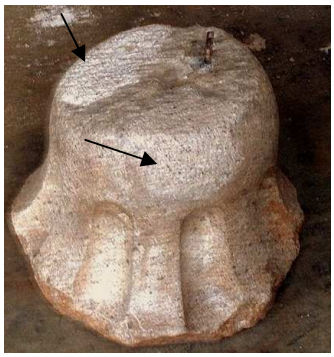

Fig. 3 – Colour Tests

Arrows on Fig.3 mark two different zones of testing. In both cases a hole (10 cm deep) was previously excavated on the stone for developing a close connection between both phases. The composition of the stone concrete that was used is mentioned on Table 2.

Table 2. Composition of Stone Concrete

Metakaolin Metamax	Metakaolin Mibal	Aggregates	Alkaline Activator
100 gr (80%)	25 gr (20%)	504 gr	170 gr

MK Metamax is a commercial metakaolin white colored and MK Mibal (which is pink in color) is prepared in laboratory from a Portuguese kaolin.

The alkaline activator was a mixture in weight of 1 part of sodium silicate (D-40 commercial type) for 2 parts of sodium hydroxide 15 molal of concentration. Mechanical strength at 7 days of age in compression and flexural tension indicates average values well above 50 MPa and 6.50 MPa respectively, on 4x4x16 cm^3 samples. Results are mentioned on Table 3.

Table 3. Mechanical Strength of Stone Concrete

Sample	Age	Compression [MPa]	Flexural Traction [MPa]
1	7 days	54.2	6.52
2	7 days	57.1	7.18
3	7 days	52.9	6.83

The adhesion between natural rock and the reagglomerated (**) rock was also determined, using stone samples of the same size (4x4x16 cm^3), that after being mechanically tested were restored with a reagglomerated micro-concrete and cured. Probes were tested at 7 and 14 days and results are displayed in Table 4 together with the mechanical strength of the stone original samples.

Table 4. Flexural Strength of Joint (adhesive bonding)

Flexural Strength of Stone Probes [MPa]	Age	Flexural Strength of Mixed Probes [MPa]
5.83	7 days	2.86
5.83	14 days	5.72

At 7 days, the mixed sample has broken by the joint between the different phases, but after 14 days the result was more than expected, as the probe has broken by the stone as it is clearly shown in Fig.4. This has a major importance in terms of the common behaviour of natural and reagglomerated rock.

Fig. 4 – Adhesion between phases

Porosity and permeability tests were also performed to verify if any difference in these aspects could jeopardize the desirable performance of the restored stone (table 5). The small difference between the two kinds of materials is partially explained by the zeolitic microstructure of the reagglomerated stone which is commonly reckoned to this type of products.

Table 5. Permeability and Porosity of Stone Concrete

Permeability [m/s]		Porosity [%]	
Natural Stone	Reagglom. Stone	Natural Stone	Reagglom. Stone
3.81E-09	2.05E-08	7.30	9.01

It is of great importance to know the size of pores and their distribution in order to anticipate the joint behaviour of the two phases, mainly considering that, for obvious reason, the reagglomerated stone is normally covering the natural stone. For natural stone, humidity changes and contacts with the aggressive external agents are now performed trough the new placed material.

Application of SAXS technique has been under development, because other common methods have indicated disperse and no reliable results. Whatsoever, the author believes that the

(**) – The terminology proposed by Davidovits[5] is herein used.

difference in porosity is not large enough to imply any major concern on the common performance.

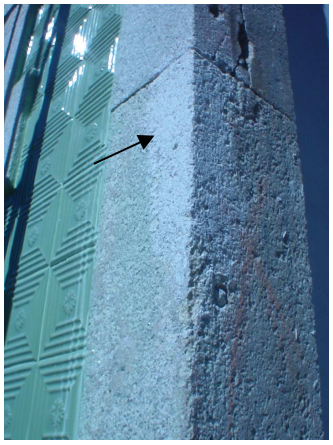

Fig. 5 – Final result

Fig. 6 – Final Result

Final results are shown in Figs. 5 and 6 which present an acceptable aspect.

Another example of reconstruct stones was performed in one of the University's building, 5 years ago (Fig. 7). It must be said that this test was performed using regular concrete technology. The paste was prepared in a small concrete batching plant using normal granite aggregates. Conventional wooden formwork was used and the paste was poured with a small vibrator.

To obtain a good connection between the two phases (natural stone and paste), the stone surface was previously (20 minutes before) painted with the alkaline activator using a simple brush. After one day the paste hardened but the forms were removed only seven days later. No particular cure process has been used, to give all chances for the formation or appearance of cracks or fissures. When the forms were removed, there were no visual signs of any cracks, particularly all along the joint between the two materials. The photo of Fig. 7 was taken after a surface treating, using a pick tool in order to have a similar carved surface as the existing stones.

Fig. 7 – Wedge Repairing

After 5 years**,** some samples were obtained and tested. Its mechanical strength, in terms of compression has increased about 11% over the previous value, but in flexo-traction the increase was a little more than 40%, showing behind any doubt the development of chemical adhesion between both phases. One important aspect of this example is the appearance of the joint between natural and reagglomerated rock (arrows on Figs. 8&9). No trace of retraction is seen, and even in SEM examination (20X magnification) the joint seems closed and well done (Fig.10).

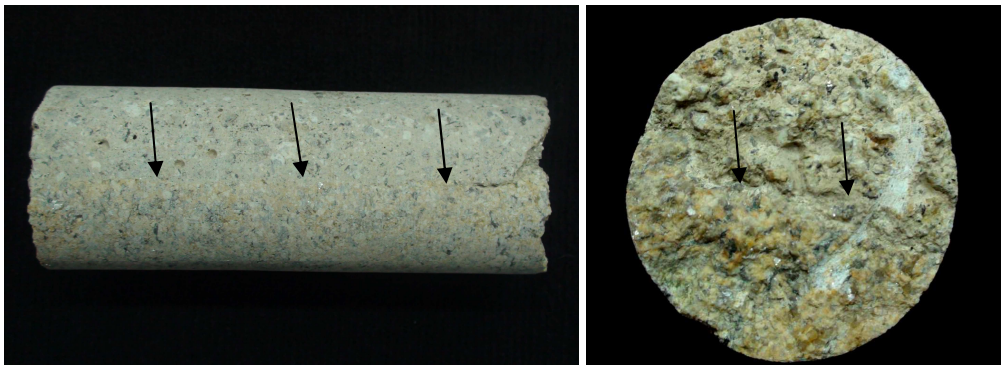

Figs. 8 and 9 – Sample (above reagglomerated rock, below natural stone)

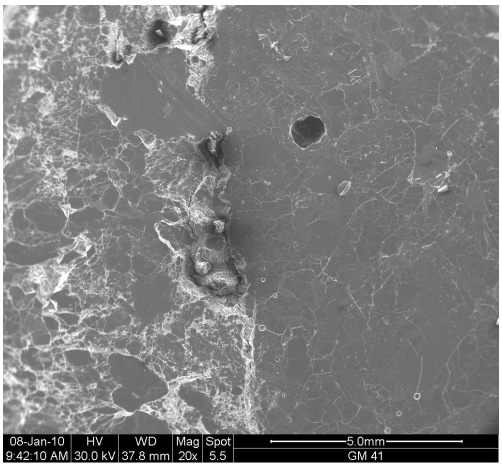

Fig.10 – EDS micrograph of joint
(left natural stone, right reagglomerated rock)

The differences are clearly seen, the reagglomerated stone matrix is much more regular, due to the amorphous character of the paste (besides the presence of aggregate elements), and the presence of air bubbles (very difficult to avoid) is one of the marks of this sort of products.

Being important to determine the behaviour of the reagglomerated stone what would be, we previously made some test, about permeability, porosity and the quality of joint in mechanical terms.

Final Results and Conclusions

Figs. 8 and 9 are self-explanatory, showing the zone of the joint between both phases. It is evident that no cracks or other characteristic sign of the joint are detected. The connection between natural and reagglomerated stone is almost perfect.

After finishing the repaired stones (arrows on Figs.5 and 6) show an acceptable integration, considering the fact that to restore the effects of Time it is not possible. It is nevertheless expected that as time elapses a natural weathering of the surface will approach the aspect of the remaining stone.

Therefore the Alkaline Activation technique seems to present a great potential for the maintenance and repairing of stone buildings and monuments, presenting a good, natural and integrated solution to solve some specific problems.

To finalize

Certainly we have to consider the philosophical aspects and concepts established as guidelines for monuments and building restoration, by the Letters of Athens (1931) Venecia (1964), Krakov (2000) and others. It is not my intention to discuss those principles. I cite here John Ruskin(1819-1900): "*Restoration is the most complete destruction than a building can suffer*" and I only leave a thought: - what could be the future of our monuments and cultural objects (paintings, books, and so on) if we just keep them follow the natural degradation and weathering as time goes on?

This is a technique, not a philosophy. I'm not trying to impose it or to justify it. It can be freely used or not as other available solutions for the same problem.

References

[1] Aires-Barros, L. – "As Rochas dos Monumentos Portugueses – Tipologias e Patologias", Instituto Português do Património Arquitectónico (IPPAR), Vol.1, Lisboa, 2001.
[2] Castro, E. – "Tratamentos de Conservação de Pedras em Monumentos", ICT Informação Técnica, Geotecnia, LNEC – Lisboa, 1994
[3] Davidovits, J. – " Geopolymers: Inorganic Polymeric New Materials", Journal of Thermal Analysis, Vol.37 (1991).
[4] Teixeira-Pinto, A. – "Sistemas Ligantes Obtidos por Activação Alcalina dos Metacaulinos", PhD Thesis, Universidade do Minho (2004)
[5] Davidovits, J. – "Chemistry of Geopolymeric Systems. Terminology", Proceedings of the Second International Conference Géopolymère '99, pp 9-40 (1999)
Davidovits, J. – "Ils Ont Bâti les Pyramides", Ed. SELD/Jean-Cyrille Godefroy, Paris, 2002.

doi:10.4028/www.scientific.net/AST.69.174

Geopolymers as waste encapsulation materials: impact of anions on the materials properties.

FRIZON Fabien[1, a], DESBATS-LE CHEQUER Charlène[1, b]

[1] Atomic Energy and Alternative Energy Commission, DEN, Marcoule, Waste Treatment and Conditioning Research Department, F-30207, Bagnols-sur-Cèze, France.

[a]fabien.frizon@cea.fr, [b]charlène.desbats@cea.fr

Keywords: geopolymer, waste encapsulation, zeolite.

Abstract. One of the most promising applications of geopolymers is their use as waste encapsulating matrix. These binders are indeed compatible with aqueous waste streams and capable of activating several chemical and physical immobilization mechanisms for a wide range of inorganic waste species. Several works have investigated the immobilization of cations, mainly heavy metals or radioactive wastes, but very few studies are taking counterions, namely anions, into account. The aim of this work is to experimentally investigate the impact of anions with different valences on the materials' properties in regard to the requirements of an industrial process at ambient or slightly elevated temperature: among others setting time, maximum achievable compressive strength or resistance to leaching. The modifications caused by the introduction of monovalent and divalent anions, such as sulphate and nitrate, are also monitored in term of mineralogy, porosity and microstructure. Their immobilization seems to be related to the advancement of geopolymerization reaction. On another hand, depending on the alkali ions used in the activation solution, the anionic species considered may also enhance the precipitation of some zeolites.

Introduction

Geopolymers are a class of largely X-ray amorphous three-dimensional aluminosilicate binder materials, usually synthesized by reaction of an aluminosilicate powder with a concentrated alkali metal silicate or hydroxide solution, cured at ambient or slightly elevated temperature [1]. These low-cost binders, compatible with aqueous waste streams, were largely considered as immobilizing materials for heavy-metals or low-level radioactive wastes [2-6]. Surprisingly, despite the fact that aqueous waste streams may contain various anionic species [7], and that it is well established that some anionic species, like PO_4^{3-}, SO_4^{2-} or NO_3^- promote the formation of zeolites [8], there is very few studies dedicated to the effects of anions on the formation and evolution of geopolymer systems [9-11]. These studies focus mainly on the impact of chloride, carbonate and phosphate anions on early-age and strength properties. To the authors' knowledge, none of them consider a possible geopolymers/zeolites secondary transformation, despite the fact that starting materials and process of synthesis are close to those involved in the formation of zeolites and that the presence of zeolitic structures embedded in geopolymer matrix has been reported [12-15]. Some authors suggested that geopolymers may be viewed as amorphous analogues of zeolites [16, 17], or that, from a thermodynamic point of view, geopolymer can be considered as metastable with regard to zeolites [18].

The aim of this work is to investigate the impact of sulfate and nitrate incorporation in alkali-activated metakaolin systems on the setting time and mechanical properties of the binders. The geopolymer systems obtained are also investigated in term of geopolymers/zeolites secondary transformation, mineralogical and microstructural evolutions of the different mixtures. In this study, the chosen variables are the chemical nature of alkali used, the chemical nature and concentration of anionic species.

Experimental methods

Materials. In order to focus on a model system and avoid the precipitation of calcium silicate hydrate phases mixed with geopolymeric materials [19], the choice was made to synthesize metakaolin-based geopolymer paste. This product was purchased under the brand name of Pieri Premix MK from Grace Construction Products. The chemical composition of metakaolin determined by X-ray Fluorescence (XRF) can be found in Table 1. X-ray Diffraction (XRD) analysis showed that the metakaolin contained anatase, kaolinite and quartz as impurities. The Brunauer-Emmet-Teller (BET) surface area was 19.9 m²/g and the mean particle size (d50) determined by laser granulometry was 5.9 µm.

Table 1: Chemical composition of metakaolin used in this study

	SiO_2	Al_2O_3	CaO	Fe_2O_3	TiO_2	K_2O	Na_2O	MgO	L.o.I*
Weight %	54.4	38.4	0.10	1.27	1.6	0.62	< 0.2	< 0.2	1.90

*Loss on ignition

Alkali hydroxide activating solutions were prepared by dissolving NaOH, KOH (Prolabo, Rectapur, 98%) pellets in Milli-Q water, with all containers kept sealed to minimize contamination by atmospheric carbonation. Silica added to the mix is amorphous silica provided by Rhodia (Tixosil 331) with a mean particle size equal to 9.19 µm. Sulfate and nitrate ions were mixed in the activating solution starting from potassium nitrate, potassium sulfate, sodium nitrate or sodium sulfate pellets (Prolabo, Rectapur, 98%)

Geopolymer Synthesis and Hydrothermal Treatment. The five series of mixtures prepared are summarized in Table 2 in term of molar ratios. Each set is incorporating the same SiO_2, Al_2O_3 and M_2O content with SiO_2/Al_2O_3=3.6, Al_2O_3/M_2O=1, which is a typical composition for metakaolin geopolymers reported in the literature. The Al_2O_3/M_2O ratio was adjusted to 1 to maximize geopolymerisation reactions [20] and mechanical properties [21]. This geopolymer composition is also known to be composed of a stable amorphous phase with no tendency toward phase transformation under moderate curing temperature during six months [22]. The water content varies among the formulation mix in order to reach a good fluidity of the geopolymer immediately after casting, but stay low enough to be representative of geopolymer materials.

Table 2: Mix formulations used in this study in term of molar ratios.

Sample	Chemical nature of alkali used	SiO_2/Al_2O_3	M_2O/SiO_2	H_2O/M_2O	MOH/M_2SO_4	MOH/MNO_3
Na ref	Na	3.6	1	12	-	-
K ref	K	3.6	1	10	-	-
Na S 60	Na	3.6	1	12	60	-
Na S 30	Na	3.6	1	12	30	-
Na S 10	Na	3.6	1	12	10	-
K S 60	K	3.6	1	10	60	-
K S 30	K	3.6	1	10	30	-
K S 10	K	3.6	1	10	10	-
Na N 20	Na	3.6	1	12	-	20
Na N 6	Na	3.6	1	12	-	6
K N 20	K	3.6	1	10	-	20
K N 6	K	3.6	1	10	-	6

The mix was performed in two steps. First alkali silicate solutions were prepared by dissolving and mixing amorphous silica in alkali containing solution during 30 minutes. The alkali solutions were prepared by dissolution of appropriate pellets (alkali hydroxide, alkali sulfate or alkali nitrate) in Milli-Q water. During the second step, geopolymer samples were prepared by mixing metakaolin and alkali solution. Mixing was performed at low speed for one minute and at high speed for two minutes in a standardized laboratory mixer (European Standard EN 196-1). The material was then transferred to 4*4*16 cm PTFE mould, vibrated for few seconds and sealed from the atmosphere. Samples were cured during 1 day at 20°C and at atmospheric pressure before removal from the mold and stored in an airtight bag at room temperature and pressure during 28 day. Mechanical and leaching tests as well as hydrothermal treatment were performed on this material. The hydrothermal treatment consists in placing the samples in sealed conditions in an oven at 90°C during a period ranging from 5 to 10 days.

Analytical Methods. The setting time was measured with a Vicat needle as per European standard EN 196 3. Ultimate compressive strength measurements were conducted as per European standard EN 196 1 on samples of geopolymer paste, using a 3R testing machine.

Laboratory X-Ray powder diffraction (XRPD) patterns were recorded in a Bragg-Brentano X'Pert Pro diffractometer (PANanalytical) using copper anode $\lambda K\alpha 1 = 1.54056$ Å generated at 40 mA and 40 kV. Samples were scanned from 5° to 60° 2θ, in continuous mode. The step size was 0.017° with a time per step of 200 seconds and a scan speed of 0.01°/s.

Leaching behaviour was studied on material suspensions prepared by mixing crushed geopolymer paste samples (< 100 µm) with ultrapure water (liquid to solid ratio of 9 $mL.g^{-1}$) and stirring for 24 hours, 7 days and 28 days. In some experiments, complete solution renewal was performed at the end of these periods. Ionic concentrations were determined by ion chromatography on a Dionex DX 500.

Results and Discussion

Setting Time. The impact of the chemical nature of alkali used and of the chemical nature and concentration of anionic species on setting time are summarized in Table 3.

Table 3: Setting time measurements conducted on Vicat apparatus as function of anions and alkali used for geopolymer synthesis.

Sample	Na ref	K ref	Na S 60	Na S 30	Na S 10	K S 60	K S 30	K S 10	Na N 20	Na N 6	K N 20	K N 6
Setting time [h]	3h12	12h30	3h03	3h05	3h48	7h14	5h58	6h57	4h19	5h24	5h23	5h52

The results clearly show that the setting time of a geopolymer material is dependent on the alkali used for its synthesis. For each given activation solution composition, the greater the basicity of the alkali hydroxide, the slower the setting. This point is in agreement with previous works, [5] for example.

The impact of anionic species varies with the alkali considered:

- If sulphate ions seem to have almost no impact on sodium-based geopolymers, the setting time of potassium-based geopolymers is reduced by 5 to 6 hours. No clear effect of sulphate concentration is noted.
- In the case of sodium-based geopolymer, nitrate ions act as retarders, the higher the concentration, the slower the setting. Introduced in potassium-based geopolymers, nitrates accelerate the setting, with few variations induced by their concentration.

As previously noted [10], increasing solution ionic strength thought inorganic salts, which is known to enhance or exert no influence on dissolution of aluminosilicates, should be expected to accelerate or have no effect on the geopolymeric gel formation, i.e. setting time. This is not the case here and the solidification process is not controlled only by the kinetics of the mineral dissolution. As

sodium-based geopolymer seem to be less disturb by the presence of anionic species than potassium-based geopolymer, the structure making ability of smaller cations in comparison to larger ones [23] should also be taken into account.

Mechanical properties. The ultimate compressive strengths of the five series of geopolymers prepared are summarized in Table 4.

Table 4. Ultimate compressive strength of geopolymers after 7 and 28 days of curing.

Sample		Na ref	K ref	Na S 60	Na S 30	Na S 10	K S 60	K S 30	K S 10	Na N 20	Na N 6	K N 20	K N 6
Ultimate compressive strength [Mpa]	7 days	24.5	28	25.3	23.2	24.4	28.9	26.2	22.9	31	22	21.6	24.2
	28 days	24.4	31.4	23.3	26	30.7	43.2	36	31.5	32.1	27	33.2	32.1

The results highlight several points. First, whatever the anions considered, the potassium-based geopolymers present better mechanical properties than those sodium-based and these properties increase with time. Second, the introduction of anions in activating solutions leads to an increase of the compressive strength of the geopolymers in comparison to the reference materials. For sulphate ions in sodium-based geopolymers, the higher the amount the stronger the material; behaviour in potassium-based geopolymers is the exact opposite. For nitrate ions in sodium based geopolymers, mechanical properties decrease with increasing concentration.

Leaching Experiments. The results of the leaching experiments are presented in Table 5 in terms of percentage of initial species introduced during the geopolymer synthesis.

Table 5. Leaching results on geopolymers after curing for 28 days.

Sample	Anions leached [%]		Cations leached [%]	
	SO_4^{2-}	NO_3^-	Na^+	K^+
Na ref	-	-	3.27	-
K ref	-	-	-	1.85
Na S 30	13	-	4.2	-
Na S 10	14.9	-	6	-
K S 30	14.4	-	-	2.2
K S 10	14.3	-	-	4.3
Na N 20	-	14.7	4.1	-
Na N 6	-	13.7	5.5	-
K N 20	-	12.8	-	2.2
K N 6	-	12.6	-	3.7

At these concentrations, the introduction of anions in activating solutions leads to an increase in alkali leaching, the higher the amount of anions added, the higher the leaching. This means that alkalis ions are less incorporated in the material in presence of anions species. This could be linked to a modification in the step of raw materials dissolution or in the step of gel solidification process. Furthermore, the amount of anions released during this experiment is quite stable around 14.1% for sulphate ions for both alkali, and a little less for nitrate ions 14.2% and 12.7% for sodium and potassium respectively.

Geopolymers/Zeolites Secondary Transformation. From a thermodynamic point of view, geopolymers can be considered as metastable with regard to zeolites [18]. Initial mix formulation and curing conditions are of primary importance for the chemistry and nature of final products as well as for the transformation of geopolymers into crystalline materials [24]. Although high temperatures (>100°C) and pressures it is usual that the medium-term phase stability of geopolymer systems is studied at moderated temperature [22, 25].

Table 6. Zeolites obtained from geopolymer samples under hydrothermal treatment at 90°C in sealed conditions and identified by XRD experiments.

Sample	Zeolites obtained at 90°C	
	After 5 days	After 10 days
Na ref	none	none
K ref	none	none
Na S 60	X-Y	X-Y-Gmelinite
Na S 30	X-Y-Gmelinite-Herschelite	X-Y-Gmelinite-Herschelite-Dachiardite
Na S 10	X-Y	X-Y
K S 30	none	none
K S 10	none	none
Na N 20	X-Y	X-Y
K N 20	W-Chabazite-Phillipsite	W-Chabazite-Phillipsite
K N 6	W	W

In agreement with previous findings, metakaolin systems with SiO_2/Al_2O_3 molar ratios of around 3.6 (with Na_2O/Al_2O_3=1) are stable materials with no tendency, or at least very low tendency, towards the amorphous/crystalline transformation [22]. But when anions are added to the system, this property changes depending on the chemical nature of alkalis and anions used: zeolites can be formed even under moderated hydrothermal conditions.

The zeolites formed starting with sodium based geopolymers are zeolites X, zeolites Y, Gmelinite, Hershelite and Dachiardite in the sulphate containing materials and zeolites X and zeolites Y in the nitrate containing materials. Furthermore, among these phases, zeolites X are metastable with regards to zeolite P [26]: the nucleation of secondary zeolite phases occurs as the result of the arrangement and decomposition of the lattice of primary crystals. In the present study, such transformations were not detected. Beside possible failure of curing conditions to favour the nucleation of zeolite P as secondary zeolite, this result is in agreement with the findings of Bosnar et al. [27]. For these authors, the introduction of sodium sulfate in zeolitics systems inhibit the transformation of zeolite A into zeolite P or hydroxysodalite, which are yet more stable in a thermodynamic point of view. This inhibition seems to be extensible to geopolymer systems and probably to nitrate ions, at least for the curing conditions and time period investigated.

Under the considered hydrothermal conditions, potassium-based geopolymers become zeolite only when nitrate ions are involved. The zeolites formed are zeolites W, Chabazite and Phillipsite.

Conclusions

Anions that can commonly be found in aqueous waste streams, such as nitrates and sulphates modify the properties of geopolymers. Setting time and mechanical properties varies lightly, even if their evolutions suggest a change in geopolymerisation reactions. Leaching behaviour is also changed and more alkalis are released from the materials when these anions are added into the system. The proportion of sulphates and nitrates leached remains stable over the composition range investigated in this study.

The major changes are linked to the secondary transformation of geopolymers into zeolites under moderate hydrothermal treatment. This could suggest that these geopolymeric systems are metastable with regards to some zeolites, depending on mix formulation, temperature of treatment and possibly time. Such a change has to be taken into account prior to any use of geopolymer as waste encapsulating materials: zeolites are indeed well known for their ion-exchange abilities.

These geopolymeric systems should be investigated in several ways. First, the evolution of geopolymeric systems with time should be considered: are these zeolites representative of the natural evolutions of the materials? Are they the thermodynamically stable phases or is the system still in evolution? Second, these transformations may induce some changes in mechanical properties

that have to be assessed. Third, leaching behaviour of the zeolites formed has to be evaluated to guaranty that these transformations are not deleterious on this property, which is crucial for immobilizing materials.

References

[1] J. Davidovits, Journal of Thermal Analysis Vol. 37 (1991), p. 1633-1656.
[2] A. Palomo and M. Palacios, Cem. Conc. Res. Vol. 33(2) (2003), p. 289-295.
[3] A.M. Fernandez Jiminez, et al., Cem. Conc. Comp. Vol. 26(8) (2004), p. 1001-1006.
[4] A. Fernandez-Jimenez et al., Journal of Nuclear Materials Vol. 346(2-3) (2005), p. 185-193.
[5] S. Berger, F. Frizon and C. Joussot-Dubien, Adv. in App. Ceram. Vol. 108 (2009), p. 412-417.
[6] J.Z. Xu et al., Mat. Lett. Vol. 60(6) (2006), p. 820-822.
[7] C. Cau Dit Coumes and S. Courtois, Cem. Conc. Res. Vol. 33(3) (2003), p. 305-316.
[8] R. Kumar, et al., Nature Vol. 381 (1996), p. 298-300.
[9] W.K.W. Lee and J.S.J. Van Deventer, Cem. Conc. Res. Vol. 32 (2002), p. 577-584.
[10] W.K.W. Lee and J.S.J. Van Deventer, Indus. Eng. Chem. Res. Vol. 41 (2002), p. 4550-4558.
[11] W.K.W. Lee and J.S.J. Van Deventer, Coll. and Surf. A: Physicochem. and Eng. Asp. Vol. 211 (2002), p. 115-126.
[12] J.L. Provis, G.C. Lukey, and J.S.J. Van Deventer, Chem. of Mat. Vol. 17 (2005), p. 3075-3085.
[13] A. Palomo et al., Cem. Conc. Res. Vol. 29(7) (1999), p. 997-1004.
[14] J.G.S. Van Jaarsveld, J.S.J. Van Deventer, and G.C. Lukey, Chem. Eng. Journ. Vol. 89 (2002), p. 63-73.
[15] M. Rowles and B. O'Connor, J. of Mat. Chem. Vol. 13(5) (2003), p. 1161-1165.
[16] A. Palomo and J.I. Lopez de la Fuente, Cem. Conc. Res. Vol. 33(2) (2003), p. 281-288.
[17] H. Xu and J.S.J. van Deventer, Int. J. of Min. Process. Vol. 59 (2000), p. 247-266.
[18] W.M. Kriven, M. Gordon and J. Bell. *Geopolymers: Nanoparticulate, Nanoporous Ceramics made under Ambient Conditions*. in *Microscopy and Microanalysis'04 (Proc.62nd Annual Meeting of Microscopy Society of America)*. 2004.
[19] C.K. Yip, G.C. Lukey, and J.S.J. van Deventer, Cem. Conc. Res. Vol. 35(9) (2005), p. 1688-1697.
[20] V.F.F. Barbosa, K.J.D. MacKenzie and C. Thaumaturgo, Int. J. of Inorg. Mat. Vol. 2(4) (2000), p. 309-317.
[21] P.S. Singh, et al., Mat. Sc. and Eng. A Vol. 396 (2005), p. 392-402.
[22] P. De Silva and K. Sagoe-Crenstil, Cem. Conc. Res. Vol. 38(6) (2008), p. 870-876.
[23] S.D. Kindare and D.L. Pole, Inorg. Chem. Vol. 31 (1992), p. 4558-4563.
[24] R.A. Fletcher et al., J. Eur. Ceram. Soc. Vol. 25(9) (2005), p. 1471-1477.
[25] M. Criado et al., Cem. Conc. Res. Vol. 37 (2007), p. 671-679.
[26] D.W. Breck, *Zeolite Molecular Sieves : Stucture, Chemistry and Use*. (Wiley Interscience, USA 1974).
[27] S. Bosnar, T. Antonic-Jelic, and J. Bronic, J. Crystal Growth Vol. 267 (2004), p. 270-282.

doi:10.4028/www.scientific.net/AST.69.180

Recycling of industrial wastewater by its immobilization in geopolymer cement

Dorith Tavor [a], Tal Meyohas, Shlomi Ronen, Adi Wolfson[b]

Green Processes Center, Chemical Engineering Department, Sami Shamoon College of Engineering, Bialik/Basel Sts. Beer-Sheva, 84100 Israel.

[a]dtavor@sce.ac.il, [b]adiw@sce.ac.il

Keywords: Geopolymer; Cement; Wastewater; Industrial waste; Recycling; Leaching; Fly ash

Abstract. In this work, wastewater from Teva Pharmaceutical Industries Ltd., which comprises several organic and inorganic compounds, was solidified in a geopolymer matrix. The addition of wastewater to the polymerization mixture of fly ash based geopolymers yielded a high compressive strength of 50-75 MPa that is similar to that of wastewater-free geopolymer. The leaching of organic compounds from the matrix was examined and it was found to be negligible, about 0.2%wt, and comparable to the amount that leached from a geopolymer matrix made without wastewater. The results indicate that the immersion temperature and the time of immersion have negligible influences on carbon leaching.

Introduction

With increasing environmental awareness, industrial wastewater (IWW) has become one of the main concerns of the chemical, petrochemical, and process industries. Because it typically contains a variety of contaminants including organic compounds that can pollute the soil, and the underground water, while also producing toxic gases, IWW has a high potential to cause marked environmental damage [1]. Currently, various biological and chemical methods are employed to treat IWW, but their ability to reduce organic compounds to required levels is limited. Furthermore, treatments are usually compound-specific and in many cases they require extreme conditions [1-6].

Recently it was reported that the global production of pulverized coal combustion (PCC) fly ash is growing, and it is estimated that it will amount to 800 million tons per year in 2010 [7, 8]. Thus developing new technologies to recycle these large amounts of PCC fly ash into added-value products is essential. Fly ash based geopolymer is just such a product low cost and environmentally friendly materials with cementing properties for construction and which represents a feasible alternative for stabilizing metallic and radioactive wastes or IWW [9-17].

Geopolymers are amorphous, three-dimensional, alumino-silicate binder materials that were first discovered by Prof. Glukhovsky in the former Soviet Union in the 1950s. Later in 1970s, Davidovits, in France, began similar work and named those materials geopolymers [9]. Geopolymer binder materials can be synthesized by mixing alumino-silicate reactive materials and strong alkaline solutions, followed by curing at room temperature. Under such strong alkaline conditions, the alumino-silicate forms free SiO_4 and AlO_4 tetrahedral clusters that link together to yield polymeric precursors {-SiO_4-AlO_4-} [9, 18, 19]. Any pozzolanic material that contains mostly silicon and aluminum in an amorphous form such as fly ash, metakaolin, and silica fumes, is a possible source for geopolymer manufacture [18-20].

The unique properties of geopolymers, such as fast hardening, high compressive strength, high temperature resistance, and long-term durability, render geopolymerization a promising technology

with many attractive commercial applications [20-22]. In addition, these properties make geopolymer cement an excellent potential substitute for Portlant cement and part of a solution for waste stabilization.

Recently, we studied the recycling of IWW with residual organic compounds by its solidification in a geopolymer matrix as a generic method to treat a variety of industrial waste streams with various organic compounds [15]. The addition of phenol, which was chosen as the representative organic contaminant, to the polymerization mixture of fly ash based geopolymer yielded a geopolymer matrix with high compressive strength that is similar to that of a phenol free geopolymer. It was found that phenol leaching from fly ash based geopolymer reached measurable levels only when the solution contained amounts of phenol close to its saturation concentration.

In this work wastewater from Teva Pharmaceutical Industries Ltd., which comprises several organic compounds, was solidified in a geopolymer matrix for the first time, and organic compound leaching from the matrix was examined.

Experimental

Materials. Fly ash (SiO_2 47.04%; Al_2O_3 29.37%; Fe_2O_3 3.56%; TiO_2 1.97%) was provided by the Ashkelon-Israel power station. Solutions of 47% NaOH and sodium silicate (Na_2O 10.9-12%; SiO_2 25.6-29.3%; H_2O 58.2-63.5%) were purchased from Romicol Ltd. Other materials were bought from the following companies: quartz sand from Ashdod; Admixture of poly naphthalene- sulfunate sodium salt 50% in water [SA] and superplasticizer FEYZAL ASTM C-494 Type F from Advanced Chemicals & Technology S.A.E. [SL]; Borresperse NA sodium lignosulphonate (50% water) from Lignotech; Gileneum 51 (70% water) from Degus. The wastewater was provided by Teva Pharmaceutical Industries Ltd. from its plant in Ramat Hovav, Israel.

Synthesis. Inorganic geopolymers were synthesized by reacting Fly ash, sodium silicate, NaOH solution, and quartz sand at room temperature. The dry materials were weighed, added to a mixer, and then mixed for 2 min. Next, the liquid materials were weighed and slowly added to the mixture in the following order: Sodium silicate, water, and admixture.

A waste water solution from Teva was added at the end of mixing to prevent the contents of the mixture from reacting with the NaOH. Wastewater quantity was calculated as the sum of its amount in NaOH solution, admixture, sodium silicate, and added tap water. The viscous mixture was mixed for 6 minutes and then transferred to a mold of 12 cubes (size 25 × 25 × 25 cm) that were placed on a vibrating table. The molds were covered and cured at 50 °C for 24 h and then dried in the oven or in the air**.**

Analysis. Compressive strength of the geopolymer was measured using a press (ADR300 Ele). The Total organic carbon (TOC) and total carbon (TC) were measured using multi N/C 2100s (including solid test HT-1330) instrument from Analytik-Jena. For organic compound leaching experiments, model and grounded geopolrymer were immersed in water for several days and at different temperatures. After filtration, the immersion water and the dried geopolymer were analyzed for TOC/TC. Both compressive strength and organic component leaching were tested for in at least three different molds. In addition, since the distribution of the organic component in the mold was not homogeneous, several samples from different locations in the same mold were tested. The numbers presented in the results are average of the analyses of all these samples.

Results and discussion

As previously, mentioned geopolymers have unique mechanical properties that make them attractive alternative materials for waste stabilization and building. Thus, the effect of curing time on the mechanical properties of the geopolymers prepared with and without IWW was tested via two methods differentiated by their curing temperatures room temperature and oven temperature (Fig 1). Compressive strength increased with time up to 28 days of curing for all geopolymer samples, indicating that the polymerization process takes about 28 days. Yet, the samples with and without IWW that were dried in the oven showed higher compressive strengths (74MPa, 77MPa) than thos dried in air (44MPa, 55MPa). These results indicate that not only does temperature accelerate the polymerization process, but that it also helped condense the mold. The results in Fig. 1 also show that the addition of IWW affected geopolymer compressive strength only at the beginning of curing, but after 28 days the compressive strengths of the molds with and without IWW were the same, within the range of the experimental error. These results support the results that we reported previously [15] and indicate that the addition of IWW, which contains several organic and inorganic compounds, does not influence the mechanical properties of the geopolymer mold, and its compressive strength was higher that of the Portland cements.

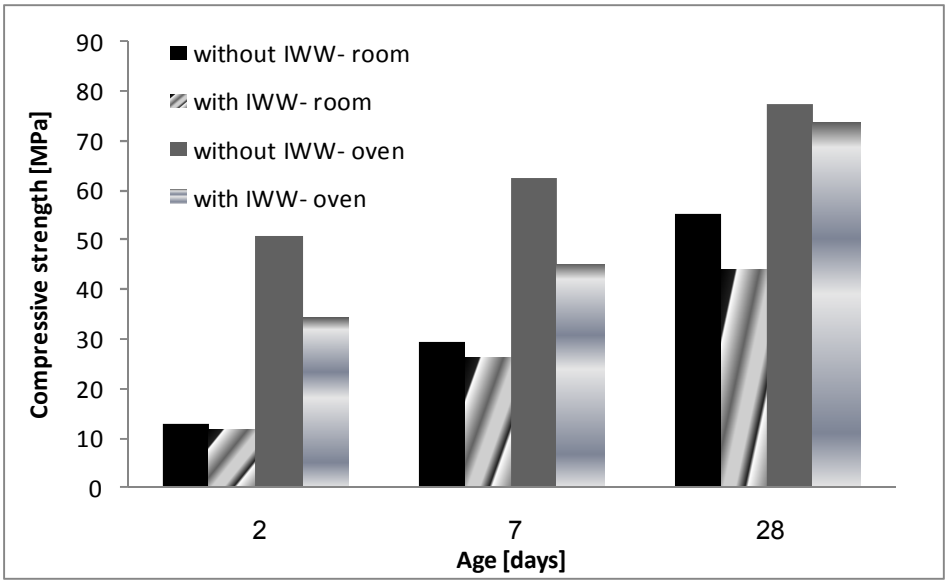

Fig. 1: Influence of added IWW on the compressive strength of geopolymers.
IWW: Industrial wastewater; room-dry in air at room temp; oven-dry in the oven at 50^0C

After the compressive strength of the geopolymer mold with the added of IWW was found to be good, the mold was tested for organic compound leaching. The samples of complete and crushed molds were immersed in 100 mL of distilled water for 1 h. After filtration of the molds from the water, the water was analyzed for TOC and TC. The leached carbon weight percentage (compared to the total weight of the molds) was calculated and summarized in Table 1. In general, it can be seen that the amount of carbon leaching was very low and that the difference between the leaching from geopolymer that was prepared with and without IWW is negligible (0.0033% and 0.0039%, respectively). As expected, the amount of carbon leaching as measured by TC is higher than that measured by TOC. In light of these results, it seems that the majority of the compounds that leached from the geopolymer came from the fly ash itself and not from the organics in the IWW that was added to the polymerization process. To verify these findings, HPLC analyses of the immersion solutions after geopolymer filtration and of a solution of fly ash in water after filtration were carried out. The HPLC spectra were similar with peaks of the fly ash, as we suspected. These results

indicate that in addition to the inorganic carbon, the fly ash contains the remains of organic compounds.

Table 1: Leaching of carbon compounds based on carbon weight percentage.

Test/Sample	Geopolymer mold without IWW[d]	Geopolymer mold with IWW	Crushed geopolymer molds without IWW	Crushed geopolymer molds with IWW
%wt leaching (TOC)[b]	0.0039	0.0033	0.2220	0.2035
%wt leaching (TC)[c]	0.0049	0.0063	0.2472	0.2287

[a] The leaching was measured after 1 h of immersion; [b] Calculated from Total Organic Carbon measured; [c] Calculated from Total Carbon measured; [d] Industrial wastewater.

Because of the low levels of carbon leaching from the geopolymer mold surface it was suggested that most of the organic compounds present in the IWW were immobilized in the geopolymer. To examine that suggestion, the crushed molds also underwent carbon leaching analysis. The weight percentages of the carbon that leached from the crushed geopolymer were higher by two levels of magnitude than that of the whole mold, and the difference between the geopolymer with and without IWW was small, within the range of the experimental errors (Table 1). Cumulatively, these results indicate that the organic compounds from the IWW were stabilized in the geopolymer matrix.

Because the leaching of organic compounds may depend on immersion time and temperature, their effects on carbon leaching were also studied (Fig. 2).

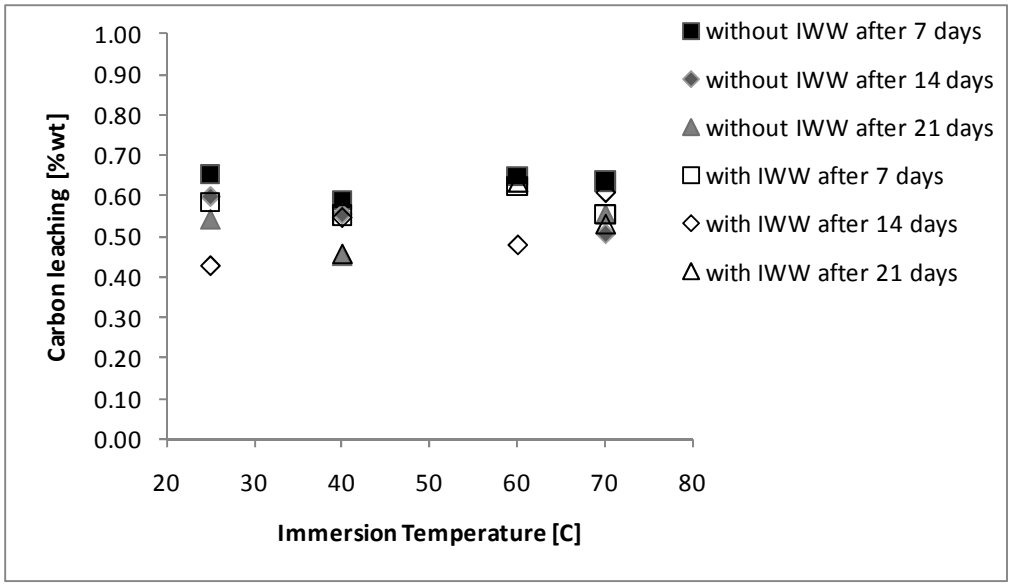

Fig. 2: Influence of temperature and length of immersion on carbon leaching.
IWW: Industrial wastewater; Crushed geopolymer; Dry in tair at room temperature; Calculated from Total carbon analysis.

In general, the effect of immersion temperature on carbon leaching was negligible in all samples (Fig. 2). In addition, immersion time had a small influence on one carbon leaching only at 25 °C. Furthermore, it can be seen that carbon leaching from the geopolymer with or without IWW was the same. Differences in the extent of carbon leaching may have resulted from both the experimental error and from the non homogenous dissemination of the materials in the matrix.

To further substantiate the assumption that the organic compounds present in IWW indeed remained in the geopolymer matrix, TC analyses of the solid geopolymers before and after immersion were also done. The calculated weight percentages of the carbon indicated that, and the as was previously concluded, the carbon leaching from the geopolymer prepared without IWW originated from the fly ash itself (Table 2). TC analyses of geopolymer after the addition of the IWW provided further support, as the percentage of carbon detected in the solid (from 0.040 to 0.046%) increased after IWW was added.
Moreover, the decrease in carbon weight percentages after geopolymer immersion was found to be the same with and without IWW.

Finally, it can be seen that the amount of carbon in the geopolymers prepared with IWW is higher than in those prepared without IWW, before and after immersion, which provides further support that the organic compounds present in the IWW are indeed immobilized in the polymer matrix. In addition, as was already shown (Fig. 2), immersion temperature had no significant influence on carbon weight percentage.

Table 2: Carbon weight concentration in solid geopolymer.

Geopolymer		Without IWW[C]		With IWW	
	Immersion Temp. [°C]	Dried in room Temp.	Dried in oven	Dried in room Temp.	Dried in oven
C[a] before immersion [%wt]		0.0428	0.0400	0.0463	0.0461
C[a] after immersion[b] [%wt]	25	0.0424	0.0408	0.0450[d]	0.0457
	40	0.0414	0.0429	0.0422	0.0433[d]
	60	0.0411	0.0417	0.0432[d]	0.0423
	70	0.0379	0.0399	0.0438	0.0441

[a] Calculated from Total Carbon analysis; [b] after 21 h immersion; [C] Industrial wastewater; [d] after 14 h immersion.

Conclusions

To conclude, the addition of IWW to fly ash during geopolymer formation did not influence the compressive strength of the final mold, and the polymerization process ended after 28 days. The fly ash based geopolymer contained the remains of organic compounds in addition to the inorganic carbon, both of which leached out of the matrix after its immersion in water. The amount of carbon that leached from the geopolymer prepared with IWW was similar to that leached from geopolymer prepared without IWW, but TC measurements of the two samples were different. In addition, leaching experiments with the immersion solutions and with the solid geopolymers that were prepared with and without IWW showed no difference.
These results indicated that the IWW was indeed immobilized in the polymer matrix.
This work supports the feasibility of the concept of IWW recycling by its immobilization in fly ash based geopolymers.

Acknowledgements

We thank Teva Pharmaceutical Industries Ltd. for providing the IWW from its plant in Ramat Hovav, Israel. We thank the Sami Shamoon College of Engineering Fund for supporting this study.

References

[1] G.Tchobanolous, F.L. Burton, H.D. Stensel, *Wastewater Engineering Treatment and Reuse*, 4th Ed., McGraw-Hill (2003)
[2] A. Sonune, R. Ghate: Desalination Vol 167 (2004), p.55
[3] B. Van der Bruggen, L. Braeken: Desalination Vol 188 (2006), p. 177
[4] M.D. Bermejo, M.J. Cocero: Journal of Hazardous Material Vol 137 (2006), p. 965
[5] A. Bozzi, T. Yuranova, P. Lais, J. Kiwi: Water Research Vol 39 (2005), p. 1441
[6] K. Laursen, L.D. Benefield, C.W. Randall, *Biological Process Design for Wastewater Treatment*, Prentice-Hall Inc, (1980)
[7] M. Izquierdo, X.Querol, C. Phillipart, Charles, D. Antenucci: World of Coal Ash: Science, Applications and Sustainability, Proceedings, 3rd, Lexington, KY, United States (2009)
[8] A. Fernandes-Jimenez, A. Palomo: Cem. Concr. Res. Vol 35 (2005), p. 1984
[9] J. Davidovits: J. Therm. Anal.Vol 37 (1991), p. 1633
[10] A. Palomo, M. Grutzeck, M. Blanco: Cem. & Con. Res. Vol 29 (1999), p. 1323
[11] H. Xu, J. van Deventer: Int. J. Min. Proc. Vol 59 (2000), p. 247
[12] H. Xu, J. van Deventer: Min. Eng. Vol 15 (2002), p. 1131
[13] C. Fernandez-Pereira, Y. Luna, X. Querol, D. Antenucci, J. Vale: Fuel Vol 88 (2008), p. 1185
[14] T. Hanzlicek, M. Steinerova, P. Straka: J. Am. Ceram. So. Vol 89(11) (2006), p. 3541
[15] D. Tavor, A. Wolfson, A. Shamaev, A. Shvarzman: Ind. Eng. Chem. Res. Vol 46 (2007), p. 6801
[16] D. Khale, R. Chaudhary, Rubina: J. oSo. Waste Tech.& Man. Vol 33 (3) (2007), p. 148
[17] J. Zhang, J.L. Provis, D. Feng, J.s.j.van Deventer: J. Haz. Mat. Vol 157(2-3) (2008), p. 587
[18] J. Davidovits: J. Mater. Educ.Vol 16 (1994), p. 91
[19] W. Sun, Y. Zhang, W. Lin, Z. Liu: Cement & concrete Res. (2004) Vol 34, p. 935
[20] A. Shvarzman , K. Kovler, G. Grader, G. Shter: International Symposium on Non-Traditional Cement & Concrete, (2002), Brno
[21] J. Swanepoel, S. Strydom: App. Geochem. Vol 17 (2002), p. 1143
[22] S. Zhang, K. Gong, J. Lu: Mat. Lett. Vol 58 (2004), p. 1292

doi:10.4028/www.scientific.net/AST.69.186

How to assess the environmental sustainability of geopolymers ? A live cycle perspective

Marcel Weil[1,a], Anja Buchwald[2,b] and Katja Dombrowski-Daube[3,c]

[1] Karlsruher Institute of Technology (KIT), Institute for Technology Assessment and Systems Analysis, Department of Technology-Induced Material Flow (ITAS-ZTS), Germany

[2] Bauhaus-University Weimar, Chair of Building Chemistry, Germany

[3] Freiberg University of Mining and Technology, Institute for Ceramic, Glass, and Construction Materials, Germany

[a] marcel.weil@kit.edu, [b] a.buchwald@ascem.nl, [c] katja.dombrowski@ikgb.tu-freiberg.de

Keywords: Geopolymer, Alkali Activated Alumosilicatic Binder, Ceramic, Cement, Concrete, Life Cycle Assessment, Sustainability, Secondary Resources

Abstract. Geopolymers as an alternative binder system gains growing attention in research and development. Outstanding technical properties like high strength, high acid resistance, or high temperature resistance can be unerringly achieved. Thus geopolymers are not only suitable for the development of building products, but are also interesting binder systems for ceramic applications.
Besides the technical performance of geopolymers, which is well investigated, only limited scientific knowledge exists about the environmental sustainability of geopolymers [1].
Due to the wide range of suitable raw materials and hence resulting, different geopolymer compositions for distinct application fields a generally statement about the environmental implications cannot be addressed to geopolymers. A more detailed analysis and assessment is needed, to provide more diversified statements.

Introduction

The sustainability assessment -by examining the economic, environmental and social aspects of new technologies or new materials- is a vital element for advancing sustainable development (Fig. 1).

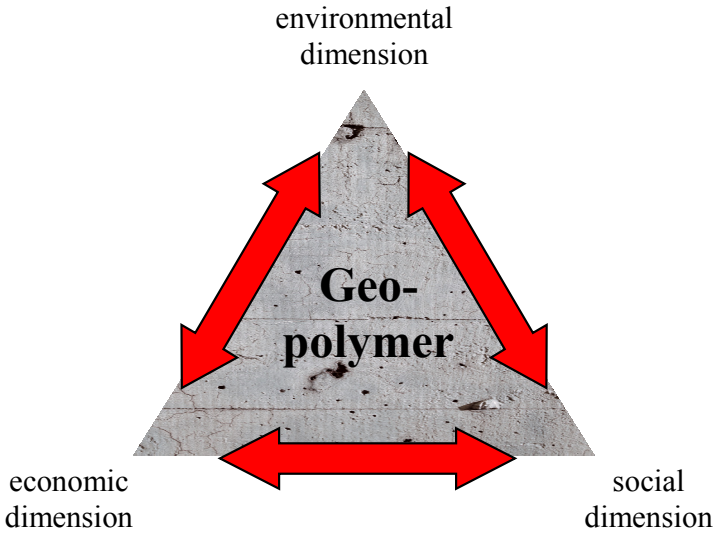

Figure 1: Dimensions for sustainable assessment of geopolymers

The economic assessment of geopolymers is heavily dependent on the regional context (with specific conditions) and on time (e.g. fluctuating raw material costs). For the region central Europe an economic analysis of geopolymer concrete production is conducted. The results exhibit the principal competitiveness with cement based systems [2].
A study so far which focuses on the social impacts or social implications of geopolymers is not known. But it can be assumed, that the quantitative assessment of social impacts will be quite difficult, especially due to the lack of specific production data and suitable social indicators because the methodology for social Life Cycle Assessment is under development [3]. Therefore the comparison of alternative materials or alternative technologies for specific applications regarding social aspects is still a challenging task.
On the contrary the presented work will focus on aspects regarding environmental sustainability of general geopolymer production, especially to identify the dependencies between geopolymer composition and environmental impacts. For this purpose Life Cycle Assessment (LCA) is an appropriate method [4, 5].

Geopolymer components

Geopolymeric binders are composed of solid and fluid (activator) raw materials. Traditionally metakaolin, different qualities of ground slag and fly ashes are used as solid components. Potassium or sodium silicate and/or potassium or sodium hydroxide solutions are used as activators within the geopolymer system.

Solids

- Metakaolin

Metakaolin is refined kaolin clay that is calcined by 500-800 °C in a burning process. Due to dehydroxylization process (during burning) the kaolin loses water and forms an amorphous aluminosilicate, which is very reactive. The production process of metakaolin is relatively energy intensive, especially the burning process. Therefore the ecological footprint is rather distinctive. Different products are available on the EU market. MetaMax from BASF (Former Engelhard) is designed for cement concrete applications, but is also suitable for geopolymer applications. The same is applicable for the product Metastar from the company Imerys. According to J. Davidovits [6] ARGICAL M 1200S by the French kaolin clay company AGS (which belongs to the Imerys group) is especially designed for geopolymer application. MEFISTO is a Czech brand of metakaolin by the company České lupkové závody. According to the company MEFISTO (Type K05/L05) is suitable for geopolymer and cement applications.

- Slag

Ground granulated blast furnace slag (GGBFS) is often used for geopolymer production and is a nonmetallic byproduct of iron production. It consists primarily of silicates, aluminosilicates, and calcium-alumina-silicates. GGBFS is in great demand, especially for cement production. In Germany, for instance, there is nearly no GGBFS available on the market, because all cement producer possess long term contracts with the iron producing industry. In Germany (2009) approximately 80% of the produced iron slag is used for cement production. The remaining 20% are mostly used as aggregates in building products or for road constructions [7]. The grinding of slag for cement or geopolymer applications is a material and energy intensive process, which induce a certain environmental impact.

- Fly ash

Fly ash is a fine-grained or powdery material and is produced by the burning of pulverized coal in a coal-fired power plant.

It is carried off in the flue gas and usually collected from the flue gas by means of electrostatic precipitators.

Fly ash requires neither extra burning process and nor kilning process (in comparison to slag) and therefore cause only little energy related environmental impact.

It can be distinguished between fly ash from hard coal combustion ("class F fly ash" and fly ash from lignite-fired power plants ("class C fly ash"). Approximately 80 % of the hard coal fly ash produced in Germany is used for concrete or cement applications. In contrast, only little amounts of brown coal fly ash is used for concrete and cement production, e.g. the product Jävament of the power plant Jänschwalde in Germany. For geopolymer production both qualities (from hard and brown coal) are suitable [8, 9, 10].

Fluids/Activator

- Sodium Hydroxide

Sodium hydroxide is produced by the electrolysis of an aqueous solution of sodium chloride. Further products of the electrolysis process are chlorine and hydrogen (coupled product). There are three important production processes at present:

- Mercury cell process
- Diaphragm cell process
- Membrane cell process

The latter causes the lowest electric energy consumption (electric energy and process energy). Thus the trend can be identified, that the market penetration of the membrane cell process is growing. In 2007 the capacity of membrane cells was grown beyond 45% of total installed chlorine production capacity in Europe [11]. The electrolysis of sodium chloride is a relatively energy intensive process.[1] The efforts (energy, raw material, etc.) of the production of chlorine, sodium hydroxide and hydrogen are in general allocated by mass and economic value.

- Sodium Silicate

The synthesis of the solid substance Sodium Silicate (Na_2O x SiO_2), also known as water glass, .involves a melting of sodium carbonate (Na_2CO_3) and silicon dioxide (SiO_2) under high temperature conditions (1100-1200 °C[2]). In addition to the energy related CO_2 emissions, the chemical reaction cause further CO_2 emissions. To produce fluid sodium silicate a dissolving process (under pressure and with water vapour) is necessary. Due to the melting process and the dissolving process, the production of silicate solution (whole pre chain) is a relative energy intensive process.[3]

Identification of drivers for environmental impact

For a streamlined life cycle assessment (gradle to gate) the following environmental impact indicators are considered:

- CED: Cumulative Energy Demand, in MJ
- ARC: Abiotic Resource Consumption, in kg Sb equivalent
- GWP: Global Warming Potential, in kg CO_2 equivalent

In Figure 2 the environmental impact of traditionally used raw materials is highlighted.

[1] Potassium hydroxide is also produced (in industrial scale) by electrolysis. Thus it can be assumed, that the environmental impact is comparable to sodium hydroxide.

[2] In literature temperature up to 1400 °C are also described

[3] Potassium silicate is also manufactured by melting process of silica sand with potassium carbonate at a temperature of approximately 1200 °C. Thus it can be assumed, that the environmental impact is comparable to sodium silicate.

Obviously the fluid activators have the highest specific environmental impact, regarding the considered indicators. The energy intensive production process is responsible for the environmental impact in both cases. The substitution of the energy intensive activators turns out to be very difficult. There are efforts to use a waste stream of the pre chain of aluminum production as a substitute of sodium hydroxide. But the heavy metal content of the waste stream impedes a real application.

In contrast, the secondary resource blast furnace slag and fly ash [12] represent widely used solids in binder systems. Due to their waste character only the transport, processing and storage after the formation is considered in LCA investigations. Thus the environmental impact of fly ash, but also of ground blast furnace slag is relatively low. Metakaolin is of primary origin and thus the burning process (with fossil fuels) causes a noteworthy environmental impact. The displayed data for metakaolin represents an average value for EU. Depending on the origin of kaolin (EU, US, Brazil, …) and even more important, depending on the specific burning process the values can differ significantly. The substitution of primary metakaolin is the object of several investigations. Coal deposits are often accompanied by kaolin containing rock [13]. According to J. Davidovits [6] the use of kaolin containing coal tailings for metakaolin production is a promising and environmental friendly option. But also other tailings are under investigation for metakaolin substitution [14].

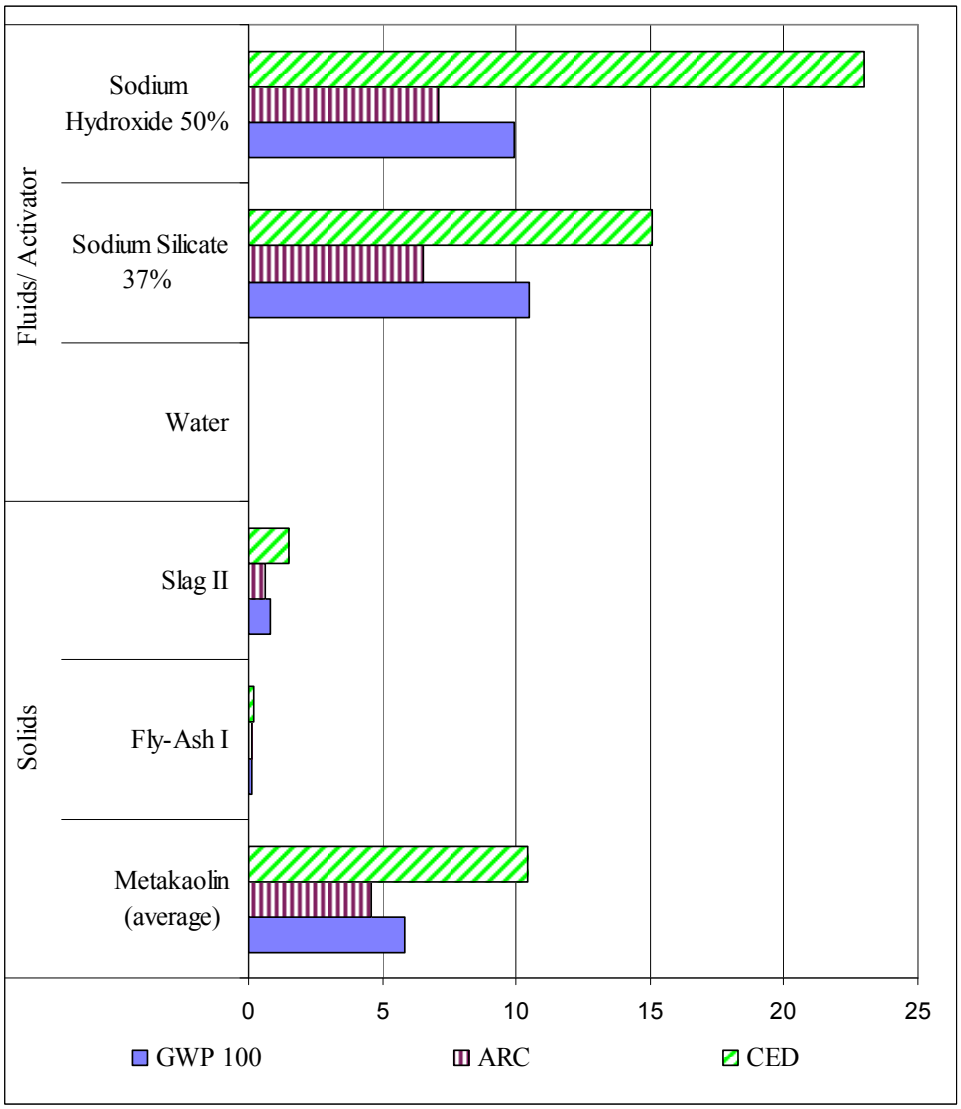

Figure 2: Environmental impact indicator values (CED, GWP, ARC) for common geopolymer raw materials. Values per kg raw material - without transport efforts.

The environmental profile of geopolymers depends obviously on the composition (Fig. 3). Especially the different amounts of activators used in geopolymers have a strong influence on the environmental impact, which is shown for CED in Figure 3. Already small mass percentage of silicate solutions or sodium hydroxide solution causes a significant contribution to the total CED. Metakaolin and slag contributes noteworthy to the total CED. In contrast aggregates and fly ash contributes only slightly to CED. Regarding other environmental impact indicators, like GWP or ARC the investigation gained comparable results.

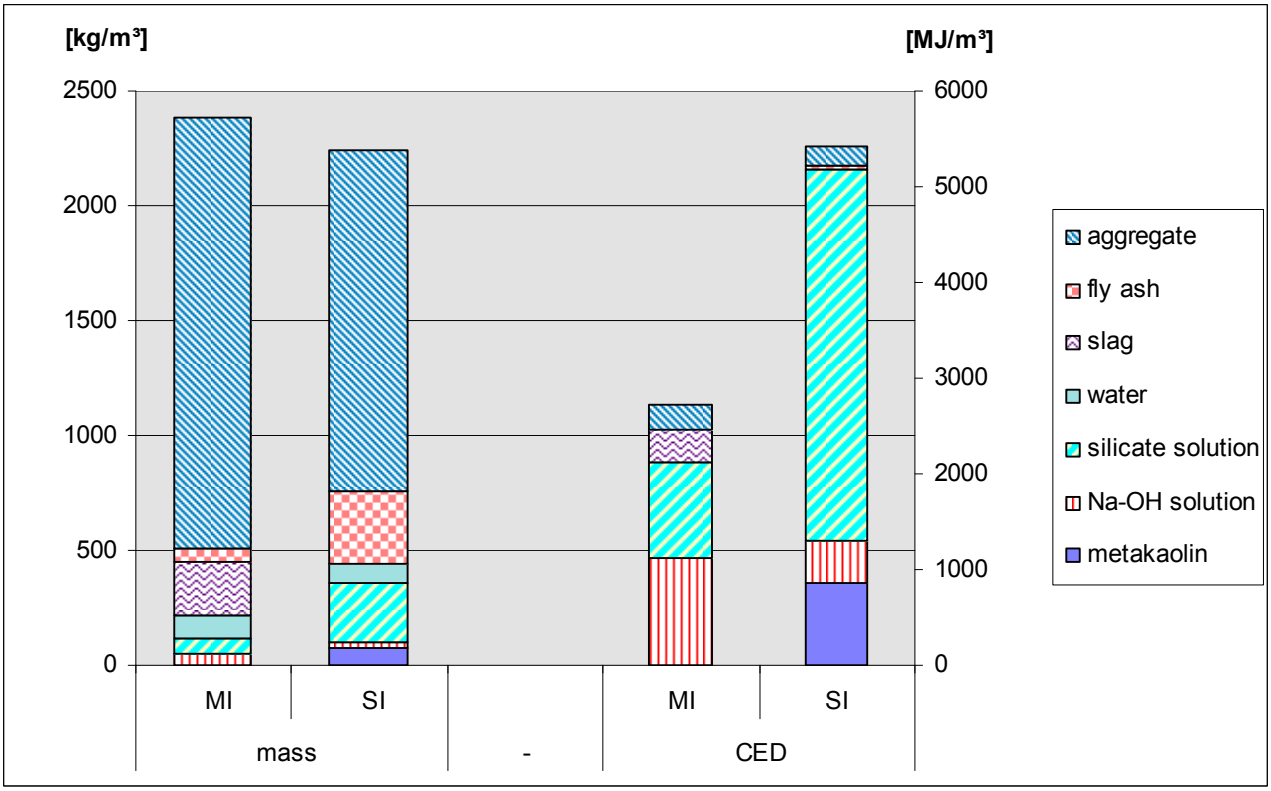

Figure 3: Two different geopolymer compositions (MI, SI) and the environmental impact regarding CED

Conclusions

Geopolymers are a very promising material group with excellent technical performance. A general statement about the environmental friendliness of geopolymers can not be drawn, because it depends on several factors. One factor is the composition of geopolymers, which was the focus of the paper. It could be identified by the investigations that the common use of silicate solution or hydroxide solution has a great impact on the environmental profile. Beside the activators only the use of slag and especially metakaolin influence noteworthy the environmental profile. The use of fly ash for geopolymer production turns out to be advantageous from an environmental point of few.

It has to be mentioned, that the production is only one phase of the whole live cycle of a product. Thus a detailed LCA has to consider the whole live cycle, especially if geopolymers are compared with competing systems like ceramics.

Acknowledgement

This research work was made possible by the support provided by the foundation Volkswagen Stiftung.

References

[1] M. Weil, A. Buchwald, K. Dombrowski, W.R. Poganietz: Managing emerging technologies – Sustainable design for geopolymers. 17th Conference of the Society of Environmental Toxicology and Chemistry (SETAC) Europe: Multiple stressors for the environment - present and future challenges and perspectives. Porto (2007)

[2] M. Weil, A. Buchwald, K. Dombrowski: Geopolymer Binders. Teil 3: Ökologische und ökonomische Analysen von Geopolymerbetonmischungen für Außenbauteile. ZKG International - accepted -.

[3] UNEP SETAC: Guidelines for social life cycle assessment of products. United Nations Environmental Programme (2009)

[4] ISO 14040 ff: Environmental management – Life cycle assessment – Principles and framework. International Organization for Standardization (2006).

[5] M. Weil, K. Dombrowski, A. Buchwald: Life cycle analysis of geopolymers. In Geopolymers – Structure, processing, properties and industrial applications. Provis, L., Deventer, J. (Eds.). Woodhead Publishing, Cambridge (2009), pp 194-210

[6] J. Davidovits: http://www.geopolymer.org/news/first-supplier-of-geopolymer-raw-material , last call 04/2010

[7] Th. Merkel: Erzeugung von Eisenhüttenschlacken im Jahr 2008. In Institut für Baustoff Forschung Report (2009), 16 (1). Personal communication with Th. Merkel - preliminary version of "Erzeugung von Eisenhüttenschlacken im Jahr 2009".

[8] E.I. Diaz, E.N. Allouche, S. Eklund: Factors affecting the suitability of fly ash as source material for geopolymers. Fuel, 89 (2010), pp 992-996

[9] Dombrowski, K., Buchwald, A., Weil, M.: The influence of calcium content on the structure and thermal performance of fly ash based geopolymers. Journal of Materials Science (2007), 42 (9), pp 3033-3043.

[10] J. Xie, J. Yin, J. Chen, J. Xu,: Study on the Geopolymer Based on Fly Ash and Slag, International Conference on Energy and Environment (2009), vol. 3, pp 578-581

[11] http://www.eurochlor.org/makingchlorine

[12] H. Li, D. Xu :The future resources for eco-building materials: II. Fly ash and coal waste. Journal of Wuhan University of Technology - Materials Science Edition (2009), 24 (4), pp 667-672

[13] K. Burger: Kaolin-Kohlentonsteine im flözführenden Oberkarbon des Niederrheinisch-Westfälischen Steinkohlenreviers. Geologische Rundschau (1980), 69 (2)

[14] F. Pacheco-Torgal, J. P. Castro-Gomes, S. Jalali: Investigations on mix design of tungsten mine waste geopolymeric binder. Construction and Building Materials (2008), 22, pp 1939–1949

[15] D. S. Perera, R. L. Trautman: Geopolymers with the Potential for Use as Refractory Castables. The Azo Journal of Materials Online - AZojomo (ISSN 1833-122X) - (2006), vol. 2

doi:10.4028/www.scientific.net/AST.69.192

Chemical and biological characterization of geopolymers for potential application as hard tissue prostheses.

Michelina Catauro[1,a], Flavia Bollino[1,b]; Isabella Lancellotti[2,d], E. Kamseu[2,e], Cristina Leonelli[2,f]

[1] Department of Aerospace and Mechanical Engineering, Second University of Naples, Via Roma 21, 81031 Aversa, Italy.

[2] Department of Materials and Environmental Engineering, University of Modena and Reggio Emilia, Via Vignolese 905, I-41100 Modena, Italy.

[a]michelina.catauro@unina2.it, [b]flavia.bollino@unina2.it, [d]isabella.lancellotti@unmore.it, [e]elie.kamseu@unimore.it, [f]cristina.leonelli@unimore.it.

Keywords: Geopolymers, FTIR, Bioactivity.

Abstract. In this study different geopolymers have been investigated and characterized as potential biomaterials. The work presents exhaustive FT-IR, SEM/EDS and X-Ray studies of two geopolymer formulations, where water content, water to solid content and curing conditions have been varied during mixing stage, maintaining constant the ratios among Na-Al-Si. The amorphous matrix is typical of sodium aluminosilicates, as shown by the FT-IR spectra. The presence of zeolitic phases has been observed by XRD at the surface of the material while the main matrix was characterized by amorphous aluminosilicate phases. The compressive strength of all the compositions was higher than 50 MPa. In order to study their bioactivity, samples of the studied materials were soaked in a simulated body fluid (SBF). The bioactivity of the synthesized geopolymers was shown by the formation of a layer of hydroxyapatite on the surface of the materials by using the SEM.

Introduction

In the biomaterials field, some system based on amorphous silicate network like bioactive glasses [1], calcium phosphate [2, 3], aragonite [4], are successfully applied in bony surgery. The numerous synthetic aluminosilicates [5, 6], possess chemical properties which offer employment as bone graft biomaterial.

Geopolymers are a class of cementious materials that are formed by mixing aluminosilicate materials (e.g., metakaolin, low-calcium fly ash) with alkali or an alkali-silicate solution [7-10].

The formation of $[M_z(AlO_2)x(SiO_2)_y.MOH.H_2O]$ gel, which essentially relies on the extend dissolution of alumino-silicates materials, is a dominant step in geopolymerisation. The gel, then, diffuses outward from the particles surface into larger interstitial spaces between the particles with precipitation of gel and concurrent dissolution of new solid. When the gel phase hardens, the separate alumino-silicate particles are therefore bound together with the gel which acts as bender[11]. Authors[12, 13] described the reaction process of the gel formation indicating that Al-Si solid particles in alkaline solution conduct to the formation of monomer $^{-}OSi(OH)_3 + Al(OH)_4^{-}$. The successive reactions between these monomers, alkali ions and water result on the formation of dimer. Moreover, adding concentrated silicate anion, the tetramer, pentamer, hexamer, octamer, nonamer, etc and their compound will appear[14]. Geopolymers are then formed with tightly packed polycrystalline structure so as to give better mechanical properties.

The reaction mechanism involves the dissolution of Al and Si in the alkali medium, transportation of dissolved species, followed by polycondensation, forming a 3D network of alumino-silicate structure. Condensation occurs between alumino-silicate species or silicate species themselves, depending on the concentration of Si in the system. When $Si/Al > 1$, the silicate species formed as a result of hydrolysis of SiO_2, tend to condense among themselves to form oligometric

silicates whose condense with $Al(OH)_4^-$ forming a rigid 3D network of geopolymer structures[15, 16]. Typically, better strength behavior are obtained for mixtures with SiO_2/Al_2O_3 ratios in the range of 1.65-2.10 with an Na_2O/SiO_2 ratio near 1. Higher amounts of hydroxyl ions facilitate the dissociation of different silicate and aluminate species, promoting thus further polymerization. NaOH promotes Na^+ ions whose strong pair formation (better dissolution) of silicate oligomers. KOH promotes K^+ that favours the formation of larger silicate oligomers with which $Al(OH)_4^-$ prefers to bind. Therefore in KOH solutions more geopolymer precursors exist resulting thus in better setting and stronger compressive strength since K^+ would promote high degree of condensation[17]. It was found that by combining NaOH and KOH, highly dissolved and crossed linked samples of geopolymer materials can be obtained. The multiple alkali sources can act in a synergistic way to promote samples of optimal characteristics[13, 14].

High-performance materials for construction, adhesives, coatings, hydroceramics and an ever-growing range of niche applications are produced by the reactions sequence described above. The mechanical strength results on the rapid solidification within hours and rapid early strength development. The strength for these materials is believed to originate from the strong chemical bonding in the alumino-silicate gel formed, as well as the physical and chemical reactions occurring between the geopolymer gel, non or partly reacted phases, and particulate aggregates. The compressive strength of geopolymer materials depends on a number of factors including gel phase strength, the ratio of gel phase/undissolved Al-Si particles size, the distribution and the hardness of the undissolved Al-Si particles, the amorphous nature of geopolymers or the degree of crystallinity as well as the surface reaction between the gel phase and the undissolved Al-Si particles[12, 18]. After geopolymerisation, the undissolved particles remain bonded in the matrix, so that the hardness of the minerals correlates positively with the final compressive strength[18]. The significance of the Si/Al ratio during alkaline dissolution of the individual minerals indicates that compressive strength is acquired by complex reactions between the mineral surface, alumino-silicate and the concentrated sodium silicate solution.

In this study different geopolymers have been synthesized. The aim of the present paper is to describe the preparation, chemical characterization and to investigate them as potential biomaterials.

Materials and experimental procedure

Metakaolin was used as the principal source of alumino-silicate. The choice was based on the fact that it is the cheapest alumino-silicate that presents a good degree of purity. Metakaolin improves mechanical strength and reduces the transport of water and salts in the final product Metakaolin is important in the production of geopolymer materials for applications as adhesives, coatings and hydroceramics [19].

Two different formulations of geopolymer materials were prepared as shown in Table 1. Metakaolin (MK) was prepared by calcining kaolinitic clay at 700°C in muffle oven for 2 hrs. Laboratory grade NaOH pellets and distilled water were used to prepare 8M alkaline solution. Sodium silicate solution (grade N, RM3,0 from Ingessil s.r.l., Verona, Italy) had a mol/mol ratio of SiO_2/Na_2O equal to 2,99.

Table 1 Formulation of the 2 geopolymers prepared for this study

Compositions	NaOH 8M solution	Na silicato solution	SiO_2/Al_2O_3
GP120	20 ml/100g MK	30 ml/100g MK	2.10
BGP130	30 ml/100g MK	30 ml/100g MK	2.10

Two different Na/Al were tested. The ratio of the solutions to MK mass used was 2:3 for both samples. Designated quantities of sodium hydroxide solutions were mixed with 100 g batches of metakaolin, and the resulting slurries were stirred mechanically for about 10 min to reach good

homogenization, than poured in a polyethylene mould for 12 hrs at room temperature before being demoulded and allowed to dry. The final geopolymers composition was calculated from Schimadzu EDX 720 X-ray fluorescence. The presence of zeolitic phases has been observed by XRD (model PW 1730 Philips Electronic Instruments) at the surface of the material.

The Bulk density and porosity were determined following the ASTM standard C20.

The compressive and bi-axial flexural strength was determined by using type MTS 810, USA. Specimens end surface were polished flat and parallel to avoid the requirement for capping. The cylinders and prisms were centered in the compression-testing machine and loaded to complete failure. The compressive strength was calculated by dividing the maximum load (N) at failure by the average cross-sectional area (m^2). For the bi-axial four point flexural strength, the piston-on-three-ball test was applied.

In order to study their bioactivity, the discs of the studied materials was soaked in a simulated body fluid (SBF) with ions concentration nearly equal to those in human blood plasma (Table 2), at 37°C and in a polystyrene bottle, as scheduled by biocompatibility test in vitro [20]. The SBF was prepared by dissolving reagent grade chemicals NaCl, $NaHCO_3$, KCl, $MgCl_2$, HCl 1M, $CaCl_2 \bullet 6H_2O$, Na_2SO_4 (Sigma-Aldrich) in ultra-pure water and buffered at pH 7.4 using tris(hydroxymethyl)-aminoethane (Sigma-Aldrich) and 1M HCl.

In this tests the ratio between the total surface (ST) of the material in contact with the SBF solution and the volume (V_{SBF}) of such solution, influence the reaction of formation of an hydroxyl-apatite layer. A constant ratio of $ST/V_{SBF} = 50 mm^2/ml$ will be used.

After immersion periods of 7, 14 and 21 days, the materials were removed from the SBF, gently washed with ultra-pure water, and dried at 40°C. The ability to form an apatite layer was studied by submitting reacted samples to Scanning Slectron Microscopy (SEM) and EDS microscopy.

Table 2 SBF composition

Ion	Ions concentration (mM)	
	Human blood plasma	SBF
Na^+	142.0	142.0
K^+	5.0	5.0
Mg^{2+}	1.5	1.5
Ca^{2+}	2.5	2.5
Cl^-	103.0	147.0
HCO_3^-	27.0	4.2
HPO_4^{2-}	1.0	1.0
SO_4^{2-}	0.5	0.5
pH	7.2-7.4	7.4

Results and discussion

The physical and mechanical properties are reported summarized in table 3: The compressive strength of the two compositions were > 50 MPa which is indicative for the suitability of the obtained products for applications as hard tissue protheses. The mechanical properties of geopolymers obtained, together with the bulk density and porosity are indicative for the higher degree of reactivity and polycondensation [21].

Table 3 Physical and mechanical properties

Bulk density	1.56-1.55 g/cm3
Compression strength	68.0 + 4.4 MPa
Bi-axial Flexural strength	20.0 4.5 MPa
Porosity	25 wt%

In the geopolymers FTIR spectra, an approximate relationship between the frequency of the absorption bands and the ratio of Si:Al in the alluminosilicate framework was observed by Milkey (1960): the higher the Al inclusions, the lower the wave length.

In Fig. 1 GP120 and BGP1 FTIR spectra are shown. The spectra consist of the strongest vibration found in all aluminosilicates, which are assigned to internal vibrations of Si-O-Si and Si-O-Al. All contain absorption bands at about 3450 and 1650 cm^{-1} resulting from hydration water, a strong Si-O stretching vibration at about 1080-1100 cm^{-1} and Si-O bending vibration at about 450-470 cm^{-1}. The Si-OH bending vibrations are at 840 cm^{-1} while Al-OH stretching vibrations are at 914-916 cm^{-1}. Moreover, the bends between 600-800 cm^{-1} are due to Al-O-Si vibrations [22, 23]: in particular, the bends at 798 cm^{-1} are due to Al-O stretching vibrations. The absence of a band at 1460 cm^{-1} indicates that sodium carbonate species are not present in this sample [24].

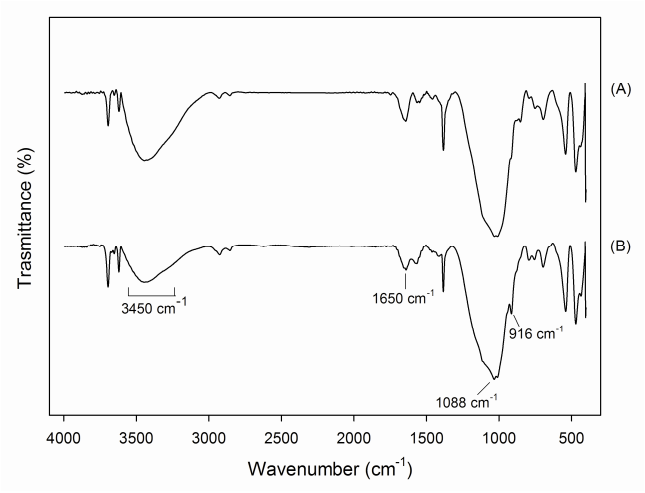

Fig. 1 FTIR of A) BGP130 and B)GP120

The final geopolymers composition was calculated from X-ray fluorescence (XRF) and quantitative are reported in Table 4.

Table 4 Composition of geopolymers as determined by X-ray Fluorescence (wt %)

Composition	SiO_2	Al_2O_3	Fe_2O_3	CaO	TiO_2
GP120	60.409	23.225	7.881	1.004	2.229
BGP130	62.380	27.923	8.466	0.126	6.441

The XRD shows the main matrix was characterized by amorphous aluminosilicate phases.

Moreover an evaluation of the morphology of the apatite deposition and a qualitative elemental analysis were carried out by electron microscopy (SEM) observations on pelletized discs previously coated with a thin Au film.

Fig. 2 A) show the SEM micrographs of GP120 soaked in SBF for 21 days. The layer of apatite isn't visible on simple surface, proving that GP120 isn't bioactive. BGP130, on the contrary, is very bioactive, in fact the characteristic apatite globular crystals are clearly visible, as shown in Fig. 2 B) and C).

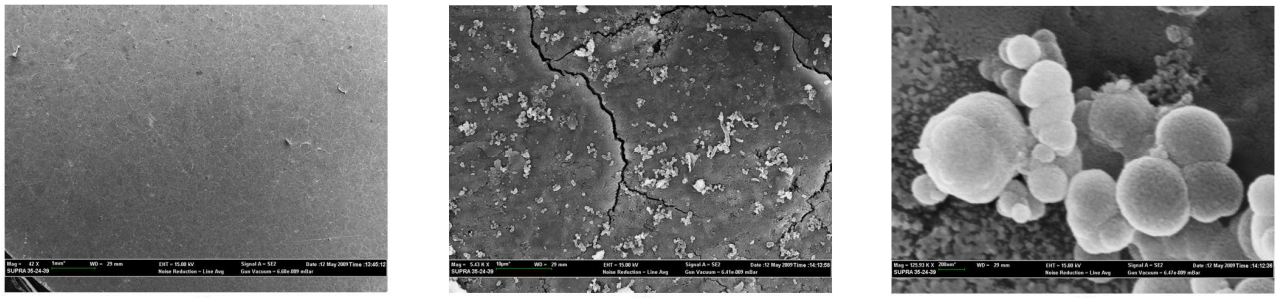

Fig. 2 SEM micrograph of (A) GP120 and (B) BGP130 after soak in SBF for 21 days. (C) Typical apatite globular crystals

The formation of the apatite on the materials incubated in SBF may be explained by the presence of groups with negative charge on the surface of the materials. These groups combine with the Ca^{2+} ions present in the fluid bringing the increase of positive charge on the surface. The Ca^{2+} ions combine with the negative charge of the phosphate ions to form amorphous phosphate, which spontaneously transforms into hydroxyl-apatite $[Ca_{10}(PO_4)_6(OH)_2]$ where the atomic ratio is Ca/P è 1.60 [25]. The EDS analysis confirms that the surface layer observed in the SEM micrographs consists of calcium phosphate (Table 5)

Table 5 Ca and P contents in BGP130 after soak in SBF for 21 days

Contents of Ca (Atomic %)	Contents of P (Atomic %)	Ratio Ca/P
3.14	1.95	1.61

Conclusions

The compressive strength of the two formulations (GP120 and BGP130) were > 50 MPa which is indicative for the suitability of the obtained products for applications as hard tissue prostheses; however, BGP130 only is bioactive. It's possible, therefore, to synthesize geopolymers bioactive and with good mechanical properties, that can serve in different applications in the bone graft biomaterial.

References

[1] L. L. Hench: Biomaterials. Vol. 19 (1998), p. 1419

[2] H.-W. Kim and H.-E. Kim: J. Biomed. Mater. Res. - B. Vol. 77B (2006), p. 323

[3] G. X. Ni, W. W. Lu, K. Y. Chiu, Z. Y. Li, D. Y. T. Fong and K. D. K. Luk: J. Biomed. Mater. Res. - B. Vol. 77B (2006), p. 409

[4] H. Oudadesse, A. C. Derrien and A. Lucas-Girot: Eur. Phys. J. Appl. Phys. Vol. 31 (2005), p. 217

[5] H. Oudadesse, A. Derrien, M. Lefloch and J. Davidovits: J. Mater. Sci. Vol. 42 (2007), p. 3092

[6] H. Oudadesse, A. C. Derrien, M. Mami, S. Martin, G. Cathelineau and L. Yahia: Biomed. Mater. Vol. 2 (2007), p. S59

[7] J. Davidovits: J. Therm. Anal. Calorim. . Vol. 37 (1991), p. 1633

[8] A. Palomo, M. T. Blanco-Varela, M. L. Granizo, F. Puertas, T. Vazquez and M. W. Grutzeck: Cement. Concrete Res. Vol. 29 (1999), p. 997

[9] A. Palomo, M. W. Grutzeck and M. T. Blanco: Cement. Concrete Res. Vol. 29 (1999), p. 1323

[10] J. G. S. Van Jaarsveld, J. S. J. Van Deventer and L. Lorenzen: Miner. Eng. Vol. 10 (1997), p. 659

[11] R. Cioffi, L. Maffucci and L. Santoro: Resour. Conserv. Recy. . Vol. 40 (2003), p. 27

[12] J. S. J. van Deventer, J. L. Provis, P. Duxson and G. C. Lukey: J. Hazard. Mater. Vol. 139 (2007), p. 506

[13] H. Xu and J. S. J. Van Deventer: Int. J. Miner. Proces. Vol. 59 (2000), p. 247

[14] W. M. Hendricks, A. T. Bell and C. J. Radke: The Journal of Physical Chemistry. Vol. 95 (1991), p. 9513

[15] M. R. Anseau, J. P. Leung, N. Sahai and T. W. Swaddle: Inorg. Chem. Vol. 44 (2005), p. 8023

[16] M. R. North and T. W. Swaddle: Inorg. Chem. Vol. 39 (2000), p. 2661

[17] J. W. Phair and J. S. J. Van Deventer: Int. J. Miner. Proces. Vol. 66 (2002), p. 121

[18] K. Komnitsas and D. Zaharaki: Miner. Eng. Vol. 20 (2007), p. 1261

[19] P. Duxson, G. Lukey and J. van Deventer: J. Mater. Sci. Vol. 42 (2007), p. 3044

[20] T. Kokubo, H. Kushitani, S. Sakka, T. Kitsugi and T. Yamamuro: J. Biomed. Mater. Res. Vol. 24 (1990), p. 721

[21] C. Leonelli, E. Kamseu and V. M. Sglavo: Ceramic Engineering and Science Proceedings. Vol. 29 (2009), p. 155

[22] R. W. Parker and R. L. Frost: Clay. Clay Miner. Vol. 44 (1996), p. 32

[23] R. L. Frost, P. M. Fredericks and H. F. Shurvell: Can. J. Appl. Spectrosc. Vol. 41 (1996), p. 10

[24] J. A. Gadsden: *Infrared spectra of minerals and related inorganic compounds* (Butterworths, London, 1975).

[25] C. Ohtsuki, T. Kokubo and T. Yamamuro: J. Non-Cryst. Solids. Vol. 143 (1992), p. 84

Keywords Index

N

P

R

S

T

W

X

Z

Authors Index

Q

R

S

T

W

Y

Z